



**HAL**  
open science

# Role of the nuclear receptor $ROR\alpha$ expressed by myeloid cells in metabolic diseases

Benan Pelin Sermikli

► **To cite this version:**

Benan Pelin Sermikli. Role of the nuclear receptor  $ROR\alpha$  expressed by myeloid cells in metabolic diseases. Human health and pathology. Université de Lille, 2020. English. NNT : 2020LILUS019 . tel-03917130

**HAL Id: tel-03917130**

**<https://theses.hal.science/tel-03917130>**

Submitted on 1 Jan 2023

**HAL** is a multi-disciplinary open access archive for the deposit and dissemination of scientific research documents, whether they are published or not. The documents may come from teaching and research institutions in France or abroad, or from public or private research centers.

L'archive ouverte pluridisciplinaire **HAL**, est destinée au dépôt et à la diffusion de documents scientifiques de niveau recherche, publiés ou non, émanant des établissements d'enseignement et de recherche français ou étrangers, des laboratoires publics ou privés.

Université de Lille  
École Doctorale Biologie et Santé de Lille (EDBSL, 446)  
Inserm, Institut Pasteur de Lille, Université de Lille, CHU Lille  
UMR 1011-EGID Récepteurs nucléaires, maladies métaboliques et cardiovasculaires  
(Prof. Bart STAELS)  
Équipe 3 : Dialogue immunométabolique dans l'obésité et ses pathologies associée  
(Dr. David DOMBROWICZ)

# Role of the nuclear receptor ROR $\alpha$ expressed by myeloid cells in metabolic diseases

Benan Pelin Sermikli

Directeur de thèse  
Dr. David Dombrowicz

## **Jury:**

Professeur Bart STAELS (Université de Lille, France), Président

Professeur Isabelle LECLERCQ (Université Catholique de Louvain (UCL), Belgium), Rapporteur

Dr. Stoyan IVANOV (Université de Nice, France), Rapporteur

Dr. David DOMBROWICZ (Université de Lille, France), Examineur

Présente et soutenue publiquement le 14 décembre 2020 pour l'obtention du titre  
de Docteur de l'Université de Lille

## ABSTRACT

Retinoic acid receptor-related orphan receptor-alpha ( $ROR\alpha$ ) is a transcription factor from the nuclear receptor superfamily expressed by immune and non-immune cells involved in the regulation of obesity, insulin resistance (IR) and non-alcoholic steatohepatitis (NASH). Cholesterol, cholesterol-sulfate, 7-oxygenated sterols and oxysterols have been identified as potential endogenous  $ROR\alpha$  ligands. To better understand the mechanisms of macrophage-expressed  $ROR\alpha$  regulation in obesity and IR, we generated a macrophage-specific  $ROR\alpha$ -deficient (MKO) mouse line by using a LysM-Cre and floxed  $ROR\alpha$  mouse line. We report that  $ROR\alpha$  deletion in macrophages does not impact on HFD-induced obesity and IR. Surprisingly, we did not confirm an earlier report on the effect of HFD on NASH development upon HFD feeding nor in the more severe and obesity-independent choline-deficient, L-amino acid-defined diet model. We thus, suspected that LysM copy number may play a role in this discrepancy, as the genotype at the LysM locus is a major difference between the two independent lines of work. The LysM-Cre mice carry an insertion of Cre recombinase into the *Lyz2* gene, leading to Cre expression under the control of the *Lyz2* promoter and enhancers, but abolishing endogenous *Lyz2* expression. While we intentionally maintained similar *Cre* and *Lyz2* expression between WT and MKO by using only hemizygous animals for this locus (comparing *Rora*<sup>+/+</sup>*Lyz2*<sup>Cre/+</sup> with *Rora*<sup>fl/fl</sup>*Lyz2*<sup>Cre/+</sup>), floxed mice (*Rora*<sup>fl/fl</sup>*Lyz2*<sup>+/+</sup>) were used as WT control and compared with MKO mice missing information about the *Lyz2* locus (*Rora*<sup>fl/fl</sup>*Lyz2*<sup>Cre/?</sup>) in the earlier study. As, we hypothesized that the observed impact of  $ROR\alpha$  deletion in macrophages on NASH in the earlier study likely did not result from a specific effect of  $ROR\alpha$  deletion, but rather from a different *Lyz2* copy number between WT and MKO mice, we decided to verify this hypothesis experimentally. Surprisingly, our preliminary findings showed that the *Lyz2*-deficient mice exhibit slight protection, rather than a detrimental effect, in HFD-induced obesity and IR, as determined by lower body weight and adipose tissue masses, significantly improved glycemic control and decreased epiAT inflammation. Interestingly, whole body *Lyz2* deficiency had no impact on hepatic steatosis (NAFL) in HFD-fed mice. Nonetheless, our preliminary findings even suggest that *Lyz2* deficiency might protect against advanced and obesity-independent choline-deficient, L-amino acid-defined diet-induced NASH. Taken together, these preliminary findings indicate that different *Lyz2* gene copy number in control mice is unlikely to account for the discrepancy between our work and the earlier study. Overall, our results show that  $ROR\alpha$  deletion in macrophages does not alter the development of obesity and IR and question its role in NASH. On the other hand, we believe that further investigations are of significant interest in the context of obesity, IR, and advanced NASH, as *Lyz2* might possess a therapeutic value.

## RÉSUMÉ

ROR $\alpha$  (Retinoic acid receptor-related orphan receptor-alpha) est un facteur de transcription de la superfamille des récepteurs nucléaires exprimé par des cellules immunitaires et non immunitaires impliqué dans le contrôle de l'obésité, de l'insulinorésistance (IR) et de la stéatohépatite non alcoolique (NASH). Le cholestérol, le cholestérol-sulfate, les stérols 7-oxygénés et les oxystérols ont été identifiés comme des ligands endogènes potentiels ROR $\alpha$ . Pour mieux comprendre le rôle de ROR $\alpha$  exprimé par les macrophages dans l'obésité et l'IR, nous avons généré une lignée de souris déficientes en ROR $\alpha$  spécifiques aux macrophages (MKO) en utilisant des lignées de souris LysM-Cre et ROR $\alpha$  foxée. Nos résultats montrent que l'inactivation de ROR $\alpha$  dans les macrophages n'a pas d'impact sur l'obésité et l'insuline-résistance induites par un régime riche en graisses (HFD). Étonnamment, contrairement à des travaux, notre étude ne montre pas d'effet sur le développement de la NASH ni suite à un régime HFD, ni dans le modèle d'alimentation défini par les acides aminés L, plus sévère et indépendant de l'obésité et déficient en choline. Nous avons donc soupçonné que le nombre de copies de LysM pouvait jouer un rôle dans cette divergence, car le génotype des souris au locus LysM est une différence majeure entre les deux études indépendantes. Les souris LysM-Cre portent une insertion de la recombinaison Cre dans le gène *Lyz2*, ce qui conduit à l'expression de *Cre* sous le contrôle du promoteur *Lyz2* et ses activateurs, mais abolit l'expression endogène de *Lyz2*. Alors que nous avons intentionnellement maintenu une expression similaire de *Cre* et de *Lyz2* entre WT et MKO en utilisant uniquement des animaux hémizygotés pour ce locus (en comparant *Rora*<sup>+/+</sup>*Lyz2*<sup>Cre/+</sup> avec *Rora*<sup>fl/fl</sup>*Lyz2*<sup>Cre/+</sup>), des souris foxées (*Rora*<sup>fl/fl</sup>*Lyz2*<sup>+/+</sup>) ont été utilisées comme contrôle de WT et comparées avec des souris MKO pour lesquelles il manquait des informations sur le locus *Lyz2* (*Rora*<sup>fl/fl</sup>*Lyz2*<sup>Cre/?</sup>) dans l'étude antérieure. Aussi, nous avons émis l'hypothèse que l'impact observé de la délétion de ROR $\alpha$  dans les macrophages sur la NASH dans l'étude précédente ne résultait probablement pas d'un effet spécifique de la délétion de ROR $\alpha$ , mais plutôt d'un nombre de copies *Lyz2* différent entre les souris WT et MKO et avons décidé de vérifier cette hypothèse expérimentalement. De manière surprenante, nos résultats préliminaires ont montré que les souris déficientes en *Lyz2* présentent une légère protection, plutôt qu'un effet néfaste, dans l'obésité et l'IR induites par le HFD, comme le montre la diminution du poids corporel et des masses de tissu adipeux, l'amélioration significative du contrôle de la glycémie et la diminution de l'inflammation de l'épiAT. Il est intéressant de noter que la déficience totale en *Lyz2* n'a eu aucun impact sur la stéatose hépatique (NAFL) chez les souris nourries au HFD. Néanmoins, nos résultats préliminaires suggèrent même que la carence en *Lyz2* pourrait protéger contre la NASH induite par le régime alimentaire, carence en choline. Dans leur ensemble, ces résultats préliminaires indiquent que le nombre différent de copies du gène *Lyz2* chez les souris de contrôle n'explique probablement pas la différence entre notre travail et l'étude précédente. Globalement, nos résultats montrent que la délétion de ROR $\alpha$  dans les macrophages ne modifie pas le développement de l'obésité et de l'IR et remettent en question son rôle dans la NASH. D'autre part, nous pensons que des recherches plus approfondies sur le rôle du lysozyme présentent un intérêt significatif dans le contexte de l'obésité, de l'IR et de la NASH avancée, car *Lyz2* pourrait avoir un intérêt thérapeutique.

## ACKNOWLEDGMENTS

First of all, I am thankful to my thesis advisor Dr. David DOMBROWICZ for the opportunity to welcome me in his team at unit 1011, designing the project and for his supportive as well as tolerant mentoring during those years.

Secondly, I am grateful to Dr. Laurent L'HOMME for his day-to-day supervision as a post-doctoral fellow, which I gained a bunch of experiences from him. I can't thank you enough for the contribution you have been made to this work experimentally and intellectually as well as your effort to help me in administrative procedures. I also appreciated the scientific and non-scientific conversations we had that help me to understand general Belgian, and French culture, especially the culture of the beers. I am so glad to support the "Belgian Red Devils" with you in the World Cup 2018 against all our French colleagues. What would I do without a bench and project partner like you! Thank you for making the lab such a great place to work every day, literally every day, including almost all the weekends and holidays, with the support of a sheer volume of coffee and the Monster energy drink! Thank you for being a kind, supportive, friendly, and extremely organized role model for me.

I want to declare my appreciation to Prof. Dr. Bart STAELS for the high-level scientific meetings, discussions, and all the helpful advices, which are always making a huge difference in our work.

I am also thankful to the jury members of the international Ph.D. students fellowship competition (2017-2018) for deem me worthy of this fellowship and to the École Doctorale Biologie et Santé de Lille (EDBSL, 446) for funding me as a Ph.D. student.

I want to acknowledge my Ph.D. thesis follow-up committee members Prof. Dr. Jean MARIANI and Dr. Stoyan IVANOV for improving the quality of the thesis and scientific discussions. Importantly, I am much obliged to Dr. Stoyan IVANOV for his support for me to initiate the LysM project.

Importantly, I am very grateful to all the people of unit 1011 for their understanding of how bad I am at speaking in French and their effort to communicate with me in English. Besides, I appreciate their positive attitude and good-humor that constitutes an excellent atmosphere to work in it. I am grateful to have the opportunity to be part of this unit.

I am thankful to Barbara GROSS and Christian DUHEM for their effort in the generation of macrophage-specific ROR $\alpha$ -deficient mice. Also, I want to thank Olivier MOLENDI-COSTE for the obtained preliminary data from those mice, for cell sorting experiments, and for together with Sandrine QUEMENER to take care of the ROR mice breeding. I am also grateful to Marie-Laure JOSEPH for the genotyping of our mice. Besides, I want to thank Sandrine QUEMENER, Sébastien FLEURY, and Laurent PINEAU for their technical supports during sacrifices. I am much obliged to Sébastien FLEURY for his assistance in our histology applications. I appreciate Mathilde LE MAITRE for the technical supports of her. Last but not least, I want to express my gratitude to Emmanuelle VALLEZ and Anne TAILLEUX for their support in the biochemical analysis by KONELAB.

It was a great pleasure to do some qPCR, RT, RNA extraction, or western blot at the same time as Christian DUHEM that he always made it very entertaining thanks to his sincere personality. I will never forget how much I enjoyed it, in particular when I got very nice results, while he failed. Thank you for being such a magnificent, high-minded person.

Special thanks to Bruno DERUDAS for providing me qPCR, RT-PCR, and Trizol reagents that I spent like water when I needed it.

Apart from their technical support, I am pleased to meet a lot of people from the unit, and I am deeply honored to get to know them.

It was always a happiness to share a glass or bottle of wine and/or beer with Marion GIMENEZ outside of the lab. Thank you for being such a good friend to me and making my first Christmas in France unforgettable.

I am so much thankful to other Ph.D. candidates Audrey DEPRINCE, Marine ANDRES, Quentin THROEL, Valentine GUINOT, Cécilia BELLENGIER, and the other members of the unit that includes Artemii NIKITIN, Denis MOGILENKO, Marion GIMENEZ, Justine BEAUCHAMP, Lise FERRI, Stephan DELHAYE, Yasmin SEBTI, Benoit POURCET, Alicia MAYEUF-LOUCHART, Laurent L'HOMME, Emilie DORCHIES, Nathalie HENNUYER, Joel HAAS, and Delphine EBERLE for the laughs we had together, for the time we spent together outside of the lab.

Many thanks to the members of the coffee, and the Monster breaks Laurent L'HOMME, Sébastien FLEURY, and Emilie DORCHIES for the highly enjoyable short but long enough to get some "fresh air" times.

I want to thank Corinne COPIN and Jacques FRAMAUX for playing the role of the bad cop in the lab to maintain the order, specifically, to Corinne for her "gentle" reminders to the mutual tasks.

Special thanks to Marie-Hélène DERUDAS and Rosamée JAFEU first for their patience with me about French and secondly for their help in administrative works.

I want to express my gratitude to François DECLORIX from the École Doctorale Biologie et Santé de Lille (EDBSL, 446) for his incessant and effective supports in administrative acts throughout my Ph.D..

During those years, I crossed paths with many special people outside the lab, few in France, mostly from Belgium who supported me and reminded me that there is a life next to science, which needs to be lived! My friends, I want to deeply thank you for making me feel part of the big Belgian family.

I have a tremendous appreciation, which is inexpressible to my real friends from Turkey, Gülizar AYDOĞDU, Kubra KUCUKER, Nuray GULEC, who stayed in contact with me during those years and supported me psychologically against all the trials and tribulations.

The next one goes to my family. Canım annem üç sene içerisinde sadece iki kere Türkiye'ye gelebildiğim ve her birinde ikişer hafta kalabildiğim, özetle üç yılda bir ay yanında olabildiğim için çok üzgünüm. Doğduğun ülkenin dışında, dilini bilmediğin, ailenden, arkadaşlarından, sevdiklerinden uzakta üç yıl geçirmenin bana kazandırdığı iş anlamındaki büyük tecrübelerin yanı sıra, hayatla ilgili de birçok öğretisi oldu. Ben ileride başarılı bir bilim insanı olabilmek için burada neredeyse 7/24 çalışırken hayatın da bir yandan akıp gittiği ve beni beklemediği gerçeğiyle ne yazık ki pamuk prensesim canım anneannemi son bir kez görmeden kaybederek, biricik annişkolatam senin ciddi bir medikal operasyonunda ve canım abişkolatam senin eşinden ayrıldığı dönemde yanınızda size destek olmak için bulunamayarak öğrenmiş oldum. Güçlü olup bana ihtiyacınız olduğu halde ben üzülmeiyim, etkilenmeiyim, işlerim aksamasın diye bana tek bir şey yansıtmayan canım annem Gülseren DEMIRBILEK ve abim HILMI ALP SERMIKLI'ye olan vefa borcumu asla ödeyemem. Bir tanecik güzeller güzeli canım annem sen benim bu hayattaki tek gerçek dostumsun. Bu kadar mükemmel bir anne olduğun için en önemlisi dostum olabilen bir anne olduğun için sana çok ama çok minnettarım. Canım abim sana da harika bir abi olduğun için ve benim yokluğumu anneme aratmayacak şekilde ona destek olduğun için ne kadar teşekkür etsem az. Sizleri çok ama çok seviyorum. İyi ki varsınız iyi ki benim ailemsiniz.

# TABLE OF CONTENTS

ABSTRACT .....	i
RÉSUMÉ .....	ii
ACKNOWLEDGMENTS .....	iii
LIST OF FIGURES .....	viii
LIST OF TABLES .....	viii
INTRODUCTION .....	1
1. OBESITY.....	1
1.1 Obesity and Type 2 Diabetes .....	2
a. Classification of diabetes and type 2 diabetes .....	2
b. Insulin Receptor Signaling .....	3
c. Classification of adipose tissue.....	4
d. Obesity and Type 2 Diabetes .....	6
1.2 Obesity, Metaflammation and Insulin Resistance .....	6
a. Crosstalk between white adipose tissue and resident immune cells in obesity .....	6
b. Mechanisms of insulin resistance .....	8
1.3 Role of Gut Microbiota in Obesity .....	10
1.4 Impact of Immune Cells on Health and Obesity in White Adipose Tissue.....	11
1.4.1 Immune cells at homeostasis in white adipose tissue .....	12
a. Monocytes .....	12
b. Macrophages .....	12
c. Dendritic cells .....	14
d. Eosinophils .....	15
e. Type 2 Innate Lymphoid Cells .....	16
f. CD4 <sup>+</sup> T cells.....	16
g. Regulatory T cells .....	17
h. $\gamma\delta$ T cells.....	17
i. Natural Killer T cells.....	18
j. B cells .....	18
1.4.2 Immune drivers of inflammation in obese white adipose tissue.....	19
a. Adipose tissue macrophages, recruited monocytes and macrophages.....	19
b. Dendritic cells.....	21
c. Neutrophils.....	21
d. Mast cells .....	23
e. Type 1 Innate Lymphoid Cells and Natural Killer Cells .....	23
f. Invariant Natural Killer T cells .....	24
g. CD4 <sup>+</sup> T cells .....	24
h. CD8 <sup>+</sup> T cells.....	25
i. B cells .....	25
2. NON-ALCOHOLIC FATTY LIVER DISEASES .....	26
2.1 Pathogenesis of obesity-dependent non-alcoholic fatty liver diseases .....	27
2.2 Pathogenesis of obesity-independent non-alcoholic fatty liver diseases .....	29
2.3 Role of gut microbiota in non-alcoholic fatty liver diseases .....	30
2.4 Impact of immune cells on health and non-alcoholic fatty liver diseases in Liver .....	33
2.4.1 Immune guardians of homeostasis in liver.....	35
a. Kupffer cells.....	35
b. Dendritic Cells .....	36
c. Natural Killer Cells .....	37
d. $\gamma\delta$ T cells.....	37
e. Invariant Natural Killer T cells .....	37
f. Mucosal-associated invariant T cells.....	38
g. Regulatory T cells .....	38
h. CD8 <sup>+</sup> Memory T cells .....	39
i. B cells .....	39
2.4.2 Immune drivers of inflammation in Non-Alcoholic Fatty Liver Diseases .....	39
a. Kupffer Cells, recruited monocytes, and macrophages .....	39

b.	Dendritic Cells .....	42
c.	Neutrophils .....	44
d.	Natural Killer Cells .....	44
e.	Natural Killer T cells .....	45
f.	CD4 <sup>+</sup> T cells .....	45
g.	CD8 <sup>+</sup> cytotoxic T cells .....	46
h.	B cells .....	47
3.	NUCLEAR RECEPTORS .....	47
3.1	<i>Structural and Functional Organization of the Nuclear Receptors</i> .....	49
3.2	Nuclear Receptor Signaling: Mechanism of Action .....	51
3.3	Retinoic Acid Receptor-related Orphan Receptors (RORs) .....	53
<b>SCOPE OF THE THESIS .....</b>		<b>61</b>
1.	IMPACT OF MACROPHAGE-SPECIFIC ROR $\alpha$ DELETION ON METABOLIC DISEASES .....	61
2.	IMPACT OF LYSOZYME M ( <i>Lyz2</i> ) DELETION ON METABOLIC DISEASES .....	61
3.	SATURATED FATTY ACIDS PROMOTE GROWTH DIFFERENTIATION FACTOR 15 (GDF-15) EXPRESSION IN MACROPHAGES THROUGH THE PERK/ELF2/CHOP SIGNALING PATHWAY. (THIS WORK WILL BE PRESENTED IN THE ANNEX). .....	61
<b>MATERIALS AND METHODS .....</b>		<b>62</b>
1.	GENERATION OF MACROPHAGE-SPECIFIC ROR $\alpha$ KNOCK OUT MICE .....	62
2.	MOUSE GENOTYPING .....	62
3.	MOUSE STUDIES .....	62
4.	INSULIN AND GLUCOSE TOLERANCE TESTS .....	63
5.	BONE MARROW-DERIVED MACROPHAGES .....	63
6.	CELL SORTING .....	64
7.	METABOLIC PARAMETERS .....	65
8.	MEASUREMENT OF LIVER TRIGLYCERIDES .....	65
9.	HISTOLOGY .....	65
10.	RT-QPCR .....	66
11.	WESTERN BLOTTING .....	66
12.	STATISTICAL ANALYSES .....	66
<b>RESULTS .....</b>		<b>70</b>
1.	IMPACT OF MACROPHAGE-SPECIFIC ROR $\alpha$ DELETION ON HFD-INDUCED OBESITY, IR, NAFL AND OBESITY-INDEPENDENT NASH DEVELOPMENT .....	70
A.	Generation and characterization of the macrophage-specific ROR $\alpha$ -deficient mice .....	70
B.	ROR $\alpha$ deletion in macrophages does not affect LPS-induced inflammation <i>in vitro</i> .....	74
C.	ROR $\alpha$ deletion in macrophages does not affect obesity, IR nor hepatic steatosis .....	76
D.	ROR $\alpha$ deletion in macrophages does not affect NASH .....	83
E.	Effect of ROR $\alpha$ deletion in KC is offset by high ROR $\gamma$ expression .....	88
2.	GENE REGULATION BY ROR $\alpha$ IN ALVEOLAR MACROPHAGES .....	91
3.	IMPACT OF <i>Lyz2</i> DELETION ON HFD-INDUCED OBESITY, IR, NAFL AND OBESITY-INDEPENDENT NASH DEVELOPMENT ....	92
A.	Generation and validation of <i>Lyz2</i> -deficient mice .....	92
A.	<i>Lyz2</i> deficiency slightly protects against HFD-induced obesity and IR, however, has no impact on NAFL .....	93
B.	<i>Lyz2</i> deficiency might protects against obesity-independent NASH .....	97
<b>DISCUSSION AND PERSPECTIVES .....</b>		<b>99</b>
1.	IMPACT OF THE LYSM-CRE-MEDIATED MACROPHAGE-SPECIFIC ROR $\alpha$ DELETION ON METABOLIC DISEASES .....	99
2.	GENE REGULATION BY ROR $\alpha$ IN ALVEOLAR MACROPHAGES .....	101
3.	IMPACT OF <i>Lyz2</i> DEFICIENCY ON METABOLIC DISEASES .....	103
<b>REFERENCES .....</b>		<b>107</b>
<b>ANNEXES .....</b>		<b>165</b>

## LIST OF FIGURES

FIGURE 1: IMPAIRED ENERGY BALANCE IN OBESITY. ....	1
FIGURE 2: INSULIN'S ACTION IN METABOLIC TISSUES AND INSULIN SIGNALING PATHWAY.....	3
FIGURE 3: COMPARISON BETWEEN HUMAN AND RODENT WHITE ADIPOSE TISSUE (WAT) DEPOTS. ....	5
FIGURE 4: WAT-RESIDENT IMMUNE CELLS IN LEAN AND OBESE INDIVIDUALS. ....	7
FIGURE 5:INSULIN SIGNALING PATHWAY IN INSULIN RESISTANCE. ....	8
FIGURE 6: SIGNALING CROSSTALK IN HEALTHY AND OBESE WAT BY IMMUNE CELLS. ....	11
FIGURE 7: WAT-LIVER CROSSTALK IN THE PATHOGENESIS OF OBESITY-DEPENDENT NAFLD. ....	28
FIGURE 8: OVERVIEW OF THE NAFLD PATHOGENESIS.....	32
FIGURE 9: HEPATIC IMMUNE AND STROMAL CELLS.....	33
FIGURE 10: CROSSTALK BETWEEN HEPATIC STROMAL AND IMMUNE CELLS IN NAFLD. ....	34
FIGURE 11: SCHEMATIC REPRESENTATION OF THE NUCLEAR RECEPTOR DOMAIN ORGANIZATION, OLIGOMERIC COMPLEXES OF THE NUCLEAR RECEPTORS AND DNA RESPONSE ELEMEN REPERTOIRES. ....	50
FIGURE 12: SCHEMATIC OF THE NUCLEAR RECEPTOR SIGNALING MECHANISMS.....	52
FIGURE 13: MODULATION OF THE GENE EXPRESSION BY NUCLEAR RECEPTORS. ....	53
FIGURE 14: SCHEMATIC REPRESENTATION OF THE ROR FAMILY MEMBERS.....	54
FIGURE 15: REGULATION OF THE CIRCADIAN RHYTHM AT MOLECULAR LEVEL.....	56

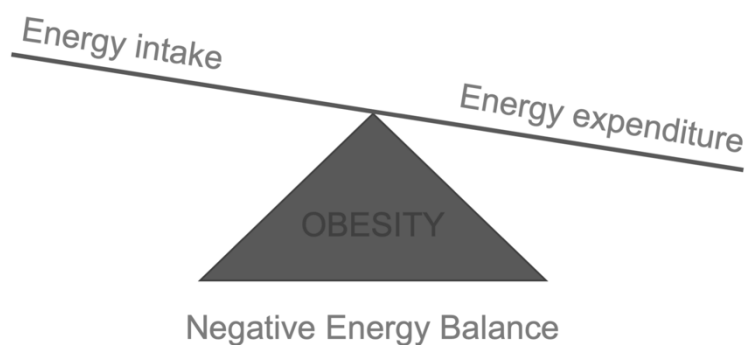
## LIST OF TABLES

TABLE 1: CLASSIFICATION OF THE DIABETES.....	2
TABLE 2: CRITERIA FOR THE DIAGNOSIS OF DIABETES. ....	2
TABLE 3: CLASSIFICATION OF HUMAN NUCLEAR RECEPTOR SUPER FAMILY. ....	48
TABLE 4: LIST OF THE PRIMERS USED IN MOUSE GENOTYPE AND qPCR.....	68
TABLE 5: LIST OF THE ANTIBODIES USED IN CELL SORTING. ....	69
SUPPLEMENTARY TABLE 1: LIST OF THE MODULATED GENES FROM MICROARRAYS PERFORMED ON ALVEOLAR MACROPHAGES .....	172

# INTRODUCTION

## 1. OBESITY

Obesity is a medical condition characterized by redundant fat accumulation in the body, arising from genetic factors, excessive dietary intake, and sedentary lifestyle (Figure 1). The widely used method to quantify obesity is body mass index (BMI) calculated by dividing the individual's body weight to the individual's height ( $\text{kg}/\text{m}^2$ ). According to the World Health Organization (WHO), the BMI value over 25 is considered as overweight, and over 30 as obesity in adults <sup>1</sup>. The prevalence of obesity nearly tripled since 1975 worldwide. The latest available data reveal that almost 2 billion world adult population is overweight (39%) among them, 650 million are obese (13%). Furthermore, 340 million children and adolescents aged between 5 and 19 were overweight or obese (10%) in 2016 <sup>2</sup>. Obesity is strongly associated with Type 2 Diabetes (T2D), Non-alcoholic Fatty Liver Diseases (NAFLD), and Cardio Vascular Diseases (CVD) <sup>3</sup>. Consequently, overweight and obesity are the 5<sup>th</sup> leading risk factor for global mortality in the 21<sup>st</sup> century <sup>4</sup>. Mutation in some key genes that regulate appetite leads to a monogenic form of obesity, including leptin (*LEP*), leptin receptor (*LEPR*), melanocortin 4 receptor (*MC4R*), pro-opiomelanocortin (*POMC*), and fat mass and obesity associated gene (*FTO*), which are extremely rare <sup>5</sup>. Nonetheless, heredity only cannot explain the global increase in the prevalence of obesity over the past decades. Thus, it is essential to identify underlying mechanisms involved in the pathogenesis to identify new therapeutic targets against obesity and associated complications.



**Figure 1:** Impaired energy balance in obesity. Negative energy balance in obesity arising from genetic factors, high calorie intake and sedentary lifestyle. Management of the energy balance one of the best strategies to prevent obesity and associated complications.

## 1.1 Obesity and Type 2 Diabetes

### a. Classification of diabetes and type 2 diabetes

<b>Table 1: Classification of the diabetes</b>
I. Type 1 Diabetes (T1D)
II. Type 2 Diabetes (T2D)
III. Gestational Diabetes
IV. Other Diabetes
A. Genetic defects of $\beta$ -cell MODY1 (OMIM # 125850) MODY2 (OMIM # 125851)
B. Genetic defects in insulin action Leprechaunism (OMIM # 246200) Rabson-Mendenhall syndrome (OMIM # 262190)
C. Diseases of the exocrine pancreas Pancreatitis Cystic fibrosis
D. Endocrinopathies Acromegaly Cushing's syndrome
E. Drug- or chemical-induced diabetes Glucocorticoids

*Adapted from American Diabetes Association, 2019<sup>6</sup>*

Diabetes is a cluster of diseases as characterized by increased blood glucose levels resulting from either the defects in insulin secretion, and/or resistance to insulin's action (Table 1). Diagnosis of the diabetes depends on either, the fasting plasma glucose (FPG) value or the 2h-plasma glucose (2-h PG) levels through the oral glucose tolerance test (OGTT), and glycated hemoglobin (HbA1C) criteria (Table 2). Obesity is closely associated with type 2 diabetes (T2D), which is characterized by hyperglycemia and hyperinsulinemia. Overall, 85 % of individuals developing T2D are overweight or obese <sup>7</sup>. The global prevalence of the

T2D in adults was 8.5% (422 million) in 2014 <sup>8</sup>. T2D is the most frequent type of diabetes accounting for 90-95 % of all types of diabetes worldwide. Individuals with T2D exhibit peripheral insulin resistance in spite of normal insulin secretion, which means cells cannot respond to insulin accurately <sup>6</sup>. As a result of T2D, insulin resistance occurs at adipose tissue, liver, and skeletal muscle, which is triggered by multiple mechanisms, including genetic factors, lipotoxicity, inflammation, endoplasmic reticulum (ER) stress, mitochondrial dysfunction, and reactive oxygen species (ROS) production <sup>9</sup>.

<b>Table:2 Criteria for the diagnosis of diabetes</b>
FPG $\geq$ 126 mg/dL (7.0 mmol/L). Fasting is defined as no caloric intake for at least 8 h.
2-h PG $\geq$ 200 mg/dL (11.1 mmol/L) during the OGTT. The test should be performed as described by the WHO.
HbA1C $\geq$ 6.5% (48 mmol/mol) The test should be performed in a laboratory using a method that is NGSP certified and standardized to the DCCT assay.
In a patient with classic symptoms of hyperglycemia or hyperglycemic crisis, a random plasma glucose $\geq$ 200 mg/dL (11.1 mmol/L).

NGSP: National Glycohemoglobin Standardization Program. DCCT: Diabetes Control and Complications Trial. WHO: World Health Organization *Adapted from American Diabetes Association, 2019<sup>6</sup>*.

## b. Insulin Receptor Signaling

Insulin is secreted from the pancreatic beta cells in parallel with the increased blood glucose levels after a meal. Insulin is an anabolic hormone that regulates glucose, lipid, and protein metabolism through the insulin receptor signaling pathway in adipose tissue, liver, and skeletal muscle (Figure 2A). The insulin receptor (IR) is a hetero-tetrameric receptor with tyrosine kinase activity that comprises of two extracellular  $\alpha$  subunits and two transmembrane  $\beta$  subunits that are linked by disulfide bonds (Figure 2B). Insulin binds to the extracellular  $\alpha$ -subunits of the IR in the target tissue that include adipose tissue, liver, and skeletal muscle, stimulating tyrosine kinase activity. Tyrosine phosphorylation leads to the recruitment of the downstream members of insulin receptor substrate family (IRS, referred to as IRS-1 through IRS-6). This results in recruitment and activation of the phosphoinositide-3-kinase (PI3K), which rapidly phosphorylates phosphatidylinositol-4,5-biphosphate (PIP<sub>2</sub>) to generate second lipid messenger phosphatidylinositol-3,4,5-triphosphate (PIP<sub>3</sub>) on the plasma membrane, that activate and translocate the cytosolic serine/threonine kinase AKT, also known as the protein kinase B (PKB) to the plasma membrane, triggering glucose import into the adipose tissue and skeletal muscle or liver by Glucose Transporter Type 4 (GLUT4) or GLUT2, respectively <sup>10</sup>.

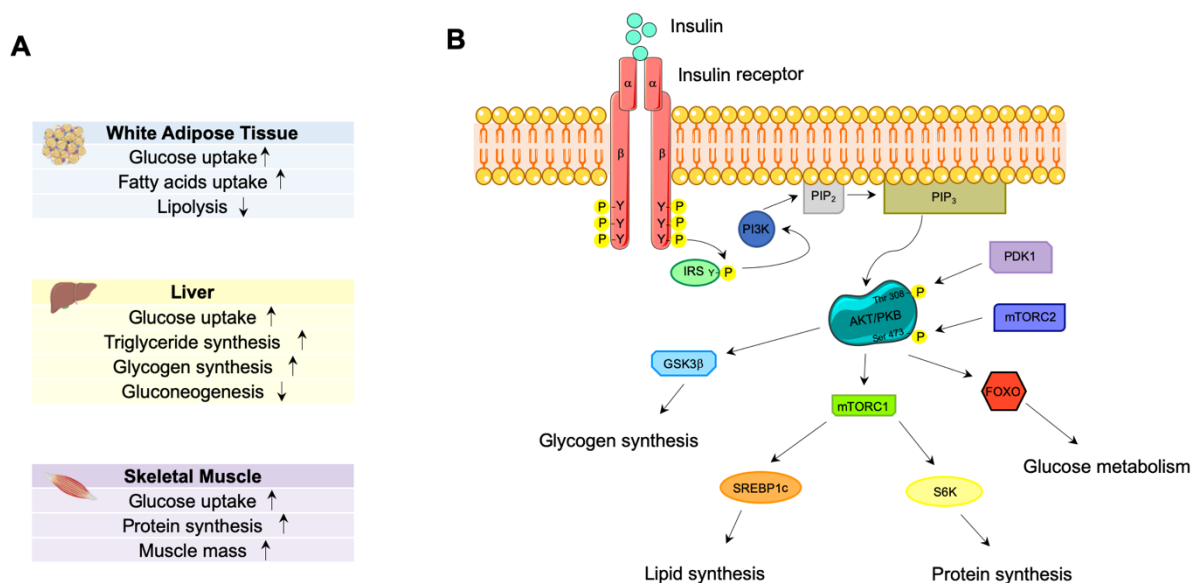


**Figure 2:** Insulin's action and Insulin Signaling Pathway. **(A)** Insulin's action on the white adipose tissue, liver, and skeletal muscle metabolism. **(B)** The insulin receptor signaling pathway. IRS, Insulin receptor substrate; PI3K, Phosphoinositide 3-kinase; PIP<sub>2</sub>, Phosphatidylinositol-4,5-bisphosphate; PIP<sub>3</sub>, Phosphatidylinositol-3,4,5-triphosphate; AKT/PKB, Protein kinase B; PDK1, Phosphoinositide-dependent kinase 1; mTORC1, mammalian target of rapamycin complex 1; mTORC2, mammalian

target of rapamycin complex 2; FOXO, Forkhead family box O; GSK3 $\beta$ , Glycogen synthase kinase 3 beta; SREBP1c, Sterol regulatory element-binding protein 1; S6K, Ribosomal protein S6 kinase.

Besides mediation of the glucose uptake by glucose transporters, the AKT/PKB is considered as a central regulator of the insulin's distal actions, such as glycogen synthesis by the glycogen synthase kinase three beta (GSK3 $\beta$ ), protein and lipid synthesis by mammalian target of rapamycin (mTOR), glucose metabolism by forkhead family box O (FOXO) <sup>11</sup>. So far, three AKT isoforms identified in mammalian, which are AKT1 (PKB $\alpha$ ), AKT2 (PKB $\beta$ ), and AKT3 (PKB $\gamma$ ). The AKTs possess two key phosphorylation residues to ensure stabilization and become activated, which is the first one a threonine residue (Thr) on the catalytic domain, and the second one is a serine (Ser) residue in the regulatory region of the carboxy-terminal <sup>12</sup>. Regarding this, the phosphoinositide-dependent kinase one (PDK1) phosphorylates AKT1 at the Thr-308 residue afterward, the mammalian target of rapamycin complex two (mTORC2) phosphorylates the Ser-473 residue <sup>13, 14</sup>. Following this, successive phosphorylations also occurs on the corresponding residues of the AKT2 (Thr-309 and Ser-474) and the AKT3 (Thr-305 and Ser-472) <sup>15</sup>. It has been reported that activated AKTs be able to phosphorylates several protein substrates with diverse subcellular localizations <sup>16</sup>.

Some rare forms of severe insulin resistance have been associated with mutations in the insulin receptor gene, which are leprechaunism, Rabson-Mendenhall syndrome, or the type-A syndrome. Patients with these syndromes have non-sense or missense mutations in the extracellular ligand binding domain ( $\alpha$  subunits) or intracellular tyrosine kinase domain ( $\beta$  subunits) of the insulin receptor that hampers insulin signaling pathway <sup>17, 18</sup>. One of the common polymorphisms is the G972R polymorphism of IRS-1 observed in patients with T2D, leading to decreased insulin signaling through impaired PI3K activity <sup>19, 20</sup>. Even though it slightly affects the insulin signaling, the M326I polymorphism in the p85 $\alpha$  regulatory subunit of the PI3K has been identified as a risk factor for T2D occurrence <sup>21, 22</sup>. Furthermore, in diabetic patients, a rare missense mutation, which is the R274H in AKT2 has been reported, ruining the kinase activity <sup>23</sup>.

### c. Classification of adipose tissue

Adipose tissue is classified on the basis of the major cell type component. White adipose tissue (WAT), which is predominantly composed of large, adipocytes with unilocular lipid droplets and represents the majority of the lipid mass as an energy storage. Brown adipose tissue (BAT) and beige/brite adipose tissue, which is mainly consist of cells with multilocular lipid droplets

and abundant mitochondria that perform thermogenesis via uncoupled mitochondrial respiration, in response to cold or adrenergic stimulation <sup>24</sup>. The majority of the WAT is categorized as either visceral (VAT) or subcutaneous (SAT) adipose tissue. VAT depots includes, surroundings of the epicardial/pericardial area and intra-abdominal organs, like mesenteric, omental, perigonadal, perirenal, and retroperitoneal in both humans and rodents. The main difference between humans and rodents VAT depots is that large omental VAT exist in humans and rather large perigonadal VAT, also known as epididymal WAT (eWAT) is found in rodents (Figure 3). SAT is subdivided into upper (abdominal) and lower (gluteal and femoral) depots in humans, which corresponds to anterior and posterior depots, so-called inguinal WAT (ingWAT) in rodents <sup>25</sup>.

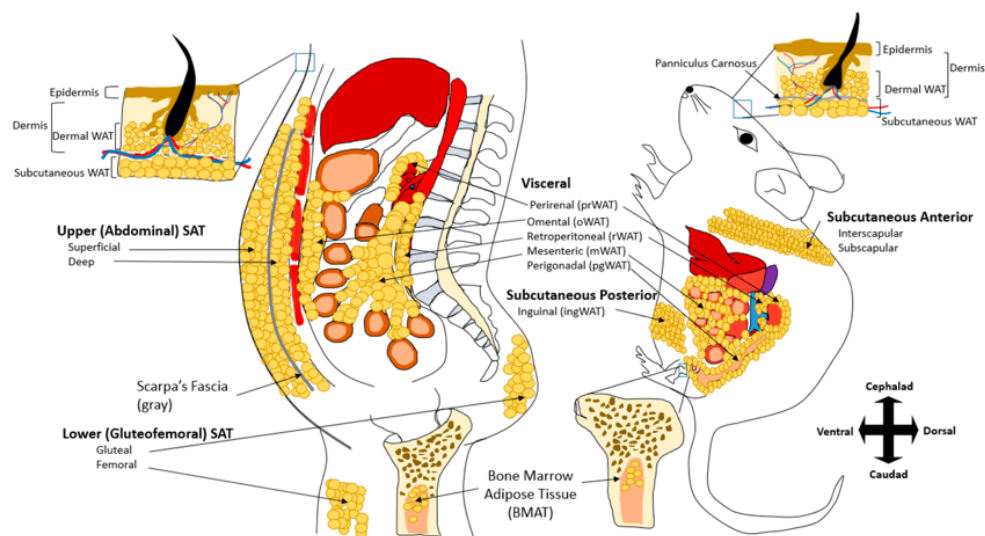


**Figure 3:** Comparison between human and rodent white adipose tissue depots. White Adipose Tissues (WAT) are mostly visceral adipose tissue (VAT) and subcutaneous adipose tissue (SAT). Major visceral depots common in both humans and rodents include epicardial/pericardial (not shown), perirenal (prWAT), retroperitoneal (rWAT), and mesenteric WAT (mWAT). While humans have large omental (oWAT) fat, mice have large perigonadal (pgWAT) fat. SAT in humans can be divided into upper (abdominal) and lower (gluteofemoral). Abdominal fat in human can be further divided into superficial and deep, which are separated anatomically by Scarpa's Fascia. In mice, SAT is divided into anterior and posterior. Dermal WAT (dWAT) is another fat depot that exists in both humans and mice. dWAT is located in the dermis and above the SAT (note: this separation is visible by the presence of striated muscular layer known as panniculus carnosus only found in mice). Bone marrow adipose tissue (BMAT or MAT) is also another adipose depot common in both species. Cephalad and caudad are also referred to as anterior and posterior in mice, respectively <sup>25</sup>.

#### d. Obesity and Type 2 Diabetes

T2D is known to be related to visceral adiposity. Risk of the T2D can be determined by waist circumference (WC) and waist to hip ratio (WHR) measurements. Thus, if the waist circumference in male equal or more than 102 centimeters, whereas in female equal or more than 88 centimeters, individuals are classified as at high risk. Moreover, the waist / hip ratio should not exceed 1 in men and 0.8 in women <sup>26</sup>. Indeed, in some rare cases, like T2D patients who are not overweight or obese have an increased proportion of body fat distribution mainly, in the visceral depots rather than subcutaneous <sup>27</sup>. Interestingly, it has been shown that fat accumulation in the subcutaneous depots rather than visceral depots has a beneficial effect against obesity and associated complications, which is known as metabolically healthy obesity <sup>28</sup>. Notably, SAT transplantation into VAT improve glucose homeostasis, attenuate body weight, and total fat mass in rodents, implying different effects of the SAT and VAT depots on metabolism rather than anatomical position that needs further investigations to clarify by which mechanism/s <sup>29, 30</sup>. Recently, distinct type of WAT depots comprising the dermal WAT (DAT), and bone marrow adipose tissue (MAT) have been reported <sup>31, 32</sup>. It has been shown that DAT is important for hair development, wound healing, and pathogen resistance <sup>33</sup>. On the other hand, MAT consist of two subtypes constitutive MAT (cMAT), located in distal skeletal bones, and regulated MAT (rMAT) found in proximal/skeletal regions that is controlled by local osteoporotic factors, depending on bone metabolism and osteoblastic activity <sup>34</sup>. Ambrosi et al. suggested that adipocyte accumulation in the bone marrow during obesity and aging impairs stem cell-based hematopoietic and bone regeneration <sup>35</sup>.

### 1.2 Obesity, Metaflammation and Insulin Resistance

#### a. Crosstalk between white adipose tissue and resident immune cells in obesity

WAT is not only storing energy but is also, known as an endocrine organ, that regulates both glucose and lipid metabolism by secreting adipokines. Adipokines, comprises of hormones (leptin, adiponectin, resistin, visfatin etc.) and cytokines (TNF $\alpha$ , IL-1 $\beta$ , IL-6, IL-8, IL10, TGF $\beta$  etc.) that possesses autocrine and paracrine properties <sup>36</sup>. For this reason, to be under control, WAT contain several immune cell types within its stromal vascular fraction. Lean and obese WAT immune compartment differ considerably regarding the number and cell type composition (Figure 4), which we will further discuss in detail (see section 1.4).

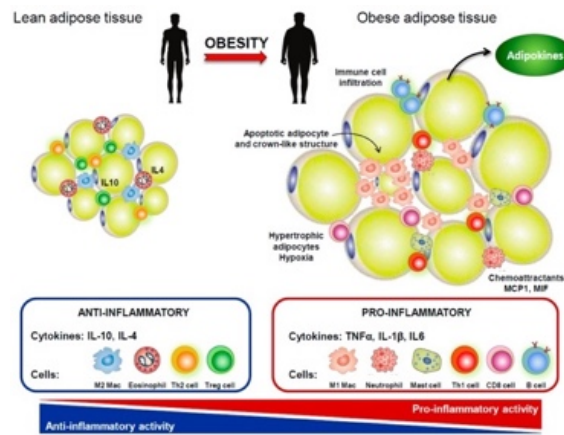


**Figure 4:** WAT- resident immune cells in lean and obese individuals. In lean adipose tissue, the cross-talk between adipocytes and resident immune cells maintains tissue homeostasis that include M2-like macrophages, eosinophils,  $T_{reg}$ s,  $T_H2$  cells (see section 1.4). Obesity leads to the expansion of WAT, resulting secretion of chemoattractants and infiltration of pro-inflammatory immune cells (see section 1.4). Therefore, dysregulated production of adipokines and pro-inflammatory cytokines, like  $TNF\alpha$ ,  $IL-1\beta$ , and  $IL-6$  contributes to the chronic low-grade inflammation <sup>37</sup>.

In the lean state, some specific subsets of WAT-resident immune cells (see section 1.4) restrict inflammation and insure tissue homeostasis via immuno-regulatory cytokine production <sup>38, 39</sup>. In obesity, WAT expands through hypertrophy, due to the lipid accumulation and to some extent, through hyperplasia, due to proliferation and differentiation of the preadipocytes, leading to extracellular matrix disposition <sup>40</sup>. Obese WAT, secrete increased amount of adipokines that includes several inflammatory mediators, like leptin, MCP-1, RANTES,  $TNF\alpha$ ,  $IL-6$ ,  $IL-1\beta$ , promoting infiltration of the pro-inflammatory immune cells (see section 1.4). Consequently, pro-inflammatory immune cells become predominant within the WAT and leads to chronic, low-grade inflammation also, known as *metaflammation*, as a result, WAT became dysfunctional <sup>41</sup>. Dysfunctional WAT will overproduce and secrete FFAs into the circulation due to the uncontrolled lipolysis <sup>42</sup>. Recently, has been shown that WAT-resident immune cells fundamental mediators of the healthy expansion and tissue remodeling during weight gain <sup>43</sup>. However, in advanced obesity, adipocytes are no longer being able to expand and undergo a necrosis process due to the decreased oxygen tension <sup>44</sup>. Pro-inflammatory macrophages are recruited around dead cells and form a crown-like structure, supporting NLRP3 inflammasome activation <sup>45</sup>. Excessive triglycerides and FFAs, which are released by WAT and stored in ectopic tissues, such as liver, heart, pancreas, and kidneys, yielding to lipotoxicity, further contributing to the pro-inflammatory milieu <sup>46</sup>. Another sign of lipotoxicity is that increased production of lipid intermediates, like diacylglycerol, ceramide, and fatty acyl-coenzyme A negatively regulates insulin signaling pathway, as we will discuss in the following section <sup>47</sup>.

## b. Mechanisms of insulin resistance

Pro-inflammatory cytokines, such as  $\text{TNF}\alpha$ ,  $\text{IL-1}\beta$ ,  $\text{IL-6}$ , ER stress, and FFAs activate the c-Jun N-terminal kinase (JNK) and the inhibitor of nuclear  $\kappa$ -B kinase subunit beta ( $\text{IKK}\beta$ ) serine/threonine (Ser/Thr) stress kinases<sup>48, 49</sup>. Activation of the JNK and  $\text{IKK}\beta$ , impairs insulin receptor signal transduction by phosphorylation of IRS-1 on inhibitory serine instead of stimulatory tyrosine residues consequently, represses P13K/AKT signal transduction (Figure 5).  $\text{IKK}\beta$  also activates the nuclear factor  $\kappa$  light chain enhancer of activated B cells (NF- $\kappa$ B) and translocate to the nucleus where promotes transcription of inflammatory genes that directly influences insulin signaling<sup>50</sup>. The key negative regulator of insulin and leptin sensitivity, protein tyrosine phosphatase 1B (PTP1B) has been shown to be upregulated by NF- $\kappa$ B in the adipose tissue and liver<sup>51</sup>. Moreover, saturated fatty acids induce ceramide biosynthesis that interfere with the insulin signaling via toll-like receptor 4 (TLR4) and NF- $\kappa$ B signaling<sup>52</sup>.

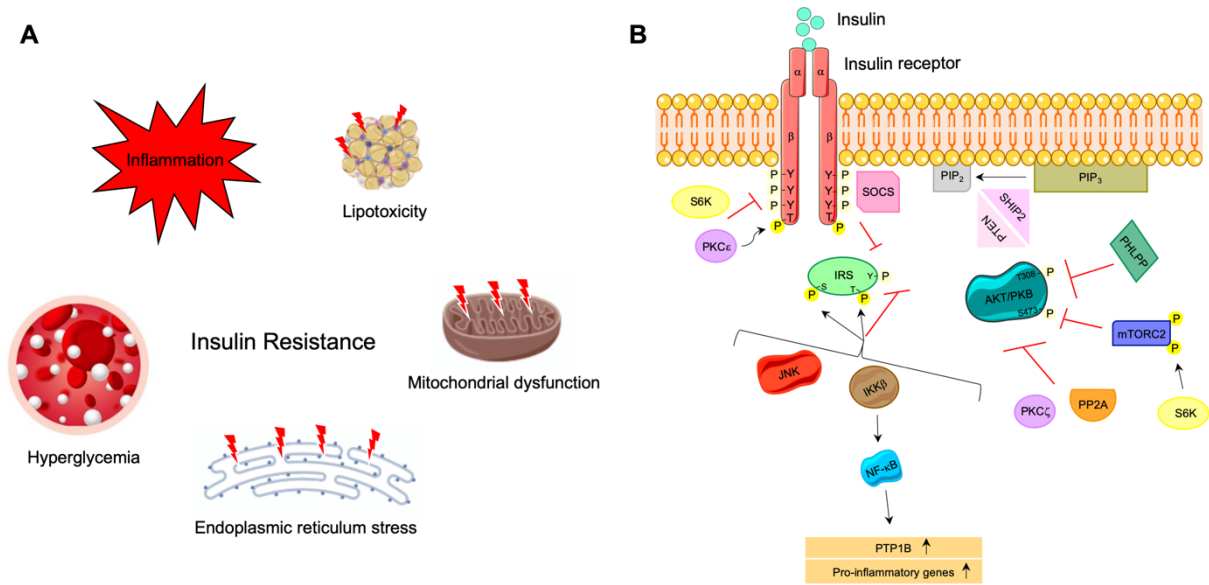


**Figure 5:** Insulin Signaling Pathway in insulin resistance. **(A)** Underlying mechanisms of the insulin resistance. **(B)** Representative suppressors of the insulin signaling pathway that causing insulin resistance. IRS: Insulin receptor substrate, PI3K: Phosphoinositide 3-kinase, PIP<sub>2</sub>: Phosphatidylinositol-4,5-bisphosphate, PIP<sub>3</sub>: Phosphatidylinositol-3,4,5-trisphosphate, PTEN: Phosphatase and tensin homolog, SHIP2: Src-homology 2-containing inositol phosphatase 2, PKC $\epsilon$ : protein kinase C epsilon, JNK: c-Jun N-terminal kinase,  $\text{IKK}\beta$ : inhibitor of nuclear kappa-B kinase subunit beta, AKT/PKB: Protein kinase B, mTORC2: mammalian target of rapamycin complex 2, S6K: Ribosomal protein S6 kinase, NF- $\kappa$ B: nuclear factor kappa light chain enhancer of activated B cells, PTP1B: protein tyrosine phosphatase 1B, PP2A: protein phosphatase 2A, PKC $\zeta$ : protein kinase C zeta, PHLPP: pleckstrin homology domain and leucine-rich repeat protein phosphatase.

The ribosomal protein S6 kinase (S6K) suppresses insulin signaling by phosphorylation of IRSs on multiple Ser/Thr domains<sup>53</sup>. Moreover, the pleckstrin homology domain and leucine-rich repeat protein phosphatase 1 and 2 (PHLPP1-2) family de-phosphorylates AKT and impairs Akt signaling<sup>54, 55</sup>. Likewise, S6K-mediated phosphorylation of mTORC2 components rictor and sin1 inhibits phosphorylation of AKT at Ser473 domain<sup>56, 57</sup>. Additionally, protein kinase C  $\epsilon$  (PKC $\epsilon$ ), which is activated via diacylglycerols, interfere insulin signaling by phosphorylating Thr1160 residue in the activation loop of the IR<sup>58</sup>. Similarly, activation of the protein kinase C  $\zeta$  (PKC $\zeta$ ) and protein phosphatase 2A (PP2A) by ceramides, alters membrane localization of the AKT consequently, abolishes AKT function<sup>59, 60</sup>.

Phosphatase and tensin homolog (PTEN) and Src-homology 2-containing inositol phosphatase 2 (SHIP2) are two significant lipid phosphatases that de-phosphorylate lipid messenger PIP3 thereby, attenuate insulin signaling transduction<sup>61</sup>. PTEN is a 3' phosphatase that turn PIP3 into its precursor PIP2 and disengage insulin signaling<sup>62</sup>. Moreover, studies showed that tissue-specific deletion of PTEN protects against insulin resistance and associated outcomes in the adipose tissue, liver and muscle<sup>63, 64, 65</sup>. SHIP2 is a 5' phosphatase which also converts PIP3 to PIP2 and has been shown to protects against obesity and insulin resistance<sup>66</sup>.

Growth factor receptor-bound proteins (GRBs), also known as insulin receptor-binding proteins (Grb-IRs) are pseudo-substrates of the IR kinase that has two essential domains. One of them is BPS (between PH and SH2) domains which binds to the substrate-binding slit of the IR. The second domain is an SH2 domain, which binds to the phosphorylated tyrosine residues on the IR. Mice deficient for GRB10 and GRB14, or both displayed better insulin sensitivity, underlying the biological importance of these proteins<sup>67, 68, 69</sup>. Furthermore, SNPs located inside or nearby *GRB10* gene have been associated with fasting hyperglycemia, and insulin resistance<sup>70</sup>. Similarly, SNPs proximate to the *GRB14* gene have been correlated with insulin resistance, adiposity, and body fat disruption<sup>70</sup>.

The Janus kinase/signal transducer and activator of transcription (JAK/STAT) pathway is a downstream mediator for various cytokines, growth factors, and hormones. Various receptors upon ligand binding, recruit cell-surface JAK proteins to their intracellular domains that lead to dimerization and activation through autophosphorylation. Thereafter, JAKs, phosphorylate and activate STAT proteins which result in dimerization and translocation to the nucleus where they regulate gene expression<sup>71</sup>. In mammals, four members of the JAK family (JAK1-3 and TYK2), and seven members of the STAT family (STAT1-4, STAT5A-B, and, STAT6) have been identified<sup>72</sup>. It has been shown that adipocyte-specific *Jak2*-deficient mice had impaired

lipolysis in response to insulin thereby, displaying insulin resistance, greater body weight and adiposity in basal conditions with ageing <sup>73</sup>. Furthermore, similar results have been reported for the adipocyte-specific *Stat3* and *Stat5*-deficient mice resulting in dysregulation of the lipolytic genes in WAT <sup>74, 75</sup>.

The suppressor of cytokine signaling (SOCS) is a family of proteins that regulate JAK/STAT pathway. Thus, modulating various biological processes, like immunity, apoptosis, cell proliferation and differentiation <sup>76</sup>. Four members of the SOCS (SOCS1, SOCS3, SOCS6, and SOCS7) family attenuate insulin signaling, via their SH2 domain that binds to phospho-tyrosine domain of the IR. A SOCS protein recruits a ubiquitin ligase to target IRS proteins for proteasomal degradation via SOCS box domain <sup>77</sup>. Among other SOCS, SOCS3 gained special attention since, its expression is increased in various tissues of obese animals <sup>78</sup>. Even though, SOCS3 is a key protein reducing the activity of the inflammatory cytokines that has been associated with various inflammatory diseases <sup>79</sup>, additional studies showed that SOCS3 modulates energy metabolism via dampening not only insulin but also leptin signaling in obesity, pregnancy, and refeeding period after fasting <sup>80, 81</sup>. Brain specific SOCS3-deficient mice displayed reduced weight gain, adiposity in high fat diet (HFD)-induced obesity model <sup>82</sup>. Importantly, SOCS3-deficient mice only in leptin receptor-expressing cells showed no differences either in weight gain, adiposity or food intake suggesting that the mechanism/s involved in prevent diet-induced obesity depends on specific neuron populations <sup>83</sup>.

### 1.3 Role of Gut Microbiota in Obesity

Depletion or alteration of gut microbiota is a prominent contributor to the development of the obesity and insulin resistance in both rodent models and humans <sup>84, 85, 86, 87</sup>. As primarily observed, the germ-free mice are protected from HFD-induced obesity and insulin resistance <sup>88</sup>, whereas fecal microbiota transplantation (FMT) from obese to germ-free mice triggers obesity and insulin resistance <sup>89</sup>. In line, FMT of the lean donors to obese patients improves insulin sensitivity <sup>90, 91</sup>. Similarly, dyslipidemia, insulin resistance, and inflammation has been associated with low bacterial diversity, determined by low microbial gene count in fecal DNA <sup>92</sup>. Correlatively, it has been shown that compensation of the bacterial richness with dietary intervention in individuals with low microbial gene count lead to improved metabolic outcomes <sup>93</sup>. In obesity, dysbiosis is associated with increased intestinal permeability due to the reduced expression of epithelial tight junction proteins, causing to leakage of bacteria or bacterial products, like inflammatory lipopolysaccharide (LPS), across the intestinal barrier that triggers intestinal immune system <sup>94</sup>. Eventually, systemic circulation of the bacterial products has been

reported in peripheral tissues, such as WAT, contributing to the pro-inflammatory milieu in obesity<sup>95, 96, 97</sup>.

#### 1.4 Impact of Immune Cells on Health and Obesity in White Adipose Tissue

As described above, crosstalk between WAT and immune cells is the critical process in the pathophysiology of obesity. Healthy AT harbors type 2 immune cells and communicate with each other via the production of type 2 cytokines that contribute to protective and regulatory response at homeostasis (see below). In contrast, obese AT mostly contains proinflammatory type 1 and 17 immune cells that produces type 1 and type 17 cytokines (Figure 6).

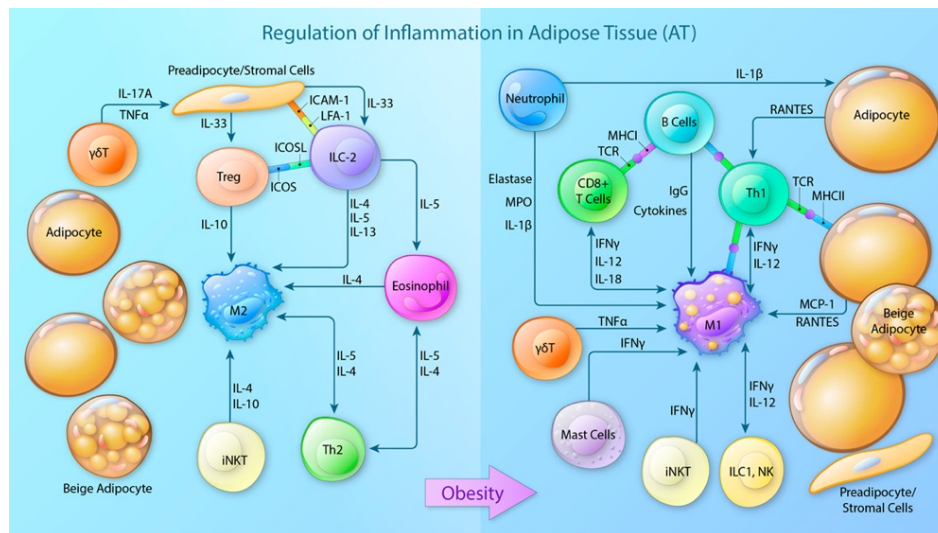


**Figure 6:** Signaling crosstalk in healthy and obese WAT by immune cells. In lean conditions (left part), AT-resident type 2 immune cells insure tissue homeostasis by secreting type 2 cytokines.  $\gamma\delta T$  cells by immune modulator IL17A and  $TNF\alpha$  secretion stimulate preadipocytes/stromal cells to produce IL-33, which activates  $T_{regs}$  and ILC-2. Preadipocytes/stromal cells and ILC-2 directly interact with each other by ICAM-1 and LFA-1, similarly  $T_{regs}$  and ILC-2 interact via ICOS and ICOSL. In turn,  $T_{regs}$  secrete IL-10 and ILC-2 cells IL-4, and IL-13 to support M2-like phenotype of ATM and IL-5 to induce eosinophils. Eosinophils also contribute to IL-4 secretion, supporting M2-like phenotype for ATM. iNKT cells also produce IL-4 and IL-10 type 2 cytokines to sustain M2-like phenotype for ATM.  $T_h2$  cells contribute as well to that process by secreting IL-5 and IL-4 cytokines. In obesity (right part), enlarged adipocytes secrete pro-inflammatory cytokines, like  $TNF\alpha$ , IL-1 $\beta$  as well as chemokines, such as RANTES and MCP-1 and DAMPs not only to induce phenotypic switch of the resident ATM toward M1-like phenotype but also to recruit neutrophils, monocytes, monocyte-derived macrophages, mast cells,  $T_h1$  cells, cytotoxic  $CD8^+T$  cells, B cells, ILC-1, and NK cells to the AT, promoting type 1 inflammation.  $T_h1$  cells and  $CD8^+T$  cells secrete  $IFN\gamma$ , IL12, and IL-18, supporting M1-like phenotype of ATM. Mast cells, iNKT

cells, ILC-1 and NK cells contribute type 1 inflammatory milieu by being additional sources of  $\text{IFN}\gamma$  and IL-12, respectively. Adipocytes and macrophages directly interact with  $\text{T}_\text{H}1$  cells for MHC-II-restricted antigen presentation and TCR-mediated activation. Similarly, B cells directly interact with  $\text{T}_\text{H}1$  cells in a MHC-II-restricted manner to stimulate TCR-mediated activation. In addition,  $\text{CD}8^+$  T cells directly interact with B cells through TCR and MHC-I-mediated interactions, which stimulate B cells to produce antigen-specific IgG that contribute M1-like phenotypic switch of ATM. Neutrophil elastase, MPO, IL1 $\beta$  secretion by neutrophils and  $\text{TNF}\alpha$  secretion by  $\gamma\delta\text{T}$  cells, supporting M1-like phenotypes of the ATM. ICAM-1, intercellular adhesion molecule 1; ICOS, inducible costimulator; ICOSL, inducible costimulator ligand; IFN, interferon; iNKT, invariant natural killer T cells; LFA-1, leukocyte function-associated antigen-1; MCP-1, monocyte chemoattractant protein-1; MHC, major histocompatibility complex; MPO, myeloperoxidase; NK, natural killer cells; RANTES, regulated on activation, normal T-cell expressed and secreted; TCR, T-cell receptor; and  $\text{TNF}\alpha$ , tumor necrosis factor alpha <sup>98</sup>.

#### 1.4.1 Immune cells at homeostasis in white adipose tissue

##### a. Monocytes

Monocytes are circulating, short-lived mononuclear phagocytes and one of the fast-responsive cells to the inflammation. Monocytes originate from hematopoietic stem cells (HSCs) in the bone marrow and subdivided into three distinct subsets based on their surface markers: classical monocytes ( $\text{CD}14^+ \text{CD}16^-$  in human,  $\text{CX}_3\text{CR}1^{\text{int}} \text{CCR}2^+ \text{CD}62\text{L}^+ \text{CD}43^{\text{low}} \text{Ly}6\text{C}^{\text{hi}}$ , shortly,  $\text{Ly}6\text{C}^+$ , in mice), intermediate monocytes ( $\text{CD}14^{\text{int}} \text{CD}16^-$  in human,  $\text{CX}_3\text{CR}1^{\text{int}} \text{CCR}2^+ \text{CD}62\text{L}^+ \text{CD}43^{\text{low}} \text{Ly}6\text{C}^{\text{int}}$ , shortly,  $\text{Ly}6\text{C}^{\text{int}}$ , in mice), and non-classical monocytes ( $\text{CD}14^- \text{CD}16^+$  in human,  $\text{CX}_3\text{CR}1^{\text{high}} \text{CCR}2^- \text{CD}62\text{L}^- \text{CD}43^{\text{high}} \text{Ly}6\text{C}^{\text{low}}$ , shortly,  $\text{Ly}6\text{C}^-$ , in mice) <sup>99</sup>. The classical  $\text{Ly}6\text{C}^+$  monocytes are able to migrate into the tissues through a  $\text{CCR}2/\text{CCL}2$  receptor/chemokine dependent manner <sup>100</sup>. Silva et al. reported minor  $\text{Ly}6\text{C}^+$  subset in mouse eWAT depot at steady-state <sup>101</sup>. The  $\text{Ly}6\text{C}^{\text{int}}$  monocyte population has been identified to display transitional monocyte phenotype, which is distinct from the  $\text{Ly}6\text{C}^+$  and  $\text{Ly}6\text{C}^-$  monocyte subsets <sup>102</sup>. The non-classical  $\text{Ly}6\text{C}^-$  monocyte subset, also known as patrolling monocytes, crawl along the vasculature and maintain vascular homeostasis via LFA-1/ICAM-dependent manner under physiological conditions in mice, <sup>103, 104</sup> as well as in human <sup>105</sup>. A recent study reported that monocytes display plasticity and have a potential to differentiate into inflammatory macrophage or DC subtypes, depending on the positioned tissue environment <sup>106</sup>.

##### b. Macrophages

Macrophages are heterogeneous population of cells that phagocytose pathogens, debris, and dead cells, can trigger or regulate inflammation, tissue repair, and wound healing thanks to phenotypic plasticity, responding to the environmental demands. In addition, macrophages are

professional antigen presenting cells (APCs) that capture, process, and present antigens to the adaptive immune cells. Strategically, macrophages are located at diverse anatomic locations, such as body cavities, mucosal surfaces, and in tissues where they are transcriptionally programmed to perform diverse tissue-specific functions<sup>107</sup>, such as adipose tissue macrophages (ATMs) in the adipose tissue, Kupffer cells (KCs) in the liver, osteoclast in the bone, and microglia in the central nervous system. Macrophages are divided into two subtypes that classically polarized inflammatory (M1) and alternatively polarized reparative (M2)<sup>108</sup>. This early the M1/M2 classification, only accurately describes the *in vitro* polarization status of the macrophages that can be obtained by using the combination of the LPS and IFN $\gamma$  treatments for M1 polarization and IL-4 for the M2 polarization<sup>109</sup>. *In vivo*, the pro/anti-inflammatory phenotype represents a broad and heterogeneous spectrum with M1 and M2 markers, representing extreme cases that we will discuss some examples within the context of obesity in the following section (1.4.2)<sup>110</sup>. Intracellular energy metabolism of the macrophages is a fundamental determinant of their functional response. So, the classically polarized macrophages utilize glycolysis and pentose phosphate pathway to support microbicidal functions, like secretion of lysozyme M, cathepsin proteases, and lipocalin. By contrast, the alternatively polarized macrophages employs fatty acid oxidation<sup>111</sup>. Yet, several recent studies showed that macrophages in different tissue environments adopt a range of inflammatory phenotypes through metabolic reprogramming, which we will discuss in detail after (see section 1.4.2)<sup>112</sup>.

ATMs derived from the primitive progenitor cells during the development in the yolk sac and self-renew through proliferation independently from the HSCs at homeostasis<sup>113, 114</sup>. ATMs are characterized as, CD64<sup>+</sup>, CD68<sup>+</sup>, F4/80<sup>+</sup>, CD11b<sup>+</sup>, CD206<sup>+</sup>, CD301<sup>+</sup>, Arg1<sup>+</sup> cells in mice and CD163<sup>+</sup>, CD204<sup>+</sup>, CD206<sup>+</sup>, CD301<sup>+</sup> in humans at homeostasis, represent the most abundant immune cell population in AT<sup>115</sup>. ATMs display an alternatively polarized reparative phenotype at steady-state and produces high levels of anti-inflammatory molecules, such as IL-10, transforming growth factor-beta (TGF- $\beta$ ), and T<sub>H</sub>2-attracting chemokines CCL17 and CCL22, favoring resolution of inflammation, tissue repair and remodeling<sup>116</sup>. This subset of ATMs express the master regulator of fatty acid oxidation transcription factor peroxisome proliferator-activated receptor gamma (PPAR- $\gamma$ ) to support their intracellular energy metabolism and adapted to a lipid-rich milieu<sup>117</sup>. ATMs insure tissue homeostasis through eliminating dying adipocytes and engulfing debris from dead cells, facilitating the cellular turnover of these cells. Indeed, a recent study described a cellular process, termed exophagy, providing a mechanism for the removal of dead adipocytes by ATMs. ATMs constitute around dead adipocytes, a hydrolytic extracellular compartment, which composed of acidic lysosomal enzymes. Consequently, this process leads to the degradation of adipocyte fragments and the

release of the free fatty acids (FFAs), which are caught by the ATMs to be recycled <sup>118</sup>. High lipid-buffering capacities of the ATMs also capture lipids by the fatty acid transporter CD36 and the lipid scavenger receptor MSR1, during the some physiological processes, such as weight-loss, and fasting <sup>119</sup>. Thus, ATMs restrain ectopic lipid accumulation and peripheral lipotoxicity through their high lipid-buffering ability to maintain an anti-inflammatory environment. In addition, it has been shown that ATMs recruits preadipocytes by secretion of high-level of osteopontin to induce adipogenesis around dead adipocytes to compensate dead adipocytes with new ones <sup>120</sup>. Moreover, Buorlier et al. showed that ATMs are active players of the AT remodeling through the extension of a capillary network by release of proangiogenic VEGF-A, MMP-2, and MMP-9, promoting angiogenesis <sup>121</sup>. Thus, regulation of angiogenesis by ATMs restricts hypoxia, supplies a sufficient amount of nutrients and oxygen to maintain tissue homeostasis by ATMs.

### c. Dendritic cells

Dendritic cells (DCs) are heterogenous, professional antigen presenting cells (APCs) that patrol diverse anatomical locations, capture antigens, process and present to the adaptive immune cells <sup>122</sup>. The current classification of the DC relies on combined approaches, based on surface markers, key gene signature, and ontogeny. DCs are subdivided as conventional also known as classical DCs (cDCs), plasmacytoid DCs (pDCs), monocyte-derived DCs (MoDCs), and epidermal Langerhans cells <sup>123</sup>, expressing high-level expression of major histocompatibility complex class two (MHC-II) in mice <sup>124</sup> and humans (HLA-DR) <sup>125</sup>. cDCs and pDCs are originates from the bone-marrow resident hematopoietic precursors named "common DC progenitors" (CDPs) that is distinct from the one of monocytes/macrophages <sup>126</sup> and the tyrosine kinase receptor Fms-related tyrosine kinase 3 (Flt3) is required for their differentiation in mice <sup>127</sup> as well as in humans <sup>128, 125, 129</sup>. The cDCs are able to differentiate into either cDC<sub>1</sub> subset under the control of the interferon regulatory factor 8 (IRF8), inhibitor of DNA-binding 2 (ID2), and basic leucine zipper ATF-like transcription factor 3 (BATF3) transcription factors <sup>130</sup> or IRF4-dependent cDC<sub>2</sub> subset <sup>131</sup>. Mouse cDC<sub>1</sub> subset is identified based on the expression of MHC-II, CD11c, CD8a or CD103 and absence of CD11b and B220. CD8a is considered as a marker of lymphoid-resident cDC<sub>1</sub> subset <sup>132</sup>, while CD103 expresses in the non-lymphoid tissues (e.g. AT, liver, kidney) and serves as a migratory cDC<sub>1</sub> subset <sup>133</sup>. In addition, the mouse cDC<sub>1</sub> subset expresses cell adhesion molecule 1 (CADM1), C-type lectin receptor 9A (Clec9a) and X-C motif chemokine receptor 1 (XCR1), which are also found in human <sup>134</sup>. However, the Clec9a expression is not only restricted to mouse cDC<sub>1</sub> subset, but also detectable in the cDC progenitors and pDCs <sup>135</sup>, unlike human <sup>136</sup>. On the other hand, the cDC<sub>2</sub> subset can be distinguished by high expression of the MHC-II, CD11b, CD11c, and signal

regulatory protein alpha (SIRP $\alpha$ ) in both, mice and humans <sup>137</sup>. pDC subset is determined as MHC-II, CD11c-CD123<sup>high</sup> CD45A-B220 expressing cells as a mutual surface marker in both mice and humans. Moreover, some additional pDCs markers have been identified, including the blood DC antigen 2 (BDCA2) <sup>138</sup>, BDCA4 <sup>139</sup>, CD317, and ILT7 <sup>140</sup>, which are specific for humans as well as mice specific the bone-marrow stromal cell antigen 2 (BTS2) <sup>141</sup>, and sialic acid-binding Ig-like lectin H (SigleCH) <sup>142</sup>. The pDC subset has been suggested to originates from the both myeloid and lymphoid lineages <sup>143</sup>. As their secretory cell-like morphology implies, the pDCs are specialized to produce large amount of type-1 interferon, in response to viral infections <sup>144</sup>. The mouse eWAT depots mainly contain cDC<sub>1</sub> and cDC<sub>2</sub> subsets, while the pDC subset is extremely rare at steady-state. Indeed, the cDC<sub>2</sub> subset represents the most abundant DC population in mouse eWAT, at homeostasis, whereas the cDC<sub>1</sub> subset defines only a minor portion <sup>145</sup>. Recently, Wnt and PPAR $\gamma$  pathways, which regulate adipocyte differentiation and expansion has been shown to controlled by cDC subsets at homeostasis in VAT. Activation of the Wnt/ $\beta$ -catenin pathway in the cDC<sub>1</sub> subset, upregulates PPAR $\gamma$  signaling in the cDC<sub>2</sub> subset and control adipocyte differentiation as well as expansion in VAT. Thus, the combined action of cDC<sub>1</sub> and cDC<sub>2</sub> subsets in the regulation of Wnt/ $\beta$ -catenin pathway-dependent PPAR $\gamma$  signaling in VAT, displays a tolerogenic phenotype by controlling adipocyte differentiation and expansion in VAT at steady-state, contributing to tissue homeostasis <sup>146</sup>.

#### d. Eosinophils

Eosinophils are key players in allergic inflammation and mainly, parasitic but also bacterial and viral infections <sup>147</sup>. Eosinophils derived from bone-marrow progenitors that GM-CSF, IL3, and IL-5 are crucial mediators of the eosinophil development and survival <sup>148</sup>. Eosinophils consist of primary granules, which are filled with hydrophobic protein family Galectin-10 (Charcot-Leyden crystals) and specific/cystalloid granules that are contain vast quantities of toxic and basic proteins, including lysozyme M, major basic proteins (MBP), eosinophil-derived neurotoxin (EDN), and eosinophil cationic protein (ECP), contributing to fight against pathogens <sup>149</sup>. Eosinophils engage another defense mechanism against microbial pathogens, called catapults or extracellular eosinophilic traps (EET) in that mitochondrial DNA together with granule proteins form a structure to kill pathogens in a ROS-dependent manner <sup>150, 151</sup>. Under physiological conditions, eosinophils are mostly present in skin, respiratory and gastrointestinal tract as well as in several other tissues, such as adipose tissue, liver, kidney where exhibit protective and immunoregulatory functions to maintain tissue homeostasis <sup>152</sup>. At steady-state VAT and SAT depots, harbor a higher number of eosinophils, than in obesity where their quantity is very low. However, is reversed by a low-calorie dietary intervention <sup>153</sup>. Eosinophils in AT contributes metabolic homeostasis through IL-4 and IL-13 production

dependent stimulation of M2-like ATMs that improve glucose tolerance of mice in response to HFD feeding <sup>154</sup>. Also, it has been suggested that eosinophils involve in being process of WAT via the regulation of transcriptomic profile by the transcriptional repressor Kruppel-like factor 3 (KLF3) <sup>155</sup>.

#### e. Type 2 Innate Lymphoid Cells

Type 2 innate lymphoid cells (ILC2) originate from the inhibitor of DNA-binding 2 (ID2)<sup>+</sup> ILC precursors, under the control of GATA-binding protein 3 (GATA3) and retinoic acid receptor-related orphan receptor alpha (ROR $\alpha$ ) transcription factors, in response to IL-33 <sup>156</sup>. WAT-resident ILC2s maintain local eosinophils and M2-like macrophages by secreting T<sub>h</sub>2 cytokines, like IL-4, IL-5, and IL-13, as the primary source under homeostasis <sup>157</sup>. Moreover, WAT-resident ILC2s control the being of WAT and thermogenesis in humans via methionine-enkephalin peptides production independent from eosinophils or IL-4 receptor signaling <sup>158</sup>.

#### f. CD4<sup>+</sup> T cells

The second subset of T cells, according to the TCR composition, is the  $\alpha\beta$  T cells that further classified as two main subgroups, which are CD4<sup>+</sup> T cells and CD8<sup>+</sup> T cells. The development of naïve CD4<sup>+</sup> T cells takes place in the thymus. Subsequently, they migrate into secondary lymphoid tissues like spleen and lymph nodes and non-lymphoid organs, such as AT. Under the lean status, AT harbors not only naïve CD4<sup>+</sup> T cells, but also dominated by several effector T-helper (T<sub>h</sub>) lineages, including T<sub>h</sub>2 cells, and T<sub>regs</sub> that coordinate tissue homeostasis <sup>159</sup>.

AT-resident T<sub>h</sub>2 cells regulated by the transcription factor GATA3 and produces a high level of IL-4, IL-5 and IL-13 cytokines, which are the main cytokines to maintain M2-like phenotype for ATMs. Nearly decades ago, Winer et al. highlighted the significance of the GATA3<sup>+</sup> T<sub>h</sub>2 cells by first observing in a mouse model that the absence of T and B lymphocytes (Recombination activating gene, Rag-deficient) prone to develop more severe obese and insulin-resistant phenotype than their WT littermates, in response to HFD-feeding. Secondly, they showed that CD4<sup>+</sup> T cells displaying a T<sub>h</sub>2 profile following the adoptive transfer in obese Rag-deficient mice and converted HFD-induced metabolic outcomes. Moreover, they revealed that transferring of CD4<sup>+</sup> T cells lacking a transcription factor for T<sub>h</sub>2 polarization, which is the signal transducer and activator of transcription 6 (STAT6), led to T<sub>h</sub>2 cell depletion in AT and loss of protective effects against HFD-feeding <sup>160</sup>.

### g. Regulatory T cells

Regulatory T cells ( $T_{\text{regs}}$ ) are crucial for the maintenance of immunological self-tolerance and the prevention of various autoimmune as well as allergic diseases, like rheumatoid arthritis, psoriasis through negatively regulating B and T cell responses by immunosuppressive cytokine production (IL-10, TGF- $\beta$ )<sup>161</sup>. Tissue  $T_{\text{regs}}$  represent a unique  $T_{\text{reg}}$  population compared to the lymphoid organ resident ones<sup>162</sup>. WAT-resident  $T_{\text{regs}}$  have a more restricted TCR repertoire (limited  $\alpha$ -chain diversity and a single  $\beta$  chain) in lean mice than  $T_{\text{regs}}$  from lymphoid organs<sup>163</sup>. Tissue  $T_{\text{regs}}$  originate from the thymus, display tissue-specific transcriptional and epigenetic programs and have pleiotropic actions, like control of metabolic homeostasis in WAT, regeneration process in skeletal muscle<sup>164</sup>. Feuerer et al. showed that CD4<sup>+</sup> GATA3<sup>+</sup> Foxp3<sup>+</sup>  $T_{\text{regs}}$  enriched in eWAT of lean mice, while their number strikingly reduced with obesity in both mouse and human, moreover whole-body depletion of  $T_{\text{regs}}$  negatively correlates with metabolic parameters, like impaired glucose homeostasis and insulin signaling in WAT<sup>165</sup>. The same group also reported that the master regulator of adipocyte differentiation PPAR $\gamma$  is a crucial driver of the accumulation and phenotype of AT-resident  $T_{\text{regs}}$ <sup>166</sup>. Moreover, IL-33 the main cytokine promoting the expansion of AT-resident  $T_{\text{reg}}$  population in the lean state<sup>162</sup> by the activity of the interferon regulatory factor 4 (IRF4) and basic-leucine zipper transcription factor (BATF) transcription factors<sup>167</sup>. Recently, Schmidleithner et al. revealed that AT-resident  $T_{\text{regs}}$  suppresses conventional T cells ( $T_{\text{conv}}$ ) by the enzymatic activity of the hydroxy-prostaglandin-dehydrogenase (HPDG), which in part mediated by PPAR $\gamma$  signaling, contributing tissue homeostasis<sup>168</sup>.

### h. $\gamma\delta$ T cells

Members of the innate-like T cell family,  $\gamma\delta$ T cells are abundant at barrier surfaces, including skin, lung, gastrointestinal, and genital tracts<sup>169</sup>. In a recent study, Kohlgruber et al. reported that CD4<sup>-</sup>CD8<sup>-</sup> double negative  $\gamma\delta$ T cells, which expressing mostly V $\gamma$ 4 and enriched in various VAT depots at steady-state in mice, as well as in human omental AT depots that control age-dependent regulatory T cell ( $T_{\text{regs}}$ ) expansion through promoting preadipocytes/stromal cell production of IL33 and control core body temperature in response to environmental fluctuations by the production of IL-17A and TNF $\alpha$ <sup>170</sup>. Also, Goldberg et al. suggested that the beneficial impact of the short-term ketogenic diet feeding on metabolic control is mediated by the activation of AT-resident  $\gamma\delta$  T cells with a specific gene signature, supporting tissue repair and homeostasis<sup>171</sup>.

### i. Natural Killer T cells

Natural killer T (NKT) cells belongs to the innate-like T cell subset and displays both NK cell markers, like NK1.1 and CD56 as well as T cell characteristics, such as  $\alpha\beta$  TCR expression. NKT cells recognizes lipids and glycolipids, like  $\alpha$ -galactosylceramide,  $\beta$ -D-glucopyranosyl ceramide, isoglobotriosyl ceramide (iGb3) by an MHC-I-like molecule, CD1d. Two subtypes are identified on the basis of the expression of an invariant TCR $\alpha$  chain, which is V $\alpha$ 14-J $\alpha$ 18 in mouse and V $\alpha$ 24-J $\alpha$ 18 in human. The type I NKT cells, also known as invariant NKT (iNKT) cells, express the invariant TCR $\alpha$  chain together with definite TCR $\beta$  chains, which are V $\beta$ 8.2,7,2 in mouse and V $\beta$ 11 in humans. On the other hand, the type II NKT cells, so-called diverse NKT (dNKT) cells, display various expression patterns of TCR $\alpha$  and TCR $\beta$  chains <sup>172</sup>.

At steady-state, the AT contains iNKT cells in both mouse and human <sup>173</sup> that represents a unique tissue-resident iNKT subset with their distinct T<sub>h</sub>2 cytokine repertoire, such as IL-4 and IL10 compared to the liver and spleen resident subsets in mouse <sup>174</sup>. Lynch et al. also showed that AT-resident iNKT cells are depleted in diet-induced obesity and are restored after weight loss. Moreover, iNKT-deficient mice exhibited enhanced obesity-associated outcomes compared to the control group, and the adoptive transfer of iNKT cells into these obese mice reversed the phenotype. After the identification of CD1d expression in adipocytes and direct interaction between CD1d-expressing adipocytes and iNKT cells <sup>175</sup>, Huh et al. reported that adipocytes selectively stimulate AT-resident iNKT cells to mediate anti-inflammatory responses and attenuate excess pro-inflammatory responses in HFD-induced obese adipose tissue by using an adipocyte specific CD1d-deficient mouse model <sup>176</sup>. It has also been suggested that AT-resident iNKT cells help to maintain AT-resident T<sub>regs</sub> by being an IL-2 source <sup>177</sup>.

### j. B cells

B cells play a crucial role in host defense through immunoglobulin (antibody) production, which recognize and eliminate pathogens but also activates the CD8<sup>+</sup> T, and CD4<sup>+</sup> T cells via TCR, MHC-I, and MHC-II-mediated interactions as well as stimulates the ATM polarization towards M1-like phenotype. B cells produce five immunoglobulin isotypes that include IgA, IgD, IgE, IgG, and IgM, which are secreted or expressed on their cell surface as the main components of B cell receptors (BCR) that bind epitopes of protein, carbohydrate, or nucleic acid antigens <sup>178</sup>. Upon either a direct antigen engagement through BCR or Th cell-mediated activation, B cells initiate serial of molecular processes, like migration, proliferation, and differentiation into antibody-producing plasma cell <sup>178</sup>. Through the development of antibody-producing plasma

cells, somatic hypermutation and gene rearrangement processes lead to the production of a wide variety of antibodies against the antigens. Affinity maturation and isotype switching further increase the antibody repertoire <sup>178</sup>. B cells are subdivided into two main subsets B1 and B2 subsets. Innate like B1 cells are derived from fetal liver and are the principal source of IgM antibodies <sup>179</sup>. B1 cells are abundant in pleural and peritoneal cavities <sup>179</sup>. B2 cells arise from bone marrow progenitors and are produce all IgG isotypes in response to Th cell-mediated stimulation and migrate into secondary lymphoid organs, as follicular B cells and splenic marginal zone B cells <sup>179</sup>. Besides antibody production, B cells are also professional antigen-presenting cells and regulate both innate and adaptive immunity through immunoregulatory cytokine secretion. It has been reported that AT contains a distinctive population of IL-10-producing regulatory B cells (B<sub>regs</sub>) at steady-state to sustain AT homeostasis and limit obesity-relevant inflammation in response to stimulation by LPS, CXCL12, and free fatty acids, in mice <sup>180</sup> as well as in humans <sup>181</sup>. Lean AT-resident IL-10-producing B<sub>regs</sub> originate from B1 subset <sup>182</sup>. Nevertheless, these studies also revealed that with obesity B<sub>regs</sub>, diminished in AT <sup>180, 181, 182</sup>.

## 1.4.2 Immune drivers of inflammation in obese white adipose tissue

### a. Adipose tissue macrophages, recruited monocytes and macrophages

Two independent studies revealed that the number of macrophages considerably expands during obesity within WAT in both mice and humans, which represents more than 50% of the WAT immune population. Weisberg et al. reported that macrophage content of various WAT depots positively correlates with BMI and adipocyte size. Moreover, they also showed that macrophages are the primary sources of TNF $\alpha$  and other proinflammatory cytokines in obese WAT <sup>183</sup>. Xu et al. suggested that macrophages in WAT play an active role in morbid obesity in that macrophage-related inflammatory cytokines contribute to the pathogenesis of obesity-induced insulin resistance <sup>184</sup>. Weisberg et al. showed that antagonism or deficiency of the C-C motif chemokine receptor-2 (CCR2), which is the main chemokine for monocyte and macrophage recruitment, reduced food intake and attenuated development of obesity in mice upon HFD feeding. CCR2-deficient obese mice also exhibit alleviated hepatic steatosis and improved systemic glucose homeostasis through decrease macrophage content and the inflammatory profile of the WAT, evidencing the importance of the recruitment of circulating monocytes besides macrophages in this pathophysiology <sup>185</sup>. Nagareddy et al. revealed that adipose tissue-derived S100A8/A9 stimulates ATMs by TLR4/MyD88 and NLRP3 inflammasome-dependent IL-1 $\beta$  production that interacts with IL-1 receptor on bone marrow progenitors, inducing the monocytosis in obesity <sup>186</sup>. Feng et al. showed that clodronate

liposome-mediated depletion of visceral ATMs improves metabolic parameters of diet-induced obese mice, implying a direct role of ATMs in obesity-associated insulin resistance<sup>187</sup>. Lumeng et al. identified a CD11c<sup>+</sup> macrophage population with the M1-like proinflammatory phenotype in AT of obese mice, which does not exist in AT of lean mice. Moreover, obese CCR2-KO mice express M2-like anti-inflammatory markers at levels similar to lean conditions, suggesting obesity induces a phenotypic switch in ATM polarization<sup>188</sup>. Obesity-induced switch in ATM activation state coupled to the recruitment of inflammatory macrophage clusters from the circulation rather than conversion of resident M2-like macrophages into M1-like ATM is an essential step<sup>189</sup>. A proinflammatory CD11c<sup>+</sup> macrophage population has also been identified as a marker of insulin resistance in human obesity<sup>190</sup>. Importantly, in this study, CD11c<sup>+</sup> macrophages were also expressing CD206, which is a marker for the M2-like ATMs, illustrating the heterogeneity of ATM populations that exist in obesity, well beyond M1 and M2, besides changes in macrophage numbers, according to the pathophysiological states. In fact, the expansion of AT across models of obesity has induces a program of lysosome biogenesis in ATMs, which is associated with lipid catabolism but not a classic inflammatory phenotype, as explained in the AT homeostasis part, lipid buffering capacities of ATMs maintain tissue homeostasis<sup>191</sup>. Kraatz et al. identified that obesity induces a metabolically activated phenotype distinct from the classical activation of ATMs in mice and humans by using a proteomic approach. These metabolically activated macrophages contain a combination of M1-like pro-inflammatory markers and M2-like lipid metabolism markers<sup>192</sup>. Catecholamine norepinephrine (NE) is a monoamine neurotransmitter that regulates thermogenesis and lipolysis of the WAT. A recent study discovered a new subset of sympathetic nerve associated macrophages (SAMs) in WAT that mediates NE transport and degradation by expression of solute carrier family 6 member 2 (SLC6A2) and monoamine oxidase A (MAOA). They showed that activation of the sympathetic nervous system upregulates NE uptake by SAMs, as a result, SAM exhibits a pro-inflammatory phenotype. Moreover, they revealed that SAM population is rising with two mouse models of obesity, and Slc6a2-deficient SAMs increase brown adipose tissue mass, cause beiging of WAT, stimulate thermogenesis, leading to significant weight loss in obese mice. They further confirmed that in humans<sup>193</sup>. Hill et al. reported that obese AT of mice and humans contain multiple distinct populations of ATMs with the unique tissue distributions, transcriptomes, chromatin landscapes, and functions<sup>194</sup>. They identified three discrete ATMs in mice, which are CD11b<sup>+</sup>CD9<sup>+</sup>Ly6C<sup>+</sup>, CD11b<sup>+</sup>CD9<sup>-</sup>Ly6C<sup>-</sup> and CD11b<sup>+</sup>CD9<sup>-</sup>Ly6C<sup>+</sup>. They described that CD9<sup>+</sup> and Ly6C<sup>+</sup> ATMs are characteristic of obesity, and both of them express CD11c at different levels. However, they assumed that CD9<sup>+</sup> ATMs are most similar to the CD11c<sup>hi</sup> population identified in prior studies. According to their findings, CD9<sup>+</sup> and Ly6C<sup>+</sup> ATMs are both monocyte-derived that CD9<sup>+</sup> ATMs predominantly found around CLSs and contain high amounts of intracellular lipids in lysosome-like structures and possess

an inflammatory chromatin landscape. On the other hand, Ly6C<sup>+</sup> ATMs homogeneously spread in obese AT. Furthermore, Ly6C<sup>+</sup> ATMs overexpresses genes associated with angiogenesis and extracellular matrix remodeling while lacking intracellular lipid droplets<sup>194</sup>. In a recent study, Jaitin et al. described a novel Trem2<sup>+</sup> lipid-associated macrophages (LAMs) in AT<sup>195</sup>, possibly similar to that described by Hill et al. as CD9<sup>+</sup> macrophages<sup>194</sup>. Importantly, they showed that the genetic ablation of the lipid receptor triggering receptor expressed on myeloid cells 2 (Trem2) in mice regulates the downstream molecular program for the protective functions of the LAMs. Furthermore, Trem2 exhibited to prevents adipocyte hypertrophy, systemic hypercholesterolemia, body fat mass, and glucose intolerance<sup>195</sup>. Consistent with that, a distinct subset of the ATMs, the vasculature-associated macrophages (VAMs) identified in WAT at steady-state, adopting inflammatory phenotype in response to metabolic challenges in obesity<sup>101</sup>, presumably corresponds to previously reported monocyte-derived Ly6C<sup>+</sup> ATMs<sup>196</sup>.

#### b. Dendritic cells

The role of the DCs in obesity is not fully understood yet since the lack of specific DC markers, allowing for unambiguous distinction from macrophages. DCs expand in obese AT, promote macrophage infiltration and their increased numbers are positively correlate with HFD-induced metabolic abnormalities<sup>197</sup>. Moreover, the accumulation of DC in obese AT induces T<sub>h</sub>17 differentiation that promotes obesity-induced inflammation and IR in mice and humans<sup>198, (197)</sup>. Discrimination of AT-resident DCs from macrophages on the basis of CD64 expression allowed to determine that both cell types are independent contributors to obesity-induced inflammation and IR<sup>199</sup>. In the same study, it was also shown that monocytes, recruited to the AT in a CCR7 and to a lesser extent CCR2-dependent manner, differentiated into DCs in response to HFD feeding<sup>199</sup>. In a recent study, Ghosh et al. evidenced that the chemerin adipokine recruits circulating pDCs into VAT by chemokine-like receptor 1 (CMKLR1), in obese individuals. Moreover, adipose tissue-derived high-mobility group 1 (HMGB1) protein activates TLR9 in the recruited pDCs by transporting extracellular DNA via the receptor for advanced glycation end products (RAGE) and induces production of type 1 interferons (IFNs), further contributing to the pro-inflammatory milieu<sup>200</sup>. In line, mice, lacking the receptor for IFN $\alpha$  and deficient in pDCs has been shown to prevent diet-induced obesity and IR<sup>201</sup>.

#### c. Neutrophils

Neutrophils are dominant granulocyte subset in the circulation and the first innate immune cells that respond against pathogens or injury<sup>202</sup>. Initially, half-life of the circulating neutrophils is

defined as less than 1 day, however a recent study in humans revealed a lifespan of up to 5.4 days<sup>203</sup>. Moreover, lifespan of tissue neutrophils reported to be twice or three times longer than circulating ones<sup>204</sup>. Neutrophils originate from HSCs and differentiate into mature neutrophils through CXCL12-CXCR4 signaling in the bone marrow, where approximately  $10^7$  neutrophils in mice and  $10^{11}$  in humans are produced every day<sup>205</sup>. Indeed, a recent study by using multi-parametric analysis (lineage commitment, and transcriptional profile) evidenced three distinct neutrophil subsets in the bone marrow, the pre-neutrophil subset, which is a proliferative precursor, differentiating into the non-proliferative immature and the mature neutrophils, in mice and humans<sup>206</sup>. Following the maturation, neutrophils exit from the bone marrow and, under homeostasis, mobilize into the circulation via CXCR2, patrolling the organism for any signs of infection or injury<sup>207</sup>. Upon infection, neutrophils anti-microbial activity relies on four main mechanisms, which are phagocytosis, release of reactive oxygen species as well as cytotoxic granule components, like myeloperoxidase, cathepsins,  $\beta$ -defensins lysozyme M, and nuclear material in the form of neutrophil extracellular traps (NET)<sup>208</sup>. The granules of the neutrophils classified as azurophilic (primary), specific (secondary), and gelatinase (tertiary) granule, facilitating pathogen destruction<sup>209</sup>. NET are the neutrophil-specific structures that contains chromatin, mitochondrial DNA, granule-derived anti-microbial peptides, and enzymes, ejecting it into the extracellular space to trap and kill pathogens, as well as prime other immune cells to induce inflammatory immune response<sup>210</sup>.

Neutrophils have been reported to infiltrate into the AT early, roughly a week later, and further increase over the course of HFD feeding<sup>211</sup>. One of the key regulators of inflammation, cytosolic phospholipase  $A_2\alpha$ , is required for such a fast neutrophil recruitment (roughly a week after HFD feeding)<sup>212</sup>. Moreover, the deletion of neutrophil elastase in mice prevent HFD-induced obesity and IR by decreasing macrophage and neutrophil content of AT and limiting tissue inflammation<sup>213</sup>. On the other hand, neutrophil myeloperoxidase regulates HFD-induced obesity and IR in mice by modulating macrophage infiltration<sup>214</sup>. Furthermore, Kawanishi et al. described that exercise training attenuates neutrophil infiltration and elastase expression in AT of HFD-induced obese mice<sup>215</sup>. Interestingly, chemical inhibition of NET release by the peptidyl arginine deiminase 4 inhibitor Cl-amidine in HFD-fed obese mice fails to reduce AT inflammation<sup>216</sup>. On the other hand, Revelo et al. show that HFD feeding in mice stimulates the release of NET and autoantibody formation against nucleic acid-related antigens in VAT, and decrease systemic clearance of NET. In line, they also show that TLR7 and TLR9-deficient HFD-fed obese mice display reduced metabolic inflammation and improved glucose homeostasis. Moreover, inhibitors of the NET formation or a TLR7/9 antagonist decrease HFD-induced obesity in mice<sup>217</sup>. Clinical trials have also shown that the numbers of activated neutrophils is increased in obese individuals, as determined by increased ROS production<sup>218</sup>,

<sup>219</sup>. Interestingly, Hagman et al. reported that following bariatric surgery in humans, metabolic improvements occur without significant reduction of AT inflammation neutrophils, and macrophages numbers were even increased <sup>220</sup>. A recent study indicated that severe obesity is associated with increased production of NET, in humans. Furthermore, they also showed that weight loss after bariatric surgery is not restore dysregulated NET generation, suggesting that patients with persistent NET accumulation following bariatric surgery are at the highest risk of cardiovascular events <sup>221</sup>.

#### d. Mast cells

Even though the role of mast cells mainly associated with allergic responses, Liu et al. reported that mast cell numbers in WAT increased with obesity in both mice and humans <sup>222</sup>. Moreover, genetic or pharmacological depletion of mast cells improves metabolic outcomes of Western style-diet feeding in mice. Mast cells contribute to WAT and muscle angiogenesis, angiogenesis-related cell apoptosis, and cathepsin activity by producing IL-6 and IFN $\gamma$  in mice, thereby promoting diet-induced obesity and glucose intolerance <sup>222</sup>. Takana et al. showed that mast cell-derived 15-deoxy-delta-12,14-prostaglandin-J<sub>2</sub> is an alternative modulator of the adipogenesis through PPAR $\gamma$  activation <sup>223</sup>. It has also been shown that mast cells regulate preadipocyte to adipocyte differentiation in both obese and non-obese mice <sup>224</sup>. Moreover, Hirai et al. showed that immature mast cells infiltrate into lean AT and gradually mature with the progression of obesity. Following maturation, mast cells secrete mast-cell protease-6 (MCP-6) that induces AT fibrosis through stimulation of collagen-V expression, leading to the acceleration of IR by the suppression of preadipocyte differentiation in genetically obese and diabetic *db/db* mice <sup>225</sup>. These findings further confirmed in C57Bl/6 mice by using pharmacological mast cell stabilizers the sodium cromoglicate sodium liposomes (DSCGs) <sup>226</sup>. <sup>227</sup>. In line, Zhou et al. reported that WAT-resident mast cells in lean humans as well as mice are leptin-deficient which promote M2-like macrophage polarization, while WAT-resident mast cells in obese conditions are leptin sufficient, thus reconstitution of leptin-deficient mast cells mitigates obesity and IR in mice <sup>228</sup>

#### e. Type 1 Innate Lymphoid Cells and Natural Killer Cells

Murine T-bet<sup>+</sup>, NK1.1<sup>+</sup>, and NKp46<sup>+</sup> type 1 innate lymphoid cell (ILC1) population that produce high amounts of the immunoregulatory cytokine IFN $\gamma$  upon activation. ILC1s are divided into three subsets, which are immature natural killer cells (iNKs), mature natural killer cells (mNKs), and mixed/heterogenous ILC1s <sup>229</sup>. A recent study revealed that mNKs are circulating, while mixed ILC1s and iNKs are AT-resident in both mice and humans, furthermore a subset of AT-

resident ILC1s has ATM-killing activity and maintain ATM homeostasis at steady-state<sup>230</sup>. Furthermore, circulating ILC1s infiltrate into AT, promoting pro-inflammatory macrophages, and the AT-resident ILC1 subset loses the ability to kill ATMs<sup>230</sup>. O-Sullivan et al. discovered that diet-induced obesity drive early production of IL-12 in AT, leading to the selective proliferation and accumulation of T-bet<sup>+</sup> Nfil3<sup>+</sup> AT-resident ILC1s in an IL-12R and STAT4-dependent manner<sup>231</sup>. Furthermore, they also indicated that ILC1s-derived IFN $\gamma$  mediates pro-inflammatory macrophage polarization to promote obesity-associated IR<sup>231</sup>. In earlier study, NKp46-deficient mice, considered as lacking NK cells, displayed reduced recruitment of macrophages into AT and improved systemic insulin sensitivity<sup>232</sup>. Wensveen et al. found that obesity stimulates the ligands of the NK cell-activating receptor (NCR1) in adipocytes and leads to the proliferation of NK cells. In turn, increased NK cell numbers triggered the recruitment of pro-inflammatory macrophages and prompted IR. Eventually, NK cell ablation by using the NCR1-deficient mouse model prevented the accumulation of pro-inflammatory macrophages in VAT and improved glucose homeostasis<sup>233</sup>. Recently, Theurich et al. identified an IL-6/STAT3-dependent distinct, obesity-associated NK cell subpopulation, which defined as myeloid-signature NK cells by the authors that regulate energy and glucose homeostasis in mice<sup>234</sup>.

#### f. Invariant Natural Killer T cells

As mentioned, iNKTs mediate AT homeostasis at steady-state, Lynch et al. reported that their quantities significantly decrease in WAT of obese mice and the omentum of obese individuals<sup>173</sup>. The depletion of iNKTs via CD1d-deficient and J $\alpha$ 18-deficient mice models does not protect against metabolic abnormalities induced by either HFD feeding or choline-deficient diet feeding on two independent studies<sup>235, 236</sup>. On the other hand, Schipper et al. revealed that CD1d-deficient mice fed a low-fat diet exhibit a distinctive insulin resistance phenotype without overt AT inflammation<sup>237</sup>. Moreover, Ji et al. stimulated iNKTs by  $\alpha$ -galactosyl ceramide in HFD-induced obese CD1d-deficient mice and showed that iNKTs enhanced alternative macrophage polarization in AT and improves glucose homeostasis by IL-4/STAT6 signaling axis at different stages of HFD feeding, precisely at 4 days, 8 and 24 weeks<sup>238</sup>.

#### g. CD4<sup>+</sup> T cells

CD4<sup>+</sup> T cell populations increase in WAT of mice as well as humans in response to adipose-derived chemokine, RANTES or CCL5, which also contribute to macrophage recruitment<sup>239</sup>. T<sub>h</sub>1 subpopulation and one of the pro-inflammatory T<sub>h</sub>1 cytokine IFN $\gamma$  reported to enriched in WAT of obese mice. Accordingly, IFN $\gamma$ -deficient obese mice displayed improved metabolic

phenotype, suggesting  $\text{IFN}\gamma$  regulates AT inflammation <sup>240</sup>. Another study showed that reducing the number of the  $T_{h1}$  cell subset reversed the IR phenotype even if HFD feeding maintained in mice <sup>160</sup>. Furthermore, McGillicuddy et al. revealed that  $\text{IFN}\gamma$  attenuates insulin signaling, lipid storage, and differentiation in human adipocytes by stimulating JAK/STAT pathway <sup>241</sup>.

$T_{h17}$  cells produce IL-17 and are involved in the several pathophysiology of inflammatory diseases and are regulated by the transcription factor  $\text{ROR}\gamma\text{t}$  <sup>242</sup>. Nevertheless, the role of  $T_{h17}$  cells in obese AT and related outcomes has not been extensively studied. IL-17 seems to have opposite effects on various cell types. According to Winer et al., in mice HFD induces  $T_{h17}$  accumulation within SAT and spleen in an IL-6-dependent manner, whereas their numbers in VAT decrease <sup>243</sup>. Moreover, Shin et al. reported that IL-17 inhibits adipocyte differentiation in human mesenchymal stem cells and regulates pro-inflammatory responses in adipocytes <sup>244</sup>. Similarly, IL-17 suppressed adipocyte differentiation of mouse 3T3-L1 preadipocytes and impaired glucose homeostasis in differentiated mature 3T3-L1 adipocytes <sup>245</sup>. In the same study, IL-17-deficient mice also displayed enhanced fat mass, upon HFD feeding and even upon feeding a low-fat diet result in altered glucose homeostasis <sup>245</sup>.

#### h. $\text{CD8}^+$ T cells

$\text{CD8}^+$  T cell number increases in eWAT of HFD-fed mice and these cells are infiltrating into AT before macrophages, likewise contributing to macrophage recruitment. In line,  $\text{CD8}^+$  T cell depletion decreases macrophage infiltration, AT inflammation, and glucose sensitivity <sup>246</sup>. Moreover, CD11a, so-called integrin alpha L or ITGAL, participates in AT inflammation by facilitating  $\text{CD8}^+$  T cell infiltration and activation <sup>247</sup>.

#### i. B cells

B cells accumulate in VAT of diet-induced obese mice and impair glucose metabolism by the activation of pro-inflammatory macrophages, T cells, and production of pathogenic IgG antibodies <sup>(253), 249</sup>. Furthermore, Winer et al. showed that B cell depletion via anti-CD20 antibody treatment attenuates obesity-associated complications, while IgG transfer from obese mice to lean mice rapidly induce insulin resistance and glucose intolerance <sup>248</sup>. Additionally, they found that insulin resistance in obese individuals associated with a unique profile of IgG autoantibodies <sup>248</sup>. Moreover, Kim et al. revealed that the adipocyte-derived B-cell-activating factor (BAFF) is a pro-inflammatory adipokine and regulates adipose tissue distribution and systemic inflammation in obesity <sup>250</sup>. Furthermore, B2 subset within the AT promotes obesity-

induced IR through leukotriene LBT4/LBT4R1 signaling in mice <sup>251</sup>. In addition, activation of the IgG receptor Fc $\gamma$ RIIB in endothelium by hypo-sialylated IgG has been reported to stimulate obesity-induced insulin resistance in mice <sup>252</sup>. Subsequently, Frasca et al. identified and characterized AT-derived IgG antibodies with self-specificity in the plasma of obese individuals <sup>253</sup>.

In conclusion, even though, obesity and obesity-associated insulin resistance are multifactorial, pathophysiology is characterized by a state of chronic low-grade inflammation driven by different stimulus. Thus, targeting to inflammation hold promise against obesity-associated metabolic diseases. However, the complexity and diversity of inflammatory cells as well as pathways in response to diets, tissue micro-environments, gut microbiota-derived inflammation in obesity is challenging.

## 2. NON-ALCOHOLIC FATTY LIVER DISEASES

Non-alcoholic fatty liver diseases (NAFLD) comprise a spectrum of liver complications in individuals exclusive of significant alcohol consumption ranging from non or benign inflammatory, isolated, simple steatosis, also called Non-alcoholic fatty liver (NAFL) to inflammatory non-alcoholic steatohepatitis (NASH). According to the American Gastroenterological Association's clinical practice guideline, the diagnosis of NAFLD based on histology with steatosis that identified by triglyceride accumulation inside the hepatocytes, being the first stage <sup>254</sup>. NAFL further evolve into NASH that is characterized by lobular inflammation, hepatocyte ballooning, and potentially accompanied by some degree of fibrosis <sup>255</sup>. The predisposition of the fibrosis in NASH might ultimately progress into cirrhosis, which is a leading risk factor for the development of hepatocellular carcinoma (HCC) <sup>256</sup>. Pathogenesis of NAFLD is strongly associated with visceral obesity, T2D, and to some features of metabolic syndrome, including insulin resistance, dyslipidemia, and hypertension that are independent from the grade of obesity <sup>257</sup>. The global prevalence of NAFLD is rising dramatically in parallel to obesity, and frequently depending on the ethnicity of the population <sup>258</sup>. Highest prevalence rates are found in the Middle East (32%) and South America (31%), median proportions in Asia (27%), USA (24%), and Europe (23%), whereas the lowest ratio is in Africa (14%) <sup>259</sup>. Given the fact that no established pharmacological treatment exists for NAFLD, finding potential candidates to cure or prediction markers for the diagnosis that are the centers of interest by scientists.

## 2.1 Pathogenesis of obesity-dependent non-alcoholic fatty liver diseases

Crosstalk between AT and liver is the primary step in the development of obesity-induced NAFLD. As mentioned earlier, in advanced obesity, saturation of WAT storing capacity and enhanced lipolysis leads to excess FFAs load into the circulation. Since the liver is the central tissue for FA metabolism, the elevation of circulating FFA levels leads to excessive influx into the liver through uptake in hepatocytes via several transporters, including fatty acid transport protein 2 (FATP2), FATP5, FA-binding protein (FABP), FA-translocase (CD36), and caveolins<sup>260</sup>. FFAs are then esterified into triglyceride (TG) in the liver. Indeed, hepatic TG synthesis is considered as a protective mechanism to prevent lipotoxicity. Besides conversion into hepatic TG, FAs follow several fates in the liver, in which most circumstances they are the primary oxidative fuel that undergoes  $\beta$ -oxidation. Acetyl coenzyme-A (Acetyl-CoA) is the end product of the  $\beta$ -oxidation that support different purposes in the liver<sup>261</sup>. First of all, Acetyl-CoA can enter Krebs cycle and produce energy by oxidative phosphorylation (OXPHOS). Secondly, Acetyl-CoA is a substrate for cholesterol biosynthesis that is an active molecule for membrane, steroid hormones, and bile acid synthesis. Lastly, the liver converts unnecessary Acetyl-CoA into ketone bodies released into the circulation to supply energy to extra-hepatic tissues, such as brain, and heart, mainly during prolonged fasting<sup>261</sup>. At homeostasis, daily, the liver regulates substantial amounts of FAs, in response to dietary fat and simple carbohydrate sources, like fructose intake. However, it stores very-low quantities in the form of TG thanks to balanced FAs uptake from the plasma and hepatic *de novo* synthesis as well as the ratio of FA oxidation and excretion into the circulation by TG-rich very-low-density lipoprotein (VLDL)<sup>262</sup>. Nevertheless, this equilibrium is impaired in obesity-driven NAFLD, as a result of the increased hepatic *de novo* TG synthesis (lipogenesis) due to WAT lipolysis-induced FAs uptake, leading to the initiation of NAFL<sup>263</sup>. Hepatic *de novo* TG synthesis is catalyzed mainly by two enzymes: Acetyl-CoA carboxylase (ACC) and fatty acid synthase (FAS). These two enzymes are regulated by insulin-dependent sterol regulatory element-binding protein 1C (SREBP-1C) and glucose-dependent carbohydrate-responsive element-binding protein (ChREB) under the control of the Liver X receptor (LXR)<sup>264</sup>. Hyperinsulinemia and hyperglycemia, which are the characteristic symptoms of obesity-associated IR, possibly over-stimulate hepatic lipogenesis by the induction of the SREB1c and ChREB regulator enzymes, further contributing to the progression of NAFL. Indeed, an earlier study, using labeled isotopes, revealed that FA composition of the hepatic TG in NAFLD patients, were originating for 60% from WAT lipolysis-induced plasmatic FA uptake, for 25% from *de novo* TG synthesis, and for 15% from dietary intakes<sup>265</sup>. Recently, Roumans et al. showed that hepatic saturated FA fraction is associated with *de novo* lipogenesis and hamper hepatic insulin sensitivity in a

cross-sectional study<sup>266</sup>. The beta-oxidation of the long-chain fatty acids (LCFAs) takes place in the hepatic mitochondria following the transport and catalysis by carnitine-palmitoyl transferase-1 (CPT1), which is suppressed through insulin and malonyl-CoA, one of the intermediate products of lipogenesis<sup>267</sup>. Moreover, it has been shown that excessive FFAs in the liver are processed by omega-oxidation in a cytochrome P450 4A (CP4A)-dependent manner within the endoplasmic reticulum, which leads to hepatic IR, and apoptosis, contributing to NAFLD<sup>268</sup>. Eventually, the over-accumulation of TGs due to the imbalanced hepatic FA metabolism, stimulates lipotoxicity-induced hepatocellular injury and cell death<sup>269</sup>. Hepatocellular injury accompanied by mitochondrial dysfunction, oxidative and endoplasmic reticulum stresses activates the liver-resident macrophages, known as Kupffer cells (KCs) that stimulates the infiltration of other inflammatory immune cells into the liver by the release of cytokines and chemokines, triggering the transition from NAFL to NASH<sup>270</sup>. Furthermore, the persistence of inflammation and hepatocellular injury activates hepatic stellate cells (HSCs) that produce extracellular matrix (ECM) proteins in response to the transforming growth factor beta (TGF- $\beta$ ) and induce abnormal wound healing response, contributing to hepatic fibrosis (Figure 7).

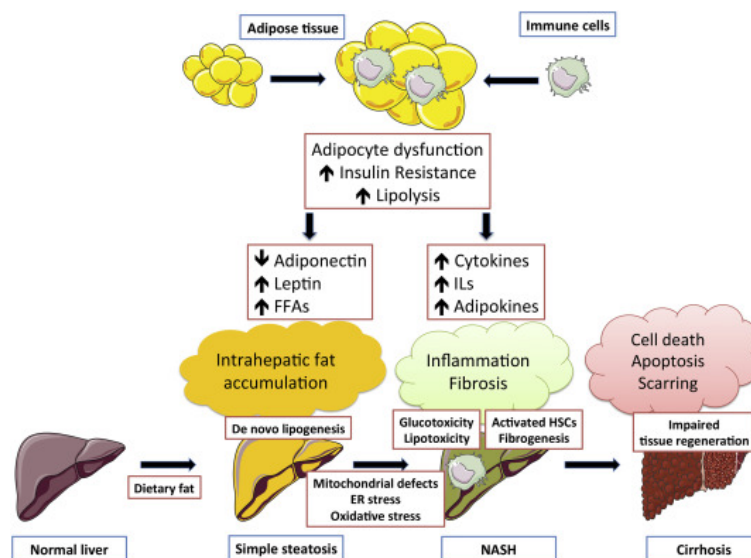


**Figure 7:** WAT-Liver crosstalk in the pathogenesis of obesity-dependent NAFLD. The expansion of adipose tissue in obesity diminishes its ability to store excess energy. Adipocyte dysfunction and IR are increased, leading to lipolysis. Consequently, circulating FFAs and leptin increase, and adiponectin decreases, resulting in intrahepatic fat accumulation (SS), which is further amplified by the high dietary fat and carbohydrates (commonly observed in obesity), the latter increasing *de novo* lipogenesis. Upon the expansion of adipose tissue, it is also infiltrated by immune cells that produce cytokines and ILs. When obesity is not successfully managed at the stage of SS, immune cells also infiltrate the liver further contributing to a low-grade, but chronic intrahepatic inflammatory process. Lipotoxicity and glucotoxicity

play central roles in both the development of SS and the subsequent progression to NASH. Mitochondrial defects, ER stress and oxidative stress link lipotoxicity and glucotoxicity with SS and NASH. When inflammation prolongs, fibrogenesis starts with HSCs as key players. Aggravation of fibrogenesis that may result in cirrhosis may represent an impaired mechanism of tissue regeneration, during the replacement of hepatocytes subjected to cell death or apoptosis is unsuccessful. Abbreviations: ER, endoplasmic reticulum; FFAs, free fatty acids; ILs, interleukins; HSCs, hepatic stellate cells; IR, insulin resistance; NASH, nonalcoholic steatohepatitis; SS, simple steatosis <sup>271</sup>.

## 2.2 Pathogenesis of obesity-independent non-alcoholic fatty liver diseases

Even though NAFLD strongly correlated with obesity, lean individuals can also suffer from NAFLD, known as lean NAFLD or non-obese NAFLD that is mostly found in the Asian population <sup>272</sup>. Several constituents have been associated with the pathophysiology of obesity-independent NAFLD, including genetic factors, diet, metabolic abnormalities, infectious-inflammatory disorders, and certain drugs <sup>273</sup>. Genetic polymorphisms in genes related to lipid metabolism have been implied as significant contributing factors in lean NAFLD patients. First, Romeo et al. revealed that genetic variations in the patatin-like phospholipase domain-containing protein 3 (*PNPLA3*) gene contribute to ancestry-related and inter-individual differences in hepatic fat content, as they found a variant allele (rs738409) that positively correlates with hepatic TG content and inflammation. In contrast, another variant allele (rs6006460), negatively correlates with this phenotype as identified by using a genome-wide association study in a population consisting of Hispanic, African American, and European American individuals <sup>274</sup>. Subsequent studies further discovered that the variants in the *PNPLA3* gene are not only correlated with hepatic TG content but also with NASH, fibrosis, and hepatocellular carcinoma dependent or independent from obesity, supporting lean NAFLD phenotype <sup>275, 276, 277, 278</sup>. Regarding this, Wei et al. reported that a large amount of non-obese individuals with NAFLD carry variants in the *PNPLA3* allele compared to obese NAFLD patients, suggesting that *PNPLA3* polymorphism is an independent risk factor for lean NAFLD by using a population-based study in China <sup>279</sup>. In addition, Adams et al. reported that the cholesteryl ester transfer protein (*CETP*) gene polymorphisms are the strong risk factor for the lean NAFLD <sup>280</sup>. Furthermore, a polymorphism in sterol regulatory element-binding factor 2 (*SREBF-2*) gene predisposes to lean-NAFLD <sup>281</sup>. Moreover, a single nucleotide polymorphism in transmembrane 6 superfamily member 2 (*TM6SF2*) allele is associated with hepatic TG content and fibrosis independently from age, obesity, insulin resistance, and *PNPLA3* genotype <sup>282</sup>. Dietary high cholesterol intake was proposed as a factor contributing to lean

NAFLD phenotype, in two independent studies comparing non-obese NASH individuals with BMI-matched control patients and obese NASH patients <sup>283, 284</sup>. In line, high cholesterol supplementation to the diet is one of the widely-used strategies to induce NAFLD in animal models without affecting obesity parameters <sup>285, 286</sup>. Overabundant cholesterol induces *de novo* lipogenesis by stimulating the LXR and oxysterol-dependent SREBP-1C pathway <sup>287</sup>. High fructose intake, especially the consumption of soft drinks, which contains large amounts of fructose corn syrup, has been associated with NAFLD, as fructose is mainly metabolized in the liver <sup>288</sup>. NAFLD has been reported in non-obese/lean individuals who display some metabolic abnormalities, such as insulin resistance, dyslipidemia, and hypertension <sup>289</sup>. This group of patients with a normal weight are known as metabolically obese and exhibit visceral adiposity more than subcutaneous adiposity <sup>290</sup>. Indeed, visceral adiposity has been recognized as an independent risk factor for lean NAFLD <sup>291</sup>. In a large cohort study, Sinn et al. found that lean NAFLD is a higher risk factor for incidence of diabetes than the presence of overweight/obesity without NAFLD, suggesting that individuals with lean NAFLD are more prone to develop metabolic abnormalities <sup>292</sup>. Chronic hepatitis C and B virus infections are the most common reasons for liver complications with prevalence of hepatic steatosis in infected individuals being about 50% of patients and with prevalence of progression into cirrhosis, and hepatocellular carcinoma being even higher <sup>293</sup>. Moreover, another cause of morbidity and mortality in chronic liver diseases is the human immunodeficiency virus (HIV) infection that leads to the whole spectrum of NAFLD and can co-exist with the chronic hepatitis C virus, worsening the phenotype <sup>294</sup>. Drug-induced steatosis is one of the well-recognized pathologies in NAFLD. Identified steatogenic drugs include acetaminophen, acetylsalicylic acid, amiodarone, diltiazem, tamoxifen, and several others <sup>295</sup>.

### 2.3 Role of gut microbiota in non-alcoholic fatty liver diseases

The portal vein mediates a functional and bidirectional interface that connects the gastrointestinal tract and liver, known as the entero-hepatic axis. Due to the symbiotic association with intestinal gut microbiota, function of the entero-hepatic axis is tightly interconnected with the immune system. As intestinal permeability is altered in obesity, bacteria and bacterium-related product, such as LPS translocation from the intestinal lumen to the circulation, and eventually into the tissues, such as liver via the portal vein, activating the immune system. Indeed, intestinal permeability has been shown to influence the pathogenesis of various chronic liver diseases, including NAFLD, not only by stimulating the immune system but also preventing the arrival of the beneficial microbial metabolites derived from the fermentation of carbohydrates and proteins by intestinal microbiome to the liver in various

animal models<sup>296</sup>. Accordingly, early clinical findings indicated that NAFLD patients display increased intestinal permeability with a high prevalence of bacterial overgrowth in small intestine compared to healthy individuals<sup>297, 298</sup>. Firstly, Le Roy et al. demonstrated that gut microbiota directly modulates NAFLD development independent from obesity by using fecal microbiota transplantation (FMT) from HFD-responder and not responder mice to the germ-free mice<sup>299</sup>. Furthermore, in a recent study, Mouries et al. showed that fecal microbiota transplantation from the HFD-fed mice into the germ-free mice causes dysbiosis-induced NASH development through WNT/ $\beta$  catenin signaling<sup>300</sup>. These findings imply that the effects of the diet on microbiome composition are able to trigger the NASH pathogenesis in the absence of the other factors related to HFD-feeding. The methionine choline-deficient (MCD) diet is another commonly used approach to induce NAFLD in experimental animals to investigate obesity-independent molecular mechanisms of the disease. It has also been reported that MCD diet-feeding leads to alteration of gut microbiota and metabolome with dysbiosis in mice<sup>301</sup>. Interestingly, a recent study, using microbiota depletion with broad-spectrum of antibiotic treatment, suggested that intestinal microbiota protect against MCD diet-induced steatohepatitis<sup>302</sup>. Moreover, Duarte et al. by comparing obese and lean patients with or without NASH, reported that gut-microbiome composition in lean individuals with NASH associated with liver damage independent from caloric intake in a small study awaiting confirmation<sup>303</sup>. Data regarding NAFLD and gut microbiota independently from obesity are quite limited. Recently, Yuan et al. observed that high ethanol-producing bacterial strain *Ksibella pneumonia* (HiAlc-*Kpn*) correlated with NAFLD in up to 60% of individuals in a Chinese cohort. Moreover, the transfer of clinically isolated HiAlc-*Kpn* from the patients to the mice by oral gavage induced NAFLD, suggesting that a high level of ethanol-producing bacterial strains in the gut microbiota contributes to NAFLD development, even without alcohol consumption<sup>304</sup>. Overall, the NAFLD pathogenesis consisting of multiple factors with a prominent role of local or systemic inflammation mediated by the immune system (Figure 8).

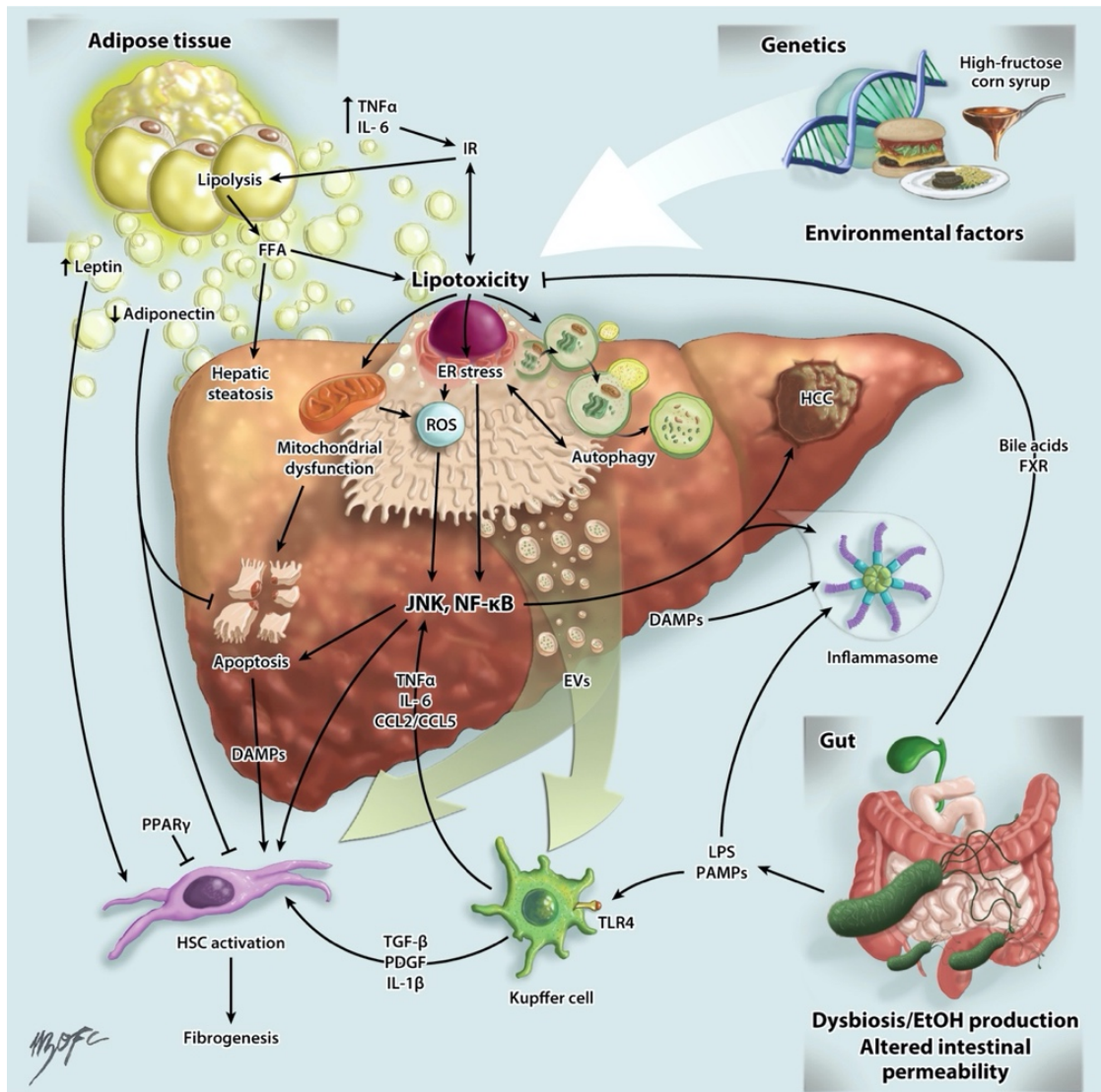


**Figure 8:** Overview of the NAFLD pathogenesis. The main components for the development and progression of the disease are diet, genetics, obesity with adipose tissue expansion and enhanced lipolysis due to IR, resulting in lipotoxicity, mitochondrial dysfunction, production of ROS, ER stress, autophagy, apoptosis, inflammasome activation, release of EVs, and ultimately HSC activation and fibrogenesis. Abbreviations: CCL2/CCL5, C-C motif chemokine ligand 2/5; DAMPs, damage-associated molecular patterns; ER, endoplasmic reticulum; EtOH, ethanol; EVs, extracellular vesicles; FFAs, free fatty acids; FXR, farnesoid X receptor; HCC, hepatocellular carcinoma; HSC, hepatic stellate cell; IL-6, interleukin 6; IR, insulin resistance; JNK, c-Jun N-terminal kinase; LPS, lipopolysaccharide; NAFLD, nonalcoholic fatty liver disease; NF- $\kappa$ B, nuclear factor kappa B; PAMPs, pathogen-associated molecular patterns; PDGF, platelet-derived growth factor; PPAR, peroxisome proliferator-activated receptors; ROS, reactive oxygen species; TGF- $\beta$ , transforming growth factor beta; TLR4, Toll-like receptor 4; TNF $\alpha$ , tumor necrosis factor  $\alpha$  <sup>305</sup>.

## 2.4 Impact of immune cells on health and non-alcoholic fatty liver diseases in Liver

As reported, the liver is a unique hemodynamic tissue in that around 30% of the total blood in the body is passing from hepatic artery and portal vessels through the liver every minute<sup>306</sup>. The hepatic portal vein provides to a large extent nutrients that represents nearly 80% of the blood flow to the liver, while the hepatic artery represents about 20% of the flow and supplies oxygen-rich blood<sup>307</sup>. Histologically, the hepatic artery, portal vein, and bile ducts are altogether known as, portal triade (Figure 9).

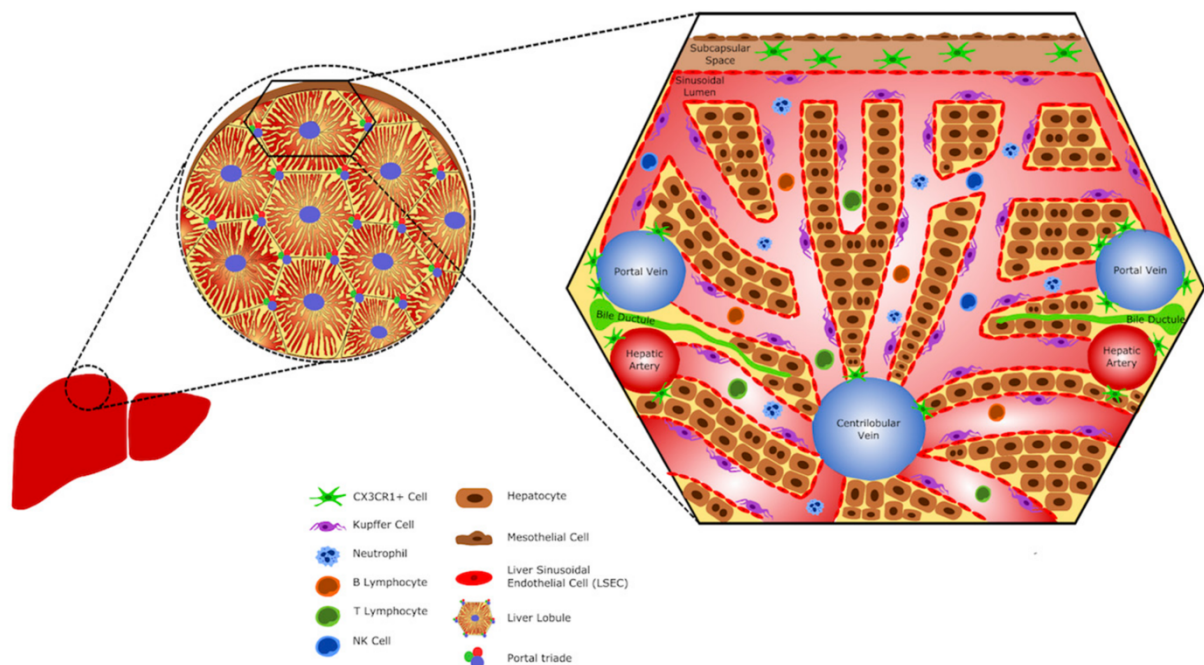


**Figure 9:** Hepatic immune and stromal cells. Schematic representation showing hepatic cells and their location. The liver harbors a large population of immune cells. Dendritic cells (CX3CR1+ cells) can be found in the subcapsular space and surround large vessels, as the centrilobular vein and the portal triade vessels (portal vein and hepatic artery). Kupffer cells are the liver resident macrophages and constitute the largest population of hepatic immune cells. They can be found within sinusoids, in contact with endothelial cells. Neutrophils, B lymphocytes, T lymphocytes, and NK cells eventually circulate in the sinusoids.<sup>308</sup>

Following its entry, the blood flowing through a honeycomb-like network of liver lobules that comprise of hepatocytes surrounded by the liver sinusoidal endothelial cells (LSECs) to be filtered within the sinusoidal lumen. Hepatic sinusoids, which are capillary-like canals that facilitate the blood filtration by slowing down the blood passage and maximizing the interaction with sinusoid-resident cells, including the LSECs, and several immune subsets, predominantly the Kupffer cells<sup>309</sup>. Indeed, the LSECs are the primary cell type involved in filtering process with the existence of the transcellular pores, named fenestrations. The pore size of the fenestrae is approximately 100nm diameter, many of which assemble into groups, known as sieve plates, allowing for the transition of specific molecules<sup>310</sup>. Due to the lack of basal lamina, the LSECs represent a gap, known as the space of Disse, which contains the hepatic stellate cells (HSCs) and further restrict direct interactions between hepatocytes and blood flow<sup>311</sup>. In fact, has been reported that hepatocytes and T lymphocytes stick out some membrane extensions by way of the fenestrae and reach out to each other in physiological settings<sup>312</sup>. Consequently, the filtered blood drains off from the liver through the hepatic centrilobular vein. Regulation of hepatic immune responses relies on the innate recognition of damage-associated molecular patterns (DAMPs) and pathogen-associated molecular patterns (PAMPs) as well as to antigen presentation to the adaptive immune cells and involved multiple interactions between hepatocytes, LSECs, HSCs, and liver-resident immune cells, which expressing cognate pattern recognition receptors (PRRs) and secrete modulator cytokines (Figure 10).

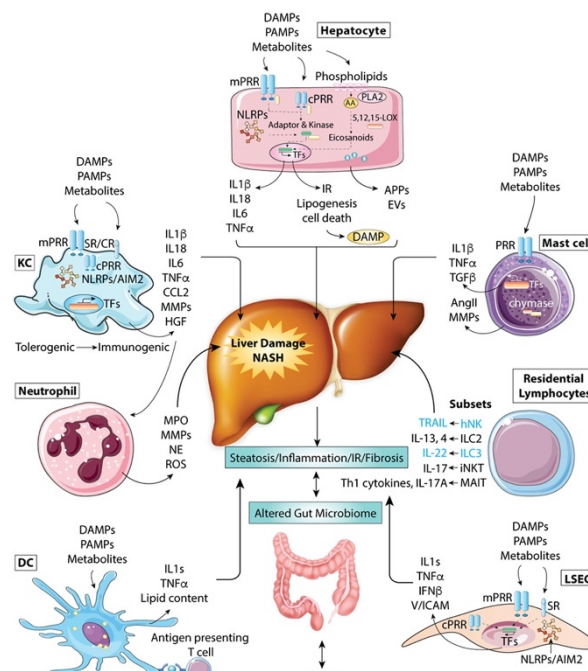


**Figure 10:** Crosstalk between hepatic stromal and immune cells in NAFLD. Liver contains a collection of immune cells. These include KCs, neutrophils, DCs, MCs, resident lymphocytes, hepatocytes, and LSECs. KCs, DCs, MCs, hepatocytes, and LSECs detect the presence of gut-derived P/MAMPs, endogenous DAMPs, and excessive metabolites mainly through PRRs, resulting in the increased release of proinflammatory cytokines and chemokines. These stressors also up-regulate expression of adhesion molecules in LSECs and, in combination with chemokines, stimulate recruitment of neutrophils and monocytes to the liver. Activated neutrophils initiate liver damage mainly by releasing enzymes and ROS. Apart from releasing proinflammatory cytokines, activated DCs also present antigens to T cells and initiate adaptive responses; KCs and hepatocytes regulate release and endocytosis of APPs, thus extending their innate immune function to extrahepatic organs; and KCs, MCs, and hepatocytes increase expression of MMPs, Ang II, TGF, and HGF to stimulate HSC activation and LF. In addition, innate immune signals also mediate metabolic changes (e.g., lipogenesis and IR) and cell apoptosis, pyroptosis, or necrosis in hepatocytes. KCs and LSECs express high levels of SR, which clears circulating molecules and organisms and is considered a critical mechanism that triggers the innate immune response. Innate-like lymphocytes, including NKs, ILCs, iNKTs, and MAITs, also generate multiple cytokines and influence their local microenvironment of the liver. Together, these events result in liver steatosis, inflammation, and fibrosis and lead to NASH and advanced complications. Abbreviations: CCL2, C-C motif chemokine 2; HGF, hepatic growth factor; MAMPs, microbe-associated molecular pattern molecules; ROS, reactive oxygen species; TF, transcriptional factor; Th1, T helper 1

313.

## 2.4.1 Immune guardians of homeostasis in liver

### a. Kupffer cells

Kupffer cells are liver-resident macrophage population, which represents a majority of total body macrophages and a sheer volume of hepatic non-parenchymal cell proportion in homeostasis that estimated to 80% and 20%, respectively<sup>314</sup>. Similar to other tissue-resident macrophages, the KCs primarily and transiently originate from c-Kit<sup>lo</sup> CD41<sup>lo</sup> primitive progenitors, in the yolk sac under the control of PU.1 transcription factor early in the mammalian development (E7.5)<sup>315</sup>. Following the formation of the heart and fetal cardiovascular system (E8-E8.5), c-Kit<sup>+</sup> CD41<sup>+</sup> CD93<sup>+</sup> FcγII and FcγIII<sup>+</sup> CD45<sup>lo</sup> hematopoietic progenitors, known as erythro-myeloid precursors (EMPs), derived from the yolk sac endothelium in a Runx-1- dependent manner, are seeded into the fetal liver at E9 and give rise to the KCs<sup>316</sup>. At the end of gestation, the hematopoietic stem cells (HSCs) migrate into the bone-marrow and take the place of the fetal liver as the site of hematopoiesis throughout the adult life<sup>317</sup>. Thus, EMP-derived tissue-resident macrophages are partly or entirely replaced by the HSCs-derived cells in the course of development except for microglia and KCs, which

are maintaining a distinct, self-renewal origin in EMPs<sup>318</sup>. Recently, Scott et al. revealed that the Clec4f surface marker is specific to KC, allowing to distinguish from the other macrophage subsets. Authors also showed that bone marrow-derived monocytes display KC-like phenotype in response to diphtheria toxin-mediated KC-depletion<sup>319</sup>. Sakai et al., in a recent study, also revealed that diphtheria toxin-induced KC depletion drives liver expression of several factors, including the delta-like canonical Notch ligand 4 (DLL4), TGF- $\beta$ , and desmosterol, which promote KC identity in bone marrow-derived monocytes by re-programming the transcriptomic landscape of KC-identity regulator, liver-X receptor (LXR)<sup>320</sup>. Thus, KCs are identified as CD11b<sup>+</sup> CD11c<sup>int</sup> F4/80<sup>hi</sup> CD64<sup>+</sup> CD68<sup>+</sup> Clec4f<sup>+</sup> (C-type lectin domain family 4, member f) cells in mice and CD68<sup>+</sup> CD14<sup>+</sup> in humans<sup>321</sup>. Presumably because of their non-monocytic origin at homeostasis, KCs are uniquely do not express fractalkine receptor CX3CR1, as reported previously<sup>322</sup>. Recently, Freitas-Lopez et al. confirmed by CXCR1 and F4/80 double staining and intravital imaging technique that at steady-state KCs do not express CX3CR1<sup>308</sup>. The principal function of the KCs is that phagocytose systemic and gut-derived pathogens from the bloodstream to sustain homeostasis at steady-state<sup>323</sup>. KCs contribute to immune homeostasis by inducing T<sub>reg</sub> response and priming tolerogenic CD8<sup>+</sup> T cells<sup>324, 325</sup>. In addition to that KCs regulate iron metabolism through eliminating hemoglobin-haptoglobin complexes<sup>326</sup> and erythrocyte-derived hemoglobin-containing vesicles from the circulation through the CD163 scavenger receptor<sup>327</sup>, likewise by modulating the hepcidin expression through IL-6-induced STAT3 signaling, which is the master regulator of body iron balance in homeostasis<sup>328, 329</sup>. Moreover, Wang et al. showed that the cholesteryl ester transfer protein (CETP), which is the regulator of high-density lipoprotein (HDL) and very-low-density lipoprotein (VLDL) levels in plasma mainly produced by KCs, suggesting KCs plays a role in cholesterol metabolism<sup>330</sup>. In addition to KCs, the hepatic portal triad-resident Ly6C<sup>hi</sup> monocyte-derived ferrotorpin-1-expressing macrophages participate cholesterol and iron metabolism at steady-state in mice<sup>331</sup>.

## b. Dendritic Cells

In homeostasis, liver contains the cDC<sub>1</sub>, cDC<sub>2</sub>, and pDC subsets that have been found in the portal triad, centrilobular vein, and space of Disse, and represent 1% of the total hepatic immune population<sup>332</sup>. Recently, a distinct subset of DCs has been identified with the particular morphological hallmarks, which possess broader and much more of numerous dendrites within the space of Disse, being the CX3CR1<sup>+</sup> cells<sup>322</sup>. Hepatic DCs originate from the HSCs and present unique characteristic features by displaying a tolerogenic and immature phenotype with lesser endocytic capacity, low MHC-II, and co-stimulatory molecule expressions at steady-state<sup>332</sup>. Furthermore, hepatic DCs have been shown to exhibit higher sensitivity to LPS-

induced maturation and provoke T cell hypo-responsiveness associated with expansion of T<sub>reg</sub> population even in homeostasis compared to splenic DCs<sup>333</sup>.

### c. Natural Killer Cells

The liver is the only tissue to harbor a vast quantity of natural killer cells (NKs) in the body, which approximately represent 50% of total hepatic lymphocytes, which are sentinel for viral and bacterial infections. NK cells regulate hepatic immune response both at homeostasis and pathological circumstances<sup>334</sup>. Indeed, liver is enriched by either hepatic-resident NK (hNK) cells and circulating NK (cNK) cells, which are distinguishable through the differential expression of the CD49a<sup>+</sup> DX5<sup>-</sup> and CD49a<sup>-</sup> DX5<sup>+</sup>, respectively in mice<sup>335</sup>. Development of hNK cells highly depends on the T-bet transcription factor, while cNK originates from Eomes<sup>336</sup>. Recently, several new transcription factors were found to be necessary for the maintenance of the NK cells among the aryl hydrocarbon receptor is specific to the hNK cells, while the  $\beta$ -interferon gene positive regulatory domain 1-binding factor (BLIMP1) and homologue of BLIMP1 in T cell (HOBIT) are common to both subsets<sup>337, 338</sup>. Functionally cNK cells primarily produce IFN $\gamma$ , whereas hNK cells produce a wide variety of cytokines and chemokines, including IFN $\gamma$ , TNF $\alpha$ , CCL3, CCL5, and CXCL16 in response to microbial stimulation<sup>339</sup>. The liver-resident NK cell subset has also been reported in humans as CD49<sup>+</sup> NK cells and their development is likewise dependent upon T-bet expression<sup>340</sup>. NK cells kill the HSCs in an inhibitory receptor NKG2D-dependent manner, thereby ameliorating fibrosis and contributing to homeostasis in mice as well as in humans<sup>341, 342</sup>.

### d. $\gamma\delta$ T cells

$\gamma\delta$ T cells reflect nearly 20% of the total hepatic T cell population at the steady-state and contribute homeostasis by producing mainly IL-17 that stimulates stromal cells to secrete IL-33, retaining T<sub>regs</sub><sup>343</sup>. Recently, Li et al. showed that activation, survival, and proliferation of the hepatic  $\gamma\delta$ T cells variable with gut microbiota composition and highly dependent upon hepatocyte-expressed CD1d receptor, apart from the TLRs or IL1/IL23 receptor signaling<sup>344</sup>.

### e. Invariant Natural Killer T cells

The invariant natural killer T cells (iNKTs) represents 40% of hepatic lymphocytes in mice, but only 3-5% in humans<sup>345</sup>. Survival and maintenance of hepatic iNKTs depend on the IL-7, IL-5, and some transcription factors that include BLIMP1, HOBIT, ID2, and the intracellular adhesion molecule 1 (ICAM1)<sup>346, 338</sup>. Among these factors, the chemokine receptor CXCR6

revealed to be the most important <sup>347</sup>. At homeostasis, hepatic iNKTs cells randomly patrol within the sinusoidal lumen by a crawling movement, seeking for a potential threat either in a identical way than in blood flow or the opposite, as shown by intravital imaging <sup>348</sup>.

#### f. Mucosal-associated invariant T cells

Mucosal-associated invariant T cells (MAIT) are a member of the  $\alpha\beta$  T cells and described with their semi-invariant TCR receptors, which contain the invariant V $\alpha$ 7.2 chain in general rearranging by either with J $\alpha$ 12, 20, or 33 fragment together with the variable  $\beta$ -chains <sup>349</sup>. Predominantly, MAIT found in the gut lamina propria, but also in liver where they account for 20-50% of the hepatic innate-like T lymphocyte population <sup>350</sup>. Activation of the MAIT relies on the antigen presentation, in which bacteria-produced vitamin B metabolites, such as 6-hydroxymethyl-8-D-ribityllumazine, acetyl-6-formyl-pterin, 6-formyl-pterin by the MHC-I-related gene protein MR1 in mice as well as in humans <sup>351</sup>. Upon activation, the MAIT cells produce a vast amount of pro-inflammatory cytokines, including IFN $\gamma$ , TNF $\alpha$ , IL17, IL22, and are also able to lysis bacteria-infected cells by granzyme B and perforin secretion <sup>352</sup>. In line, MAIT are lack within the germ-free mice, and a recent study, Legoux et al. reported that microbial metabolites, such as 5-(2-oxopropylideneamino)-6-D-ribityl-amino-ouracil (5-OP-RU) control the thymic development of the MAIT <sup>353</sup>. Of note, MAIT are reported to be also activated by the MR1/TCR-independent manner in response to anti-viral cytokines, such as IL-12, IL-18, IL-15, and IFN $\alpha/\beta$  in viral infections, including HIV, hepatitis B, and C by mainly producing IFN $\gamma$  <sup>354, 355, 356</sup>.

#### g. Regulatory T cells

At steady state hepatic CD4<sup>+</sup> T cell population is less abundant than CD8<sup>+</sup> T cell population respectively, which reflects approximately 40% and %60 of total TCR $\alpha/\beta$ <sup>+</sup> T cell population. CD25<sup>hi</sup> CD127<sup>int</sup> FoxP3<sup>+</sup> T<sub>regs</sub> are prevalent among the CD4<sup>+</sup> T cell fraction <sup>357</sup>. At homeostasis, two crucial functions of the T<sub>regs</sub> are that to restrict hepatic inflammation by mainly secreting the IL-10 and TGF- $\beta$  cytokines, also maintaining self-tolerance through regulating auto-reactive T cells within the sinusoidal lumen and nearby portal tract <sup>358</sup>. Indeed, in a recent study, Li et al. revealed that hepatic neonatal T<sub>regs</sub> are critical to ensure self-tolerance and liver maturation at steady-state <sup>359</sup>. T<sub>regs</sub> are highly sensitive to IL-2 in connection with the high expression of CD25, which is the receptor for IL-2 cytokine. Production of IL-2 from other T cells activates IL-2 signaling in T<sub>regs</sub> that leads to phosphorylation of the STAT5, regulating their differentiation, proliferation, and survival <sup>360</sup>. Moreover, human hepatic T<sub>regs</sub> have also been shown to require IL-2 cytokine from the effector cells for survival <sup>361</sup>.

#### h. CD8<sup>+</sup> Memory T cells

At homeostasis, liver contain a specific CD8<sup>+</sup> T cell subset, characterized as T-bet<sup>lo</sup> Eomes<sup>lo</sup> Blimp-1<sup>hi</sup> Hobit<sup>lo</sup> CD69<sup>+</sup> CD103<sup>+</sup> CXCR3<sup>+</sup> CXCR6<sup>+</sup> liver-resident memory T cells (T<sub>RM</sub>) that patrol the space of Disse close to the hepatic veins, supplying quick and powerful responses against invasive pathogens <sup>362</sup>. The liver-resident CD8<sup>+</sup> T<sub>RM</sub> are strongly associated with malaria infection in mice and required for long-term protection <sup>363</sup>. In a recent study, Olsen et al. proposed a combined prime-and-trap strategy to fight against pre-erythrocytic malaria infection by which priming the protective liver-resident CD8<sup>+</sup> T<sub>RM</sub> <sup>364</sup>. Moreover, the inflammatory and antigenic signals dictate the development of a high amount of liver-resident CD8<sup>+</sup> T<sub>RM</sub> subsets, requiring IL-15, with a half-life of 36 days in mice <sup>365</sup>. Furthermore, Feau et al. showed that the IL-2, necessary for the expansion CD8<sup>+</sup> T<sub>RM</sub> population, is mainly provided by CD8<sup>+</sup> T cells, rather than CD4<sup>+</sup> T cells in mice <sup>366</sup>. In line, IL-2-expressing liver-resident CD8<sup>+</sup> T<sub>RM</sub>, are considered as sentinels for hepatotropic infection in the human liver <sup>367</sup>.

#### i. B cells

In mouse, hepatic B cell subsets include small numbers of B220<sup>+</sup>IgM<sup>+</sup>CD23<sup>-</sup>CD43<sup>+</sup> B1 subset and large quantities of bone marrow-derived mature B220<sup>+</sup>IgM<sup>+</sup>CD23<sup>+</sup>CD43<sup>-</sup> B2 subset at steady-state <sup>368</sup>. Functionally, B2 cells need T helper cells for proliferation and isotype switch that result in the production of highly antigen-specific antibodies <sup>369</sup>. Nonetheless, the maturation of B1 cells occurs independently from the T cells, which are the principal sources of natural, poly-specific (cross-reactive) IgM antibodies against both self and microbial antigens <sup>370</sup>. Therefore, together with their cross-reactive natural antibody production ability, IL-10-producing regulatory B cells (B<sub>regs</sub>), maintaining hepatic homeostasis <sup>371</sup>.

### 2.4.2 Immune drivers of inflammation in Non-Alcoholic Fatty Liver Diseases

#### a. Kupffer Cells, recruited monocytes, and macrophages

Since KCs express several receptors, such as the scavenger, complement, and PRRs, they sense and are quickly activated by pathogens or metabolic abnormalities. Activated KCs, initiate the hepatic immune response through expanding their number, the release of the immune modulators (cytokines i.e. TNF $\alpha$ , IL-1 $\beta$ , IL6 and chemokines i.e. CCL2/CCL5), the recruitment of other immune subsets to the liver, such as monocytes, pro-inflammatory macrophages, and, based on the state of the damage, exacerbate or resolve the injury by coordinating the tissue-repair process. Besides infection, KCs are also at the center of the

initiation, progression, and regression of NAFLD, as revealed by several experimental settings. One of the robust evidence in that the depletion of KCs, by gadolinium chloride or clodronate liposome techniques, protects against diet-induced hepatic steatosis and insulin resistance in rodents <sup>372, 373</sup>. In the pathophysiology of the NAFLD, KCs are activated by diverse stimuli. Lipotoxicity-induced hepatocellular injury, characterized by oxidative stress, endoplasmic reticulum stress, mitochondrial dysfunction, and cell death causes the secretion of DAMPs, such as the high mobility group protein 1 (HMGB1), which believed to be the primary inducer of KCs <sup>374</sup>. Besides, cholangiocytes, which are the epithelial cells of the bile duct, LSECs, and HSCs contribute to the KCs activation by secreting DAMPs <sup>375</sup>. On the other hand, as a result of the intestinal permeability altered in NAFLD, the gut-derived PAMPs, including LPS, flagellin, bacterial-derived products that bind to TLR4, and activate KCs, leading to release of a massive amount of pro-inflammatory cytokines, including TNF $\alpha$ , and IL-1 $\beta$  <sup>376</sup>. The excessive LDL is mostly in its oxidized form (ox-LDL), due to the lipotoxicity-induced oxidative stress in NAFLD. KCs capture the toxic ox-LDL by the two principal scavenger receptors, which are the SR-A and CD36, that leads to the formation of foamy KCs with cholesterol crystals, prompting hepatic inflammation <sup>377, 378</sup>. Moreover, activated KCs stimulate fat accumulation within the hepatocytes in part due to IL1- $\beta$ -dependent suppression of the PPAR $\alpha$  activity, which in turn down-regulate fatty acid oxidation related genes, favoring hepatic steatosis <sup>379</sup>. Interestingly, Wan et al. observed an M2-like alternatively polarized KC subset that promotes M1-like proinflammatory KC apoptosis in morbidly obese patients with minimal hepatic injury and steatosis compared to patients with severe liver problems. These findings were also confirmed in animal models by the authors, suggesting the balance between anti-inflammatory and inflammatory milieu shaping the KC identity in NAFLD <sup>380</sup>. Indeed, the persistence of the hepatic inflammatory environment stimulates KCs to recruit pro-inflammatory immune cell infiltration into the liver, progressing from NAFL to NASH phenotype. During the inflammatory phase, KCs promotes hepatic monocyte infiltration mainly by producing the monocyte chemoattractant protein 1 (MCP-1/CCL2) through activation of CCR2, which is expressed by monocytes <sup>381</sup>. Indeed, a strategy to target pharmacological inhibition of CCL2 decreases macrophage infiltration and steatohepatitis <sup>382</sup>. Alternate chemokine signaling pathways, such as the, CXCR3/CXCL10, CCR1/CCL5 (RANTES), and CCR8/CCL1, contribute hepatic monocyte recruitment, favoring a NASH phenotype <sup>383, 384, 385</sup>. Idrissova et al. determined that the deletion of the TNF related apoptosis-inducing ligand (TRAIL) receptor in mice reverse metabolic outcomes in response to high saturated fat, cholesterol, and fructose feeding, implying that the TRAIL involved in bone marrow-derived monocyte/macrophage recruitment <sup>386</sup>. Circulating monocytes are considered to give rise to the hepatic monocyte-derived macrophage subset in NASH <sup>387</sup>. Indeed, Beattie et al. revealed that the bone marrow-derived macrophages and KCs exhibit distinct transcriptomic signatures, nevertheless comparable

biological functions <sup>388</sup>. In a recent study, Seidman et al. by performing single-cell RNA sequencing (scRNA-seq) on liver non-parenchymal cells from standard or NASH diet fed mice identified five major hepatic macrophage populations, which are healthy KC (KC-H), NASH KC (KC-N), recruited macrophages occupying the KC-N niche (KN-RM), Ly6C<sup>hi</sup>-RM, and Ly6C<sup>low</sup>-RM <sup>389</sup>. Authors revealed that the KC-H, KC-N, and KN-RM mutually express high levels of *Adgre1* (F4/80) and low levels of *Cd11b* as well as KC lineage-determining *Mafb* and *Maf* genes, coding for BZIP transcription factors, while Ly6C<sup>hi</sup>-RM express *Ly6c2*, *Chil3*, *F13a1*, *Fn1* and Ly6C<sup>low</sup>-RM express *Cd2091*, *CD7*, and *Itgax* <sup>389</sup>. They also performed fate-mapping analysis and found that KC-N cells are long-lived and originate from embryonic KCs, while KN-RM, Ly6C<sup>hi</sup>-RM, and Ly6C<sup>low</sup>-RM are short-lived and derive from HSCs <sup>389</sup>. Moreover, authors employed diphtheria toxin (DTR)-driven KC ablation (*Clec4f-creR26-iDTR*) and showed that KN-RM are able to re-populate KC niche and contribute to NASH pathogenesis, as similar to the embryonically derived KCs <sup>389</sup>. Furthermore, they also showed that NASH microenvironments induce apoptosis of KC-H cells and impair their regulatory transcriptomic landscape, which result in acquisition of KC-N phenotype through reprogramming the transcriptomic landscape of liver-X receptor (LXR)-mediated KC-signature <sup>389</sup>. Authors also identified by analyzing LXR CHIP-seq and gene expression data obtained from KC-N and KN-RM fate-map strategy, several potential NASH-dependent LXR binding partners that are responsible for LXR-dependent transcriptomic landscape remodeling, for example, ATF3 as a gain of function partner and Spic as a loss of function partner <sup>389</sup>. More recently, two independent studies using different NASH models also confirmed that embryonic KCs (EmKCs) are dying in the course of NASH pathogenesis and are replaced by monocyte-derived macrophages (MoKCs) <sup>390,391</sup>. Tran et al. by using BM chimerism and parabiosis strategies, identified that TIM4<sup>+</sup> Clec2<sup>+</sup> (*Clec2* was used as a KC marker instead of *Clec4f*) EmKCs were gradually replaced by TIM4<sup>-</sup> Ly6C<sup>hi</sup> MoKCs with the progression of MCD-induced NASH development in mice <sup>390</sup>. Authors showed that NASH alters EmKCs self-renewal by causing their death, while MoKCs acquire self-renewal capacity, evidenced by long-term survival and proliferation <sup>390</sup>. Importantly, they found MoKCs store less lipid droplets than EmKCs and exhibit higher pro-inflammatory markers under NASH diet, suggesting that MoKCs are more prone to lipid-induced stress and inflammation <sup>390</sup>. They also showed that DTR-mediated EmKC depletion leads to enrichment of MoKCs and severe liver damage as well as hepatic fibrosis development in response to NASH-inducing diet <sup>390</sup>. Remmerie et al. by combining CITE-seq technology and BM chimerism approach, found a similar gradual loss of Clec4f<sup>+</sup> TIM4<sup>+</sup> EmKC and their replacement with monocyte-derived Clec4f<sup>+</sup> TIM<sup>-</sup> MoKCs with the progression of Western diet-induced NASH development in mice <sup>391</sup>. In line with the findings of Tran et al. <sup>390</sup>, authors also discovered MoKCs contain less lipid droplet than EmKCs <sup>391</sup>. Interestingly, they identified a distinct monocyte-derived macrophage population,

characterized as Ly6C<sup>hi</sup> Clec4f<sup>-</sup> Spp1<sup>+</sup> Trem2<sup>+</sup> CD9<sup>+</sup> cells that resemble to recently described lipid-associated macrophages (LAMs) in obese WAT<sup>194</sup> thus, named hepatic LAMs<sup>391</sup>. Authors revealed that LAMs exhibit an altered transcriptome compared to MoKCs and EmKCs with the highest lipid metabolism rate in response NASH, however function of these osteopontin-expressing cells has not been explored in detail<sup>391</sup>. Pro-inflammatory milieu found during NASH stimulates hepatocytes to produce a large number of complement proteins. Following the binding to their target antigens, the complement proteins cleaved to create active fragments and complement-opsonized particles, which are efficiently phagocytosed by KCs via the complement receptors that include CR1, CR3, CR4, CR5aR, and CR1g<sup>313</sup>, contributing to the pathogenesis as also reported in NASH patients<sup>392</sup>. Additionally, KCs are involved in hepatic fibrosis development as they activate the HSCs by releasing pro-fibrotic cytokines TGF- $\beta$  and platelet-derived growth factor (PDGF). Conversely, HSCs produce the tissue inhibitors of metalloproteinases (TIMPs) and extracellular matrix components (ECM)<sup>393</sup>. KCs trigger extracellular matrix degradation being the primary source of the various matrix metalloproteinases, including MMP9, -12, and -13, thus leading to resolve the fibrosis<sup>394, 395, 396</sup>. Recruited Ly6C<sup>hi</sup> monocyte-derived proinflammatory macrophages also directly communicate and activate HSCs by TGF- $\beta$  to promote hepatic fibrosis<sup>397</sup>. Recently, the stimulator of interferon genes (STING) in monocyte-derived macrophages was found to correlate with the progression of liver inflammation and fibrosis in individuals with NAFLD<sup>398</sup>. Moreover, recruited Ly6c<sup>low</sup> monocyte-derived macrophages have also been linked to the resolution phase of the hepatic fibrosis by secreting MMPs<sup>399</sup>. Selective deficiency of infiltrating macrophages by using the CD11b-diphtheria toxin receptor transgenic mice, decreases fibrosis development, but by contrast, during the state of resolution, aggravates hepatic fibrosis<sup>400</sup>. These findings highlights the significance of phenotypic flexibility of the KCs, recruited monocyte, and macrophage entity in response to environmental and metabolic signals<sup>400</sup>.

## b. Dendritic Cells

Given the fact that lack of specific markers to target hepatic DCs and diversity in the employed animal models, i.e., diets, duration, genetic background, the role of DC in NASH remains unclear. In this regard, Henning et al. showed in mice with CD11c-DTR-mediated depleted DCs, intrahepatic inflammation is exacerbated in response to MCD-feeding, suggesting hepatic DCs are protective against NASH by ignoring the absence of DC specificity<sup>401</sup>. On the other hand, Suitti et al. claimed that the inflammatory hepatic CX3CR1<sup>+</sup> DCs, which arises from the bone marrow, contribute to NASH progression in MCD-fed mice<sup>402</sup>. Besides, Ibrahim et al. suggested that the hepatic environment and cellular lipid content determines the phenotype of

DCs, as they found that hepatic lipid-rich DCs are immunogenic, activating T, NKT, and NK cells. Nonetheless, the hepatic lipid-poor DCs are tolerogenic, which induce activation of the T<sub>regs</sub>, in both mice and humans, facilitating DC discrimination<sup>403</sup>. Moreover, Heier et al. identified that CD103<sup>+</sup> cDC<sub>1</sub> subset protects against the metabolic challenges upon high-sucrose and MCD diets in mice<sup>404</sup>. Interestingly, in a recent study, Aarts et al. revealed that DC-CD40-deficient mice obtained by crossing CD40 floxed mice with CD11c Cre mice, displayed severe obesity and liver steatosis with a considerable reduction of the T<sub>regs</sub> number compared to control group in response to the HFD-feeding. Nevertheless, under a NASH-inducing diet, hepatic inflammation decreased without affecting hepatic lipid content in DC-CD40-deficient mice, suggesting CD40<sup>+</sup> CD11c<sup>+</sup> DC subset acts as a double-edged sword by contributing inflammation in NASH and protecting against metabolic syndrome<sup>405</sup>. Likewise, Connolly et al. reported that hepatic DCs display a pro-inflammatory phenotype, which induces inflammation and progression of fibrosis, as they have been shown improved phenotype by using CD11c-DTR mice to deplete DCs in a fibrotic model<sup>406</sup>. It has also been reported that CD11c-DTR mice, which have depleted DCs, subjected to the carbon tetrachloride-induced liver fibrosis, manifests prolonged regression of fibrosis<sup>407</sup>. Our group recently demonstrated that increased extracellular free fatty acids (FFAs) profoundly affect DC immune function, primarily via modification of DC intracellular metabolism<sup>408</sup>. Compared to stimulation with TLR ligands alone, BM-derived DCs, which differentiated into mostly cDC<sub>2</sub>-like phenotype displayed a distinct cytokine and metabolic response when treated with TLR ligands in the presence of FFAs with synergistic IL-23A production as a hallmark<sup>408</sup>. Our group, also performed a comprehensive blood immunophenotyping combined with hepatic transcriptomic analysis of a large cohort of NAFLD patients<sup>409</sup>. It was found that in the blood, cDC<sub>1</sub> cells were inversely correlated with histological features of NASH (especially lobular inflammation), while cDC<sub>2</sub> were positively correlated with hepatic lesions<sup>409</sup>. In parallel, the hepatic transcriptome of patients with NASH was enriched in genes closely associated with cDC functions, especially with antigen presentation and specific cytokines and chemokine, such as IL18, CXCL10, and IL23A that are also synergistically upregulated by TLR and FFAs<sup>409</sup>. Moreover, intrahepatic immunophenotyping of a diet-induced murine model of NASH revealed changes in a number of immune cell populations that paralleled those observed in blood from NAFLD patients, notably decreased cDC<sub>1</sub> and increased cDC<sub>2</sub> in NASH<sup>409</sup>. These data highlights importance of considering the metabolic environment for the understanding the hepatic immune system activation in NAFLD<sup>409</sup>. Collectively, this paper clearly implicates hepatic cDC in the development and resolution of NASH in mice as well as in humans<sup>409</sup>.

### c. Neutrophils

Upon activation, KCs early on mainly recruit neutrophils into the inflamed liver by the CXCR1/CXCR2 chemokine signaling ligands that include CXCL1, CXCL2, and CXCL8<sup>410</sup>. There is a positive correlation between NAFLD and hepatic neutrophil infiltration, thus neutrophil myeloperoxidases (MPOs) is a good predictive marker of the severity of the disease progression<sup>411</sup>. Indeed, overproduction of neutrophil MPOs aggravates NASH in mice while, MPO-deficient mice have an opposite phenotype<sup>412</sup>. Pulli et al. revealed, by using the MCD-fed mice model, the underlying mechanism in that MPO leads to oxidative stress that directly kills hepatocytes and macrophages, increases mitochondrial permeability through pore formation and it furthermore activates the HSCs, contributing to NASH pathogenesis<sup>413</sup>. Moreover, neutrophil elastases have also been shown to mediate insulin resistance, thereby enhancing inflammation<sup>213</sup>. Consequently, the antibody-based depletion of neutrophils ameliorates diet-induced NAFLD in mice<sup>414</sup>. Besides, neutrophil extracellular trap (NET) formation upon activation by DAMPs favors the hepatic sterile inflammatory injury<sup>415</sup>. In addition, hepatocyte and neutrophil crosstalk regulates the NET formation upon bacterial antigen exposure, which might be counteract increased gut permeability associated to NASH<sup>416</sup>.

### d. Natural Killer Cells

Even though hepatic NK cells are essential to homeostasis, NK cells polarize KCs towards M1-like inflammatory phenotype in response to MCD-feeding in mice<sup>417</sup>. Moreover, a spontaneous NASH development is observed in the principal methyl donor, the glycine-methyltransferase (GMNT)-deficient mice, is NK cell-dependent, through increasing the hepatic proinflammatory milieu<sup>418</sup>. Since the proinflammatory cytokine IL-15 is necessary for NK cell maturation and function<sup>419</sup>, IL-15-driven NASH development is also mediated by NK cells<sup>419</sup>. The metabolic checkpoint kinase mTOR is the master regulator of the IL-15 signaling during the NK cell development and activation<sup>420</sup>. Likewise, osteopontin (OPN) has also been shown to regulates the development and function of the NK cells<sup>421, 422</sup>. Consequently, alteration of NK cell function in response to PPAR $\gamma$ -mediated suppression of mTOR signaling has been linked to NAFLD in obese patients<sup>423, 424</sup>. Furthermore, in a recent study, Assman et al. revealed that the Srebp-1 transcription factor regulates glucose and lipid metabolism in NK cells and leads to cytokine-induced metabolic reprogramming of NK cells from anti-inflammatory phenotype to pro-inflammatory phenotype, determining their effector function<sup>425</sup>.

#### e. Natural Killer T cells

The hepatic number of the NKT cells increases dramatically with NASH. Their recruitment mediated by hedgehog signaling-dependent production of the CXCL16 and the vascular cell adhesion molecule 1 (VCAM-1) leading to induction of OPN synthesis by NKT cells that drive fibrinogenesis in mice and humans<sup>426</sup>. Recently, Maricic et al. showed that hepatic IL-17<sup>+</sup> IL22<sup>+</sup> iNKT cells switch to an IFN $\gamma$ <sup>+</sup> IL-4<sup>+</sup> IL-13<sup>+</sup> iNKT phenotype during the progression in the choline-deficient L-amino acid-defined (CDAA) diet-induced mouse NASH model. Furthermore, steatosis and fibrosis development in this model is mediated by IFN $\gamma$ <sup>+</sup> IL-4<sup>+</sup> IL-13<sup>+</sup> iNKT cells throughout the recruitment of the inflammatory macrophages, CD8<sup>+</sup> T cell, and activation of the HSCs<sup>427</sup>. Moreover, NKT cells induce hepatocyte FA-uptake by the lymphotoxin beta receptor (LT $\beta$ R)-ligand LIGHT, also known as tumor necrosis factor superfamily member 14 (TNFSF14) and together with CD8<sup>+</sup> T cells, lead to liver damage and HCC development in response to the choline-deficient high-fat diet<sup>428</sup>. Regarding that, in a recent study, a Spanish group confirmed that the genetic deficiency of the LIGHT exhibits improved glucose homeostasis and hepatic steatosis in the high-fat high-sucrose diet-fed mice<sup>429</sup>.

#### f. CD4<sup>+</sup> T cells

The secretion of increased pro-inflammatory cytokines, like TNF $\alpha$  and immunoregulatory cytokine IFN $\gamma$  by various hepatic immune cell types not only recruits T-bet<sup>+</sup> STAT2<sup>+</sup> STAT4<sup>+</sup> CD4<sup>+</sup> T<sub>h</sub>1 cells but also induces polarization of the hepatic naïve CD4<sup>+</sup> T cell population into CD4<sup>+</sup> T<sub>h</sub>1 subset, increasing total CD4<sup>+</sup> T cell quantity in the liver of mice and humans with NASH<sup>430</sup>. The T<sub>h</sub>1 cells further contributes to the hepatic inflammation by IFN $\gamma$ , TNF $\alpha$ , and IL-2 production and stimulating pro-inflammatory macrophage polarization. Furthermore, hepatic, and circulating IFN $\gamma$ -producing T<sub>h</sub>1 cells are enriched in NASH patients and mouse models<sup>431</sup>,<sup>432</sup>. Relatedly, IFN $\gamma$ -deficient mice displayed alleviated hepatic inflammation and fibrosis, by restricting the inflammatory phenotype of macrophages in animals fed with a NASH-inducing diet<sup>433</sup>. Hepatic T<sub>h</sub>17 are also increased in mice fed with HFD, as well as in NASH patients compared to healthy control groups and neutralization of IL-17 attenuate hepatic steatosis and inflammation, thus T<sub>h</sub>17 cells facilitate the progression from simple steatosis to NASH<sup>434</sup>. Similarly, Harley et al. showed that IL-17RA-deficient mice exhibit decreased hepatocellular damage and steatosis in response to HFD feeding. Moreover, alteration of IL-17 production by modulation to the colonization of mice with segmented filamentous bacteria suggested that the IL-17 axis is central to the development and progression of NAFL to NASH<sup>435</sup>. Besides, Rau et al. confirmed that NAFL to NASH progression characterized by an increase in IL-17<sup>+</sup> T cells among the intrahepatic CD4<sup>+</sup> T cells and peripheral blood ratio of T<sub>h</sub>17/T<sub>regs</sub> as compared to

lean individuals with NAFL and NASH patients<sup>436</sup>. It has also been reported that IL-17 directly activates the HSCs to produce TGF- $\beta$ , alpha-smooth muscle actin ( $\alpha$ -SMA), collagen type-I by inducing the STAT3 signaling pathway, contributing to hepatic fibrosis formation<sup>437, 438</sup>.

#### g. CD8<sup>+</sup> cytotoxic T cells

Hepatic CD8<sup>+</sup> cytotoxic T cells expand during NAFL to NASH transition. CD8<sup>+</sup> T cells recognizes damaged or infected cells via MHC-I receptor, which are killed through the release of various cytokines and cytotoxic molecules that include perforin and granzymes in mice and humans<sup>439, 428, 409</sup>. Recently, Ghazarian et al. showed that the accumulation of CD8<sup>+</sup> cytotoxic T cells within the liver is mediated by the hepatic type-I interferon (IFN-I) responses, as suggested by increased interferon regulatory factors (IRFs), interferon stimulatory genes (ISGs), and IFN $\alpha$  protein expressions in HFD-fed mice. Furthermore, whole-body IFN $\alpha$ R1-deficient or CD8-specific IFN $\alpha$ R1-deficient chimeric mice are protected from HFD-induced liver complications, which results improved hepatic insulin sensitivity and gluconeogenesis<sup>440</sup>. Relatedly, CD8<sup>+</sup> T cell-deficient mice fed a high-fat high sucrose (HFHS) supplemented with high cholesterol diet, which is a progressive murine NASH model, exhibited alleviation of the hepatic steatosis and fibrosis together with the decreased number of activated KCs and immune cell infiltration compared to wild-type mice as well as in humans with NASH<sup>441</sup>. Moreover, Breuer et al. showed that hepatic CD8<sup>+</sup> T cells increased in obese and hyperlipidemic NASH mice, upon feeding a western diet and are positively correlated to HSCs activation, while the CD8 and LDLR (low-density lipoprotein receptor) double-deficient mice displayed a significant reduction in hepatic inflammation upon feeding with a Western diet. Furthermore, depletion of the CD8<sup>+</sup> T cells in a lean NASH model obtained by MCD diet feeding, neither affected hepatic inflammation nor HSCs activation<sup>442</sup>. Interestingly, genetic ablation of the CD8<sup>+</sup> cytotoxic T cell protein perforin in mice leads to excessive hepatic fat accumulation and lobular inflammation in response to MCD diet or HFD feeding by causing inflammatory polarization of the recruited bone marrow-derived monocytes and macrophages, pointing towards immunoregulatory role of the CD8<sup>+</sup> T cells. Moreover, perforin-deficient mice also display an increase in accumulation, survival, activation, and proinflammatory cytokine production of CD8<sup>+</sup> T cells but neither NK cells or CD4<sup>+</sup> T cells, presumably as compensatory mechanism, which confirmed by their transcriptome by RNA-sequencing data. In line, elevated plasmatic perforin levels and hepatic perforin expression were observed in individuals with NASH<sup>443</sup>. In accordance, our group also evidenced an increased in blood perforin-expressing CD8<sup>+</sup> T cells as well as in hepatic perforin and granzyme A-expressing CD8<sup>+</sup> T subset that positively correlate with the severity of disease in a large NAFLD patients cohort<sup>409</sup>.

## h. B cells

Hepatic B cell populations expand strikingly in NASH. The B cell-activating factor (BAFF) is the stimulator of the B cell differentiation and expansion accounts for increased serum immunoglobulin levels and is associated with the histological severity of NAFLD <sup>444</sup>. Surprisingly, Kawasaki et al. revealed that the BAFF receptor-deficient mice fed with HFD worsen the hepatic steatosis development by stimulating expression of the steatogenic genes compared to wild-type mice, implying the protective role of the BAFF signaling <sup>445</sup>. Nevertheless, Sutti et al. reported that MCD diet-fed mice when vaccinated with BAFF-neutralizing antibody, were protected from the NASH development leading to improved hepatic steatosis, and lobular inflammation. They identified that 40% of decreased in the circulating and hepatic B cell number and decreased CD4<sup>+</sup> T<sub>h</sub>1 activation, as evaluated by IFN $\gamma$  production. The authors also found similar findings in mice over-expressing the soluble form of the BAFF/APRIL receptor in mice fed a CDAA diet <sup>446</sup>. Compatibly, in a recent study, HFD-fed BAFF-deficient mice displayed significantly improved insulin sensitivity accompanied by attenuated inflammation and marked decreased CD11c<sup>+</sup> ATMs and fibrosis of epiAT, suggested to contribute to healthy AT expansion. Attenuated hepatic steatosis was also observed in BAFF-deficient mice, suggesting a therapeutic interest for BAFF neutralization in obesity-induced diabetes and NAFLD <sup>447</sup>.

In conclusion, diverse mechanisms and microenvironmental changes together with the heterogenous and evolving cell populations are involved in the onset and progression of NAFLD. Therefore, identifying reliable molecular players against multifactorial NASH development is difficult.

## 3. NUCLEAR RECEPTORS

Nuclear receptors (NRs) are a superfamily of transcription factors that include 48 members in humans, 49 members in mice, and 47 in rats. NRs regulate activity of the target genes mostly, in a ligand-dependent manner, involving various biological processes, such as development, metabolism, inflammation, and circadian rhythm <sup>448, 449</sup>. Due to the capability to control such essential physiological processes and to the nature of their ligands (small and often stable molecules), NRs have long been represented a valuable therapeutic targets in several pathologies that include breast cancer, T2D, fertility, NASH, and atherosclerosis <sup>450</sup>. Ligands of the NRs comprise of small lipophilic molecules and hormones, like phospholipids, steroids,

retinoids, and vitamin D that induce NRs to bind specific DNA sequences, known as DNA response elements, formerly named as hormone response elements (HRE), all along the genome <sup>450</sup>. Upon activation NRs are recruited to the DNA with co-regulator proteins, chromatin remodelers, and the principal transcriptional machinery, which in turn activate or repress the target gene expression <sup>451</sup>. Nevertheless, ligands for some of the NRs have not yet been determined and the receptors are thus considered as the “orphans” <sup>452</sup>. NRs are categorized into seven subfamilies from subfamily 0 to 6 based on the origin and evolutionary diversification (Table 3).

Family	Common name	Abbreviation	Gene	Ligand
0B	Dosage-sensitive sex reversal-adrenal hypoplasia congenital critical region on the X chromosome, Gene 1	DAX1	<i>NR0B1</i>	Orphan
	Short heterodimeric partner	SHP	<i>NR0B2</i>	Orphan
1A	Thyroid hormone receptor- $\alpha$	TR $\alpha$	<i>THRA</i>	Thyroid hormones
	Thyroid hormone receptor- $\beta$	TR $\beta$	<i>THRB</i>	Thyroid hormones
1B	Retinoic acid receptor- $\alpha$	RAR $\alpha$	<i>RARA</i>	Retinoic acids
	Retinoic acid receptor- $\beta$	RAR $\beta$	<i>RARB</i>	Retinoic acids
	Retinoic acid receptor- $\gamma$	RAR $\gamma$	<i>RARG</i>	Retinoic acids
1C	Peroxisome proliferator-activated receptor- $\alpha$	PPAR $\alpha$	<i>PPARA</i>	Fatty acids
	Peroxisome proliferator-activated receptor- $\beta$	PPAR $\beta$	<i>PPARD</i>	Fatty acids
	Peroxisome proliferator-activated receptor- $\gamma$	PPAR $\gamma$	<i>PPARG</i>	Fatty acids
1D	Reverse-Erb- $\alpha$	REV-ERB $\alpha$	<i>NR1D1</i>	Heme
	Reverse-Erb- $\beta$	REV-ERB $\beta$	<i>NR1D2</i>	Heme
1F	Retinoic acid-related orphan- $\alpha$	ROR $\alpha$	<i>RORA</i>	Sterols
	Retinoic acid-related orphan- $\beta$	ROR $\beta$	<i>RORB</i>	Sterols
	Retinoic acid-related orphan- $\gamma$	ROR $\gamma$	<i>RORC</i>	Sterols
1H	Farnesoid X receptor- $\alpha$	FXR $\alpha$	<i>NR1H4</i>	Bile Acids
	Farnesoid X receptor- $\beta$	FXR $\beta$	<i>NR1H5P</i>	Orphan
	Liver X receptor- $\alpha$	LXR $\alpha$	<i>NR1H3</i>	Oxysterols
	Liver X receptor- $\beta$	LXR $\beta$	<i>NR1H2</i>	Oxysterols
1I	Vitamin D receptor	VDR	<i>VDR</i>	1 $\alpha$ ,25-dihydroxyvitamin D3
	Pregnane X receptor	PXR	<i>NR1I2</i>	Endobiotics and xenobiotics
	Constitutive androstane receptor		<i>NR1I3</i>	Xenobiotics
2A	Hepatocyte nuclear Factor-4- $\alpha$	HNF4 $\alpha$	<i>HNF4A</i>	Fatty acids
	Hepatocyte nuclear Factor-4- $\gamma$	HNF4 $\gamma$	<i>HNF4G</i>	Fatty acids
2B	Retinoid X receptor- $\alpha$	RXR $\alpha$	<i>RXRA</i>	9- <i>Cis</i> retinoic acid
	Retinoid X receptor- $\beta$	RXR $\beta$	<i>RXRB</i>	9- <i>Cis</i> retinoic acid
	Retinoid X receptor- $\gamma$	RXR $\gamma$	<i>RXRG</i>	9- <i>Cis</i> retinoic acid
2C	Testicular Receptor 2	TR2	<i>NR2C1</i>	Orphan
	Testicular Receptor 4	TR4	<i>NR2C2</i>	Orphan
2E	Tailless homolog orphan receptor	TLX	<i>NR2E1</i>	Orphan
	Photoreceptor-cell-specific nuclear receptor	PNR	<i>NR2E3</i>	Orphan

2F	Chicken ovalbumin upstream promoter-transcription factor $\alpha$	COUP-TF $\alpha$	<i>NR2F1</i>	Orphan
	Chicken ovalbumin upstream promoter-transcription factor $\beta$	COUP-TF $\beta$	<i>NR2F2</i>	Orphan
	Chicken ovalbumin upstream promoter-transcription factor $\gamma$	COUP-TF $\gamma$	<i>NR2F6</i>	Orphan
3A	Estrogen receptor- $\alpha$	ER $\alpha$	<i>ESR1</i>	Estrogens
	Estrogen receptor- $\beta$	ER $\beta$	<i>ESR2</i>	Estrogens
3B	Estrogen-related receptor- $\alpha$	ERR $\alpha$	<i>ESRRA</i>	Orphan
	Estrogen-related receptor- $\beta$	ERR $\beta$	<i>ESRRB</i>	Orphan
	Estrogen-related receptor- $\gamma$	ERR $\gamma$	<i>ESRRG</i>	Orphan
3C	Androgen receptor	AR	<i>AR</i>	Androgens
	Glucocorticoid receptor	GR	<i>NR3C1</i>	Glucocorticoids
	Mineralocorticoid receptor	MR	<i>NR3C2</i>	Mineralocorticoids and glucocorticoids
	Progesterone receptor	PR	<i>PGR</i>	Progesterone
4A	Nerve growth Factor 1B	NGF1-B	<i>NR4A1</i>	Orphan
	Nurr-related Factor 1	NURR1	<i>NR4A2</i>	Unsaturated fatty acids
	Neuron-derived orphan Receptor 1	NOR-1	<i>NR4A3</i>	Orphan
5A	Steroidogenic Factor 1	SF-1	<i>NR5A1</i>	Phospholipids
	Liver receptor Homolog-1	LRH-1	<i>NR5A2</i>	Phospholipids
6A	Germ cell nuclear factor	GCNF	<i>NR6A1</i>	Orphan

**Table 3:** Classification of the human NRs together with the gene names and their activating ligands <sup>453</sup>.

### 3.1 Structural and Functional Organization of the Nuclear Receptors

Nuclear receptors possess a common structural organization, which comprises five functional domains in their polypeptide backbone (Figure 11A). The first one is the A/B, or the amino (N)-terminal domain (NTD) is variable in size and sequence that contains the ligand-independent activation function 1 (AF-1) region, which cooperates with numerous co-regulator proteins based on the cell types and promoter usage <sup>454</sup>. Moreover, the post-translational modifications and the formation of the multiple isoforms takes place in the NTD upon alternative splicing <sup>455</sup>.

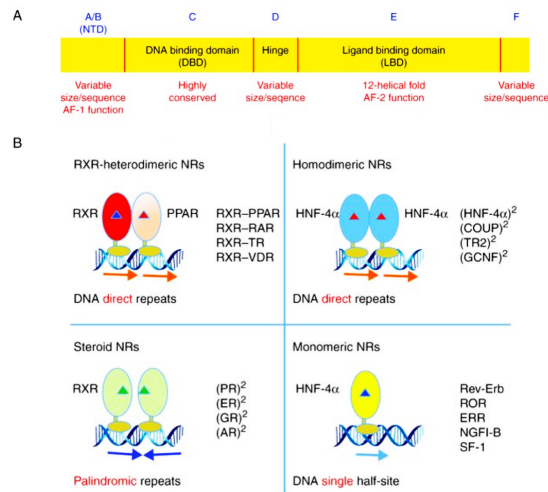


**Figure 11:** Schematic representation of the **(A)** NRs domain organization. NR polypeptides have an N-terminal domain (NTD) that is variable in size and sequence, a conserved DBD, a variable hinge region, and a 12-helical LBD. Several NRs also contain a variable F-domain positioned at their C-termini. **(B)** Oligomeric complexes of NRs and DNA response element repertoires. Receptors can be organized into distinct oligomeric states such as heterodimers with the common partner retinoid X receptor (RXR), homodimers, or monomers. The non-steroid receptor heterodimers and many homodimers bind to direct repeat response elements with various inter-half-site spacings. Steroid receptor homodimers mainly use palindromic DNA elements, where the two half sites are in an inverted repeat arrangement. Other receptors use monomeric sites extended at their 5'-end with short sequences used for selectivity. Several examples of receptors falling into each of these four categories are shown <sup>456</sup>.

The C or the DNA-binding domain (DBD) is the highly conserved domain, among NRs <sup>457</sup>. The DBD possesses two zinc finger motifs, which are both constituted by four cysteine residues that match with a zinc ion to facilitate canonical DNA-binding. The first zinc finger motif carries the DNA reading helix, which cooperates with the major groove to create base-specific interactions within the P-box polypeptide loop by the DNA <sup>458</sup>. The second zinc finger helix makes non-specific contacts with the DNA backbone that includes a distal box (D-box) in the peptide loop and promotes receptor dimerization <sup>459</sup>. The D domain or hinge region is a small adjustable linker connecting the DBD and the ligand-binding domain (LBD), which has the smallest size and sequence similarity among the NRs that contains a nuclear localization signal and supply an additional target for post-translational modifications <sup>460</sup>. The E or the LBD is the most conserved domain that comprises eleven  $\alpha$ -helixes and four  $\beta$ -sheets that coil up three parallel zones to build an  $\alpha$ -helical sandwich, creating a hydrophobic ligand-binding pocket <sup>461</sup>. The LBD binds to the ligands by the assistance of the ligand-dependent activation function 2 (AF-2) region and immediately cooperates with the co-regulator proteins at the

center of the receptor <sup>462</sup>. The carboxy (C)-terminal domain of the NRs is the most variable one, and their functional properties have not yet been fully understood. NRs often act on the DNA in the form of homodimers or heterodimers with one of the RXRs (RXR $\alpha$ , RXR $\beta$  or RXR $\gamma$ ), which makes them a unique member of the superfamily (Figure 11B). This binary format constitutes a large interaction surface for co-regulator proteins and post-translational modifications. Also, a pair of LBD enhances the ligand specificity as a regulatory mechanism <sup>463</sup>. Nonetheless, some NRs, like ROR $\alpha$ , GCNF, and LRH-1 binds as a monomer to the DNA with the assistance of a C-terminal extension (CTE) sequence in their DBD, which creates supplemental base-specific DNA contacts within the minor groove as a compensatory mechanism to stabilize monomer binding <sup>464</sup>. NRs binds to the multiple DNA response elements that contain one of the following nucleotide sequences, the direct repeats, palindromic repeats, or extended monomeric sites (Figure 11B) <sup>465</sup>.

### 3.2 Nuclear Receptor Signaling: Mechanism of Action

Mechanistically NRs subdivided into four groups as I to IV (Figure 12). The type I NRs contain the steroid receptors (SRs) that are activated by the cholesterol-derived steroid hormone ligands, like estrogens, androgens, and corticoids <sup>466</sup>. In the inactive state, SRs localize at the cytoplasm and are coupled with the chaperone proteins to keep open steroid-binding cleft, leading to accessibility for a steroidal ligand. Following the ligand-dependent activation, chaperones facilitate migration of the SRs throughout the microtubular paths to the nucleus <sup>467</sup>. Then, the SRs binds to the DNA response element, as a homodimer, containing palindromic repeats <sup>468</sup>. During that time, chaperone machinery still in contact with the receptor and interacts with transcriptional regulatory complexes to terminate transcriptional activation when it is necessary <sup>467</sup>. The type II NRs reside in the nucleus even in the absence of a cognate ligand bound to the co-repressor protein complexes that include, for example, the RAR and LXR. Upon ligand-binding, co-repressors are displaced by co-activators and the transcriptional machinery complexes, forming heterodimers with one of the RXRs on the direct repeat DNA response sequences <sup>469</sup>. Type III and type IV NRs share the same mechanism of action with type II NRs except upon activation, they binds to the DNA as a homodimers on direct repeat sequences, and as a monomers on extended single half-site, respectively <sup>470</sup>.

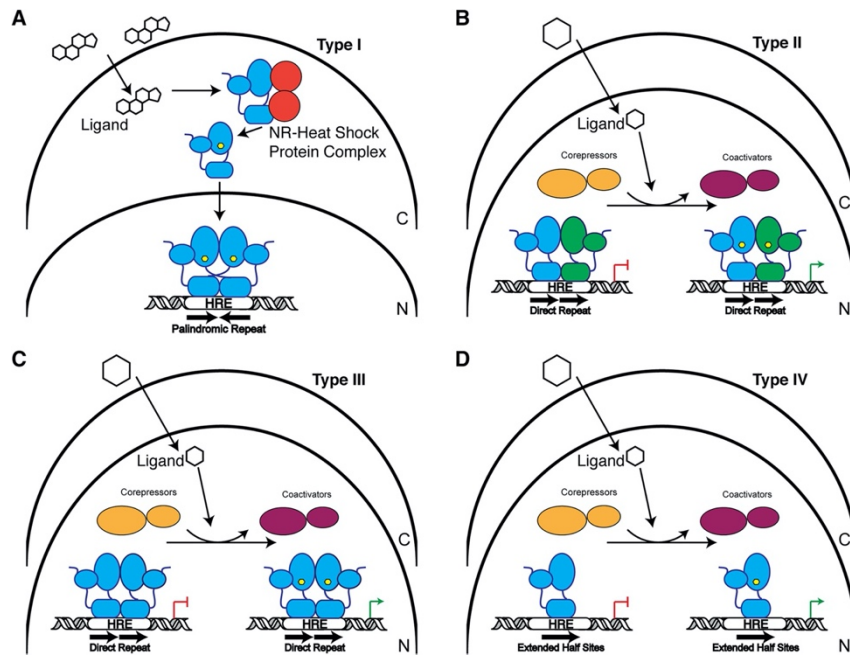


**Figure 12:** Schematic of NR signaling mechanisms. (A) Type I receptors reside in the cytoplasm (C) in complex with chaperone proteins. Upon ligand binding (hexagon), the receptor is released from this complex and is trafficked into the nucleus (N) where they typically bind to palindromic hormone response elements (HREs) as a homodimer to regulate transcription. (B) Type II receptors are localized in the nucleus. In their unliganded state, they interact with co-repressor proteins, but upon ligand binding are exchanged for co-activators. NRs in this group generally form heterodimeric complexes with RXR. (C) Similar to Type II receptors, Type III receptors reside in the nucleus and exchange bound co-repressors and co-activators. These receptors bind to direct repeat HREs as homodimers. (D) Type IV receptors are almost identical to Type III except they bind HREs that are extended half sites as monomers <sup>453</sup>.

In the positive regulation of the transcription, NRs recruits the co-activator scaffold proteins to start building of the large protein complexes that include the histone-modifying enzymes, for instance, histone acetyl-transferases (HATs) or histone methyl-transferases (HMTs) (Figure 13A). The histone modifiers support chromatin accessibility by keeping it open for other regulatory proteins <sup>471</sup>. Eventually, the general transcription machinery and RNA polymerase II lead to the transcription of the target genes. Alternatively, repression of the transcription by NRs is accomplished through two distinct mechanisms (Figure 13B). In the first scenario, like in the case of the inactive type II to IV, NRs keep interacting with the co-repressor proteins, which in turn engage the histone deacetylases (HDACs) that tighten the chromatin by contrast with the HATs, resulting in the prevention of the transcription <sup>472</sup>. In the second scenario, NRs bind to negative DNA response elements on the DNA, altering the conformational structure and favoring use of co-repressor to suppress the transcription <sup>473</sup>.

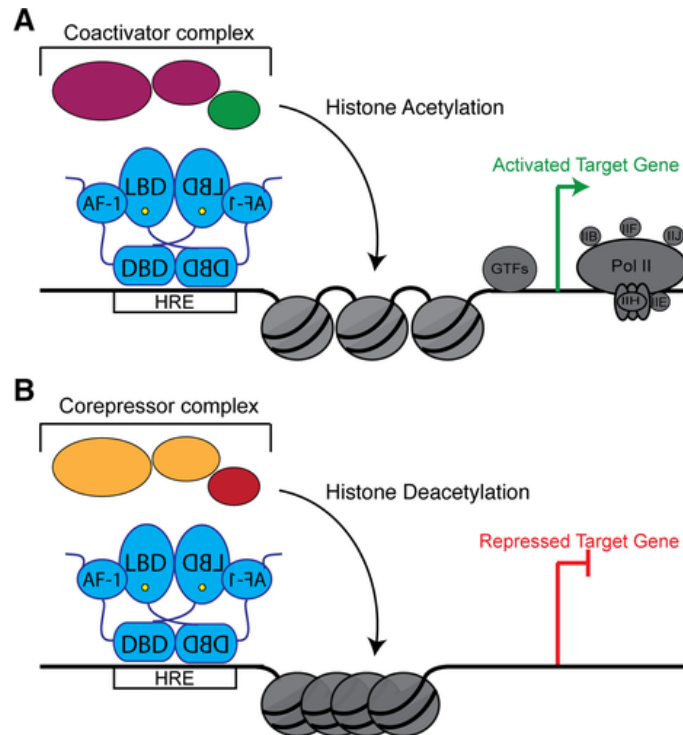


**Figure 13:** Modulation of the gene expression by NRs. NRs both activate and repress transcription. (A) To activate gene expression, NRs (blue) interact with their DNA response elements. DNA-bound NRs recruit co-activator proteins (magenta), which in turn recruit histone-modifying enzymes. These histone-modifying enzymes are commonly histone acetylases (green), which acetylate histone tails. This modification is a mark of active chromatin. Ultimately, the general transcriptional machinery and RNA Polymerase Pol II (gray) are recruited to drive gene expression. (B) To repress transcription, NRs recruit co-repressor proteins (orange). These proteins recruit other histone deacetylases (red) that reverse histone acetylation and restrict chromatin accessibility. This condensation prevents the transcriptional machinery from accessing the DNA, thus repressing gene expression <sup>453</sup>.

### 3.3 Retinoic Acid Receptor-related Orphan Receptors (RORs)

The nuclear receptor superfamily member Retinoic-Acid-Related (RAR) Orphan Receptors (RORs) subfamily comprises of ROR $\alpha$  (NR1F1), ROR $\beta$  (NR1F2), and ROR $\gamma$  (NR1F3) that exhibit discrete tissue expression patterns and play a role in diverse pathological conditions <sup>474</sup>. RORs have the common NR structural organization constituted by the variable N-terminal A/B domain, the DBD with two zinc finger motifs, a hinge region, the LBD, and a C-terminal domain. All of the ROR genes create several isoforms by alternative exon splicing and promoter usage, which are distinguishable only in the N-terminal A/B domain sequences (Figure 14).

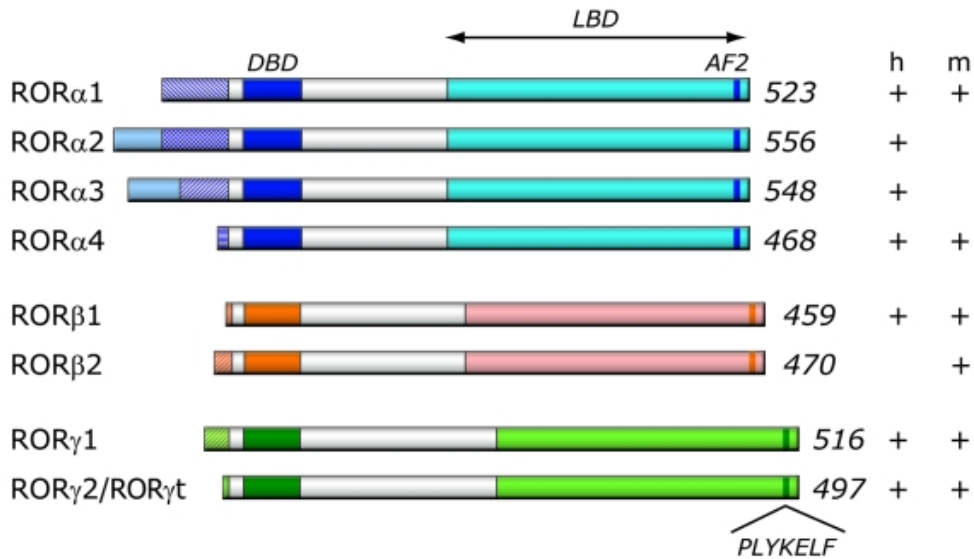


**Figure 14:** Schematic representation of ROR family members. Schematic structure of the various human (h) and mouse (m) ROR isoforms. The DNA binding domain (DBD) and ligand binding domain (LBD), and activation function 2 (AF2) are indicated. The variable regions at the N-terminus of each ROR generated by alternative promoter usage and/or alternative splicing are indicated by patterned boxes on the left. The numbers on the right refer to the total number of amino acids in RORs. The different ROR isoforms identified in human and mouse are shown on the right (+/-)<sup>475</sup>.

In humans 4 ( $\alpha$ 1 to  $\alpha$ 4), in mice 2 ( $\alpha$ 1 and  $\alpha$ 4), ROR $\alpha$  isoforms have been identified<sup>476</sup>. ROR $\alpha$ 4 is the predominant isoform that is widely-expressed, whereas ROR $\alpha$ 1 and ROR $\alpha$ 4 are consistently expressed in the cerebellum of the mice<sup>477</sup>. In mice, two ROR $\beta$  isoforms ( $\beta$ 1 to  $\beta$ 2) have been reported in which ROR $\beta$ 1 is exclusively expressed in the central nervous system while ROR $\beta$ 2 is expressed in the pineal gland and retina<sup>478</sup>. Two ROR $\gamma$  isoforms ( $\gamma$ 1 to  $\gamma$ 2) have been found in both human and mouse in which ROR $\gamma$ 1 is widely-expressed, whereas the ROR $\gamma$ 2 (ROR $\gamma$ t) is restricted to the thymus<sup>479</sup>. Since RORs binds as a monomer to the DNA<sup>480</sup> at the AT-rich sequences that contain the AGGTCA core motif<sup>481</sup>, known as the ROR response elements (RORE), the DBD is the most profoundly conserved between RORs that DBD of the ROR $\beta$  and ROR $\gamma$  are 91% and 88% identical to the DBD of ROR $\alpha$ , respectively<sup>482</sup>. Considering the importance of the CTE sequences within the DBD for the binding of monomeric NRs, that estimated similarity of the DBD is attributed to the CTE region<sup>483</sup>. Even though all ROR isoforms bind to similar ROREs, however, they display distinct affinities due to the variable N-terminal domain and promoter assembly<sup>484</sup>. REV-ERB $\alpha$  and REV-ERB $\beta$ , which are transcriptional repressors of the NR superfamily, recognize a cluster of ROREs that leads to suppression of the RORs-induced transcriptional activation of genes by competing with

RORs to bind the identical RORE<sup>485</sup>. Indeed, the competition between REV-ERBs and RORs for the RORE generates a regulatory feedback loop to control several notable physiological events, for instance, by modulation of the brain and muscle ARNT-like 1 (BMAL1 or ARNTL) gene expression. Rev-erb $\alpha$  and ROR $\alpha$  regulates the circadian rhythm<sup>486</sup>. LBD of the ROR $\beta$  and ROR $\gamma$  exhibit 63% and 58% analogy, respectively, compared to the LBD of the ROR $\alpha$ <sup>482</sup>, containing twelve  $\alpha$ -helices (H1 to H12). The AF-2 domain in the H12 comprise a completely conserved PLYKELF sequences among the RORs<sup>487</sup>. As reported, the deletion or mutation within the H12 lead to lack of the ROR transactivation property, prompting a dominant-negative ROR phenotype<sup>488</sup>.

### 3.3.1 Retinoic Acid Receptor-related Orphan Receptor Alpha and Circadian Rhythm

The circadian clock, (biological clock) is a molecular oscillator that enables organisms to adjust their physiology, including their metabolism, to adapt predictable to periodic changes in the environment in response to the rotation of the Earth within 24 hours, which is known as the circadian rhythm<sup>489</sup>. Suprachiasmatic nuclei (SCN) of the hypothalamus harbor a central timekeeper, known as the master clock that receives the stimulus from the retinal photoreceptor cells and synchronizes peripheral clocks wherein theoretically every cell in the body is entrained to the circadian rhythm in a coordinated manner<sup>490</sup>. Synchronization of the peripheral clock by the master clock incorporates the neuronal outputs and hormonal signals, like melatonin and glucocorticoids in return, the daily oscillations, including dark/light exposure, feeding/fasting, and activity/rest cycles modulate body temperature, blood pressure, metabolism, and immune function. In addition, tissue specific circadian rhythm is regulated by local/environmental cues independent from the central clock<sup>491</sup>. Regulation of the circadian rhythm is governed by complex transcriptional/translational negative and positive feedback loops at the molecular level (Figure 15). The positive loop is under the control of the basic helix-loop-helix-PAS (bHLH-PAS) transcription factors, which are the brain and muscle ARNT-like protein-1 (Bmal1) and the circadian locomotor output cycles kaput protein (Clock) or its paralogue the neuronal PAS domain protein-2 (NPAS2)<sup>492</sup>. The Bmal1 constitutes a heterodimer with the Clock or NPAS2 to activate the expression of the Period (Per1, Per2, and Per3) and the Cryptochrome (Cry1 and Cry2) genes by binding to the E-box DNA response elements in their promoter region. Afterward, the Per and Cry proteins forms heterodimers and suppresses the activity of Bmal1/Clock (or NPAS2) by negative feedback loop<sup>493</sup>. Furthermore, the repressor Rev-erb $\alpha$  and activator ROR $\alpha$  creates an additional regulatory feedback loop that controls Bmal1 expression by binding to the mutual response element

(RORE) present within the promotor of the *Bmal1* by theoretically following a circadian pattern with opposing phases, regulating the gene expression of the *Bmal1* in respect to the circadian rhythm <sup>494</sup>.

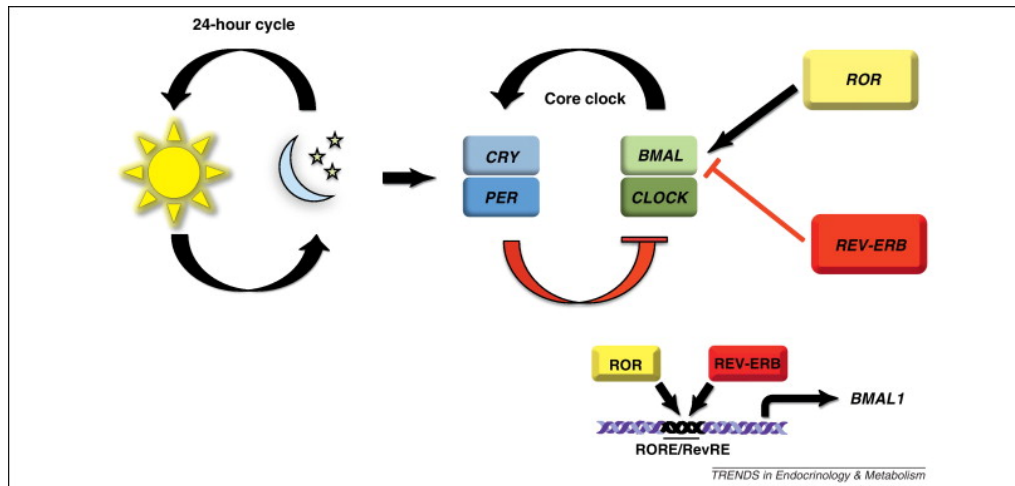


**Figure 15:** Regulation of the circadian rhythm at molecular level. Circadian rhythms are biological processes that display endogenous oscillations of approximately 24 hours and are regulated by a core circadian clock. The master circadian clock is located in the suprachiasmatic nucleus (SCN) of the hypothalamus. There are several interconnected transcriptional auto-regulatory feedback loops controlling the circadian cycle. Heterodimers of BMAL1 and CLOCK activate the expression of CRY and PER genes. Once the CRY/PER heterodimers reach a critical threshold, they enter the nucleus and repress BMAL/CLOCK transactivation. ROR $\alpha$  and REV-ERB $\alpha$  have been demonstrated to positively or negatively regulate the expression of BMAL1, respectively. ROR $\alpha$  competes with REV-ERB $\alpha$  for binding of their shared DNA response element in the BMAL1 promoter. The oscillating pattern of ROR $\alpha$  and REVERB $\alpha$  in the SCN dictates the circadian pattern of BMAL1 expression. This ROR $\alpha$ /REV-ERB $\alpha$  feedback loops interconnects the positive and negative arms of the core circadian clock <sup>494</sup>.

According to the available data and the circadian expression profiles databases, ROR $\alpha$  gene expression is not circadian but displays very weak oscillation compared to the *Bmal1* and *Rev-erbs* but, in terms of activity, ROR $\alpha$  can exhibit circadian rhythmicity <sup>495</sup>. Indeed, the activation of the *Bmal1* by ROR $\alpha$  is mediated by the transcriptional co-activator PGC1- $\alpha$  in the liver that oscillate rhythmically and PGC-1 $\alpha$ -deficient mice display altered circadian rhythm <sup>496</sup>. It has also been reported that the naturally inactivated ROR $\alpha$  *staggerer* mice (see below) exhibit abnormal circadian rhythm with the decreased expressions of the clock genes, including *Clock*, *NPAS2*, and *Cry1*. Nonetheless, *Bmal1*, *Clock*, *Cry1*, and *Per2* expressions continue to oscillate with rhythmicity in the fibroblasts of the *staggerer* mice, suggesting ROR $\alpha$  is not

necessary for circadian oscillations of the clock genes but regulates their level of expression<sup>497</sup>.

### 3.3.2 Retinoic Acid Receptor-related Orphan Receptor Alpha as a Metabolic Regulator

Primarily, ROR $\alpha$  has been shown to activate apolipoprotein A-I, which is the principal component of the HDL that transports cholesterol from the periphery to the liver and inhibits excessive cholesterol accumulation in the arterial walls, suggesting a regulatory role for ROR $\alpha$  in the plasma cholesterol level<sup>498</sup>. Subsequent studies have also demonstrated that ROR $\alpha$  regulates expression of several genes involved in lipid metabolism, including apoC-III in humans and mice<sup>499</sup>, apo-AV in humans<sup>500</sup>, and the fibroblast growth factor-21 (FGF-21) in human liver cancer cell line HepG2 cells<sup>501</sup>. Cholesterol, cholesterol derivatives, like cholesterol sulfate, and oxysterols have been identified as the potential endogenous ligands for ROR $\alpha$ <sup>502, 503</sup>. Since altered cholesterol metabolism or transport observed in aging, ROR $\alpha$  has been involved in atherosclerosis and Alzheimer's diseases, ROR $\alpha$  has been implied to possess protective effects in the vascular system by modulating intracellular cholesterol content<sup>504</sup>. Indeed, in a recent study, Choi et al. determined that the cholesterol 25-hydroxylase (CH25), the 25-hydroxycholesterol 7-hydroxylase (CYP7B1)-ROR $\alpha$  axis of cholesterol metabolism in chondrocytes is a catabolic regulator of osteoarthritis pathogenesis, which is one of the most common forms of the age-related degenerative whole-joint disease<sup>505</sup>. Additionally, Chopra et al. identified that hepatic gluconeogenesis, in response to fasting, regulated by ROR $\alpha$  and the transcriptional co-activator steroid receptor co-activator-2 (SRC-2), through the modulation of the rate-limiting enzyme glucose-6 phosphatase (G6Pase) expression<sup>506</sup>. In line, Kumar et al. identified the benzene sulfonamide (T0901317) as a first high-affinity synthetic ROR $\alpha$  and ROR $\gamma$  ligand that suppresses the G6Pase gene expression via inhibition of the SRC-2 recruitment by ROR $\alpha$  in HepG2 cells<sup>507</sup>. The same group also identified that the 7- $\alpha$ -hydroxycholesterol (7- $\alpha$ -OHC), which is the intermediate molecule of the bile acid metabolism, acts as a natural inverse agonist of the ROR $\alpha$  by repressing expression of the ROR target genes, such as the G6Pase and phosphoenolpyruvate carboxykinase (PEPCK)<sup>508</sup>.

In 1962, Sidman et al. reported several spontaneous mutant mice with the neuropathological features, which they called them *staggerer* mice as they exhibited cerebellar defects leading to severe ataxia, motor defect, and tremor in a stock of obese mice at the Jackson Memorial Laboratory in 1955<sup>509</sup>. A few decades later, Hamilton et al. identified the mutant gene in

*staggerer* mice as the *Rora* gene, which hereupon are known as,  $ROR\alpha^{sg/sg}$  mice. A spontaneous mutation leads to a shift in the reading frame, causing a premature stop codon within the LBD<sup>510</sup>. This discovery highlighted the significance of  $ROR\alpha$  in Purkinje cell development of the cerebellum. Steinmayr et al. generated  $ROR\alpha$ -deficient mice by using a targeted insertion of a lacZ reporter gene vector, encoding beta-galactosidase that replaced the second zinc finger of the DBD of  $ROR\alpha$ . The generated mice displayed a *staggerer* phenotype<sup>511</sup>. Subsequently, this validation initiated a comprehensive analysis of the *staggerer* mice to seek for functional properties of the  $ROR\alpha$ . Mamontova et al. revealed that lipid metabolism was altered in *staggerer* mice with low levels of total plasma HDL, apoA-I, and apoA-II observed at steady-state, leading to severe atherosclerosis development in response to atherogenic diet feeding<sup>512</sup>. On the other hand, the *Srebp-1c* and fatty-acid synthase, which are the key genes for the regulation of lipid homeostasis are dysregulated in *staggerer* mice, leading to a lower AT masses and hepatic TG content, suggesting a protective role against obesity<sup>513</sup>. Relatedly, *staggerer* mice are protected from HFD-induced obesity, IR, and NAFLD<sup>514</sup>. One of the underlying mechanisms accounting for this protection is attributed to increased thermoregulation in the SAT and BAT depots of the *staggerer* mice<sup>515</sup>. Consistent with this finding, recently, Monnier et al. determined that  $ROR\alpha$  controls thermogenesis-related gene expression, which are overlapping with those previously published genes, in the inguinal and perigonadal WAT depots via in a circadian-dependent manner<sup>516</sup>. Nonetheless, several additional defects were found in *staggerer* mice, which makes poorly suited for the precise delineation of pathophysiological mechanisms. Abnormalities include thymopoiesis and lymphocyte development, evidenced by the reduced spleen and thymus masses, as well as hyper induction of the cytokine secretion by macrophages that might directly impact on metabolic parameters<sup>517, 518</sup>. Concomitantly, the development of new synthetic ligands that include the SR1078 ( $ROR\alpha$  and  $ROR\gamma$  double agonist) and JC1-40 ( $ROR\alpha$  agonist) also provided evidence for a role of  $ROR\alpha$  in IR and NAFLD by modulating endoplasmic reticulum stress and hepatic oxidative stress<sup>519, 520</sup>. Recently, to decipher the precise function of  $ROR\alpha$  in NASH pathogenesis several independent groups generated hepatocyte-specific  $ROR\alpha$ -deficient mice. Firstly, Zhang et al. showed that hepatocyte-specific  $ROR\alpha/\gamma$ -double knock-out mice up-regulate the expression of lipogenic genes at a definite time of day (circadian), highlighting the importance of the time in a day, as a key parameter in the treatment of liver diseases<sup>521</sup>. Secondly, Kim K. et al. determined that hepatocyte-specific deletion of  $ROR\alpha$  leads to dysregulation of  $PPAR\gamma$  signaling and increases hepatic glucose and lipid metabolism in response to HFD feeding<sup>522</sup>. Another group suggested that lack of  $ROR\alpha$  in hepatocytes leads to the development of severe NASH due to mitochondrial dysfunction in HFD-fed mice<sup>523</sup>. Nevertheless, in an independent study, no effect of hepatocyte-specific  $ROR\alpha$  deletion on

NASH was observed, leaving open the question about how ROR $\alpha$  influences NASH<sup>524</sup>. Besides, in humans, mutations in the *RORA* gene have been associated with obesity<sup>525</sup>, T2D<sup>526</sup>, and liver diseases<sup>527</sup>.

### 3.3.3 Retinoic Acid Receptor-related Orphan Receptor Alpha as an immune regulator

Initial data about the role of ROR $\alpha$  as an immune regulator arose from observation of the *staggerer* mice that display limited thymus development, swollen lymph nodes, and decreased spleen mass<sup>518</sup>. Moreover, in the same study, it was also surprisingly shown that *staggerer* mice generated normal proportions of the T helper cells and antibody-producing B cells following the SRBC immunization. However, they exhibited prolonged immune response and delay in the generation of suppressor T-cells following the challenge, suggesting impaired regulatory feedback mechanisms<sup>518</sup>. In response to LPS-induced inflammation, *staggerer* mice found to be highly sensitive, causing hyper activation of macrophages leading to increased production of the pro-inflammatory cytokines, like IL-1 and TNF $\alpha$ , suggested a reduced regulator activity of ROR $\alpha$  in inflammation<sup>528</sup>. Relatedly, Dzhagalov et al. revealed that ROR $\alpha$  indirectly governs the development of T and B cells by supplying the necessary environment and controls immune responses through limiting cytokine production in innate immune cells and lymphocytes by using *staggerer* and Rag-2<sup>-/-</sup>ROR<sup>sg/sg</sup> bone marrow chimeric mice<sup>529</sup>. Furthermore, Delerive et al. reported that over-expression of ROR $\alpha$  in smooth muscle cells activates I $\kappa$ B $\alpha$  that represses the NF- $\kappa$ B signaling pathway by reducing the p65 translocation and suppresses TNF $\alpha$ -induced cytokine production, confirming ROR $\alpha$  is a negative regulator of the inflammatory response<sup>530</sup>. Additionally, human aortic smooth muscle cells have been shown to predominantly express ROR $\alpha$ 1, while in atherosclerotic plaques, it was decreased significantly, supporting the absence of protective ROR $\alpha$  in *staggerer* mice provokes atherosclerosis development<sup>531</sup>. By contrast, Sun et al. demonstrated that ROR $\alpha$  drives the oxygen-induced retinopathy by repressing the suppressors of cytokine signaling 3 (SOCS3) expression, which is a negative regulator of the inflammation, implying immune regulator activity of the ROR $\alpha$  depends on the pathology<sup>532</sup>. It has also been reported that *staggerer* mice are protected from ovalbumin-induced allergic airway inflammation, evidenced by decreased mucus cell hyperplasia, T<sub>h</sub>2 cytokine responses, like IL-4, IL-5, and IL-13, infiltration of the neutrophils, eosinophils, and lymphocytes into the lung and bronchoalveolar fluids<sup>533</sup>. Similarly, Stapleton et al. found that *staggerer* mice heightened susceptibility to intratracheal LPS-induced T<sub>h</sub>17 and neutrophilia-dependent lung inflammation<sup>534</sup>. Importantly,

they also identified that the engagement of the attenuated I $\kappa$ B $\alpha$ -dependent mechanism was not responsible for this protection, as previously shown in smooth muscle cells, highlighting that ROR $\alpha$  possibly affects various inflammatory pathways as a negative immune modulator<sup>534</sup>. These findings suggest that ROR $\alpha$  plays a significant role in the development of T<sub>h</sub>2-driven allergic lung inflammation in mice as a potential asthma target. Indeed, in a recent study, the RORA gene has been identified as a high risk for asthma in a large-scale genome-wide association study<sup>535, 536</sup>. Besides, ROR $\alpha$  is widely-expressed within the immune system and play key roles in the development and function of various immune cell types. Friesenhagen et al. by using genome-wide microarray analysis revealed that monocytes display reduced immune response against a highly pathogenic avian influenza virus (HPAIV), H5N1 compared to human influenza A virus<sup>537</sup>. They showed that ROR $\alpha$  is activated in monocytes upon H5N1 infection and inhibited NF- $\kappa$ B signaling, suggesting that ROR $\alpha$  regulate immune function of monocytes in response to viral infection<sup>537</sup>. In a recent study, Saini et al. reported that ROR $\alpha$  expression is increased in murine macrophages and DCs as well as in human PBMCs upon *Mycobacterium tuberculosis* infection without providing a functional mechanism<sup>538</sup>. It has been shown that ROR $\alpha$  regulate development of group 2 innate lymphoid cells (ILC2)<sup>539</sup>, which are crucial cell types in allergic asthma as well as to maintain metabolic homeostasis in AT<sup>540</sup>. Moreover, Yang et al. revealed that T<sub>h</sub>17 lineage differentiation is programmed by ROR $\alpha$  and ROR $\gamma$  nuclear receptors<sup>541</sup>. Furthermore, ROR $\alpha$  regulate differentiation of T follicular helper (T<sub>FH</sub>) cells<sup>542</sup>, which are specialized to stimulate B cell growth, differentiation, immunoglobulin isotype switching, and affinity maturation. In line, ROR $\alpha$  control survival of IgG2<sub>a</sub>-producing memory B cells<sup>543</sup>. Recently, Malhotra et al. showed that ROR $\alpha$  expression in T<sub>regs</sub> control allergic skin inflammation through TNF ligand-related molecule 1 (TL1A) and death receptor 3 (DR3)-mediated suppression of ILC2 and eosinophil infiltration<sup>544</sup>.

The role of ROR $\alpha$  as a metabolic regulator and immune modulator were mostly documented by using *staggerer* mice. However, as mentioned, due to their pleiotropic immune and metabolic abnormalities, this model is not suitable to determine cell-specific contribution of ROR $\alpha$  to pathophysiology. Given the well-established function of several myeloid cell subsets, in particular macrophages in the initiation and progression of the metabolic diseases, such as obesity-driven T2D, or NAFLD and due to the wide cell distributions of ROR $\alpha$  within the immune system, its potential contribution to both metabolic homeostasis and immunoregulation can only be studied by a cell-specific ROR $\alpha$ -targeting strategy. As we indeed hypothesize that its impact on these pathologies, might in part, mediated by a direct action on macrophages. Therefore, we generated a macrophage-specific ROR $\alpha$ -deficient mouse model and evaluated its impact on models of obesity, IR, and NASH.

## SCOPE OF THE THESIS

1. Impact of macrophage-specific ROR $\alpha$  deletion on metabolic diseases
  - A. HFD-induced obesity, insulin resistance, and NAFL
  - B. obesity-independent diet-induced NASH
2. Impact of lysozyme M (*Lyz2*) deletion on metabolic diseases
  - C. HFD-induced obesity, IR, and NAFL
  - D. obesity-independent diet-induced NASH
3. Saturated fatty acids promote Growth Differentiation Factor 15 (GDF-15) expression in macrophages through the PERK/eIF2/CHOP signaling pathway. (This work will be presented in the annex).

## MATERIALS AND METHODS

### 1. Generation of macrophage-specific ROR $\alpha$ knock out mice

We generated mice harboring a floxed allele of *Rora* (*Rora<sup>fl/fl</sup>*) by flanking exon 3 with two *loxP* sequences. Briefly, a targeting vector containing loxP sites, an FRT-floxed neomycin cassette and homologous regions surrounding exon 3 was constructed and transfected in embryonic stem (ES) cells derived from 129/Sv. After screening for homologous recombination by southern blot and PCR, ES cells were injected into C57BL/6 blastocysts. Neomycin cassette was removed in vivo by using FLP deleter mice in C57BL/6 background. Finally, mice were backcrossed with C57BL/6J mice for at least six generations. To achieve the deletion of ROR $\alpha$  in myeloid cells, *Rora<sup>fl/fl</sup>* mice were crossed with LysM-Cre transgenic mice (Jackson laboratory) in which Cre recombinase is expressed under the control of endogenous *Lyz2* promoter. Littermates ROR $\alpha$ -deficient (MKO, *Rora<sup>fl/fl</sup> Lyz2<sup>Cre/+</sup>*) and WT (*Rora<sup>+/+</sup> Lyz2<sup>Cre/+</sup>*) mice were generated by crossing *Rora<sup>fl/+</sup> Lyz2<sup>Cre/Cre</sup>* with *Rora<sup>fl/+</sup> Lyz2<sup>+/+</sup>* mice. All mice were genotyped twice.

### 2. Mouse genotyping

DNA was extracted from tail with REDEExtract-N-Amp Tissue PCR Kit (Sigma, #XNAT-1000RXN). Floxed *Rora* was detected by PCR with the *Rora* genotyping primers (Supplementary table 1) and the following cycling conditions: 1 cycle at 94°C for 3 min; 35 cycles at 94°C for 30 s, 55°C for 30 s, 72°C for 1 min; and 1 cycle at 72 °C for 10 min; hold at 4°C. Samples were separated by gel electrophoresis on a 1.5% agarose gel. *Rora<sup>+/+</sup>* gave a single band at 250 bp, *Rora<sup>fl/fl</sup>* at 340 bp and *Rora<sup>fl/+</sup>* had both bands. Endogenous *Lyz2* and *Cre* were detected with the *Lyz2* genotyping and *Cre* genotyping primers respectively (Table 4) and the following cycling conditions: 1 cycle at 94°C for 3 min; 35 cycles at 94°C for 1 min, 63°C for 1 min, 72°C for 90 s; and 1 cycle at 72 °C for 10 min; hold at 4°C. Samples were separated by gel electrophoresis on a 1.5% agarose gel. *Lyz2<sup>+/+</sup>* gave a single band at 350 bp for *Lyz2* PCR while *Lyz2<sup>Cre/Cre</sup>* gave a single band at 700 bp for *Cre* PCR. *Lyz2<sup>Cre/+</sup>* gave bands for both *Lyz2* and *Cre* PCR.

### 3. Mouse studies

Mice were kept on a 12-hours light/dark cycle in the SPF animal facility from the Institute Pasteur de Lille with *ad libitum* access to food and water. Littermate WT and MKO mice were

maintained all along the experiment procedures in 904 cm<sup>2</sup> cages (Green line GR900, Tecniplast) with 6-12 mice per cage and a ratio WT:MKO tending to 1:1. Only male mice were used for the experiments. All animal procedures were approved by the ethical committee for animal experimentation of the Nord-Pas-de-Calais Region (CEEA75) (APAFIS#7160-2017040313471173) in accordance with European guidelines on the protection of animals used for scientific purposes (2010/63/UE). Ten-week-old ROR $\alpha$  WT and their littermates ROR $\alpha$  MKO mice were fed with a 60% high-fat diet (HFD, Research Diet, D12492) for 12 weeks or maintained under chow diet (SAFE, #A04). To induce a NASH-like disease, ten-week-old ROR $\alpha$  WT and MKO mice were fed with a choline-deficient, L-amino acid-defined (CDAA) diet with 35% sucrose, 21% fat and 2% cholesterol (Ssniff, custom diet) for 8 weeks. In addition to CDAA diet, mice also received monosaccharides in the drinking water (42g/L, fructose: glucose ratio of 55:45). Weight of mice was measured weekly. Before sacrifice, mice were fasted for 5 hrs. Mice were sacrificed at ZT3 (10 am) for HFD and at ZT7 (2 pm) for CDAA experiment.

#### 4. Insulin and glucose tolerance tests

After 10 weeks of HFD, a Glucose Tolerance Test (GTT) was performed by intraperitoneal injection of glucose (1g/kg). Tail blood sample was collected before glucose injection to measure fasting insulin by ELISA (Mercodia #10-1247-10) according to manufacturer instruction. After 11 weeks of HFD, an Insulin Tolerance Test (ITT) was performed by intraperitoneal injection of human insulin (1IU/kg) (Actrapid, Novo Nordisk). Glycemia was measured from tail before and 15, 30, 60, 90 and 120 min after glucose or insulin injection by using a glucose meter (Accu-Check performa, Roche). Before GTT and ITT, mice were fasted for 5h at ZT2 (9 am) and the tests were performed at ZT7 (2 pm).

#### 5. Bone marrow-derived macrophages

Bone marrow was isolated from tibia and femur of mice. Bone marrow cells were culture in RPMI 1640 with Hepes and L-glutamine supplemented with 10% fetal bovine serum, 20% L929-conditioned medium and 25  $\mu$ g/mL gentamycin for one week. After three days of culture, fresh medium was added. After one week of culture, supernatant was discarded and adherent bone marrow-derived macrophages (BMDMs) were washed two times with PBS. BMDMs were collected by using a cell scraper, counted and plated at a concentration of 10<sup>6</sup> cells/ml. After 24 hours, BMDMs were treated with 100nM dexamethasone (Sigma, #D1756) for 2 hours to synchronize cells, washed and maintained in complete medium for 32 hours to reach the pic of ROR $\alpha$  activity corresponding to ZT0 *in vivo*.

## 6. Cell sorting

Mice were sacrificed at ZT0 (7 am) and tissue kept in PBS on ice until processing. For epididymal adipose tissue, between 3 and 4 mice were pooled. Spleen was gently pressed on a 70  $\mu$ m cell strainer by using a 1 mL syringe plunger. Adipose tissue, liver and lung were minced with scissors and digested in RPMI containing 1 mg/mL collagenase D (Roche # 11088882001) at 37°C under agitation for 30, 45 and 60 min respectively and then carefully passed several times through an 18 or 19 G needle to obtain a single cell suspension. Red blood cells were lysed with ammonium chloride-based buffer and cells were blocked by using a combination of anti-CD16/CD32 (clone 2.4G2) (BD Biosciences, #553142) and anti-Fc $\gamma$ RIV (clone 9E9) (BioLegend, #149502). Antibodies used for staining are provided in table 5. Cell suspension was directly run into an Influx sorter (Becton Dickinson®) (Plateau d'Immunophenotypage Metabolique, Inserm U1011) equipped with an 86  $\mu$ m nozzle and tuned at a pressure of 24.7 psi and a frequency of 48.25 kHz. Sample fluid pressure was adjusted to reach an event rate of maximum 10 000 events/sec. In spleen, cells of interest were selected in the following order: T cells (CD45<sup>+</sup> CD3 $\epsilon$ <sup>+</sup> TCR $\beta$ <sup>+</sup> MHC-II<sup>-</sup>), B cells (CD45<sup>+</sup> CD19<sup>+</sup> MHC-II<sup>+</sup>), Neutrophils (CD45<sup>+</sup> CD3 $\epsilon$ <sup>-</sup> TCR $\beta$ <sup>-</sup> CD19<sup>-</sup> CD11b<sup>+</sup> Ly6G<sup>+</sup>), Macrophages (CD45<sup>+</sup> CD3 $\epsilon$ <sup>-</sup> TCR $\beta$ <sup>-</sup> CD19<sup>-</sup> Ly6G<sup>-</sup> F4/80<sup>+</sup>), monocytes (CD45<sup>+</sup> CD3 $\epsilon$ <sup>-</sup> TCR $\beta$ <sup>-</sup> CD19<sup>-</sup> Ly6G<sup>-</sup> F4/80<sup>-</sup> CD11b<sup>+</sup> CD115<sup>+</sup>) and DCs (CD45<sup>+</sup> CD3 $\epsilon$ <sup>-</sup> TCR $\beta$ <sup>-</sup> CD19<sup>-</sup> Ly6G<sup>-</sup> F4/80<sup>-</sup> CD115<sup>-</sup> CD11c<sup>+</sup> MHC-II<sup>+</sup>). In liver, cells of interest were selected in the following order: T cells (CD45<sup>+</sup> CD3 $\epsilon$ <sup>+</sup> TCR $\beta$ <sup>+</sup> CD19<sup>-</sup> CD20<sup>-</sup>), B cells (CD45<sup>+</sup> CD19<sup>+</sup> CD20<sup>+</sup> MHC-II<sup>+</sup>), Kupffer cells (CD45<sup>+</sup> CD3 $\epsilon$ <sup>-</sup> TCR $\beta$ <sup>-</sup> CD19<sup>-</sup> CD20<sup>-</sup> F4/80<sup>+</sup> Clec4F<sup>+</sup>) and other (CD45<sup>+</sup> CD3 $\epsilon$ <sup>-</sup> TCR $\beta$ <sup>-</sup> CD19<sup>-</sup> CD20<sup>-</sup> F4/80<sup>-</sup> Clec4F<sup>-</sup>). Adipose tissue macrophages were selected as CD45<sup>+</sup> CD3 $\epsilon$ <sup>-</sup> TCR $\beta$ <sup>-</sup> CD19<sup>-</sup> CD20<sup>-</sup> F4/80<sup>+</sup> CD64<sup>+</sup> and lung macrophages as CD45<sup>+</sup> CD3 $\epsilon$ <sup>-</sup> TCR $\beta$ <sup>-</sup> CD19<sup>-</sup> F4/80<sup>+</sup> CD64<sup>+</sup> CD11b<sup>low</sup> SiglecF<sup>+</sup>.

For bone marrow (BM) neutrophils, BM was first isolated from tibia and femur of mice. Red blood cells were lysed with ammonium chloride-based buffer and BM cells were blocked by using a combination of anti-CD16/CD32 (clone 2.4G2) (BD Biosciences, #553142) and anti-Fc $\gamma$ RIV (clone 9E9) (BioLegend, #149502). Cells were incubated with PE rat anti-mouse Ly-6G (Clone 1A8) (BD Biosciences, #551461) for 30 min and purified by magnetic separation with anti-PE MicroBeads (Miltenyi Biotec, #130-048-801) according to the manufacturer's instructions.

## 7. Metabolic parameters

Before sacrifice and after 5 hours of fasting, blood samples were collected from the retro orbital sinus of mice. Plasma alanine aminotransferase (ALAT), aspartate aminotransferase (ASAT), total cholesterol and triglycerides were measured on a Konelab 20 (Thermo Fisher) with reagents from Thermo Scientific for ALAT (#981769) and ASAT (#981771) and reagents from DiaSys for cholesterol (#113009910026) and triglycerides (#157109910026). The plasma ALAT and ASAT measurement under CDAA diet was performed without fasting for the time point T0, 2, 4 and 6 weeks.

## 8. Measurement of liver triglycerides

Lipids were extracted from the liver caudate lobe. A weighted piece of tissue was homogenized with T10 Ultra-Turrax (Ika) in PBS 1% Triton. Samples were transferred into glass tubes and mixed with a 2:1 chloroform: methanol mixture. After centrifugation, upper- and inter-phase were discarded. The lower organic phase was evaporated under nitrogen flow and reconstituted in 1% Triton X100. Triglyceride content was measured with Triglycerides FS kit (DiaSys, #157109910026).

## 9. Histology

The median lobes of liver were collected and fixed in 4% paraformaldehyde for 48 to 72 hrs. Tissues were embedded in paraffin by using a STP 120 Spin Tissue Processor (Microm Microtech) and an EG1160 Tissue Embedding Station (Leica). Paraffin-embedded samples were cut at a thickness of 3 $\mu$ m and sections were transferred on a gelatin-coated slide for hematoxylin and eosin (H&E) staining and on a Superfrost Plus slides (Thermo Scientific, # J1800AMNZ) for Sirius Red staining. Staining was performed with a Leica autostainer XL and the following steps for H&E staining: xylene (2 min), xylene (2 min), 100% ethanol (2 min), tap water (2 min), hematoxylin (Sigma, #HHS128) (3 min), tap water (2 min), 70% ethanol 0.25% HCl (6 s), tap water (2 min), 90% ethanol (2 min), eosin (Sigma, #HT1101128) (2 min), 90% ethanol (6 s), 100% ethanol (1 min) and finished in xylene before mounting with Mercoglas (Merck, # 103973). For Sirius red staining, the process was the following: xylene (2 min), xylene (2 min), 100% ethanol (2 min), tap water (2 min), 0.1% Direct Red 80 (Sigma, #365548) in saturated picric aqueous solution (60 min), tap water (8 min), 100% ethanol (1 min) and finished in xylene before mounting with Mercoglas. Images were acquired on an Eclipse Ti-U microscope (Nikon) and quantified with Image J software.

## 10. RT-qPCR

Total RNA was extracted from the snap-frozen tissues or sorted cell pellets by using TRIzol reagent (Ambion, #15596018) according to the manufacturer's instructions. DNase treatment was performed (Thermo Scientific, #EN0521) and RNA was reverse-transcribed to complementary DNA (cDNA) by using the high capacity cDNA reverse transcription kit (Applied Biosystems, #4368813). qPCR was performed by using Brilliant II SYBR Green QPCR Master Mix (Agilent, #600828) and ran on a Mx3000P qPCR system (Agilent). Relative changes in mRNA expression (Fold change, FC) were calculated by the  $2^{-\Delta\Delta CT}$  method. Absolute changes in mRNA expression were calculated with the formula  $2^{\Delta CT} \times 100$  and expressed as arbitrary unit (AU). The mean of four housekeeping genes (*Rplp0*, *Ppia*, *Rpl4* and *Rps29*) was used to normalize mRNA expression. The primers used for qRT-PCR are listed in table 4.

## 11. Western blotting

Tissues were weighted and homogenized with a T10 Ultra-Turrax (Ika) in protect buffer (water with cOmplete protease inhibitor cocktail (Roche, #11836145001) and PhosSTOP (Roche, #04906837001)) (3.75  $\mu$ L/mg for adipose tissue and 7.5  $\mu$ L/mg for muscle and liver). Next, total protein lysates were mixed with 4X Laemmli buffer (Tris-HCl 250mM pH 6.8, 40% glycerol, 8% SDS, 12%  $\beta$ -mercaptoethanol and bromophenol blue) and heated at 100°C for 5 min. Total protein extracts were subjected to SDS-PAGE (10% polyacrylamide gel) and transferred on a 0.22  $\mu$ m nitrocellulose membrane (Li-Cor, #P/N 926-31092). After blocking in 5% BSA, membranes were probed with mouse anti-Akt (Cell Signaling, #2920) and rabbit anti-phospho-Akt (Ser473) (Cell Signaling, #4058) monoclonal antibodies. The secondary antibodies used for the revelation were Alexa Fluor 680 anti-mouse IgG (Jackson ImmunoResearch, #715-625-150) and Alexa Fluor 790 anti-rabbit IgG (Jackson ImmunoResearch, #711-655-152). Immunoblots were scanned with an Odyssey CLx Imaging System (LI-COR) and quantified with Image studio software (LI-COR).

## 12. Statistical analyses

All statistical analyses were carried out using GraphPad Prism 8 for Windows (GraphPad Software) and presented as means  $\pm$  SEM. The study was done blinded for genotype. Only one mouse (WT) was excluded from the analysis because it did not reach an appropriate weight gain under HFD feeding (Body weight: 31.2 g; ingAT: 0.165 g; epiAT: 0.348 g). No mice were excluded in CDAA diet group. Data were analyzed with 2-way ANOVA and Sidak's

multiple comparisons post-hoc test or Student's *t*-test. Values with  $P < 0.05$  were considered as significant. All statistical details including statistical test used and exact value of *n* are described in each figure legend. Each data point represents genuine replication, also called true replicate, and were obtained from a single measurement or multiple measurements illustrated by the mean, such as gene expression by RT-qPCR that was assessed in duplicate or histology quantification made on five random fields per mice. For sake of clarity, results of statistical comparisons between WT and MKO mice upon Chow feeding were not illustrated on the figures but were not significant for all the parameters.

	Forward	Reverse
<b>Genotyping</b>		
<i>Rora</i> (PCR1)	CATGCATACACCCACACACATCACAACC	CTTGATGCACTGATGTAATAACATATCC
<i>Lyz2</i>	CTTGGGCTGCCAGAATTTCTC	TTACAGTCGGCCAGGCTGAC
<i>Cre</i>	CTTGGGCTGCCAGAATTTCTC	CCCAGAAATGCCAGATTACG
<b>Excision</b>		
<i>Rora</i> (PCR2)	CATGCATACACCCACACACATCACAACC	CAGCCGTGTGAACTTACGGGAAATACC
<b>qPCR</b>		
<i>Rplp0</i>	GGGAAGGTGTAATCAGTCTCCACAG	CATGCTGAACATCTCCCCCTTCTCC
<i>Ppia</i>	GCATACGGGTCTGCGCATCTTGTC	ATGGTGATCTTCTTGCTGGTCTTGC
<i>Rpl4</i>	CTGAACCCTTACGCCAAGAC	CCTTCTCGGATTTGGTTGCC
<i>Rps29</i>	GATCCGCAAATACGGGCTG	CCATTC AAGGTCGCTTAGTCC
<i>Rora</i> Exon 3	TTCCATGCAAGATCTGTGGAGAC	TGCAGCCTTCACACGTAAT
<i>Rorb</i>	CCCACACCTACGAGGAAATCAA	CATGAAGCCTGTTATCCGCTTG
<i>Rorc</i>	GGTACCATATGCCTCTCTGA	ATCTCCCACATTGACTTCCT
<i>Lyz2</i>	CAATGTGCAAAGAGGGTGGTG	TAGAGGGGAAATCGAGGGAATG
<i>Cre</i>	CCTGAAAATGCTTCTGTCCG	CAGGGTCTTATAAGCAATCCC
<i>Arntl</i>	GGACTTCGCCTCTACCTGTTT	ACCCGATTTCCCGTTC
<i>Ob</i>	GGTGTGAAAGAACCTGAGCTGAGG	CAGTGGATGCTAATGTGCCCTG
<i>Tnf</i>	AGCACAGAAAGCATGATCCG	CCCGAAGTTCAGTAGACAGAAGAG
<i>Il1b</i>	GCCACCTTTTGACAGTGATGAG	CCTGAAGCTCTTGTGATGTGC
<i>Il6</i>	CCAGTTGCCTTCTTGGGACTG	CAGGTCTGTTGGGAGTGGTATCC
<i>Il10</i>	AGGCGCTGTGCATCGATTCTC	TGGCCTTGACACACCTTGGTC
<i>Col1a1</i>	AGGCATAAAGGGTCATCGTGG	GAGACCGTTGAGTCCGTCTTT
<i>Col3a1</i>	TGGCAATGTAAAGAAGTCTC	CCCAGTGTGTTTAGTACAGC
<i>Acta2</i>	GCCGAGATCTCACCGACTAC	CAATCTCACGCTCGGCAGTA
<i>Cd19</i>	ACCTGACCATCGAGAGGCACGTG	CCTGGCGGGGTCAGTCATTGCTT
<i>Cd3e</i>	ACTGGAGCAAGAATAGGAAG	GGATGGGCTCATAGTCTG
<i>Adgre1</i>	CTTTGGCTATGGGCTTCCAGTC	GCAAGGAGGACAGAGTTTATCGTG
<i>Clec4f</i>	CCCAGGACCCTGCGGCACGTC	CCGAAGCAGGAGGGAGGGAGGCTC
<i>Ly6g</i>	TGATGGATTTTTCGTTGCTCTG	GTATTGTCCAGAGTAGTGGGGC
<i>Ccr2</i>	ATTCTCCACACCCTGTTTCG	CATGGCCTGGTCTAAGTGCT

**Table 4:** List of the primers used in mouse genotyping and qPCR.

	<b>Source</b>	<b>Identifier</b>
<b>Spleen</b>		
BV510 Anti-CD45 (Clone 30-F11)	BioLegend	#103137
PE-CF594 Anti-CD3e (Clone 145-2C11)	BD Biosciences	#562286
PE-CF594 Anti-TCR $\beta$ Chain (Clone H57-597)	BD Biosciences	#562841
PE-CF594 Anti-CD19 (Clone 1D3)	BD Biosciences	#562291
BUV395 Anti-CD11b (Clone M1/70)	BD Biosciences	#563553
BV421 Anti-Ly-6G (Clone 1A8)	BioLegend	#127627
PE/Cy7 Anti-F4/80 (Clone BM8)	BioLegend	#123113
FITC Anti-I-A/I-E (MHC class II) (Clone M5/114.15.2)	BioLegend	#107605
PE Anti-CD115 (CSF-1R) (Clone AFS98)	BioLegend	#135505
APC/Cy7 Anti-CD11c (Clone N418)	BioLegend	#117323
<b>Liver</b>		
BV510 Anti-CD45 (Clone 30-F11)	BioLegend	#103137
APC Anti-CD3e (Clone 145-2C11)	BD Biosciences	#553066
APC Anti-TCR $\beta$ Chain (Clone H57-597)	BD Biosciences	#553174
PE Anti-CD19 (Clone 1D3)	BD Biosciences	#557399
PE Anti-CD20 (Clone AISB12)	eBioscience	#12-0201-82
AF700 Anti-I-A/I-E (MHC class II) (Clone M5/114.15.2)	BioLegend	#107622
AF488 Anti-F4/80 (Clone BM8)	BioLegend	#123120
Anti-CLEC4F/CLECSF13 (Clone 370901)*	Bio-Techne	#MAB2784
<b>Adipose tissue</b>		
BV510 Anti-CD45 (Clone 30-F11)	BioLegend	#103137
APC Anti-CD3e (Clone 145-2C11)	BD Biosciences	#553066
APC Anti-TCR $\beta$ Chain (Clone H57-597)	BD Biosciences	#553174
PE Anti-CD19 (Clone 1D3)	BD Biosciences	#557399
PE Anti-CD20 (Clone AISB12)	eBioscience	#12-0201-82
AF700 Anti-I-A/I-E (MHC class II) (Clone M5/114.15.2)	BioLegend	#107622
AF488 Anti-F4/80 (Clone BM8)	BioLegend	#123120
BV711 Anti-CD64 (FcyRI) (Clone X54-5/7.1)	BioLegend	#139311
<b>Lung</b>		
BV510 Anti-CD45 (Clone 30-F11)	BioLegend	#103137
PE-CF594 Anti-CD3e (Clone 145-2C11)	BD Biosciences	#562286
PE-CF594 Anti-TCR $\beta$ Chain (Clone H57-597)	BD Biosciences	#562841
PE-CF594 Anti-CD19 (Clone 1D3)	BD Biosciences	#562291
PE/Cy7 Anti-F4/80 (Clone BM8)	BioLegend	#123114
BV711 Anti-CD64 (FcyRI) (Clone X54-5/7.1)	BioLegend	#139311
BUV395 Anti-CD11b (Clone M1/70)	BD Biosciences	#563553
AF647 Anti-Siglec-F (Clone E50-2440)	BD Biosciences	#562680

\* Anti-CLEC4F antibody was coupled with PE/Cy7 by using PE/Cy7 Conjugation Kit - Lightning-Link (Abcam, #ab102903).

**Table 5:** List of the antibodies used in cell sorting.

## RESULTS

### 1. Impact of macrophage-specific ROR $\alpha$ deletion on HFD-induced obesity, IR, NAFL and obesity-independent NASH development

#### A. Generation and characterization of the macrophage-specific ROR $\alpha$ -deficient mice

We generated *Rora* floxed mice by introducing *loxP* sites flanking exon 3 (Figure 1A). Exon 3, the first common exon of isoforms 1 and 4, encodes for the DBD and includes the first zinc finger motif. Deletion of exon 3 leads to a frameshift, resulting in a premature stop codon and the absence of functional domains (Figure 1B-C).

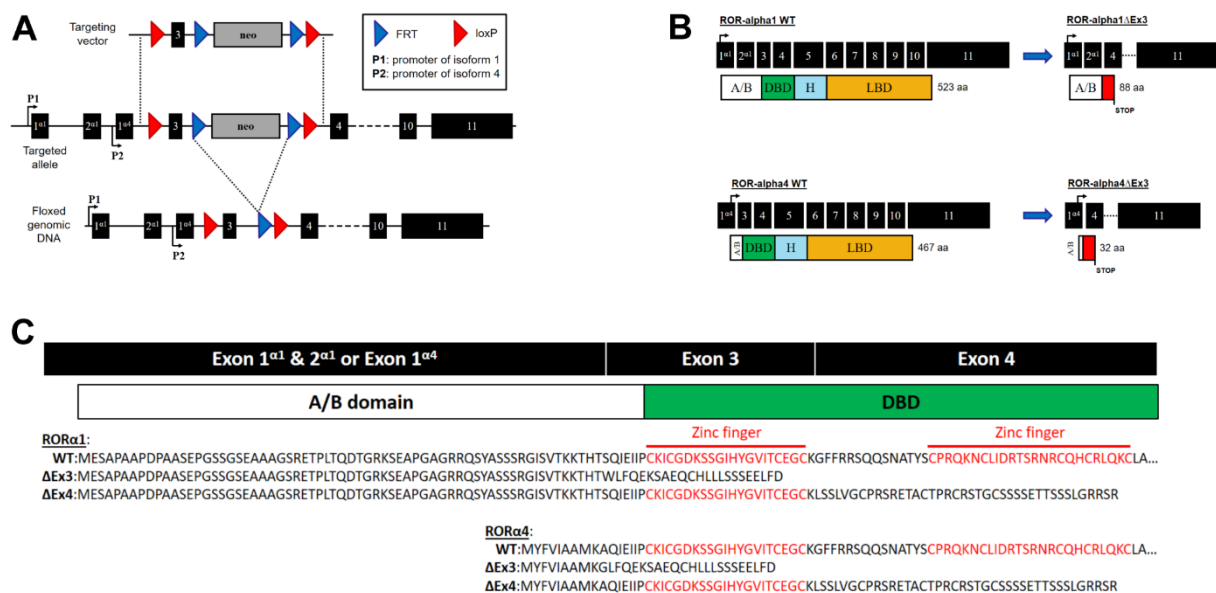


**Figure 1:** Generation of macrophage-specific ROR $\alpha$ -deficient (MKO) mice.

**(A)** Schematic representation of the strategy to target exon 3 of *Rora*. **(B)** mRNA structures of ROR $\alpha$ 1 and ROR $\alpha$ 4 and the resulting proteins in both WT and MKO ( $\Delta$ Ex3) mice. Exons are represented in black. Protein predictions are illustrated below mRNA and functional domains are indicated with colors. **(C)** Comparison of *Rora* exon 3 and exon 4 deletion on protein translation. Zinc finger motifs are indicated in red. Protein predictions were generated with Translate tool from ExPASy (<https://web.expasy.org/translate>) by using GenBank sequences for ROR $\alpha$ 1 (NM\_013646.2) and ROR $\alpha$ 4 (NM\_001289916.1).

To achieve ROR $\alpha$  deletion in macrophages, the floxed mice were subsequently crossed with the LysM-Cre mice. *Rora*<sup>fl/fl</sup> *Lyz2*<sup>Cre/+</sup> (MKO) mice and their littermate controls *Rora*<sup>+/+</sup> *Lyz2*<sup>Cre/+</sup> (WT), exhibiting comparable expression of *Lyz2* and *Cre* (Figure 2A), were further studied. To validate and characterize the ROR $\alpha$  deletion in MKO mice, we demonstrated the excision of exon 3 in DNA from sorted splenic macrophages (Figure 2B).

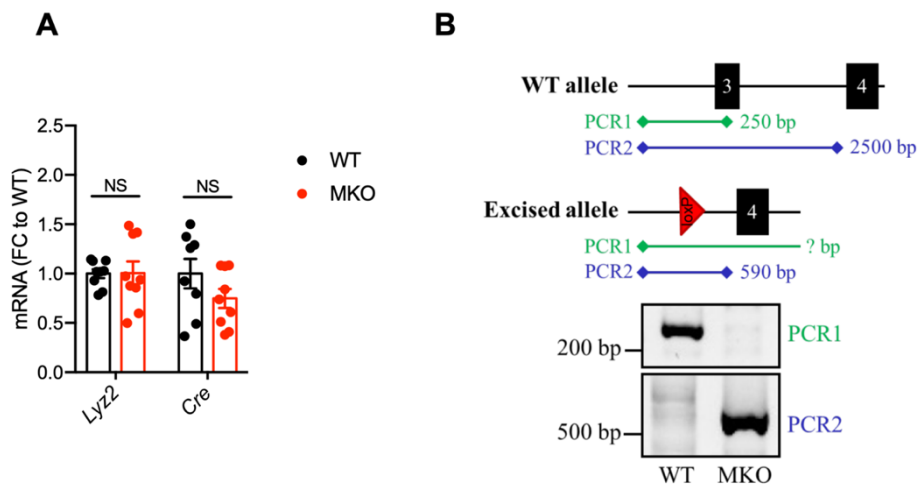


**Figure 2:** Characterization of ROR $\alpha$  MKO mice. **(A)** mRNA expression levels measured by RT-qPCR for *Lyz2* and *Cre* genes in spleen from WT (*Rora*<sup>+/+</sup> *Lyz2*<sup>Cre/+</sup>) and MKO (*Rora*<sup>fl/fl</sup> *Lyz2*<sup>Cre/+</sup>) mice. **(B)** PCR analysis of genomic DNA extracted from sorted splenic macrophages of WT and MKO mice. Locations of primer hybridization are represented with  $\blacklozenge$ . Data are shown as mean  $\pm$  SEM. \*  $p < 0.05$ ; \*\*  $p < 0.01$ ; \*\*\*  $p < 0.001$  by 2-way ANOVA followed by Sidak's multiple comparisons test or unpaired t test. n= 8-10 mice per genotype for **A**. NS: Not significant; AU: Arbitrary unit; FC: Fold change.

Since the LysM-Cre mouse model mainly targets macrophages and neutrophils, but also a fraction of monocytes and DCs, we sorted these populations from spleen and quantified the deletion of exon 3 in *Rora* mRNA by RT-qPCR (Figure 3A). MKO mice displayed an important deletion of exon 3 in macrophages and to a lesser extent in monocytes and DCs, but surprisingly not in neutrophils. No deletion of exon 3 in *Rora* mRNA was observed in T cells and B cells. To confirm the absence of deletion in neutrophils, we also analyzed the bone marrow (BM) cells, which mainly contain neutrophils. Neither total BM cells nor purified neutrophils from BM showed a deletion of exon 3, while bone marrow-derived macrophages (BMDM) did (Figure 3B). Collectively, our results show that macrophages, monocytes and DCs, but not neutrophils, exhibit a LysM-Cre-induced deletion of *Rora* exon 3.

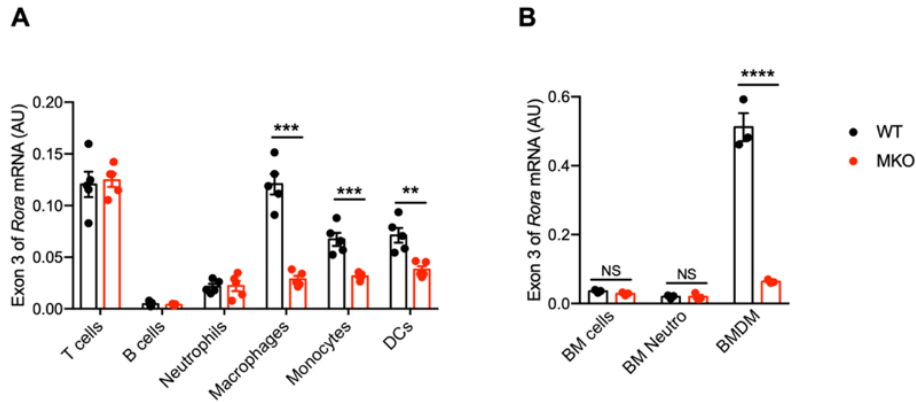


**Figure 3:** Characterization of ROR $\alpha$  MKO mice. **(A)** mRNA expression levels measured by RT-qPCR for the exon 3 of *Rora* in B cells, T cells, neutrophils, macrophages, monocytes, and dendritic cells (DCs) sorted from the spleen of WT and MKO mice. **(B)** mRNA expression levels measured by RT-qPCR for the exon 3 of *Rora* in total bone marrow (BM) cells, in neutrophils purified from BM and in BM-derived macrophages (BMDM) from WT and MKO mice. Data are shown as mean  $\pm$  SEM. \*  $p < 0.05$ ; \*\*  $p < 0.01$ ; \*\*\*  $p < 0.001$  by 2-way ANOVA followed by Sidak's multiple comparisons test or unpaired t test  $n = 5$  mice per genotype for **A** and  $n = 3$  mice per genotype for **B**. NS: Not significant; AU: Arbitrary unit; FC: Fold change.

*Rorc* expression was not affected by *Rora* deletion (Figure 4A) and *Rorb* was undetectable in both WT and MKO immune cells (data not shown), suggesting no compensatory regulation of other ROR genes. The expression of a key ROR target gene *Arntl*, encoding for BMAL1, was significantly lower in ROR $\alpha$ -deficient splenic macrophages and BMDM (Figure 4B-C). A tendency to a lower *Arntl* expression was also observed in monocytes, but not in DCs, probably due to the high expression of *Rorc* (Figure 4A). Thus, despite the significant LysM-Cre-induced deletion of exon 3 in monocytes and DCs, MKO mice foremost displayed a phenotype in macrophages.

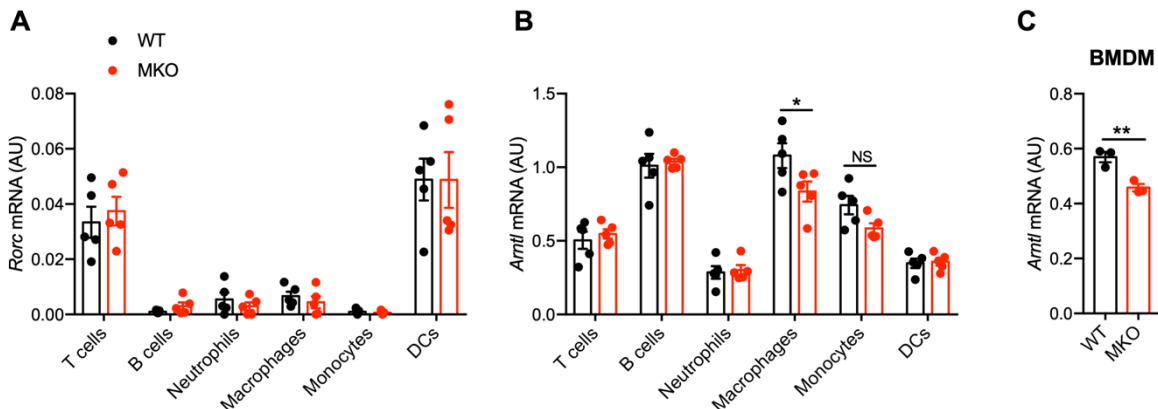


**Figure 4:** Characterization of ROR $\alpha$  MKO mice. **(A-B)** mRNA expression levels measured by RT-qPCR for *Rorc* **(A)** and *Arntl* **(B)** genes in B cells, T cells, neutrophils, macrophages, monocytes, and DCs sorted from the spleen of WT and MKO mice. **(C)** mRNA expression levels measured by RT-qPCR for *Arntl* in BMDM. Data are shown as mean  $\pm$  SEM. \*  $p < 0.05$ ; \*\*  $p < 0.01$ ; \*\*\*  $p < 0.001$  by 2-way ANOVA followed by Sidak's multiple comparisons test or unpaired t test  $n = 5$  mice per genotype for **A & B**,  $n = 3$  mice per genotype for **C**. NS: Not significant; AU: Arbitrary unit; FC: Fold change.

As macrophages display some tissue-specific characteristics, we sorted ATM (CD45<sup>+</sup> CD3 $\epsilon$ <sup>-</sup> TCR $\beta$ <sup>-</sup> CD19<sup>-</sup> CD20<sup>-</sup> F4/80<sup>+</sup> CD64<sup>+</sup>) from epididymal AT to evaluate the efficiency of *Rora* deletion in these cells. Similar to the splenic macrophages and BMDM, MKO mice showed a significant deletion of exon 3 and a significant decrease of the ROR target gene *Arntl* in ATM (Figure 5A). No significant deletion of exon 3 occurred in total epididymal AT, liver nor skeletal muscle (Figure 5B), suggesting the absence of an unwanted recombination in parenchymal cells of metabolic tissues.

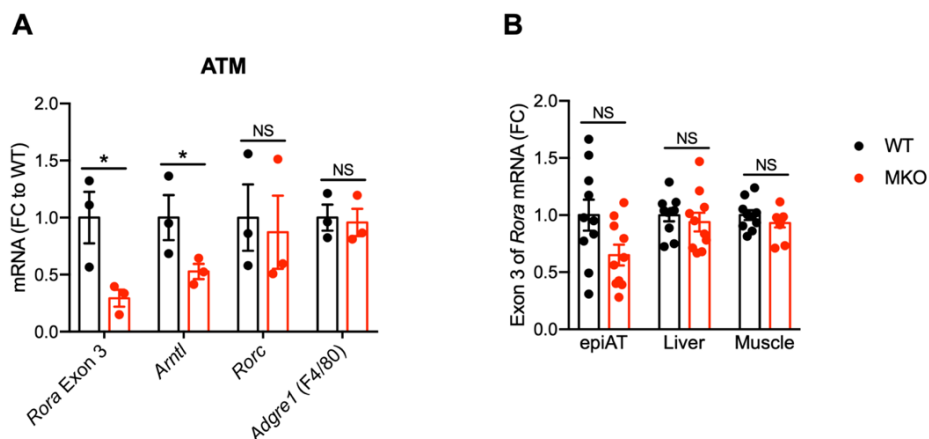


**Figure 5:** Characterization of ROR $\alpha$  MKO mice. **(A)** mRNA expression levels measured by RT-qPCR for the exon 3 of *Rora*, *Arntl*, *Rorc* and *Adgre1* in adipose tissue macrophages (ATM) sorted from epididymal adipose tissue of WT and MKO mice. **(B)** mRNA expression levels measured by RT-qPCR for the exon 3 of *Rora* in liver, epididymal adipose tissue (epiAT) and skeletal muscle from WT and MKO mice. Data are shown as mean  $\pm$  SEM. \*  $p < 0.05$ ; \*\*  $p < 0.01$ ; \*\*\*  $p < 0.001$  by 2-way ANOVA followed by Sidak's multiple comparisons test or unpaired t test.  $n =$  each dot represents a pool of 3-4 mice for **A**, and  $n = 8-10$  mice per genotype for **B**. NS: Not significant; AU: Arbitrary unit; FC: Fold change.

## B. ROR $\alpha$ deletion in macrophages does not affect LPS-induced inflammation *in vitro*

As previous studies have reported super induction of several cytokines, including TNF $\alpha$ , IL-6, and IL1 $\beta$  in isolated LPS-treated ROR $\alpha$ -deficient macrophages by using *staggerer* mice<sup>545, 546, 528</sup>. Taking into consideration the impact of gut microbiota-derived LPS on metabolic diseases, we first investigated cytokine response upon LPS treatment in wild-type and ROR $\alpha$ -deficient bone marrow-derived macrophages (BMDM). We performed a time course stimulation with 50 ng/mL of LPS and analyzed the mRNA expression and secretion of TNF $\alpha$  and IL-6 in supernatant (SN) and observed no statistical differences at any time points between WT and ROR $\alpha$ -deficient BMDM (Figure 6A-B).

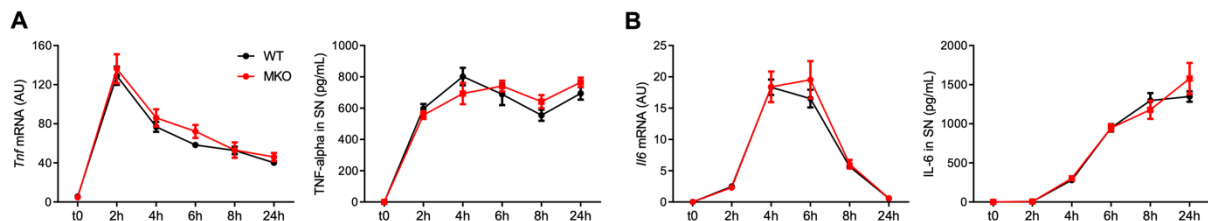


**Figure 6:** Impact of ROR $\alpha$  deletion on cytokine response upon LPS treatment in BMDM. BMDM from WT and MKO mice were treated with 50 ng/mL of LPS before analysis of **(A)** cytokine release in supernatant (SN) by ELISA and **(B)** gene expression by RT-qPCR. Data are shown as mean  $\pm$  SEM. 2-way ANOVA followed by Sidak's multiple comparisons test  $n = 4-5$  mice per genotype. AU: Arbitrary unit.

We also treated BMDM for 8 hours with a lower (10 ng/mL) and a higher (100 ng/mL) LPS concentration and observed no differences between genotypes for TNF $\alpha$  and IL-6 (Figure 7A-B).

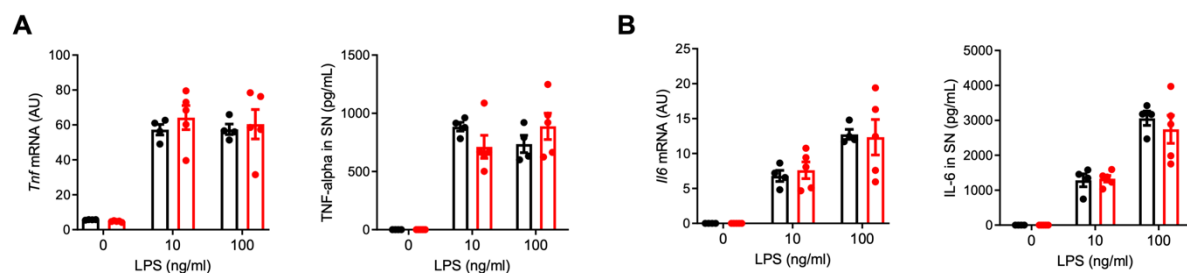


**Figure 7:** Impact of ROR $\alpha$  deletion on cytokine response upon LPS treatment in BMDM. BMDM from WT and MKO mice were treated with 10 or 100 ng/mL of LPS for 8 hours before analysis of **(A)** cytokine release in SN by ELISA and **(B)** gene expression by RT-qPCR. Data are shown as mean  $\pm$  SEM. 2-way ANOVA followed by Sidak's multiple comparisons test n= 4-5 mice per genotype. AU: Arbitrary unit.

We also measured *I11b* gene expression in time course (Figure 8A) and dose-response (Figure 8B) experiments and observed no differences between WT and ROR $\alpha$ -deficient BMDM as well. Because LPS treatment alone did not result in a detectable level of mature IL-1 $\beta$  in SN, we treated BMDM with both LPS and aluminum hydroxide, a well-known inflammasome activator leading to maturation and secretion of IL-1 $\beta$ , and detected no difference in IL-1 $\beta$  release in both genotypes (Figure 8C).

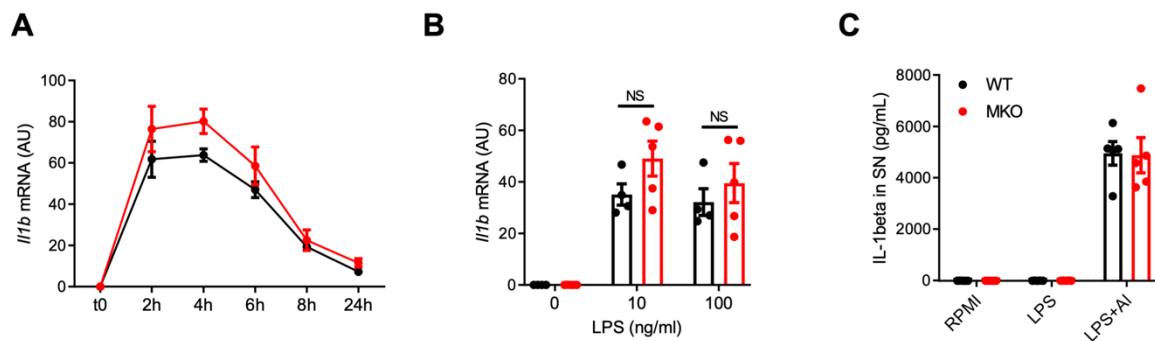


**Figure 8:** Impact of ROR $\alpha$  deletion on cytokine response upon LPS treatment in BMDM. BMDM from WT and MKO mice were treated with either 50 ng/mL or 10 ng/mL or 100 ng/mL of LPS for 8 hours before analysis of **(A-B)** gene expression by RT-qPCR. **(C)** ELISA for IL-1 $\beta$  in SN of BMDM treated with 10 ng/mL of LPS for 8 hours. 400 $\mu$ g/mL of aluminum hydroxide was added 2 hours after LPS stimulation. Data are shown as mean  $\pm$  SEM. 2-way ANOVA followed by Sidak's multiple comparisons test n= 4-5 mice per genotype. NS: Not significant, AU: Arbitrary unit.

We confirmed that deletion of *Rora* (85%, measured by exon 3 deletion) expectedly decreased expression of *Arntl* (BMAL1, ROR $\alpha$ -target gene) by 50% in untreated conditions (Figure 9A-D). Interestingly, we also observed that LPS downregulates *Rora* and *Arntl* expression, abolishing the effect of ROR $\alpha$  deletion on *Arntl* after 2-4 hours (Figure 9A). This observation is in agreement with earlier work showing that LPS decreases circadian genes, including *Arntl*<sup>547</sup>. Thus, it seems reasonable to conclude that a condition leading to a downregulation of

ROR $\alpha$  and its target genes is unlikely to reveal a major phenotype. These results show that ROR $\alpha$  does not regulate LPS-induced BMDM inflammatory response unlike reported earlier.

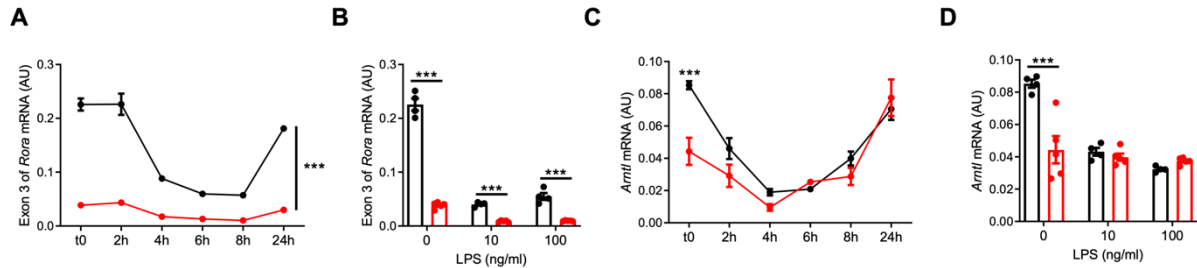


**Figure 9:** Impact of ROR $\alpha$  deletion on cytokine response upon LPS treatment in BMDM. BMDM from WT and MKO mice were treated with either 50 ng/mL or 10 ng/mL or 100 ng/mL of LPS for 8 hours before analysis of **(A-B)** exon 3 of Rora **(C-D)** *Arntl* gene expression by RT-qPCR. Data are shown as mean  $\pm$  SEM. \*\*\*  $p < 0.001$  by 2-way ANOVA followed by Sidak's multiple comparisons test.  $n = 4-5$  mice per genotype. AU: Arbitrary unit.

### C. ROR $\alpha$ deletion in macrophages does not affect obesity, IR nor hepatic steatosis

To investigate the role of macrophages ROR $\alpha$  in metabolic functions, in particular obesity and IR, we fed WT and MKO mice with a 60% high fat diet (HFD) for 12 weeks. WT and MKO mice under HFD significantly gained weight, AT mass and leptin expression increased similarly in both genotypes (Figure 10A-C).

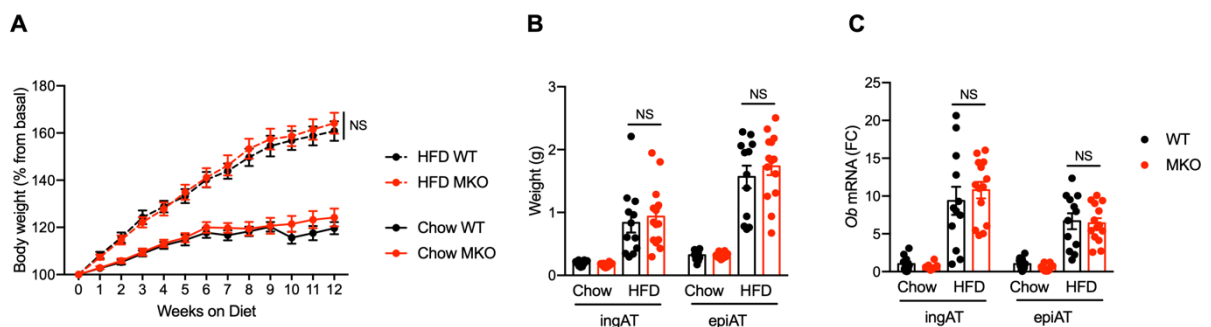


**Figure 10:** Effect of ROR $\alpha$  deletion in macrophages on HFD-induced obesity. Ten weeks old WT and MKO mice were fed with either a chow or a HFD for 12 weeks. **(A)** Body weight gain. **(B)** Weight of inguinal (IngAT) and epididymal (epiAT) adipose tissues. **(C)** mRNA expression levels measured by RT-qPCR for the *Ob* gene in both IngAT and epiAT. Data are shown as mean  $\pm$  SEM. 2-way ANOVA followed by Sidak's multiple comparisons test was performed. n=10-15 mice per group. NS: Not significant; FC: Fold Change.

Likewise, plasma cholesterol and triglyceride levels were not different between WT and MKO mice (Figure 11). Overall, these findings suggest that ROR $\alpha$  deletion in macrophages has no impact on HFD-induced obesity.

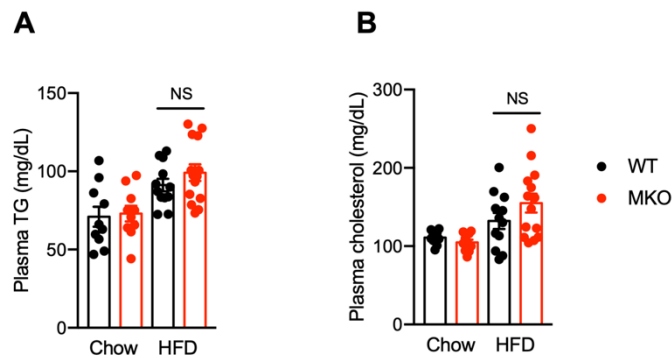


**Figure 11:** Effect of ROR $\alpha$  deletion in macrophages on HFD-induced obesity and IR. Ten weeks old WT and MKO mice were fed with either a chow or a HFD for 12 weeks. **(A)** Plasma triglyceride (TG). **(B)** Plasma cholesterol. Data are shown as mean  $\pm$  SEM. 2-way ANOVA followed by Sidak's multiple comparisons test was performed. n=10-15 mice per group. NS: Not significant; AU: Arbitrary unit.

Fasting serum glucose and insulin concentrations increased significantly upon HFD feeding although no difference between genotypes was observed (Figure 12A-B). Furthermore, we observed no difference in glucose levels between WT and MKO mice during IPGTT and IPITT (Figure 12C-D).

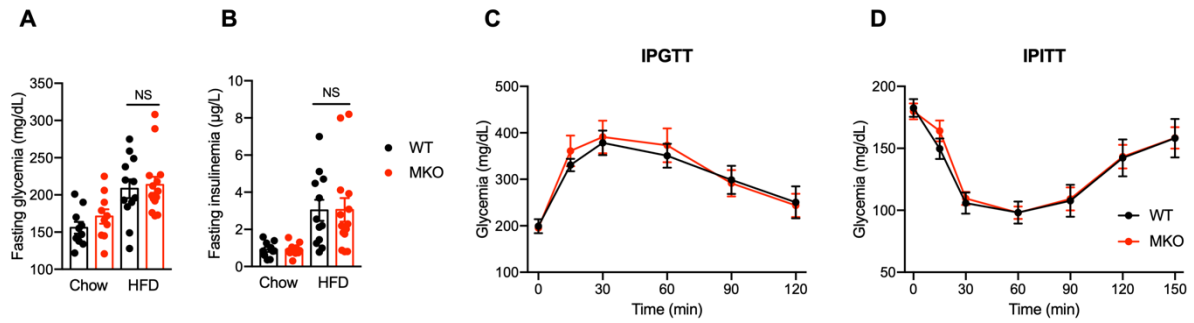


**Figure 12:** Effect of ROR $\alpha$  deletion in macrophages on HFD-induced obesity and IR. Ten weeks old WT and MKO mice were fed with either a chow or a HFD for 12 weeks. After 10 weeks of diet, mice were fasted for 5 hours and glycemia (A) and insulinemia (B) were measured, (C) then intraperitoneally injected with 1g/kg glucose for a glucose tolerance test (IPGTT). (D) Intraperitoneal insulin tolerance test (IPITT) was performed by injecting 1 IU/kg insulin after 11 weeks of diet and 5 hours of fasting. Data are shown as mean  $\pm$  SEM. 2-way ANOVA followed by Sidak's multiple comparisons test was performed. n=10-15 mice per group. NS: Not significant; FC: Fold Change.

Moreover, insulin signaling in skeletal muscle, epididymal AT and liver was similar in both genotypes (Figure 13).

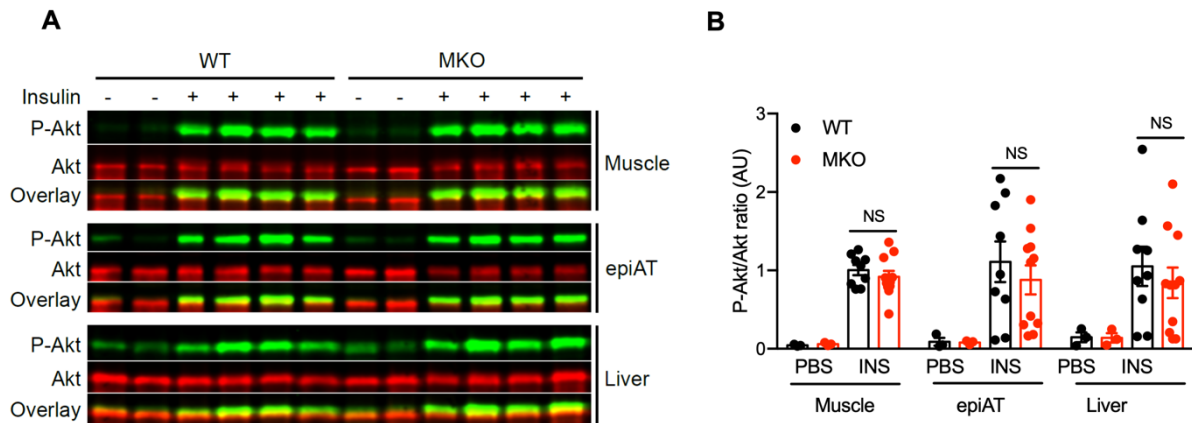


**Figure 13:** Effect of ROR $\alpha$  deletion in macrophages on HFD-induced obesity and IR. Ten weeks old WT and MKO mice were fed with either a chow or a HFD for 12 weeks. (A) Western blot of phospho-AKT<sup>Ser473</sup> in skeletal muscle, epiAT and liver. Mice were injected with either PBS or 1 IU of insulin 15 min before sacrifice. Images were cropped for sake of clarity. (B) Quantification of western blot for phospho-Akt in skeletal muscle, epididymal adipose tissue (epiAT) and liver. Data are shown as mean  $\pm$  SEM. 2-way ANOVA followed by Sidak's multiple comparisons test was performed. n=10-15 mice per group. NS: Not significant; FC: Fold Change.

Considering AT inflammation is a central driver for obesity-induced IR, no difference in *Tnf*, *Il1b*, *Il6*, and *Il10* expression was observed in epididymal AT between WT and MKO mice (Figure 14). Taken together, our results show that ROR $\alpha$  deletion in macrophages has no impact on obesity-induced IR.

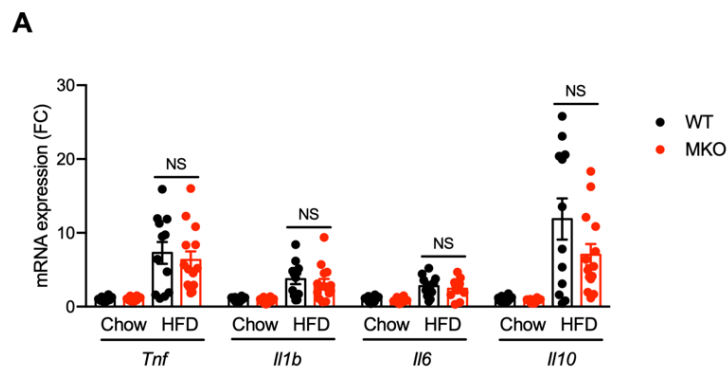


**Figure 14:** Effect of ROR $\alpha$  deletion in macrophages on HFD-induced obesity and IR. Ten weeks old WT and MKO mice were fed with either a chow or a HFD for 12 weeks. **(A)** mRNA expression levels measured by RT-qPCR for *Tnf*, *Il1b*, *Il6*, and *Il10* genes in epiAT. Data are shown as mean  $\pm$  SEM. 2-way ANOVA followed by Sidak's multiple comparisons test was performed. n=10-15 mice per group. NS: Not significant; FC: Fold Change.

In interconnection with obesity and IR, HFD feeding also induces liver steatosis. Liver weight, hepatic triglyceride content, and steatosis level determined by histology were increased upon HFD feeding to the same extent in WT and MKO mice (Figure 15).

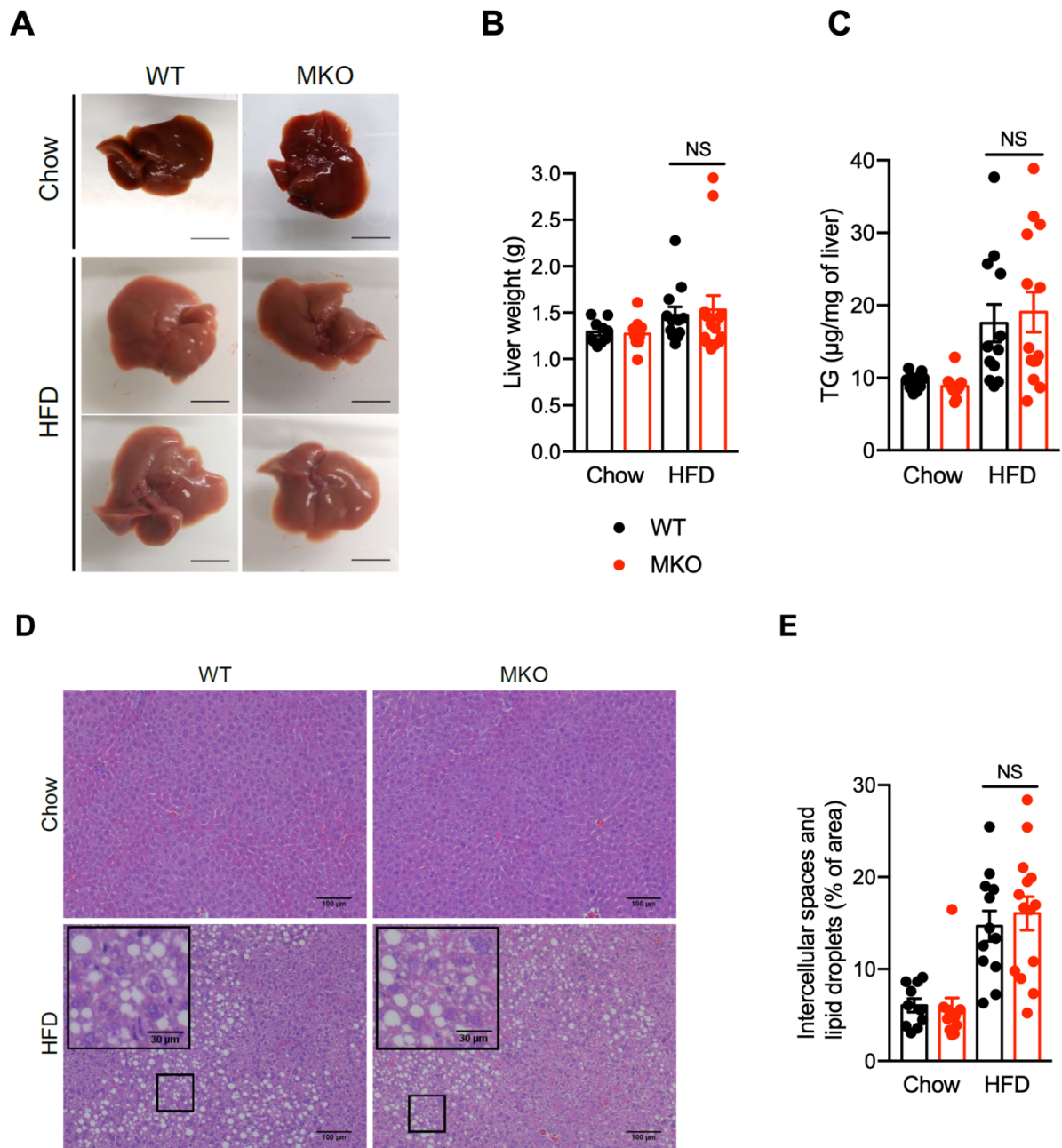


**Figure 15:** Effect of ROR $\alpha$  deletion in macrophages on liver upon HFD feeding. Ten weeks old WT and MKO mice were fed with either a chow or a HFD for 12 weeks. **(A)** Representative liver gross morphology. **(B)** Liver weight. **(C)** Hepatic triglycerides (TG) content. **(D)** Hematoxylin & Eosin staining of liver sections and **(E)** quantification of lipid droplets. Data are shown as mean  $\pm$  SEM. 2-way ANOVA followed by Sidak's multiple comparisons test was performed. n=10-15 mice per group. NS: Not significant; FC: Fold Change.

Histology analysis did not reveal cell infiltrates upon HFD feeding despite the significantly increased expression of inflammatory genes such as *Tnf*, *Il1b*, *Il6* and *Il10* (Figure 16A). Likewise, we did not observe any significant differences in hepatic cytokine expression between WT and MKO mice besides a tendency to a lower *Il10* expression in MKO mice ( $p=0.07$ ). HFD feeding induced a similar mild increase of plasma transaminase activity in both WT and MKO mice (Figure 16B).

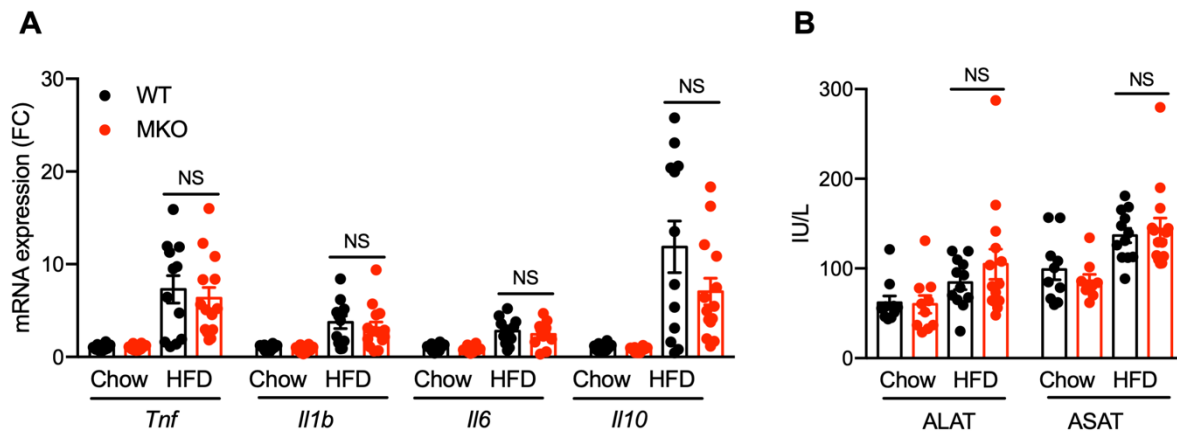


**Figure 16:** Effect of ROR $\alpha$  deletion in macrophages on liver upon HFD feeding. Ten weeks old WT and MKO mice were fed with either a chow or a HFD for 12 weeks. **(A)** mRNA expression levels measured by RT-qPCR for *Tnf*, *Il1b*, *Il6*, and *Il10* genes in liver. **(B)** Plasma transaminases activity. Data are shown as mean  $\pm$  SEM. 2-way ANOVA followed by Sidak's multiple comparisons test was performed.  $n=10-15$  mice per group. NS: Not significant; FC: Fold Change.

Liver fibrosis and expression of collagen genes slightly increased upon HFD feeding for 12 weeks at comparable level between WT and MKO mice (Figure 17). Collectively, our results display that ROR $\alpha$  deletion in macrophages has no impact on HFD-induced liver steatosis nor fibrosis.

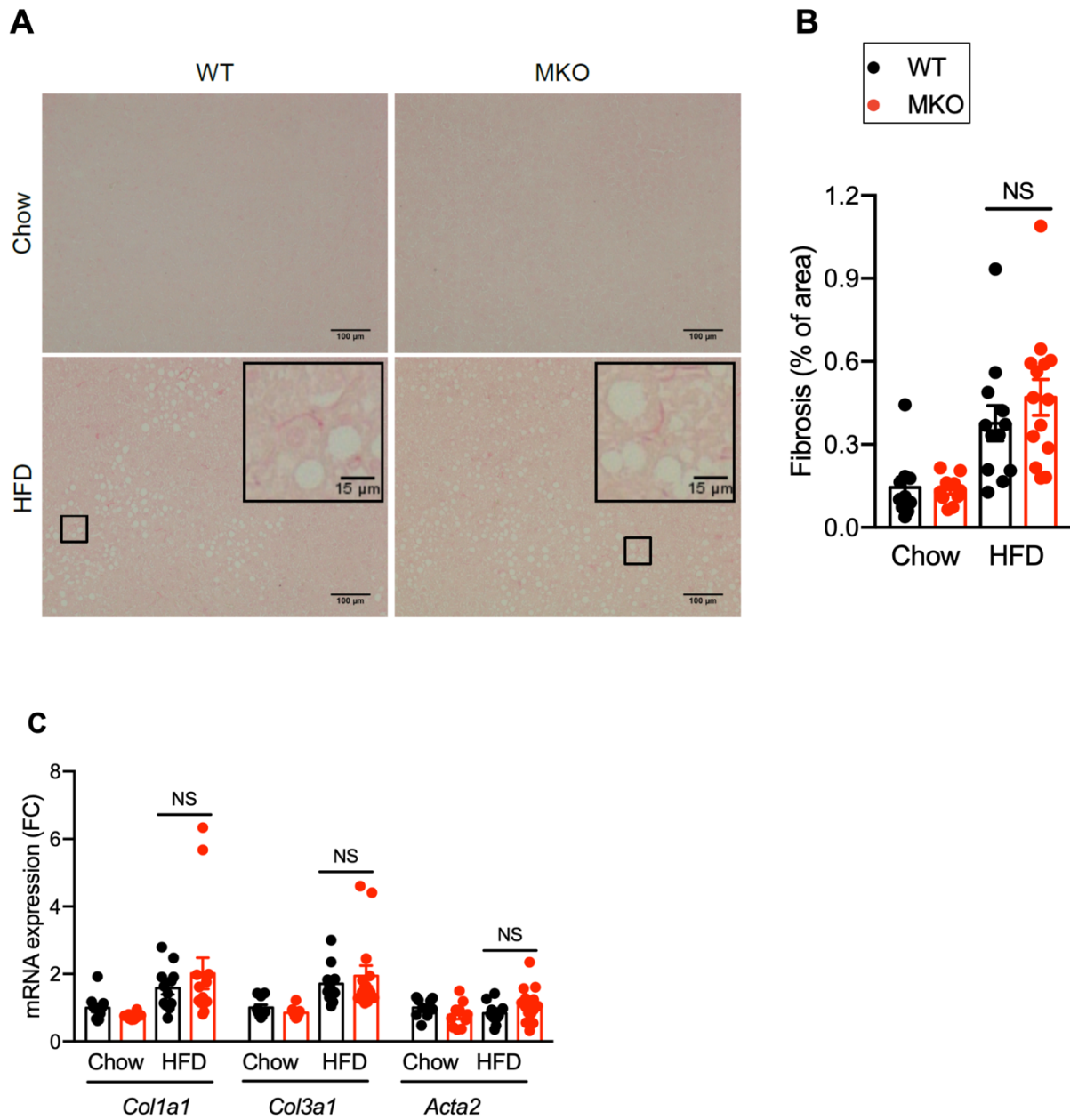


**Figure 17:** Effect of ROR $\alpha$  deletion in macrophages on liver upon HFD feeding. Ten weeks old WT and MKO mice were fed with either a chow or a HFD for 12 weeks. **(A)** Sirius red staining of liver sections and **(B)** quantification of fibrosis. **(C)** mRNA expression levels measured by RT-qPCR for *Col1a1*, *Col3a1*, and *Acta2* genes in the liver. Data are shown as mean  $\pm$  SEM. 2-way ANOVA followed by Sidak's multiple comparisons test was performed. n=10-15 mice per group. NS: Not significant; FC: Fold Change.

#### D. ROR $\alpha$ deletion in macrophages does not affect NASH

As a generally accepted fact, HFD feeding efficiently promotes obesity and IR, the liver pathology is mainly characterized by triglyceride accumulation corresponding to the NAFL stage. To investigate whether the deletion of ROR $\alpha$  in macrophages might play a role in advanced NAFLD, WT and MKO mice were fed with the choline-deficient, L-amino acid-defined (CDAA) diet supplemented with sucrose and 2% cholesterol for 8 weeks, leading to a pronounced hepatic steatosis, inflammation and fibrosis, but dissociated from obesity and IR, allowing the analysis of liver-centric responses. Thus, unlike HFD, the CDAA diet did not induce obesity, hyperglycemia nor AT inflammation, but led to a 10% weight loss and a drop of glycemia of 30% in both WT and MKO (Figure 18).

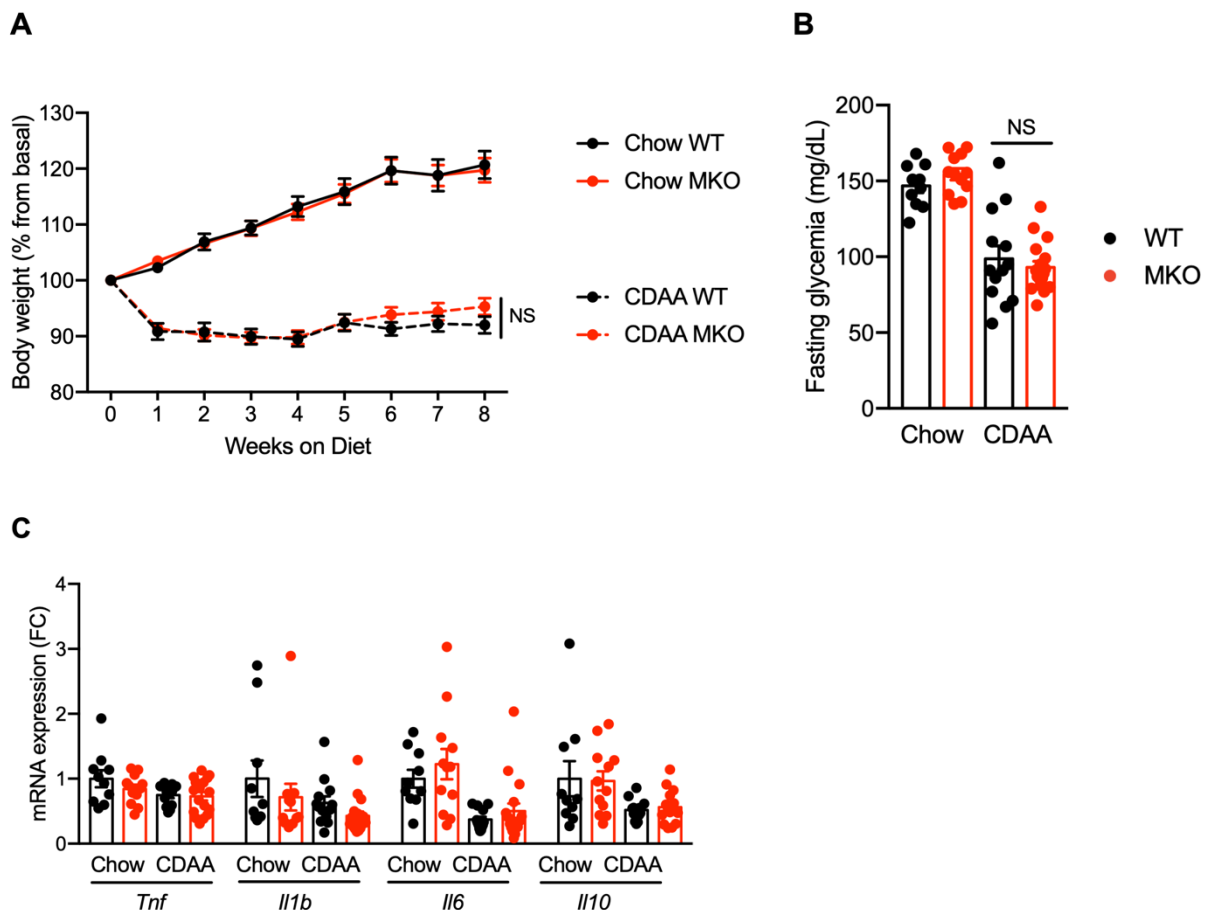


**Figure 18:** Effect of ROR $\alpha$  deletion in macrophages upon CDAA diet feeding. Ten weeks old WT and MKO mice were fed with either a chow or a CDAA diet for 8 weeks. **(A)** Body weight gain. **(B)** Fasting glycemia. **(C)** mRNA expression levels measured by RT-qPCR for *Tnf*, *Il1b*, *Il6*, and *Il10* genes in epiAT. Data are shown as mean  $\pm$  SEM. 2-way ANOVA followed by Sidak's multiple comparisons test was performed. n=10-17 mice per group. NS: Not significant; FC: Fold Change.

The CDAA diet produced a massive hepatic steatosis, but ROR $\alpha$  deletion in macrophages did not impact on liver weight nor steatosis level (Figure 19).

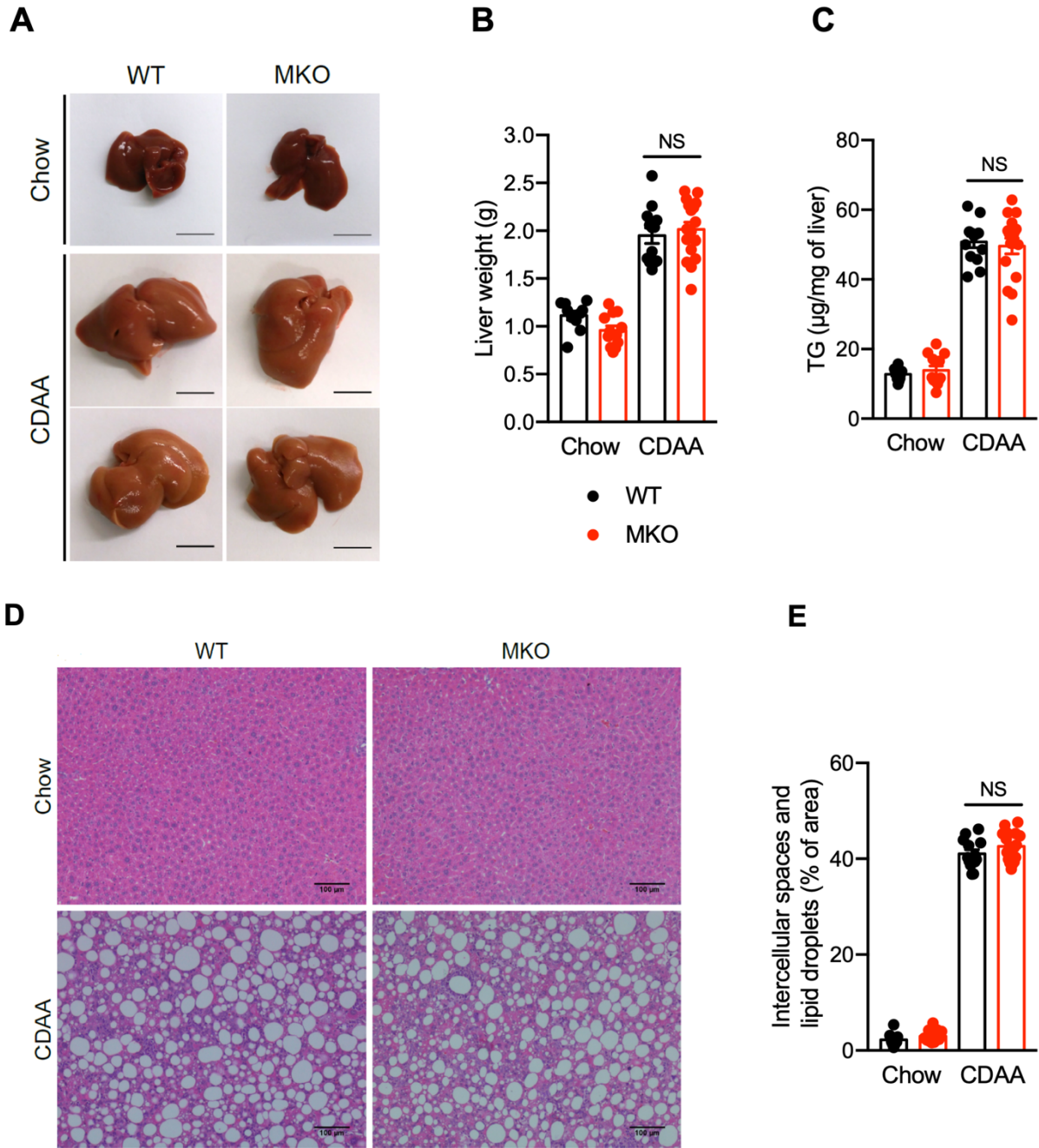


**Figure 19:** Effect of ROR $\alpha$  deletion in macrophages upon CDAA diet feeding. Ten weeks old WT and MKO mice were fed with either a chow or a CDAA diet for 8 weeks. **(A)** Representative liver gross morphology. **(B)** Liver weight. **(C)** Hepatic triglycerides (TG) content **(D)** Hematoxylin & Eosin staining of liver sections and **(E)** quantification of lipid droplets. Data are shown as mean  $\pm$  SEM. \*  $p < 0.05$  by 2-way ANOVA followed by Sidak’s multiple comparisons test.  $n = 10-17$  mice per group. NS: Not significant; FC: Fold Change.

Histological analysis showed evidences of cell infiltrates upon CDAA diet feeding but no manifest difference between WT and MKO mice was observed (Figure 20A). Further analysis of the expression of inflammatory genes revealed no difference in *Tnf* and *Il6* expression whereas *Il1b* and *Il10* mRNA significantly decreased in livers of MKO mice (Figure 20B).

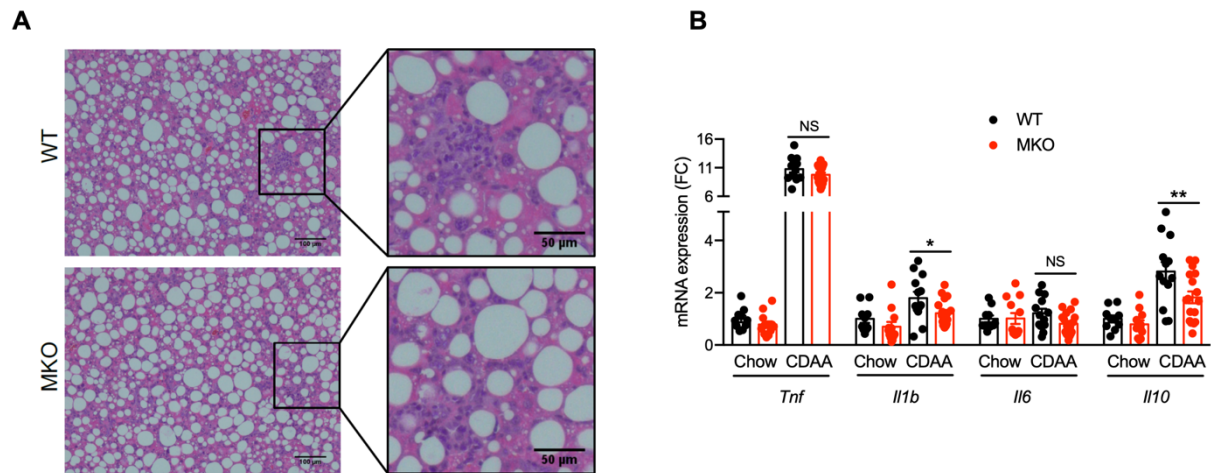


**Figure 20:** Effect of ROR $\alpha$  deletion in macrophages upon CDAA diet feeding. Ten weeks old WT and MKO mice were fed with either a chow or a CDAA diet for 8 weeks. **(A)** Hematoxylin & Eosin staining of liver sections. **(B)** mRNA expression levels measured by RT-qPCR for *Tnf*, *Il1b*, *Il6*, and *Il10* genes in liver. Data are shown as mean  $\pm$  SEM. \*  $p < 0.05$ ; \*\*  $p < 0.01$  by 2-way ANOVA followed by Sidak's multiple comparisons test.  $n = 10-17$  mice per group. NS: Not significant; FC: Fold Change.

Despite this modest decrease in cytokine expression, we did not observe any significant differences in plasma transaminase activity at sacrifice (Figure 21) and in the weekly time course measurements, while a strong effect of the CDAA diet was found on these parameters (Figure 22).

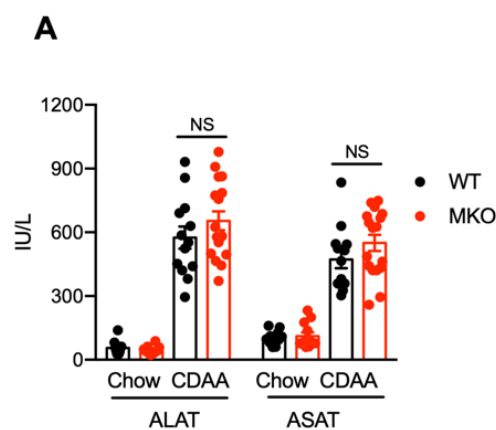


**Figure 21:** Effect of ROR $\alpha$  deletion in macrophages upon CDAA diet feeding. Ten weeks old WT and MKO mice were fed with either a chow or a CDAA diet for 8 weeks. **(A)** Plasma transaminases activity. Data are shown as mean  $\pm$  SEM. 2-way ANOVA followed by Sidak's multiple comparisons test was performed. n=10-17 mice per group. NS: Not significant; FC: Fold Change.

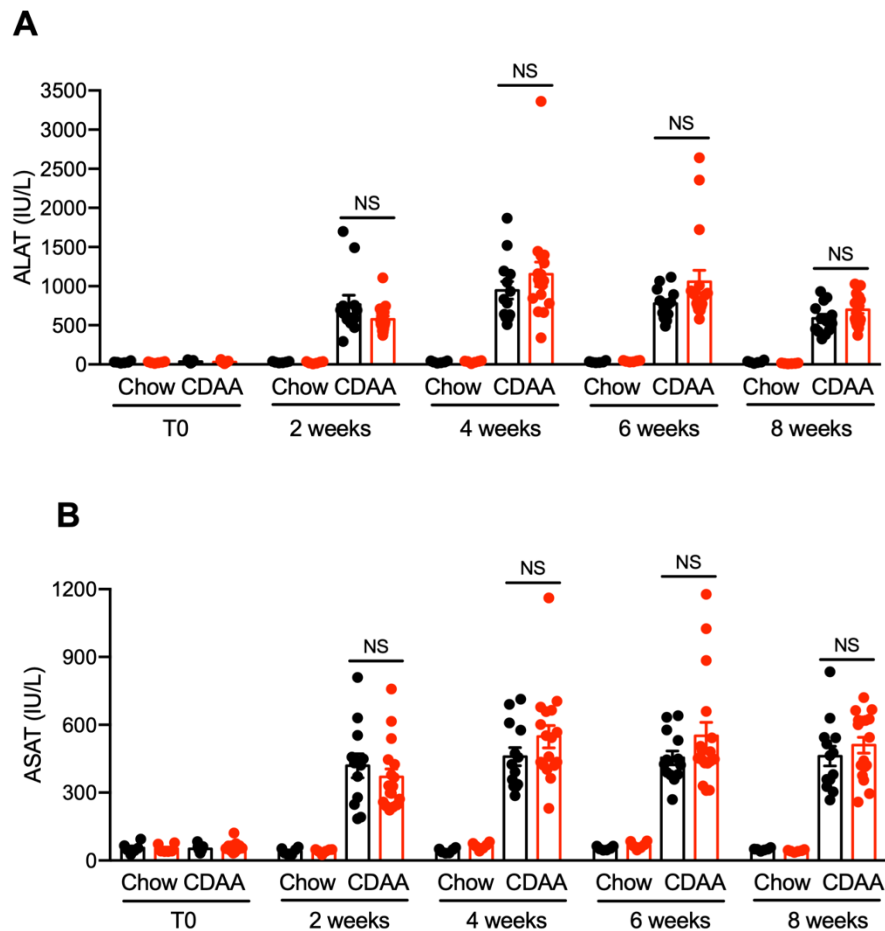


**Figure 22:** Effect of ROR $\alpha$  deletion in macrophages upon CDAA diet feeding. Ten weeks old WT and MKO mice were fed with either a chow or a CDAA diet for 8 weeks. **(A & B)** Kinetics of plasma transaminases activity. Data are shown as mean  $\pm$  SEM. 2-way ANOVA followed by Sidak's multiple comparisons test was performed. n=10-17 mice per group. NS: Not significant; FC: Fold Change.

Hepatic fibrosis and expression of collagen genes greatly increased upon CDAA diet feeding for 8 weeks at comparable level between WT and MKO mice (Figure 23). These results indicate that deletion of ROR $\alpha$  in macrophages does not affect CDAA-induced NASH.

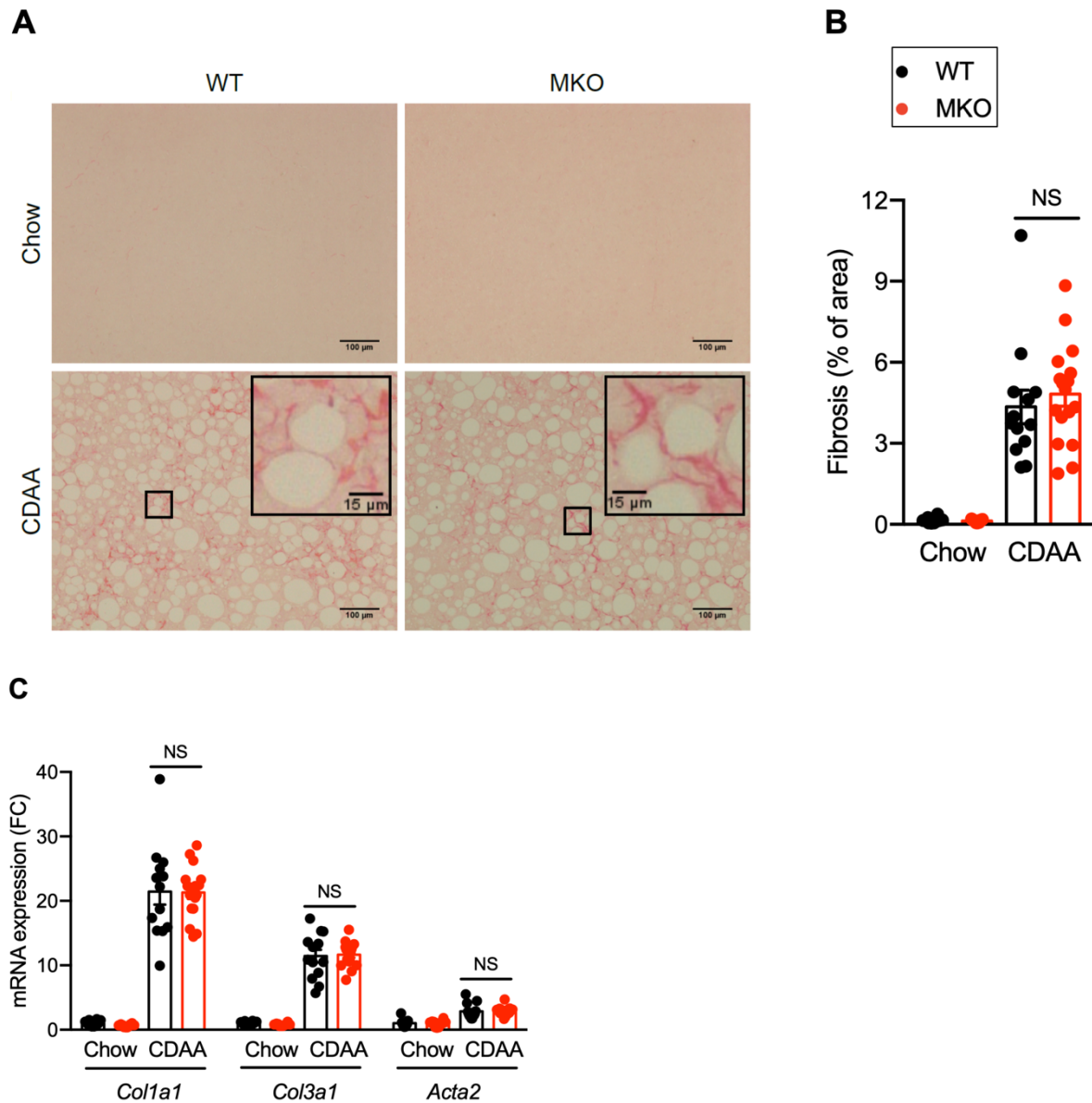


**Figure 23:** Effect of ROR $\alpha$  deletion in macrophages upon CDAA diet feeding. Ten weeks old WT and MKO mice were fed with either a chow or a CDAA diet for 8 weeks. **(A)** Sirius red staining of liver sections and **(B)** quantification of fibrosis. **(C)** mRNA expression levels measured by RT-qPCR for *Col1a1*, *Col3a1*, and *Acta2* genes in the liver. Data are shown as mean  $\pm$  SEM. \*  $p < 0.05$  by 2-way ANOVA followed by Sidak's multiple comparisons test.  $n = 10-17$  mice per group. NS: Not significant; FC: Fold Change.

## E. Effect of ROR $\alpha$ deletion in KC is offset by high ROR $\gamma$ expression

Contrasting with these results in 2 independent and complementary models of NAFLD, it was reported that ROR $\alpha$  deletion in macrophages, achieved by using a similar strategy (*Rora*<sup>fl/fl</sup> *Lyz2*<sup>Cre</sup>), predisposes mice to NASH after 12 weeks of HFD feeding<sup>548</sup>. NASH exacerbation was attributed to a key role of ROR $\alpha$  in Kupffer Cell (KC) function<sup>548</sup>. To determine a possible cause for this discrepancy, we first assessed the extent of *Rora* exon 3 deletion in KC. KC and other liver immune cell populations, sorted to a high level of purity (Figure 24-25).

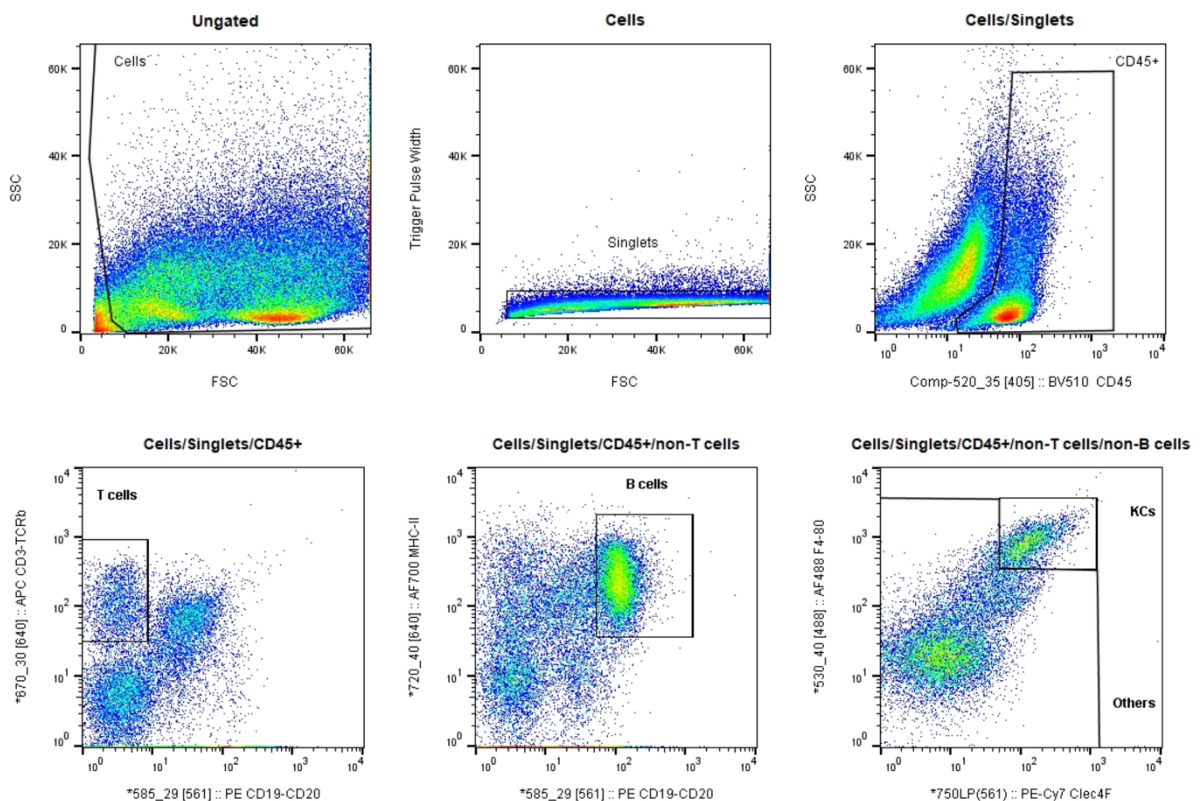


**Figure 24:** Representative gating strategy for cell sorting of T cells, B cells, KCs and other cells (CD45<sup>+</sup> non-T cells, -B cells and -KCs) from liver. Data are shown as mean  $\pm$  SEM. n=5 mice per genotype. AU: Arbitrary unit.

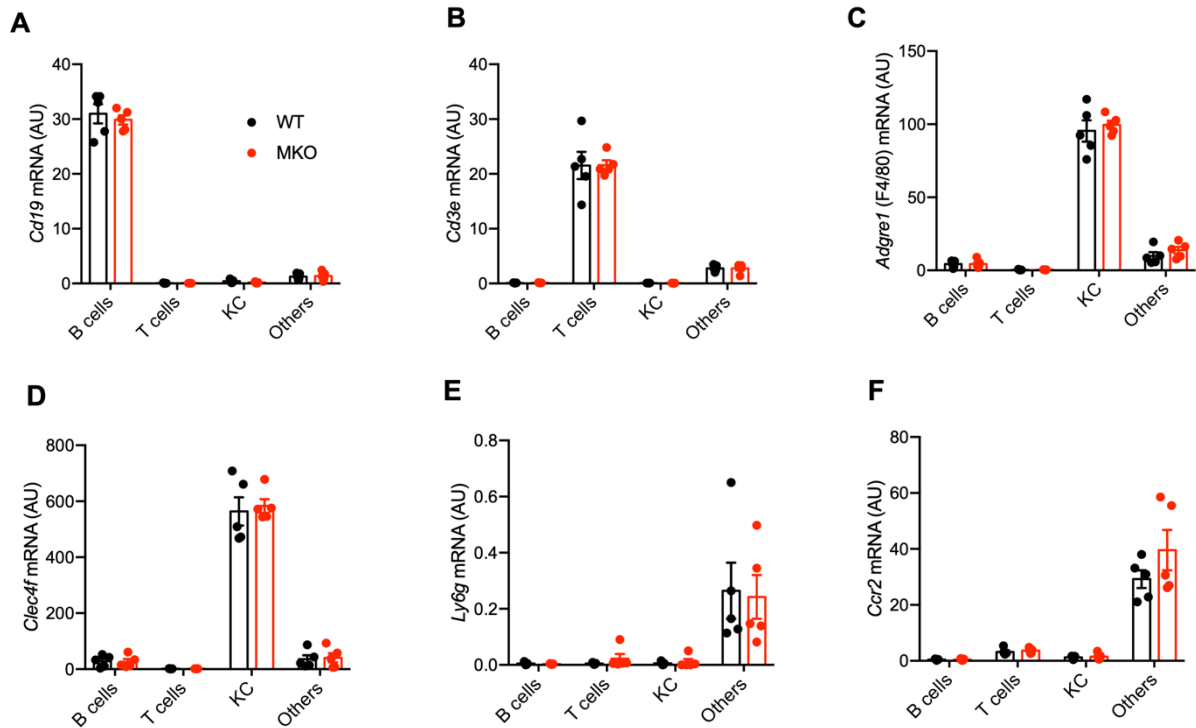


**Figure 25:** Quality control of Kupffer Cells (KCs) sorting. (A-F) mRNA expression levels measured by RT-qPCR for the *Cd19* (A), *Cd3e* (B), *Adgre1* (C), *Clec4f* (D), *Ly6g* (E) and *Ccr2* (F) genes in B cells, T cells, KCs and Others sorted from the liver of WT and MKO mice. Data are shown as mean  $\pm$  SEM. n=5 mice per genotype. AU: Arbitrary unit.

Our sorting results revealed efficient and specific deletion of *Rora* exon 3 in KC (Figure 26A). Interestingly, we observed that KC expressed lower levels of *Rora* than other macrophage populations, with lung macrophages expressing the highest level (Figure 26B), similarly to publicly available transcriptomic data (Figure 26C).

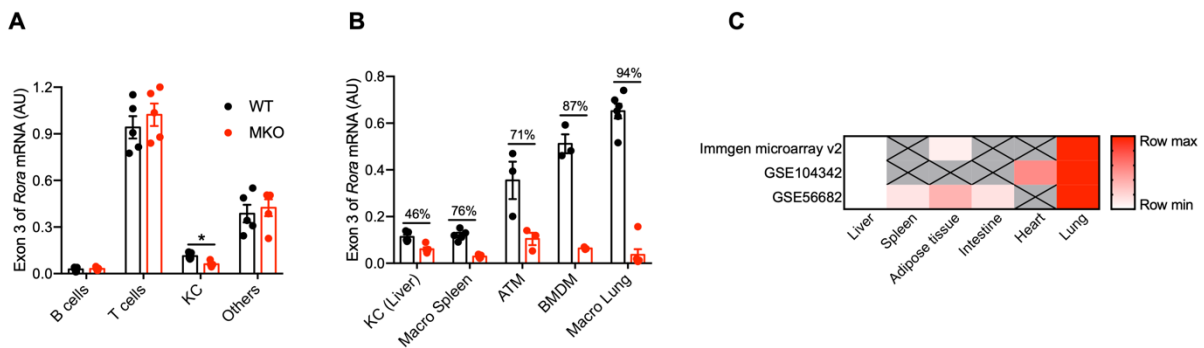


**Figure 26:** Impact of *ROR $\alpha$*  deletion on Kupffer Cells (KCs). (A-B) mRNA expression levels measured by RT-qPCR for the exon 3 of *Rora* gene in B cells, T cells, KCs, and CD45<sup>+</sup> non-T, B or KC (others) sorted from liver (A) and in different macrophage populations (B) from WT and MKO mice. (C) Heatmap

of *Rora* expression in different macrophage populations from public databases. Data are shown as mean  $\pm$  SEM. \*  $p < 0.05$  by 2-way ANOVA followed by Sidak's multiple comparisons test.  $n = 3-6$  mice per genotype except for ATM where each dot represents a pool of 3-4 mice. NS: Not significant; AU: Arbitrary unit.

Despite a significant *Rora* exon 3 deletion, expression of the ROR target gene *Arntl* did not decrease in KC, unlike lung macrophages (Figure 27A), splenic macrophages (Figure 4A), BMDM (Figure 4B) and ATM (Figure 5A). The lack of effect of ROR $\alpha$  deletion on *Arntl* expression in KC suggests a compensatory mechanism by another ROR protein. *Rorb* was not expressed in KC, similarly to other macrophage populations tested (data not shown), but *Rorc* expression was detected (Figure 27B). No compensation of *Rorc* expression was found in any macrophage subsets from MKO mice compared to littermate controls. However, basal *Rorc* expression was between 5- and 10-fold higher in KC compared to other macrophage subsets. The low *Rora* expression and the high *Rorc* expression in KC led to a *Rorc/Rora* ratio 10- to 50-fold higher than in other macrophage populations (Figure 27C). Collectively, these results suggest that ROR $\alpha$  deficiency is unlikely to induce major transcriptional effect in KC due to a concomitant high ROR $\gamma$  expression.

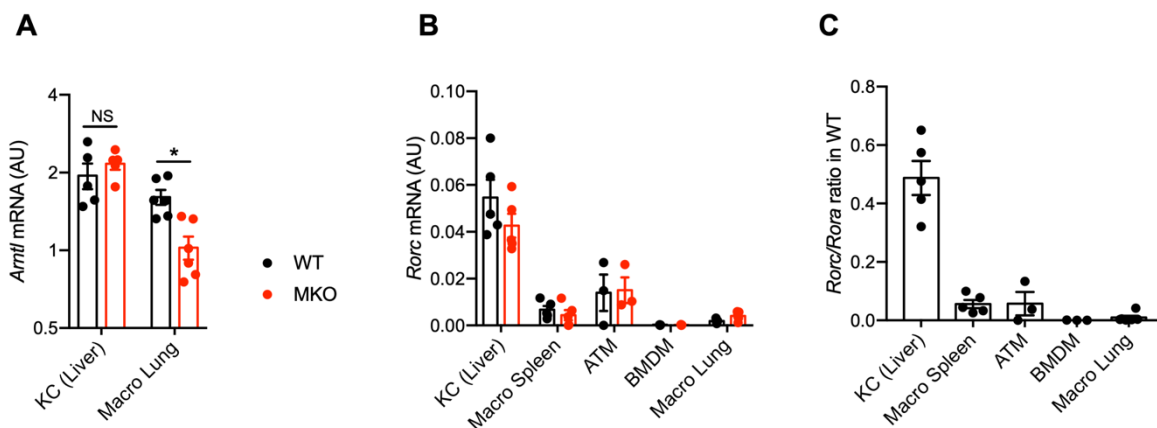


**Figure 27:** Impact of ROR $\alpha$  deletion on Kupffer Cells (KCs). (A-C) mRNA expression levels measured by RT-qPCR for *Arntl* (A) and *Rorc* (B) genes in different macrophage populations. (C) *Rorc/Rora* in different macrophage populations from WT mice. Data are shown as mean  $\pm$  SEM. \*  $p < 0.05$  by 2-way ANOVA followed by Sidak's multiple comparisons test.  $n = 3-6$  mice per genotype except for ATM where each dot represents a pool of 3-4 mice. NS: Not significant; AU: Arbitrary unit.

## 2. Gene regulation by ROR $\alpha$ in alveolar macrophages

Since ROR $\alpha$  expression is the highest in alveolar macrophages and deletion achieved is very high (94%), we reasoned that these cells would be the most appropriate to seek for differential gene expression pattern between ROR $\alpha$ -proficient and -deficient macrophages. Therefore, we performed a transcriptomic analysis by microarrays on purified ROR $\alpha$ -proficient and -deficient alveolar macrophages (Figure 28). Based on the false discovery rate (FDR), only 2 genes (*Coro2b* and *Arntl*) were significantly downregulated in ROR $\alpha$ -deficient alveolar macrophages, probably due to the modest fold change observed between the 2 genotypes. Thus, selecting on the basis of a p-value of 0.01 rather than on of a FDR of 0.05 and a log<sub>2</sub>(FC) of 0.5, we identified 200 differentially expressed genes between the ROR $\alpha$ -proficient and -deficient alveolar macrophages in basal conditions (Figure 28A). The complete list of the modulated genes can be found in the annex (Supplementary Table-1). Expectedly, *Arntl* was among the 10 most downregulated genes in ROR $\alpha$ -deficient alveolar macrophages (Figure 28B). Moreover, pathway analysis using Database for Annotation, Visualization, and Integrated Discovery (DAVID) revealed that pathways related to circadian rhythm were significantly ( $p=0.0367$ ) dysregulated in ROR $\alpha$ -deficient alveolar macrophages, in line with earlier results on the role of ROR $\alpha$  in other cell types. Taken together, these data indicate that ROR $\alpha$  regulate a restricted subset of genes of the alveolar macrophages in basal conditions, despite the high expression level and efficiency of deletion. Impact of ROR $\alpha$  deletion in activated lung macrophages and/or pathophysiological conditions remains to be investigated.

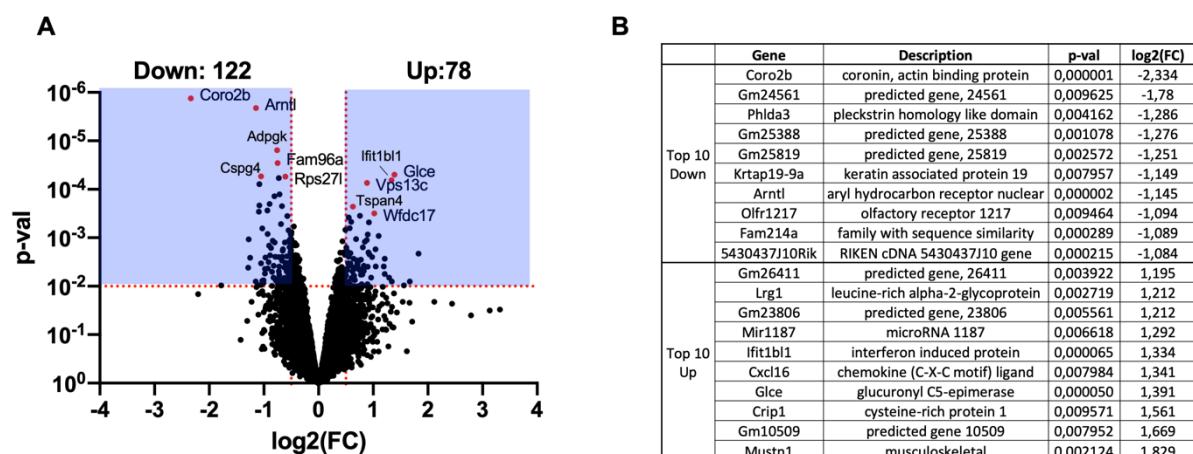


**Figure 28:** Transcriptomic analysis of ROR $\alpha$ -deficient alveolar macrophages. **(A)** Volcano plot and **(B)** top 10 modulated genes from microarrays performed on alveolar macrophages from lung of 14 weeks old naïve WT and MKO mice. n=6 mice per genotype.

### 3. Impact of *Lyz2* deletion on HFD-induced obesity, IR, NAFL and obesity-independent NASH development

We found no impact of LysM-Cre-mediated ROR $\alpha$  deletion neither on HFD-induced obesity, IR and steatosis nor on CDAA diet-induced NASH. These finding contrast with an earlier report showing that LysM-Cre-mediated ROR $\alpha$  deletion increases the susceptibility to HFD-induced NASH<sup>548</sup>, while both studies used the same HFD reference and duration of treatment. Therefore, we suspected that LysM copy number may play a role in this discrepancy, as the only difference between the two independent lines of work is the mouse genotype regarding the LysM locus. The LysM-Cre mice carry an insertion of Cre recombinase into the *Lyz2* gene, leading to Cre expression under the control of the *Lyz2* promoter and enhancers, but abolishing endogenous *Lyz2* expression. While we intentionally maintained similar Cre and *Lyz2* expression between WT and MKO by using only hemizygous animals for this locus (comparing *Rora*<sup>+/+</sup>*Lyz2*<sup>Cre/+</sup> with *Rora*<sup>fl/fl</sup>*Lyz2*<sup>Cre/+</sup>), floxed mice (*Rora*<sup>fl/fl</sup>*Lyz2*<sup>+/+</sup>) were used as WT control and compared with MKO mice missing information about the *Lyz2* locus (*Rora*<sup>fl/fl</sup>*Lyz2*<sup>Cre/?</sup>) in the earlier study<sup>548</sup>. This latter strategy results in differential Cre and *Lyz2* expression between the WT, expressing no Cre, and the MKO mice expressing less or no *Lyz2*. Thus, MKO mice generation strategy in the earlier study, possess at least one inactivated *Lyz2* allele and possibly a homozygous (whole body) *Lyz2* deletion. Indeed, based on the described genotyping strategy using a single PCR reaction to analyze Cre gene, it is highly likely that MKO mice<sup>548</sup> were actually also *Lyz2*-deficient in this earlier study.

Thus, we investigated whether or not *Lyz2* copy number affects metabolic parameters independently of ROR $\alpha$  expression. Indeed, lysozyme expression and activity is affected in various liver diseases<sup>549, 550, 551</sup>, but, to our knowledge, the role of *Lyz2* in NASH was never investigated. Besides, impact of lysozyme on obesity and obesity-associated IR is unknown. Presented results are preliminary and need to be confirmed.

#### A. Generation and validation of *Lyz2*-deficient mice

We crossed wild-type mice with homozygous *Lyz2*-Cre mice (wild-type at the ROR $\alpha$  locus) to obtain heterozygous (*Lyz2*<sup>WT/Cre</sup>) mice. Subsequently, we crossed heterozygous *Lyz2*<sup>WT/Cre</sup> mice with each other to obtain wild-type (*Lyz2*<sup>WT/WT</sup>), heterozygous (*Lyz2*<sup>WT/Cre</sup>), and *Lyz2*-deficient (*Lyz2*<sup>Cre/Cre</sup>) littermates. We validated genotypes of the mice by using single PCR reaction with three primers on extracted DNA and agarose gel electrophoresis (Figure 29A-B).

We further confirmed the *Lyz2* deficiency at mRNA level by RT-qPCR in spleen of *Lyz2*<sup>WT/WT</sup> (WT), *Lyz2*<sup>WT/Cre</sup> (Het), and *Lyz2*<sup>Cre/Cre</sup> (KO) mice (Figure 29C).

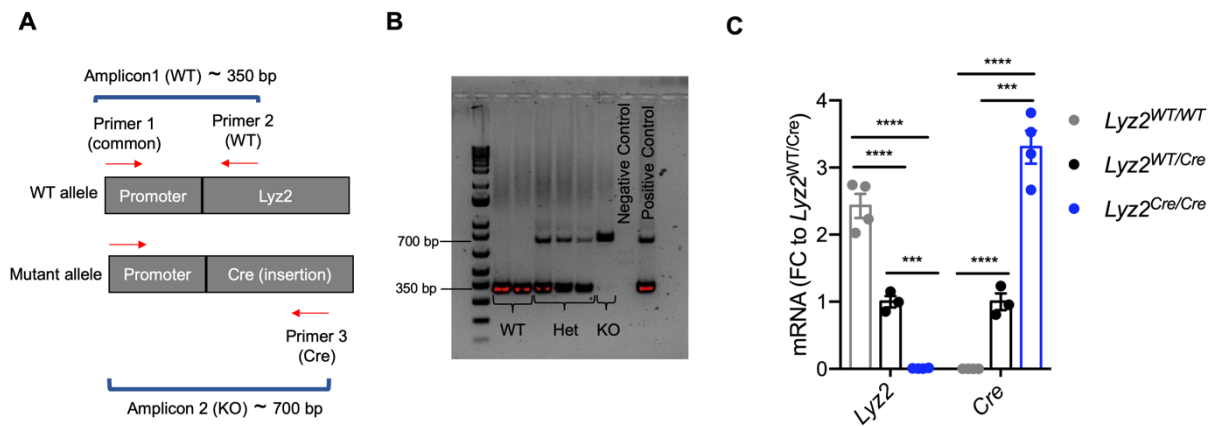


**Figure 29:** Validation of *Lyz2* deletion in mice. **(A)** Schematic representation of the genotyping strategy by PCR. Designed primer-binding sites on the genome and expected amplicons are represented for *Lyz2*<sup>WT/Cre</sup> (Het) mice. **(B)** PCR analysis of genomic DNA extracted from tails of *Lyz2*<sup>WT/WT</sup>, *Lyz2*<sup>WT/Cre</sup>, and *Lyz2*<sup>Cre/Cre</sup> mice. **(C)** mRNA expression levels measured by RT-qPCR for *Lyz2* and *Cre* genes in spleen from *Lyz2*<sup>WT/WT</sup>, *Lyz2*<sup>WT/Cre</sup>, and *Lyz2*<sup>Cre/Cre</sup> mice. Data are shown as mean ± SEM. \*\*\*  $p < 0.001$ ; \*\*\*\*  $p < 0.0001$  by 2-way ANOVA followed by Sidak's multiple comparisons test was performed  $n = 4-3$  mice per genotype. FC: Fold change.

A. *Lyz2* deficiency slightly protects against HFD-induced obesity and IR, however, has no impact on NAFL

To investigate the role of *Lyz2* in diet-induced obesity, IR, and NAFL, we fed *Lyz2*<sup>WT/WT</sup> (WT), *Lyz2*<sup>WT/Cre</sup> (Het), and *Lyz2*<sup>Cre/Cre</sup> (KO) littermate mice with a 60% of high fat diet (HFD) for 12 weeks. All the mice significantly gained weight upon HFD feeding, however KO mice displayed lower body weight gain compared to WT and Het littermates (Figure 30).

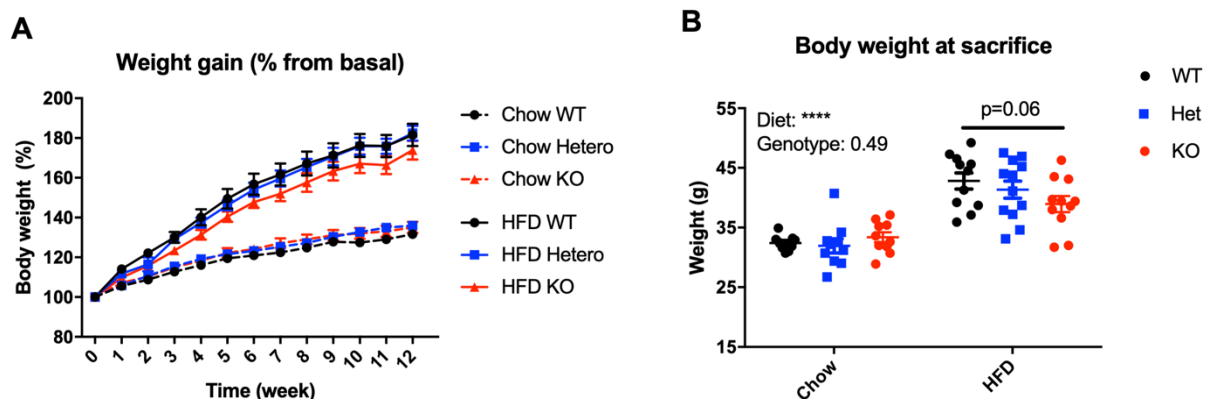


**Figure 30:** Effect of *Lyz2* deficiency on HFD-induced obesity. Eight weeks old WT, Het, and KO mice were fed with either a chow or a HFD for 12 weeks. **(A)** Body weight gain. **(B)** Weight of mice at sacrifice. Data are shown as mean  $\pm$  SEM. \*\*\*\*  $p < 0.0001$  by 2-way ANOVA followed by Sidak's multiple comparisons test was performed.  $n=10-12$  mice per group.

Similarly, KO mice displayed lower inguinal and epididymal adipose tissue masses under HFD compared to WT and Het mice (Figure 31).

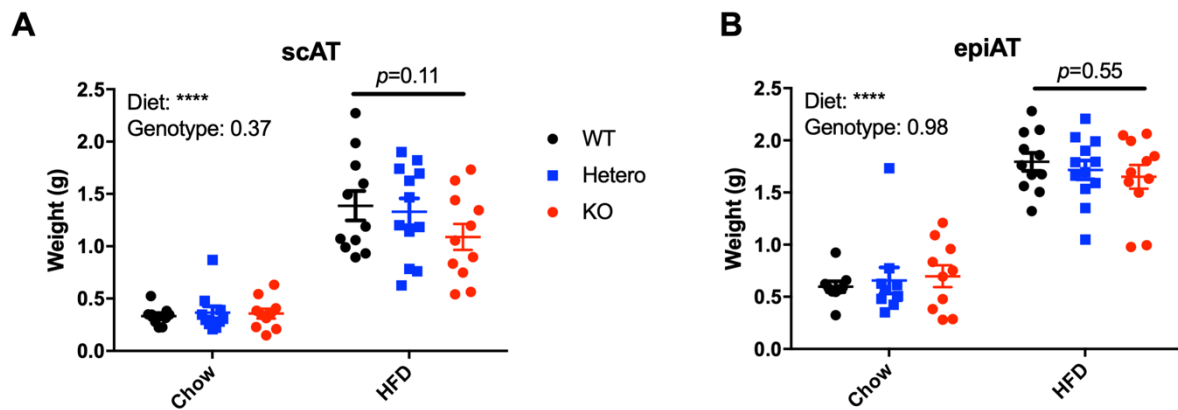


**Figure 31:** Effect of *Lyz2* deficiency on HFD-induced obesity. Eight weeks old WT, Het, and KO mice were fed with either a chow or a HFD for 12 weeks. **(A)** Weight of subcutaneous/inguinal (IngAT) and **(B)** epididymal (epiAT) adipose tissues. Data are shown as mean  $\pm$  SEM. \*\*\*\*  $p < 0.0001$  2-way ANOVA followed by Sidak's multiple comparisons test was performed.  $n=10-12$  mice per group.

Furthermore, HFD-fed KO mice exhibited significantly better glycemic control during intraperitoneal glucose tolerance (IPGTT) test compared to WT and Het mice. Nevertheless, we observed no significant difference between genotypes in fasting glucose levels at sacrifice (Figure 32).

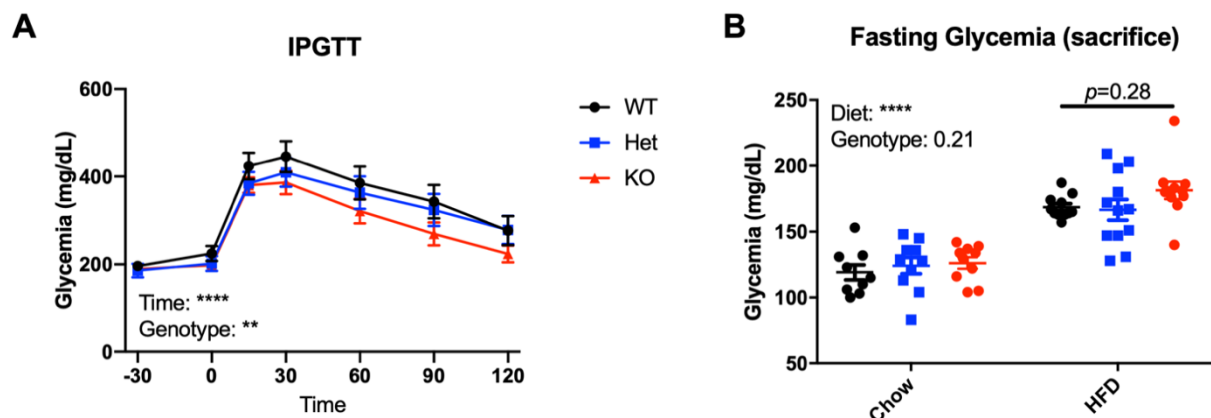


**Figure 32:** Effect of *Lyz2* deficiency on HFD-induced IR. Eight weeks old WT, Het, and KO mice were fed with either a chow or a HFD for 12 weeks. After 10 weeks of diet, mice were fasted for 5 hours (A) thereafter, intraperitoneally injected with 1g/kg glucose for a glucose tolerance test (IPGTT). (B) fasting glycemia of the mice at sacrifice. Data are shown as mean  $\pm$  SEM. \*\*  $p < 0.01$ ; \*\*\*\*  $p < 0.0001$  by 2-way ANOVA followed by Sidak's multiple comparisons test was performed. n=10-12 mice per group.

Regarding AT inflammation as a causative factor for obesity-induced IR, expression of *Tnf* and *Adreg1* genes was significantly lower, whereas *Il1b* expression tended to decrease, and *Il6* expression remained unchanged (data not shown) in epididymal AT of KO mice compared to WT and Het mice upon HFD-feeding (Figure 33). Altogether, our results suggest that *Lyz2* deficiency has a slightly protective effect against HFD-induced obesity and IR.

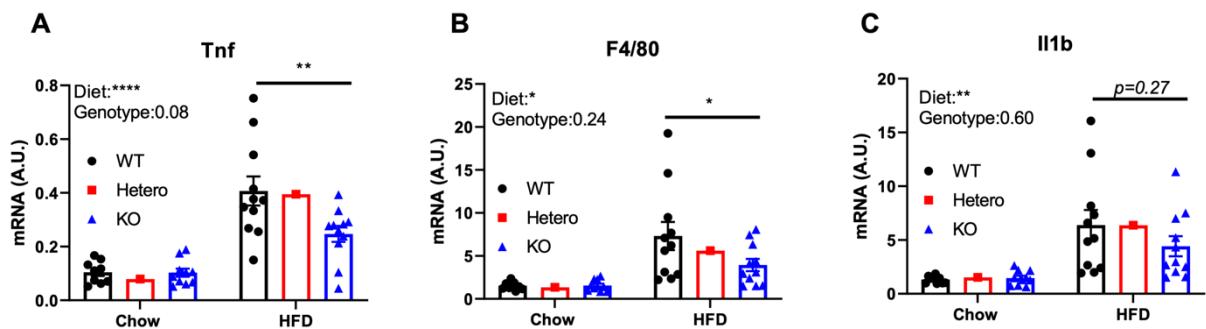


**Figure 33:** Effect of *Lyz2* deficiency on HFD-induced IR. Eight weeks old WT, Het, and KO mice were fed with either a chow or a HFD for 12 weeks. mRNA expression levels measured by RT-qPCR for (A) *Tnf*, (B) *Adreg1* (encoding for F4/80), (C) *Il1b* in epiAT. Data are shown as mean  $\pm$  SEM. \*  $p < 0.05$ ; \*\*  $p < 0.01$  by 2-way ANOVA followed by Sidak's multiple comparisons test was performed. n=10-12 mice per group for WT and KO mice. n= 1 that represents a pool of 10-12 mice for heterozygous mice. AU: Arbitrary unit.

Considering HFD-induced NAFL development, liver weight, steatosis level determined by histology were increased upon HFD feeding to the same extent regardless of the genotype of the mice (Figure 34). Furthermore, we did not observe any significant differences in hepatic cytokine expression levels but tended to increase in HFD-fed KO mice compared to WT and Het mice (data not shown). Overall, our findings suggest that *Lyz2* deficiency has no impact on HFD-induced hepatic steatosis development.

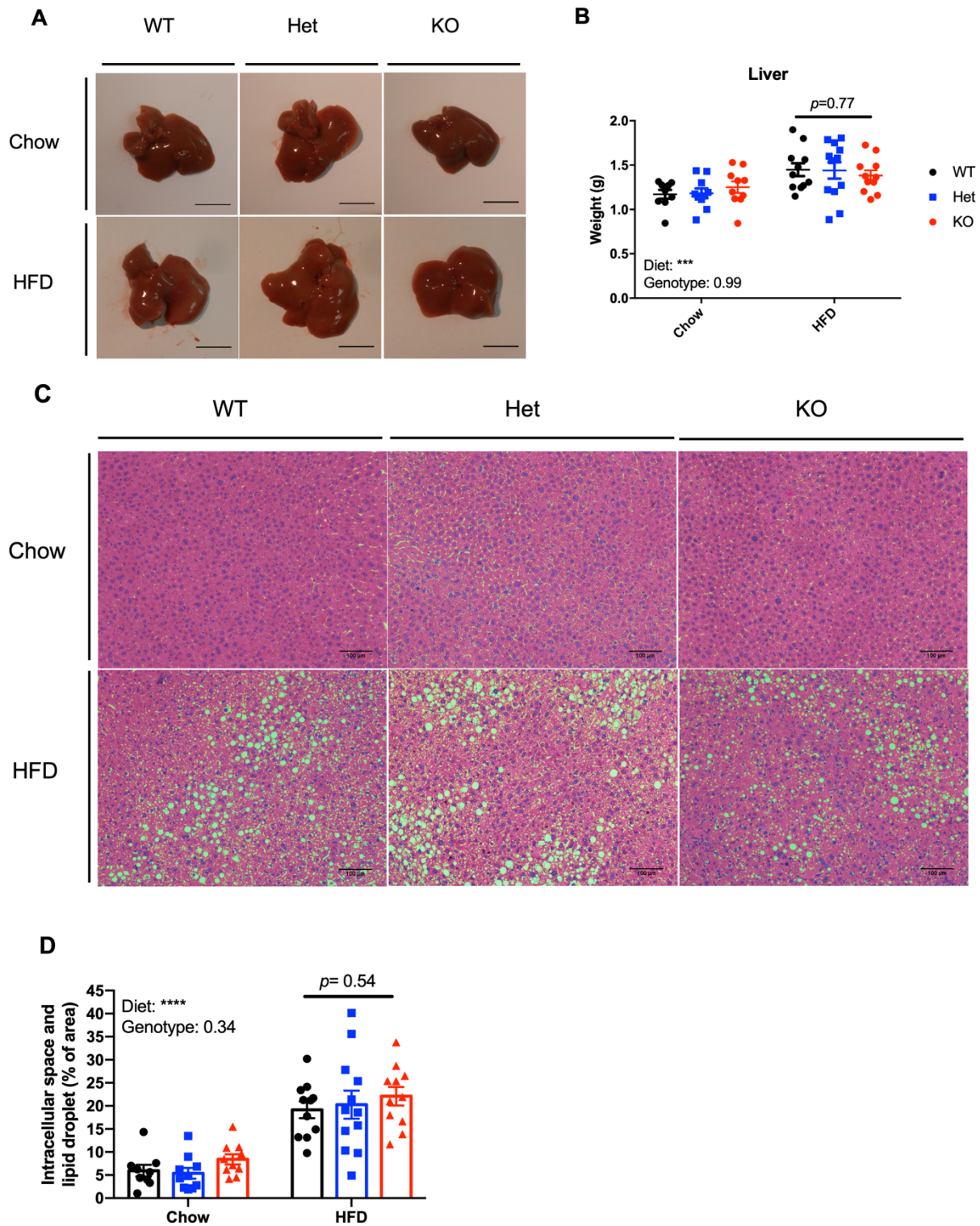


**Figure 34:** Effect of *Lyz2* deficiency on HFD-induced IR. Eight weeks old WT, Het, and KO mice were fed with either a chow or a HFD for 12 weeks (**A**) Representative liver gross morphology. (**B**) Liver weight. (**C**) Hematoxylin & Eosin staining of liver sections and (**D**) quantification of lipid droplets. Data are shown as mean  $\pm$  SEM. \*\*\*  $p < 0.001$ ; \*\*\*\*  $p < 0.0001$  by 2-way ANOVA followed by Sidak's multiple comparisons test was performed.  $n=10-12$  mice per group.

## B. *Lyz2* deficiency might protects against obesity-independent NASH

Given the fact that 12 weeks of HFD feeding only induces NAFL, we further investigated the impact of *Lyz2* deficiency on an advanced NASH model that is independent from obesity and IR. Thus, wild-type (*Lyz2*<sup>WT/WT</sup>), heterozygous (*Lyz2*<sup>WT/Cre</sup>), and *Lyz2*-deficient (*Lyz2*<sup>Cre/Cre</sup>) littermates were fed with the choline-deficient, L-amino acid-defined (CDAA) diet supplemented with sucrose and 2% cholesterol for 4 weeks. In contrast to HFD, as expected, CDAA diet feeding induced neither obesity nor hyperglycemia. Instead, as expected, the CDAA diet feeding resulted in a 15% weight loss and a decrease of nearly 40% of fasting glycemia at a similar rate in WT, Het, and KO mice (Figure 35). Accordingly, we also observed a lower subcutaneous and epididymal adipose tissue masses upon the CDAA diet at a comparable level between each genotype (data not shown).

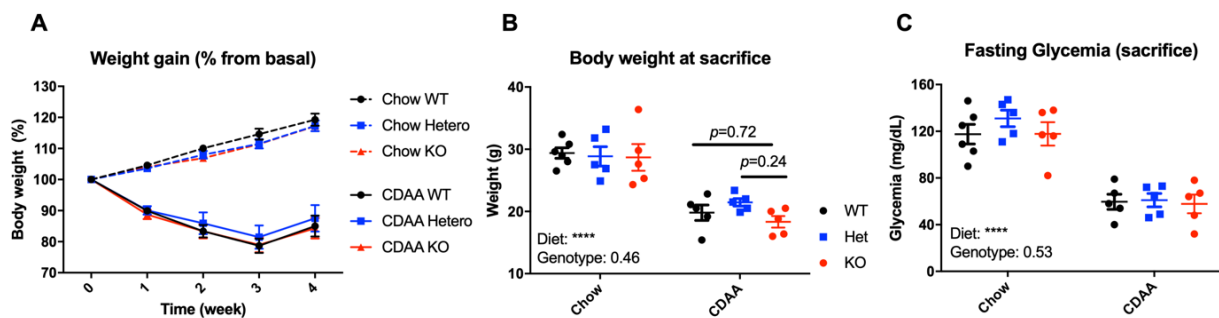


**Figure 35:** Effect of *Lyz2* deficiency on CDAA diet-induced NASH. WT, Het, and KO mice were fed with either a chow or a CDAA diet for 4 weeks. **(A)** Body weight gain. **(B)** Weight of mice at sacrifice. **(C)** Fasting glycemia of the mice at sacrifice. Data are shown as mean  $\pm$  SEM. \*\*\*\*  $p < 0.0001$  by 2-way ANOVA followed by Sidak's multiple comparisons test was performed.  $n=5-6$  mice per group.

Interestingly, our preliminary findings revealed that *Lyz2*-deficient mice exhibit significantly lower liver weight in comparison with Het mice and almost significantly than WT mice in response to CDAA diet feeding, despite the steatotic appearance of the liver (Figure 36). These results suggest that whole-body *Lyz2* deficiency might have a protective effect against NASH development.

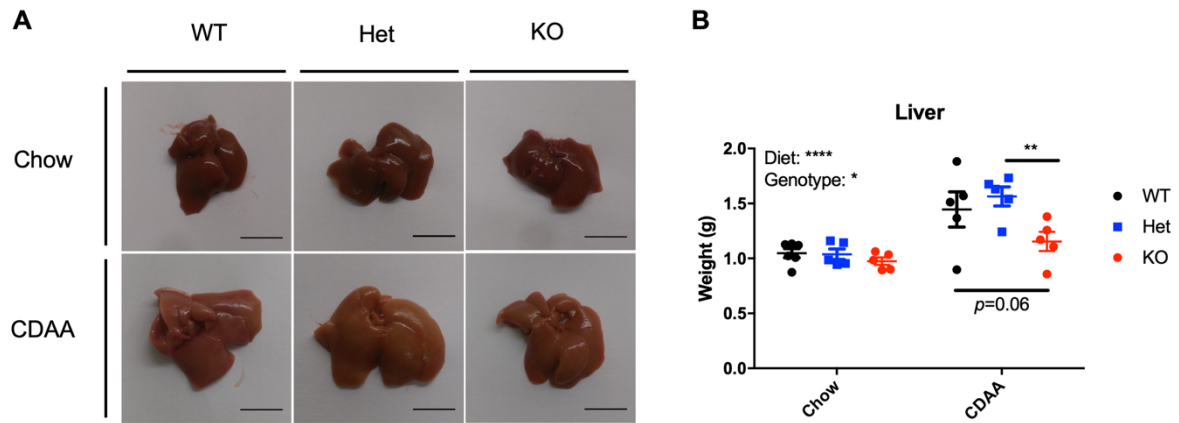


**Figure 36:** Effect of *Lyz2* deficiency on CDAA diet-induced NASH. WT, Het, and KO mice were fed with either a chow or a CDAA diet for 4 weeks. **(A)** Representative liver gross morphology. **(B)** Liver weight. Data are shown as mean  $\pm$  SEM. \*\*\*\*  $p < 0.0001$  by 2-way ANOVA followed by Sidak's multiple comparisons test was performed.  $n=5-6$  mice per group.

## DISCUSSION AND PERSPECTIVES

### 1. Impact of the LysM-Cre-mediated macrophage-specific ROR $\alpha$ deletion on metabolic diseases

Over the past years, a considerable number of studies contributed to our understanding about the role of nuclear receptors, including RORs, in the regulation of lipid and glucose metabolism, circadian rhythm as well as the development and function of the immune system. Due to the pleiotropic effects and wide cell distribution of ROR $\alpha$  and considering the key role of macrophages in metabolic diseases, we investigated the impact of ROR $\alpha$  deletion in these cells on obesity, IR and NASH by using the LysM-Cre mice. Evaluation of deletion efficiency and decreased expression of a major ROR $\alpha$  target gene in several myeloid subsets showed that macrophages were mostly impacted by ROR $\alpha$  deletion in basal conditions although we cannot formally exclude that other myeloid subsets are also affected upon metabolic challenge.

Nonetheless, we observed no effect of LysM-Cre-mediated ROR $\alpha$  deletion neither on HFD-induced obesity, IR, and steatosis nor on CDAA diet-induced NASH. These results are in contradiction with an earlier report showing that LysM-Cre-mediated ROR $\alpha$  deletion enhances the susceptibility to HFD-induced NASH<sup>548</sup>, even though both studies adopted the same HFD reference and duration of the procedure. As feeding a HFD for 12 weeks is not *per se* leading to NASH, but rather to NAFL<sup>552</sup>, only a more pronounced steatosis (higher liver weight and triglyceride content) was reported in MKO mice in the earlier study<sup>548</sup>. Indicators of increased hepatic lipotoxicity, such as higher plasma transaminase activity, increased expression of pro-inflammatory cytokines (*Tnf*, *Il1b* and *Il6*) and decreased expression of *Il10* in liver were also observed<sup>548</sup>. It was proposed that ROR $\alpha$  directly regulates M2 polarization of KCs leading to increased IL-10 production which would protect hepatocytes against lipid accumulation<sup>548</sup>. While we also observed a tendency to lower *Il10* expression in livers from MKO mice upon HFD feeding (Figure 16A) and a significant decrease upon CDAA diet feeding (Figure 20B), we did not observe any exacerbation of steatosis or NASH. As the putative protective role for IL-10 was only based on *in vitro* findings, we believe that the reduced *Il10* expression in liver of MKO mice upon HFD is unlikely to contribute to aggravated steatosis. Further supporting this finding, IL-10-deficient mice fed with a HFD for 12 weeks developed increased liver inflammation, but decreased steatosis and transaminase activity<sup>553</sup>, suggesting that beyond its well described anti-inflammatory function, endogenous IL-10 is not protective against HFD-induced steatosis.

Several other factors might account for the discrepancy between our results and these earlier findings<sup>548</sup>. The microbiological status of the animal facility and housing conditions are two underestimated factors that might account for major differences in experimental outcome and it is not uncommon for this information to be missing. Specific pathogen free (SPF) status indicates that mice are free of defined pathogens including the mouse hepatitis virus and *Helicobacter hepaticus*, which may interfere with liver function. As we discussed with the sheer volume of evidence, gut microbiota also influences NAFLD development. The microbiota composition is highly variable between animal facilities, mouse lines and even between cages, especially when two genotypes are bred separately. Generation of littermate animals is critical to ensure that both deficient and control mice harbor identical gut microbiota while post-weaning cohousing is ineffective<sup>554</sup>. Our mice were housed in SPF facility and bred to obtain WT and MKO littermate animals. Nevertheless, no information was provided in the earlier study about the animal facility and littermate status.

Additionally, used floxed mice strategy may also account for the observed discrepancies between studies. We generated mice with floxed *Rora* exon 3 while exon 4 was targeted in the earlier study<sup>548</sup>. Deletion of exon may still result in the translation of a truncated protein containing a portion of the DBD that includes the exon 3-encoded zinc finger motif (Figure 1C). This difference in deletion strategy is however unlikely to account for the observed phenotypic differences, considering the absence of C-terminal extension (CTE) sequence within the DBD domain, that stabilize DNA contact for monomeric nuclear receptors<sup>464</sup>.

By using a 12-week HFD that induces liver steatosis (NAFL) or an 8-week CDAA diet that leads to NASH, we observed no differences between WT and MKO mice for any tested hepatic parameters including liver weight, triglyceride content, inflammatory and fibrosis gene expression, histology and transaminase activity. We also found no impact on obesity and glucose homeostasis. Investigations on KC showed that, despite an effective deletion of *ROR $\alpha$* , KCs were the only macrophage population without transcriptional effect on the *ROR* target gene *Arntl*. We found no compensatory expression of other *ROR* genes in MKO, but we evidenced a high level of *Rorc* expression specifically in KC that might offset the *ROR $\alpha$*  deletion. The redundancy between *ROR* proteins is well established<sup>541, 102, 521</sup>. Hepatocytes express high levels of *ROR $\gamma$*  in addition to *ROR $\alpha$* <sup>521</sup>. It was shown that a single deletion of *ROR $\alpha$*  or *ROR $\gamma$*  in hepatocytes affects only 2 and 6 transcripts, respectively in whole liver transcriptome, while *ROR $\alpha/\gamma$*  double deletion leads to a broader effect with 299 genes affected, unambiguously demonstrating the redundancy between *ROR $\alpha$*  and *ROR $\gamma$*  in hepatocytes<sup>521</sup>.

Such a redundancy might be at play in KCs and further investigation with a double  $ROR\alpha/\gamma$  double deficient mouse model might address this question. Moreover, usage of the new KC-specific *Clec4f-Cre* mouse line would improve the specificity towards KC and may result in a better deletion efficiency than the one reached with the *LysM-Cre* mice<sup>319</sup>.

It is worth noting that the *LysM-Cre* mice model gives rise to a variability in deletion efficiency among the different macrophage populations, as previously reported<sup>555</sup>. In our mouse model, we observed the highest deletion of *Rora* in lung macrophages (94%) and the lowest in Kupffer cells (KC, 46%), while the deletion in other macrophage populations was around 75%. Despite the fact that a lower deletion efficiency occurs in KC compared to other macrophage populations using this *Cre* model, different groups succeeded to demonstrate a role of several genes, such as *Pparg*<sup>556</sup>, *Tlr9*<sup>557</sup>, and *Il4ra*<sup>558</sup> on NAFL/NASH development by employing the same *LysM-Cre*-driven gene deletion. These findings led us to conclude that  $ROR\alpha$  expressed by macrophages is not a major player in NASH development, unlike what was previously reported by Han and colleagues who employed the same *LysM-Cre*-based deletion strategy<sup>548</sup>. Furthermore, using scRNA-seq technology, heterogeneous and novel macrophage populations have been identified at basal state as well as during onset and progression of obesity, IR, and NAFLD leading to determination of tissue-specific macrophage signatures (i.e., WAT, liver) prompting for more elaborated techniques than *LysM-Cre*-mediated deletion to study the specific contribution of macrophage-expressed genes in a specific tissue. Use of dual recombinase *Dre-rox* system<sup>559</sup> might be useful to further refine cell specificity. In conclusion,  $ROR\alpha$  deletion in macrophages by using the *LysM-Cre* system has no impact on the development of obesity, IR and NASH.

## 2. Gene regulation by $ROR\alpha$ in alveolar macrophages

Our microarray data revealed that coronin 2b (*Coro2b*) and aryl hydrocarbon nuclear receptor (*Ahrntl*) are significantly ( $p=0.000001$  and  $p=0.000002$ , respectively) downregulated in  $ROR\alpha$ -deficient alveolar macrophages (Figure 28). Coronins are an evolutionarily conserved family of actin-binding proteins that regulate the actin cytoskeleton dynamics and turnover<sup>560</sup>. The actin cytoskeleton mediates various critical cellular processes, such as cell migration, endocytosis, vesicular trafficking, and cytokinesis therefore, is required for cell survival<sup>561, 562</sup>. So far, seven mammalian coronin genes have been identified and classified by the Human Genome Nomenclature Committee (HGNC) in 2011, as *CORO1A*, *CORO1B*, *CORO1C*, *CORO2A*, *CORO2B*, *CORO6*, and *CORO7*<sup>563</sup>. Based on phylogenetic analysis coronins are subdivided into 3 types<sup>564</sup>. Coronins display distinct cell and tissue expression patterns.

The best-studied type I coronin, *Coro1a* is highly enriched in several immune subsets that include neutrophils, macrophages, and T cells. *Coro1a* is involved in the generation of microbicidal superoxide burst in neutrophils by binding to p40phox, the cytosolic subunit of NADPH oxidase complex<sup>565</sup>. Moreover, *Coro1a* is required for chemotaxis and phagocytosis in human neutrophils<sup>566</sup>. *Coro1a* has also been associated with neutrophil survival<sup>567</sup>. In addition, *Coro1a* is transiently recruited to the phagosomes throughout the phagocytosis of pathogens by macrophages and it is required for the early-phase phagosome formation<sup>568</sup>,<sup>569</sup>,<sup>570</sup>,<sup>571</sup>. Phosphorylation of *Coro1a* by protein kinase C (PKC) regulate its disassociation from phagosomes after ingestion is completed and stimulate the phagosome-lysosome fusion to initiate degradation of the pathogens<sup>572</sup>. Interestingly, retention of *Coro1a* on the phagosomal membrane upon mycobacterial infection activates  $Ca^{2+}$ -dependent phosphatase calcineurin that block the lysosomal delivery and killing of mycobacteria<sup>573</sup>. Thus, the balance between the PKC and calcineurin regulatory loops for *Coro1a*, control the phagosome-lysosome fusion in response to microbial infection. Furthermore, *Coro1a*-deficient T cells are defective in chemokine-mediated migration and display impaired egress from the thymus<sup>574</sup>. A point mutation in Coronin 1A gene was identified in peripheral T cell-deficient (Ptcd) mice, which are characterized by severe defects in T cell migration and thymic egress, as well as in an atypical  $T^{-}NK^{+}B^{+}$  severe combined immunodeficiency (SCID) patients<sup>575</sup>.

The type 2 coronins are much less studied. However, *Coro2a* is associated to the control of focal adhesion turnover<sup>576</sup>. Other type II coronin, *Coro2b*, also known as, Clipin C is predominantly expressed in the brain and at lower levels in other tissues<sup>577</sup>. Immunostaining techniques revealed that *Coro2b* is localized in cerebral cortex, hippocampus, thalamus, olfactory bulb, and cerebellum in mouse brain<sup>577</sup>. Importantly, in the cerebellum, the Purkinje cell layer is reported to be intensely labeled with anti-*Coro2b* antibodies<sup>577</sup>. Considering the expression levels and the significance of  $ROR\alpha$  in the nervous system, particularly, in Purkinje cells<sup>578</sup>,<sup>579</sup>,<sup>580</sup>,<sup>581</sup>, as well as our microarray results, it appears highly relevant that *Coro2b* expression regulated by  $ROR\alpha$  and represents a potential target gene. Chip-Seq experiments would be necessary to formally demonstrate that it is actually the case. This prove might technically challenging due to the absence of reliable  $ROR\alpha$ -specific antibodies. *Coro2b* is also enriched in glomerular epithelial cells (namely podocytes) of kidney and regulates the ventral actin cytoskeleton that partially protect glomerular function and the glomerular filtration barrier<sup>582</sup>. Recently, *Coro2b* expression was found to be downregulated in podocytes of human diabetic nephropathy patients and is suggested to be involved in the pathogenesis of glomerulopathies<sup>583</sup>. More recently, *CORO2B* was identified as a member of micro RNA (miRNA) and mRNA interaction network that regulates the malignant transformation of human bronchial epithelial cells induced by cigarette smoking<sup>584</sup>. According to the ImmGen database,

Coro2b is expressed at lower levels in macrophages compared to other immune cells, for instance, ILC2 where ROR $\alpha$  shown to be essential<sup>539,585</sup>. Moreover, based on our investigation, Coro2b is expressed at similar levels than ROR $\alpha$  in various sorted macrophage populations, i.e., KCs, ATMs, and alveolar macrophages (data not shown). Nevertheless, the role of Coro2b in macrophages is completely unknown. Mammalian Coro2b share 44% of amino acid identity with Coro1a<sup>586</sup> and some of the mechanisms that identified for Coro1a might also apply to Coro2b. However, different localization and expression levels could indicate distinct functional roles of these proteins<sup>587</sup>.

Besides *Coro2b*, pathway analysis by DAVID showed that circadian rhythm pathway was significantly ( $p=0.0367$ ) dysregulated in ROR $\alpha$ -deficient alveolar macrophages. Among 9 genes belonging to circadian rhythm pathway, 2 of them were significantly downregulated in ROR $\alpha$ -deficient alveolar macrophages: *Arntl* ( $p=0.000002$ ) and *Cry1* ( $p=0.00145$ ), respectively. It has been reported that even though expression of the *Bmal1*, *Clock*, *NPAS2*, and *Cry1* were downregulated in fibroblasts of the *staggerer* mice, *Bmal1*, *Clock*, *Cry1*, and *Per2* expressions were still oscillating with rhythmicity<sup>497</sup>. These findings suggested that ROR $\alpha$  is not dispensable for circadian oscillations of the clock genes but regulates their level of expression<sup>497</sup>.

Overall, it is thus possible ROR $\alpha$  might regulate chemotaxis and/or phagosome formation of alveolar macrophages in response to microbial infection or magnitude of response upon activation in a circadian manner.

### 3. Impact of *Lyz2* deficiency on metabolic diseases

As mentioned, we hypothesized that the observed impact of ROR $\alpha$  deletion in macrophages on NASH in the earlier study<sup>548</sup> likely did not result from a specific effect of ROR $\alpha$  deletion, but rather from a different *Lyz2* copy number between WT and MKO mice and decided to verify this hypothesis experimentally. Surprisingly, our preliminary findings showed that the *Lyz2*-deficient mice exhibit slight protection, rather than a detrimental effect, in HFD-induced obesity and IR, as determined by lower body weight and adipose tissue masses, significantly improved glycemic control and decreased epiAT inflammation (Figures 30-33). Interestingly, whole body *Lyz2* deficiency had no impact on hepatic steatosis (NAFL) in HFD-fed mice (Figure 34). Nonetheless our preliminary findings even suggest that *Lyz2* deficiency might protect against advanced NASH (Figure 36). Taken together, these preliminary findings indicate that different

*Lyz2* gene copy number in control mice is unlikely to account for the discrepancy between our work and the earlier study<sup>548</sup>.

Despite the fact that our preliminary findings in *Lyz2*-deficient mice do not clarify the discrepancy between our work and the earlier study<sup>548</sup>, we believe that further investigations are of significant interest in the context of obesity, IR, and advanced NASH, as *Lyz2* might possess a therapeutic value. Lysozyme is a  $\beta$ -1,4-N-acetyl-muromoyl-hydrolase, an anti-microbial protein that catalyzes the hydrolysis of the peptidoglycan between N-acetylglucosamine (NAG) and N-acetylmuramic acid (NAM), contributing to the degradation of the both Gram-positive and Gram-negative bacterial cell walls. Hydrolysis of the peptidoglycan by lysozyme leads to release of muramyl dipeptide (MDP) that stimulate Pattern Recognition Receptor (PRR), specifically NOD2, modulating intestinal epithelia and microbiota interactions<sup>588</sup>. In addition to its enzymatic activity, lysozyme, as a cationic protein can create pores by insertion into negatively-charged bacterial membrane<sup>590, 591, 592</sup>. In humans, lysozyme is encoded by a single gene *LYZ*, whereas 2 genes exist in mouse, *Lyz1* and *Lyz2* encoding for lysozyme P and lysozyme M, respectively. *Lyz1* expression is restricted to the Paneth cells in small intestine. However, *Lyz2* is a widely-expressed lysozyme gene in mice with a high expression in the myeloid lineage, mainly neutrophils, macrophages and dendritic cells similar to what is found for human *LYZ* gene. Myeloid cells not only secrete lysozyme M extracellularly, but also deliver it to the bacterium-containing phagosomes<sup>593, 594, 595</sup>. It has been reported that *Lyz1* can compensate *Lyz2* deficiency in lung by increased mRNA and protein levels<sup>596</sup>. However, it has also been shown that lysozyme P exhibits lower muramidase and bactericidal activities compared to lysozyme M, indicating the compensatory effect of lysozyme P for lysozyme M may not be fully effective<sup>596, 591</sup>. Interestingly, *LYZ* gene is positioned in the neighborhood of an ulcerative colitis (UC) risk locus<sup>597, 598</sup>. Moreover, point mutations in *LYZ* gene have been associated with familial visceral amyloidosis that result in hepatomegaly and cholestasis liver phenotypes in humans<sup>599</sup>. Relatedly, familial visceral amyloidosis patients carrying mutant *LYZ* gene display gastritis and inflammatory bowel disease (IBD) symptoms like abdominal pain, malabsorption, diarrhea, and weight loss<sup>600, 601</sup>. Expectedly, *Lyz2*-deficient mice develop more severe bacterial infections<sup>602, 603, 604</sup>. In addition to its anti-microbial properties, lysozyme is also an anti-inflammatory factor. Lysozyme inhibits serum complement activation<sup>605</sup> and possesses a LPS-binding ability that reduces LPS-related inflammation<sup>606</sup>. Peptides derived from lysozyme cleavage inhibit production of pro-inflammatory cytokines, including TNF $\alpha$  and IL-1 $\beta$ , by macrophages<sup>607</sup>. In a recent study, Yu et al. reported that Paneth cell-derived lysozyme (*Lyz1*) defines the composition of mucolytic microbiota and the inflammatory tone of the intestine<sup>609</sup>. Authors using bulk RNA-seq analysis of ileum revealed that *Lyz1*-deficient mice exhibit diminished NLR and muramyl-dipeptide

signaling as well as suppressed cytokine production, inflammatory response, and ROS signaling in basal conditions compared to wild-type littermates, suggesting that *Lyz1* deficiency diminishes the intestinal mucosal response to bacterial molecular patterns<sup>609</sup>. Moreover, in response to dextran sulfate sodium (DSS)-induced colitis, *Lyz1*-deficient mice exhibit reduced NLR signaling and anti-colitogenic type 2 immune response compared to wild-type mice, indicating that *Lyz1* deficiency ameliorates mucosal inflammation during DSS-induced colitis<sup>609</sup>. Interestingly, authors also observed in ileum of *Lyz1*-deficient mice increased Tuft and goblet cell populations and concluded that the skewed type 2 immune profile of *Lyz1*-deficient mice in intestine was consistent with an activated goblet and Tuft cell program<sup>609</sup>. Subsequently, they identified that ILC2-derived IL13 promotes goblet and Tuft cell differentiation through ILC2-IL13-IL4Ra-Stat6 axis, and accounts for anti-colitogenic protection in *Lyz1*-deficient<sup>609</sup>. Moreover, authors by using broad-spectrum antibiotic treatment, showed that gut microbiota of *Lyz1*-deficient mice is required for the type 2 immune phenotype and anti-colitogenic effect<sup>609</sup>. Importantly, authors found no change in luminal bacterial load in cecum or mucosa-associated bacteria in ileum and colon<sup>609</sup>. In line, 16S rRNA amplicon profiling of fecal and ileal content showed unchanged  $\alpha$ -diversity (the mean species diversity in habitats at a local scale) between the 2 genotypes<sup>609</sup>. However, by using unweighted UniFrac analysis, which reflects  $\beta$ -diversity (the ratio between regional and local species diversity), they found significant differences between the 2 genotypes in fecal and ileal bacterial composition<sup>609</sup>. They identified that for ileal luminal bacteria an expansion of *Ruminococcus gnavus*, *Blautia gnavus*, and *Dorea formicigenerans* and a reduction of *Candidatus Arthromitus* in *Lyz1*-deficient mice<sup>609</sup>. Similarly, for fecal and ileal mucosal bacteria, relative expansion of *Dorea formicigenerans* and reduction of *Candidatus Arthromitus* was found, indicating that *Lyz1* deficiency alters gut bacterial landscape<sup>609</sup>. Authors next performed fecal microbiota transfer (FMT) using germ-free wild-type recipients to test the anti-inflammatory activity of *Lyz1*-deficient microbiota in DSS-induced colitis whether transferable or not<sup>609</sup>. Interestingly, they found that *Lyz1*-deficient-FMT mice exhibit an exacerbated colitis, loss of 20% of body weight, and a 20% mortality at the end of the study<sup>609</sup>. The authors suggested that transfer of *Lyz1*-deficient microbiota to lysozyme-sufficient recipients exacerbated colitis likely through enhanced bacterial processing by host lysozyme<sup>609</sup>. Thus, they concluded that transfer of *Lyz1*-deficient microbiota to lysozyme-sufficient recipients did not transfer the protection<sup>609</sup>. Taken together, authors concluded that Paneth cells possibly monitor and regulate the intestinal type 1 immunity via lysozyme, while goblet and Tuft cells are regulated by type 2 immunity<sup>609</sup>. Thus, the Th1-Paneth cell axis is balanced by goblet-tuft-Th2 circuit to maintain gut homeostasis<sup>609</sup>. The authors also proposed that such interplay between host lysozyme and microbiota might also exist in *Lyz2*-deficient mice<sup>609</sup>. In agreement with earlier published report that compare muramidase and bacterial killing activity of the lysozyme M and lysozyme

P<sup>596</sup>, the authors suggested that myeloid lysozyme M might mediate direct bacterial killing to prevent infection spreading, while luminal lysozyme P, with an intact barrier, might primarily process bacterial cell-wall to alert the immune system<sup>609</sup>.

Moreover, lysozyme improves the anti-oxidant capacity of hepatocytes *in vitro* and *in vivo*, leading to a protection against oxidative stress in liver<sup>608</sup>. Given the impact of intestinal permeability and dysbiosis on metabolic diseases and the anti-microbial activity of the lysozyme M, we suspected that its potential protection upon HFD, might in part, be mediated by a direct action on intestinal microbiota and/or permeability-derived local and distal inflammation. Thus, we will measure plasmatic endotoxin levels by ELISA of chow diet and HFD-fed wild-type (*Lyz2<sup>WT/WT</sup>*), heterozygous (*Lyz2<sup>WT/Cre</sup>*), and deficient (*Lyz2<sup>Cre/Cre</sup>*) mice to evaluate intestinal permeability to bacterial products. Moreover, to investigate impact of *Lyz2* deficiency on inflammatory response and intestinal permeability, we collected small intestine (duodenum, jejunum and ileum) and colon samples for qPCR and histological analysis from chow diet and HFD-fed wild-type (*Lyz2<sup>WT/WT</sup>*), heterozygous (*Lyz2<sup>WT/Cre</sup>*), and deficient (*Lyz2<sup>Cre/Cre</sup>*) littermates. Likewise, to examine effect of *Lyz2* deficiency on dysbiosis, we also collected fecal and cecal content in sterile conditions from these mice. Analyses are currently underway.

## REFERENCES

1. World Health Organization, (WHO). Obesity and overweight. <https://www.who.int/news-room/fact-sheets/detail/obesity-and-overweight> (2020).
2. (NCD-RisC), N.R.F.C. Worldwide trends in body-mass index, underweight, overweight, and obesity from 1975 to 2016: a pooled analysis of 2416 population-based measurement studies in 128·9 million children, adolescents, and adults. *Lancet Lond. Engl.* **390**, 2627–2642 (2017).
3. González-Muniesa, P. *et al.* Obesity. *Nat. Rev. Dis. Primer* **3**, 1–18 (2017).
4. Abdelaal, M., le Roux, C. W. & Docherty, N. G. Morbidity and mortality associated with obesity. *Ann. Transl. Med.* **5**, 8 (2017).
5. Fairbrother, U., Kidd, E., Malagamuwa, T. & Walley, A. Genetics of Severe Obesity. *Curr. Diab. Rep.* **18**, 85 (2018).
6. American Diabetes Association. 2. Classification and Diagnosis of Diabetes: *Standards of Medical Care in Diabetes—2019. Diabetes Care* **42**, S13–S28 (2019).
7. Bhupathiraju, S. N. & Hu, F. B. Epidemiology of Obesity and Diabetes and Their Cardiovascular Complications. *Circ. Res.* **118**, 1723–1735 (2016).
8. World Health Organization (WHO). Diabetes.
9. Habib Yaribeygi, Farin Rashid Farrokhi, Alexandra E. Butler & mechanisms. Insulin resistance: Review of the underlying molecular mechanisms.
10. Haeusler, R. A., McGraw, T. E. & Accili, D. Biochemical and cellular properties of insulin receptor signalling. *Nat. Rev. Mol. Cell Biol.* **19**, 31–44 (2018).
11. Manning, B. D. & Toker, A. AKT/PKB Signaling: Navigating the Network. *Cell* **169**, 381–405 (2017).
12. Alessi, D. R. *et al.* Mechanism of activation of protein kinase B by insulin and IGF-1. *EMBO J.* **15**, 6541–6551 (1996).

13. Alessi, D. R. *et al.* Characterization of a 3-phosphoinositide-dependent protein kinase which phosphorylates and activates protein kinase B. *9*.
14. Sarbassov, D. D. Phosphorylation and Regulation of Akt/PKB by the Rictor-mTOR Complex. *Science* **307**, 1098–1101 (2005).
15. Kandel, E. S. & Hay, N. The Regulation and Activities of the Multifunctional Serine/Threonine Kinase Akt/PKB. *20*.
16. Manning, B. D. & Toker, A. AKT/PKB Signaling: Navigating the Network. *Cell* **169**, 381–405 (2017).
17. Kahn CR, *et al.* The Syndromes of Insulin Resistance and Acanthosis Nigricans — Insulin-Receptor Disorders in Man | NEJM.
18. Plamper, M., Gohlke, B., Schreiner, F. & Woelfle, J. Mecasermin in Insulin Receptor-Related Severe Insulin Resistance Syndromes: Case Report and Review of the Literature. *Int. J. Mol. Sci.* **19**, 1268 (2018).
19. Hribal, M. L. *et al.* Transgenic mice overexpressing human G972R IRS-1 show impaired insulin action and insulin secretion. *J. Cell. Mol. Med.* **12**, 2096–2106 (2008).
20. Burguete-Garcia, A. I. *et al.* Association of Gly972Arg polymorphism of IRS1 gene with type 2 diabetes mellitus in lean participants of a national health survey in Mexico: a candidate gene study. *Metabolism* **59**, 38–45 (2010).
21. Baier, L. J., Wiedrich, C., Hanson, R. L. & Bogardus, C. Variant in the Regulatory Subunit of Phosphatidylinositol 3-Kinase (p85 ). **47**, 4 (1998).
22. Almind, K. *et al.* Characterization of the Met326Ile variant of phosphatidylinositol 3-kinase p85. *Proc. Natl. Acad. Sci.* **99**, 2124–2128 (2002).
23. George, S. A Family with Severe Insulin Resistance and Diabetes Due to a Mutation in AKT2. *Science* **304**, 1325–1328 (2004).
24. Kahn, C. R., Wang, G. & Lee, K. Y. Altered adipose tissue and adipocyte function in the pathogenesis of metabolic syndrome. (2019) doi:10.1172/JCI129187.

25. Luong, Q., Huang, J. & Lee, K. Y. Deciphering White Adipose Tissue Heterogeneity. *Biology* **8**, 23 (2019).
26. World Health Organization. *Waist circumference and waist-hip ratio: report of a WHO expert consultation, Geneva, 8-11 December 2008*. (World Health Organization, 2011).
27. Lukich, A., Gavish, D. & Shargorodsky, M. Normal weight diabetic patients versus obese diabetics: relation of overall and abdominal adiposity to vascular health. *Cardiovasc. Diabetol.* **13**, 141 (2014).
28. Blüher, M. Metabolically Healthy Obesity. *Endocr. Rev.* **41**, (2020).
29. Tran, T. T., Yamamoto, Y., Gesta, S. & Kahn, C. R. Beneficial Effects of Subcutaneous Fat Transplantation on Metabolism. *Cell Metab.* **7**, 410–420 (2008).
30. A Novel Role for Subcutaneous Adipose Tissue in Exercise-Induced Improvements in Glucose Homeostasis | Diabetes.
31. Driskell, R., Jahoda, C. A. B., Chuong, C.-M., Watt, F. & Horsley, V. Defining dermal adipose tissue. *Exp. Dermatol.* **23**, 629–631 (2014).
32. Paula, F. J. A. de & Rosen, C. J. Structure and Function of Bone Marrow Adipocytes. in *Comprehensive Physiology* 315–349 (American Cancer Society, 2017).  
doi:10.1002/cphy.c170010.
33. Chen, S. X., Zhang, L.-J. & Gallo, R. L. Dermal White Adipose Tissue: A Newly Recognized Layer of Skin Innate Defense. *J. Invest. Dermatol.* **139**, 1002–1009 (2019).
34. Region-specific variation in the properties of skeletal adipocytes reveals regulated and constitutive marrow adipose tissues | Nature Communications.
35. Ambrosi, T. H. *et al.* Adipocyte Accumulation in the Bone Marrow during Obesity and Aging Impairs Stem Cell-Based Hematopoietic and Bone Regeneration. *Cell Stem Cell* **20**, 771-784.e6 (2017).
36. Fasshauer, M. & Blüher, M. Adipokines in health and disease. *Trends Pharmacol. Sci.* **36**, 461–470 (2015).

37. Ruiz-Fernández, C. *et al.* Molecular Relationships among Obesity, Inflammation and Intervertebral Disc Degeneration: Are Adipokines the Common Link? *Int. J. Mol. Sci.* **20**, 2030 (2019).
38. Heo, Jin-Yeong, Park, Yoon Jeong, Ham, Mira & Kim, Jae Bum. Crosstalk between Adipocytes and Immune Cells in Adipose Tissue Inflammation and Metabolic Dysregulation in Obesity. *Mol. Cells* **37**, 365–371 (2014).
39. Brestoff, J. R. & Artis, D. Immune Regulation of Metabolic Homeostasis in Health and Disease. *Cell* **161**, 146–160 (2015).
40. Ghaben, A. L. & Scherer, P. E. Adipogenesis and metabolic health. *Nat. Rev. Mol. Cell Biol.* **20**, 242–258 (2019).
41. Unamuno, X. *et al.* Adipokine dysregulation and adipose tissue inflammation in human obesity. *Eur. J. Clin. Invest.* **48**, e12997 (2018).
42. I. S. Sobczak, A., A. Blindauer, C. & J. Stewart, A. Changes in Plasma Free Fatty Acids Associated with Type-2 Diabetes. *Nutrients* **11**, 2022 (2019).
43. Wernstedt Asterholm, I. *et al.* Adipocyte Inflammation Is Essential for Healthy Adipose Tissue Expansion and Remodeling. *Cell Metab.* **20**, 103–118 (2014).
44. Crewe, C., An, Y. A. & Scherer, P. E. The ominous triad of adipose tissue dysfunction: inflammation, fibrosis, and impaired angiogenesis. *J. Clin. Invest.* **127**, 74–82 (2017).
45. Cinti, S. *et al.* Adipocyte death defines macrophage localization and function in adipose tissue of obese mice and humans. *J. Lipid Res.* **46**, 2347–2355 (2005).
46. Rosen, E. D. & Spiegelman, B. M. What We Talk About When We Talk About Fat. *Cell* **156**, 20–44 (2014).
47. Ertunc, M. E. & Hotamisligil, G. S. Lipid signaling and lipotoxicity in metaflammation: indications for metabolic disease pathogenesis and treatment. *J. Lipid Res.* **57**, 2099–2114 (2016).

48. Kim, J. K. *et al.* Prevention of fat-induced insulin resistance by salicylate. *J. Clin. Invest.* **108**, 437–446 (2001).
49. Hirosumi, J. *et al.* A central role for JNK in obesity and insulin resistance. *Nature* **420**, 333–336 (2002).
50. Catrysse, L. & van Loo, G. Inflammation and the Metabolic Syndrome: The Tissue-Specific Functions of NF- $\kappa$ B. *Trends Cell Biol.* **27**, 417–429 (2017).
51. Zabolotny, J. M. *et al.* Protein-tyrosine Phosphatase 1B Expression Is Induced by Inflammation *in Vivo*. *J. Biol. Chem.* **283**, 14230–14241 (2008).
52. Holland, W. L. *et al.* Lipid-induced insulin resistance mediated by the proinflammatory receptor TLR4 requires saturated fatty acid–induced ceramide biosynthesis in mice. *J. Clin. Invest.* **121**, 1858–1870 (2011).
53. Shah, O. J., Wang, Z. & Hunter, T. Inappropriate Activation of the TSC/Rheb/mTOR/S6K Cassette Induces IRS1/2 Depletion, Insulin Resistance, and Cell Survival Deficiencies. *Curr. Biol.* **14**, 1650–1656 (2004).
54. Gao, T., Furnari, F. & Newton, A. C. PHLPP: A Phosphatase that Directly Dephosphorylates Akt, Promotes Apoptosis, and Suppresses Tumor Growth. *Mol. Cell* **18**, 13–24 (2005).
55. Brognard, J., Sierceki, E., Gao, T. & Newton, A. C. PHLPP and a Second Isoform, PHLPP2, Differentially Attenuate the Amplitude of Akt Signaling by Regulating Distinct Akt Isoforms. *Mol. Cell* **25**, 917–931 (2007).
56. Julien, L.-A., Carriere, A., Moreau, J. & Roux, P. P. mTORC1-Activated S6K1 Phosphorylates Rictor on Threonine 1135 and Regulates mTORC2 Signaling. *Mol. Cell. Biol.* **30**, 908–921 (2010).
57. Liu, P. *et al.* Sin1 phosphorylation impairs mTORC2 complex integrity and inhibits downstream Akt signalling to suppress tumorigenesis. *Nat. Cell Biol.* **15**, 1340–1350 (2013).

58. Petersen, M. C. *et al.* Insulin receptor Thr1160 phosphorylation mediates lipid-induced hepatic insulin resistance. *J. Clin. Invest.* **126**, 11 (2016).
59. Xia, J. Y., Morley, T. S. & Scherer, P. E. The adipokine/ceramide axis: Key aspects of insulin sensitization. *Biochimie* **96**, 130–139 (2014).
60. Chaurasia, B. & Summers, S. A. Ceramides – Lipotoxic Inducers of Metabolic Disorders. *Trends Endocrinol. Metab.* **26**, 538–550 (2015).
61. Lazar, D. F. & Saltiel, A. R. Lipid phosphatases as drug discovery targets for type 2 diabetes. *Nat. Rev. Drug Discov.* **5**, 333–342 (2006).
62. Masson, G. R. & Williams, R. L. Structural Mechanisms of PTEN Regulation. *Cold Spring Harb. Perspect. Med.* **10**, a036152 (2020).
63. Kurlawalla-Martinez, C. *et al.* Insulin Hypersensitivity and Resistance to Streptozotocin-Induced Diabetes in Mice Lacking PTEN in Adipose Tissue. *Mol. Cell. Biol.* **25**, 2498–2510 (2005).
64. Stiles, B. *et al.* Live-specific deletion of negative regulator Pten results in fatty liver and insulin hypersensitivity. *Med. Sci.* **6**.
65. Wijesekara, N. *et al.* Muscle-Specific Pten Deletion Protects against Insulin Resistance and Diabetes. *Mol. Cell. Biol.* **25**, 1135–1145 (2005).
66. Lehtonen, S. SHIPping out diabetes—Metformin, an old friend among new SHIP2 inhibitors. *Acta Physiol.* **228**, (2020).
67. Cooney, G. J. *et al.* Improved glucose homeostasis and enhanced insulin signalling in Grb14-deficient mice. *EMBO J.* **23**, 582–593 (2004).
68. Wang, L. *et al.* Peripheral Disruption of the Grb10 Gene Enhances Insulin Signaling and Sensitivity In Vivo. *Mol. Cell. Biol.* **27**, 6497–6505 (2007).
69. Holt, L. J. *et al.* Dual Ablation of Grb10 and Grb14 in Mice Reveals Their Combined Role in Regulation of Insulin Signaling and Glucose Homeostasis. *Mol. Endocrinol.* **23**, 1406 (2009).

70. DIAbetes Genetics Replication And Meta-analysis (DIAGRAM) Consortium *et al.* A genome-wide approach accounting for body mass index identifies genetic variants influencing fasting glycemic traits and insulin resistance. *Nat. Genet.* **44**, 659–669 (2012).
71. Dodington, D. W., Desai, H. R. & Woo, M. JAK/STAT – Emerging Players in Metabolism. *Trends Endocrinol. Metab.* **29**, 55–65 (2018).
72. Villarino, A. V., Kanno, Y. & O’Shea, J. J. Mechanisms and consequences of Jak–STAT signaling in the immune system. *Nat. Immunol.* **18**, 374–384 (2017).
73. Shi, S. Y. *et al.* Adipocyte-specific deficiency of Janus kinase (JAK) 2 in mice impairs lipolysis and increases body weight, and leads to insulin resistance with ageing. *Diabetologia* **57**, 1016–1026 (2014).
74. Cernkovich, E. R., Deng, J., Bond, M. C., Combs, T. P. & Harp, J. B. Adipose-Specific Disruption of Signal Transducer and Activator of Transcription 3 Increases Body Weight and Adiposity. *Endocrinology* **149**, 1581–1590 (2008).
75. Kaltenecker, D. *et al.* Adipocyte STAT5 deficiency promotes adiposity and impairs lipid mobilisation in mice. *Diabetologia* **60**, 296–305 (2017).
76. Durham, G. A., Williams, J. J. L., Nasim, M. T. & Palmer, T. M. Targeting SOCS Proteins to Control JAK-STAT Signalling in Disease. *Trends Pharmacol. Sci.* **40**, 298–308 (2019).
77. Howard, J. K. & Flier, J. S. Attenuation of leptin and insulin signaling by SOCS proteins. *Trends Endocrinol. Metab.* **17**, 365–371 (2006).
78. Pedroso, J. A. B., Ramos-Lobo, A. M. & Donato, J. SOCS3 as a future target to treat metabolic disorders. *Hormones* **18**, 127–136 (2019).
79. Rottenberg, M. E. & Carow, B. SOCS3, a Major Regulator of Infection and Inflammation. *Front. Immunol.* **5**, (2014).

80. Zampieri, T. T. *et al.* SOCS3 deficiency in leptin receptor-expressing cells mitigates the development of pregnancy-induced metabolic changes. *Mol. Metab.* **4**, 237–245 (2015).
81. Pedrosa, J. A. B. *et al.* Changes in Leptin Signaling by SOCS3 Modulate Fasting-Induced Hyperphagia and Weight Regain in Mice. *Endocrinology* **157**, 3901–3914 (2016).
82. Mori, H. *et al.* Socs3 deficiency in the brain elevates leptin sensitivity and confers resistance to diet-induced obesity. *Nat. Med.* **10**, 739–743 (2004).
83. Pedrosa, J. A. B. *et al.* Inactivation of SOCS3 in leptin receptor-expressing cells protects mice from diet-induced insulin resistance but does not prevent obesity. *Mol. Metab.* **3**, 608–618 (2014).
84. Aydin, Ö. The Gut Microbiome as a Target for the Treatment of Type 2 Diabetes. *Curr Diab Rep* **11** (2018).
85. Cornejo-Pareja, I., Muñoz-Garach, A., Clemente-Postigo, M. & Tinahones, F. J. Importance of gut microbiota in obesity. *Eur. J. Clin. Nutr.* **72**, 26–37 (2019).
86. on behalf of the Obesity Programs of nutrition, Education, Research and Assessment (OPERA) group *et al.* Gut microbiota: a new path to treat obesity. *Int. J. Obes. Suppl.* **9**, 10–19 (2019).
87. Crovesy, L., Masterson, D. & Rosado, E. L. Profile of the gut microbiota of adults with obesity: a systematic review. *Eur. J. Clin. Nutr.* (2020) doi:10.1038/s41430-020-0607-6.
88. Backhed, F. *et al.* The gut microbiota as an environmental factor that regulates fat storage. *Proc. Natl. Acad. Sci.* **101**, 15718–15723 (2004).
89. Bäckhed, F., Manchester, J. K., Semenkovich, C. F. & Gordon, J. I. Mechanisms underlying the resistance to diet-induced obesity in germ-free mice. *Proc. Natl. Acad. Sci.* **104**, 979–984 (2007).
90. Vrieze, A. *et al.* Transfer of Intestinal Microbiota From Lean Donors Increases Insulin Sensitivity in Individuals With Metabolic Syndrome. *Gastroenterology* **143**, 913-916.e7 (2012).

91. Yu, E. W. *et al.* Fecal microbiota transplantation for the improvement of metabolism in obesity: The FMT-TRIM double-blind placebo-controlled pilot trial. *PLOS Med.* **17**, e1003051 (2020).
92. MetaHIT consortium *et al.* Richness of human gut microbiome correlates with metabolic markers. *Nature* **500**, 541–546 (2013).
93. ANR MicroObes consortium *et al.* Dietary intervention impact on gut microbial gene richness. *Nature* **500**, 585–588 (2013).
94. Winer, D. A., Luck, H., Tsai, S. & Winer, S. The Intestinal Immune System in Obesity and Insulin Resistance. *Cell Metab.* **23**, 413–426 (2016).
95. Burcelin, R. *et al.* Metagenome and metabolism: the tissue microbiota hypothesis: Burcelin *et al.* *Diabetes Obes. Metab.* **15**, 61–70 (2013).
96. Anhê, F. F. Type 2 diabetes influences bacterial tissue compartmentalisation in human obesity. **2**, 17 (2020).
97. Chakaroun, R. M., Massier, L. & Kovacs, P. Gut Microbiome, Intestinal Permeability, and Tissue Bacteria in Metabolic Disease: Perpetrators or Bystanders? **30** (2020).
98. Wu, H. & Ballantyne, C. M. Metabolic Inflammation and Insulin Resistance in Obesity. *Circ. Res.* **126**, 1549–1564 (2020).
99. Guilliams, M., Mildner, A. & Yona, S. Developmental and Functional Heterogeneity of Monocytes. *Immunity* **49**, 595–613 (2018).
100. Swirski, F. K. *et al.* Identification of Splenic Reservoir Monocytes and Their Deployment to Inflammatory Sites. *Science* **325**, 612–616 (2009).
101. Silva, H. M. *et al.* Vasculature-associated fat macrophages readily adapt to inflammatory and metabolic challenges. *J. Exp. Med.* jem.20181049 (2019)  
doi:10.1084/jem.20181049.

102. Wong, K. L. *et al.* Gene expression profiling reveals the defining features of the classical, intermediate, and nonclassical human monocyte subsets. *Blood* **118**, e16–e31 (2011).
103. Auffray, C. *et al.* Monitoring of Blood Vessels and Tissues by a Population of Monocytes with Patrolling Behavior. *Science* **317**, 666–670 (2007).
104. Carlin, L. M. *et al.* Nr4a1-Dependent Ly6Clow Monocytes Monitor Endothelial Cells and Orchestrate Their Disposal. *Cell* **153**, 362–375 (2013).
105. Cros, J. *et al.* Human CD14<sup>dim</sup> Monocytes Patrol and Sense Nucleic Acids and Viruses via TLR7 and TLR8 Receptors. *Immunity* **33**, 375–386 (2010).
106. Kratofil Rachel M., Kubes Paul & Deniset Justin F. Monocyte Conversion During Inflammation and Injury. *Arterioscler. Thromb. Vasc. Biol.* **37**, 35–42 (2017).
107. the Immunological Genome Consortium *et al.* Gene-expression profiles and transcriptional regulatory pathways that underlie the identity and diversity of mouse tissue macrophages. *Nat. Immunol.* **13**, 1118–1128 (2012).
108. Shapouri-Moghaddam, A. *et al.* Macrophage plasticity, polarization, and function in health and disease. *J. Cell. Physiol.* **233**, 6425–6440 (2018).
109. Orecchioni, M., Ghosheh, Y., Pramod, A. B. & Ley, K. Macrophage Polarization: Different Gene Signatures in M1(LPS+) vs. Classically and M2(LPS-) vs. Alternatively Activated Macrophages. *Front. Immunol.* **10**, (2019).
110. Okabe, Y. & Medzhitov, R. Tissue-Specific Signals Control Reversible Program of Localization and Functional Polarization of Macrophages. *Cell* **157**, 832–844 (2014).
111. Saha, S., Shalova, I. N. & Biswas, S. K. Metabolic regulation of macrophage phenotype and function. *Immunol. Rev.* **280**, 102–111 (2017).
112. Zuo, H. & Wan, Y. Metabolic Reprogramming in Mitochondria of Myeloid Cells. *Cells* **9**, 5 (2020).

113. Gomez Perdiguero, E. *et al.* Tissue-resident macrophages originate from yolk-sac-derived erythro-myeloid progenitors. *Nature* **518**, 547–551 (2015).
114. McGrath, K. E. *et al.* Distinct Sources of Hematopoietic Progenitors Emerge before HSCs and Provide Functional Blood Cells in the Mammalian Embryo. *Cell Rep.* **11**, 1892–1904 (2015).
115. Catrysse, L. & van Loo, G. Adipose tissue macrophages and their polarization in health and obesity. *Cell. Immunol.* **330**, 114–119 (2018).
116. Italiani, P. & Boraschi, D. From Monocytes to M1/M2 Macrophages: Phenotypical vs. Functional Differentiation. *Front. Immunol.* **5**, (2014).
117. Dai, L. *et al.* Macrophage alternative activation confers protection against lipotoxicity-induced cell death. *Mol. Metab.* **6**, 1186–1197 (2017).
118. Haka, A. S. *et al.* Exocytosis of macrophage lysosomes leads to digestion of apoptotic adipocytes and foam cell formation. *J. Lipid Res.* **57**, 980–992 (2016).
119. Kosteli, A. *et al.* Weight loss and lipolysis promote a dynamic immune response in murine adipose tissue. *J. Clin. Invest.* **120**, 3466–3479 (2010).
120. Lee, Y.-H., Petkova, A. P. & Granneman, J. G. Identification of an Adipogenic Niche for Adipose Tissue Remodeling and Restoration. *Cell Metab.* **18**, 355–367 (2013).
121. Bourlier, V. *et al.* Remodeling Phenotype of Human Subcutaneous Adipose Tissue Macrophages. *Circulation* **117**, 806–815 (2008).
122. Segura, E. Review of Mouse and Human Dendritic Cell Subsets. in *Dendritic Cell Protocols* (eds. Segura, E. & Onai, N.) vol. 1423 3–15 (Springer New York, 2016).
123. Eisenbarth, S. C. Dendritic cell subsets in T cell programming: location dictates function. *Nat. Rev. Immunol.* **19**, 89–103 (2019).
124. Collin, M. & Bigley, V. Human dendritic cell subsets: an update. *Immunology* **154**, 3–20 (2018).

125. See, P. *et al.* Mapping the human DC lineage through the integration of high-dimensional techniques. *Science* **356**, eaag3009 (2017).
126. Sathe, P. *et al.* Lymphoid Tissue and Plasmacytoid Dendritic Cells and Macrophages Do Not Share a Common Macrophage-Dendritic Cell-Restricted Progenitor. *Immunity* **41**, 104–115 (2014).
127. Waskow, C. *et al.* The receptor tyrosine kinase Flt3 is required for dendritic cell development in peripheral lymphoid tissues. *Nat. Immunol.* **9**, 676–683 (2008).
128. Breton, G. *et al.* Circulating precursors of human CD1c<sup>+</sup> and CD141<sup>+</sup> dendritic cells. *J. Exp. Med.* **212**, 401–413 (2015).
129. Bourdely, P. *et al.* Transcriptional and Functional Analysis of CD1c<sup>+</sup> Human Dendritic Cells Identifies a CD163<sup>+</sup> Subset Priming CD8<sup>+</sup>CD103<sup>+</sup> T Cells. *Immunity* **53**, 335–352.e8 (2020).
130. Chandra, J., Kuo, P. T. Y., Hahn, A. M., Belz, G. T. & Frazer, I. H. Batf3 selectively determines acquisition of CD8<sup>+</sup> dendritic cell phenotype and function. *Immunol. Cell Biol.* **95**, 215–223 (2017).
131. Tamura, T. *et al.* IFN Regulatory Factor-4 and -8 Govern Dendritic Cell Subset Development and Their Functional Diversity. *J. Immunol.* **174**, 2573–2581 (2005).
132. Shortman, K. & Heath, W. R. The CD8<sup>+</sup> dendritic cell subset. *Immunol. Rev.* **234**, 18–31 (2010).
133. Edelson, B. T. *et al.* Peripheral CD103<sup>+</sup> dendritic cells form a unified subset developmentally related to CD8 $\alpha$ <sup>+</sup> conventional dendritic cells. *J. Exp. Med.* **207**, 823–836 (2010).
134. Crozat, K. *et al.* Comparative genomics as a tool to reveal functional equivalences between human and mouse dendritic cell subsets. *Immunol. Rev.* **234**, 177–198 (2010).
135. Schraml, B. U. *et al.* Genetic Tracing via DNNGR-1 Expression History Defines Dendritic Cells as a Hematopoietic Lineage. *Cell* **154**, 843–858 (2013).

136. Granot, T. *et al.* Dendritic Cells Display Subset and Tissue-Specific Maturation Dynamics over Human Life. *Immunity* **46**, 504–515 (2017).
137. Petvises, S., Periasamy, P. & O’Neill, H. C. MCSF drives regulatory DC development in stromal co-cultures supporting hematopoiesis. *BMC Immunol.* **19**, 21 (2018).
138. Pellerin, A. *et al.* Anti- BDCA 2 monoclonal antibody inhibits plasmacytoid dendritic cell activation through Fc-dependent and Fc-independent mechanisms. *EMBO Mol. Med.* **7**, 464–476 (2015).
139. Fanning, S. L. *et al.* Receptor Cross-Linking on Human Plasmacytoid Dendritic Cells Leads to the Regulation of IFN- $\alpha$  Production. *J. Immunol.* **177**, 5829–5839 (2006).
140. Cao, W. *et al.* Regulation of TLR7/9 responses in plasmacytoid dendritic cells by BST2 and ILT7 receptor interaction. *J. Exp. Med.* **206**, 1603–1614 (2009).
141. Moffat, J. M. *et al.* Targeting antigen to bone marrow stromal cell-2 expressed by conventional and plasmacytoid dendritic cells elicits efficient antigen presentation. *Eur. J. Immunol.* **43**, 595–605 (2013).
142. Davison, L. M. & Jørgensen, T. N. Sialic Acid–Binding Immunoglobulin-Type Lectin H–Positive Plasmacytoid Dendritic Cells Drive Spontaneous Lupus-like Disease Development in B6.Nba2 Mice. *Arthritis Rheumatol.* **67**, 1012–1022 (2015).
143. Reizis, B. Plasmacytoid Dendritic Cells: Development, Regulation, and Function. *Immunity* **50**, 37–50 (2019).
144. Swiecki, M. & Colonna, M. The multifaceted biology of plasmacytoid dendritic cells. *Nat. Rev. Immunol.* **15**, 471–485 (2015).
145. Macdougall, C. E. & Longhi, M. P. Adipose tissue dendritic cells in steady-state. *Immunology* **156**, 228–234 (2019).
146. Macdougall, C. E. *et al.* Visceral Adipose Tissue Immune Homeostasis Is Regulated by the Crosstalk between Adipocytes and Dendritic Cell Subsets. *Cell Metab.* **27**, 588–601.e4 (2018).

147. Shamri, R., Xenakis, J. J. & Spencer, L. A. Eosinophils in innate immunity: an evolving story. *Cell Tissue Res.* **343**, 57–83 (2011).
148. Nussbaum, J. C. *et al.* Type 2 innate lymphoid cells control eosinophil homeostasis. *Nature* **502**, 245–248 (2013).
149. Acharya, K. R. & Ackerman, S. J. Eosinophil Granule Proteins: Form and Function. *J. Biol. Chem.* **289**, 17406–17415 (2014).
150. S, Y. *et al.* Catapult-like release of mitochondrial DNA by eosinophils contributes to antibacterial defense. *Nat. Med.* **14**, (2008).
151. E, G. *et al.* Extracellular eosinophilic traps in association with *Staphylococcus aureus* at the site of epithelial barrier defects in patients with severe airway inflammation. *J. Allergy Clin. Immunol.* **139**, (2017).
152. Weller, P. F. & Spencer, L. A. Functions of tissue-resident eosinophils. *Nat. Rev. Immunol.* **17**, 746–760 (2017).
153. Bolus, W. R., Kennedy, A. J. & Hasty, A. H. Obesity-induced reduction of adipose eosinophils is reversed with low-calorie dietary intervention. *Physiol. Rep.* **6**, e13919 (2018).
154. Wu, D. *et al.* Eosinophils Sustain Adipose Alternatively Activated Macrophages Associated with Glucose Homeostasis. *Science* **332**, 243–247 (2011).
155. Knights, A. J. *et al.* Eosinophil function in adipose tissue is regulated by Krüppel-like factor 3 (KLF3). *Nat. Commun.* **11**, 2922 (2020).
156. Spits, H. *et al.* Innate lymphoid cells — a proposal for uniform nomenclature. *Nat. Rev. Immunol.* **13**, 145–149 (2013).
157. Molofsky, A. B. *et al.* Innate lymphoid type 2 cells sustain visceral adipose tissue eosinophils and alternatively activated macrophages. *J. Exp. Med.* **210**, 535–549 (2013).
158. Brestoff, J. R. *et al.* Group 2 innate lymphoid cells promote beiging of white adipose tissue and limit obesity. *Nature* **519**, 242–246 (2015).

159. Zhou, H. & Liu, F. Regulation, Communication, and Functional Roles of Adipose Tissue-Resident CD4<sup>+</sup> T Cells in the Control of Metabolic Homeostasis. *Front. Immunol.* **9**, (2018).
160. Winer, S. *et al.* Normalization of obesity-associated insulin resistance through immunotherapy. *Nat. Med.* **15**, 921–929 (2009).
161. Dominguez-Villar, M. & Hafler, D. A. Regulatory T cells in autoimmune disease. *Nat. Immunol.* **19**, 665–673 (2018).
162. Kolodin, D. *et al.* Antigen- and Cytokine-Driven Accumulation of Regulatory T Cells in Visceral Adipose Tissue of Lean Mice. *Cell Metab.* **21**, 543–557 (2015).
163. Panduro, M., Benoist, C. & Mathis, D. Tissue Tregs. *Annu. Rev. Immunol.* **34**, 609–633 (2016).
164. Lui, P. P., Cho, I. & Ali, N. Tissue regulatory T cells. *Immunology* **161**, 4–17 (2020).
165. Feuerer, M. *et al.* Lean, but not obese, fat is enriched for a unique population of regulatory T cells that affect metabolic parameters. *Nat. Med.* **15**, 930–939 (2009).
166. Cipolletta, D. *et al.* PPAR- $\gamma$  is a major driver of the accumulation and phenotype of adipose tissue T reg cells. *Nature* **486**, 549–553 (2012).
167. Vasanthakumar, A. *et al.* The transcriptional regulators IRF4, BATF and IL-33 orchestrate development and maintenance of adipose tissue-resident regulatory T cells. *Nat. Immunol.* **16**, 276–285 (2015).
168. Schmidleithner, L. *et al.* Enzymatic Activity of HPGD in Treg Cells Suppresses Tconv Cells to Maintain Adipose Tissue Homeostasis and Prevent Metabolic Dysfunction. *Immunity* **50**, 1232-1248.e14 (2019).
169. Nielsen, M. M., Witherden, D. A. & Havran, W. L.  $\gamma\delta$  T cells in homeostasis and host defence of epithelial barrier tissues. *Nat. Rev. Immunol.* **17**, 733–745 (2017).
170. Kohlgruber, A. C. *et al.*  $\gamma\delta$  T cells producing interleukin-17A regulate adipose regulatory T cell homeostasis and thermogenesis. *Nat. Immunol.* **19**, 464–474 (2018).

171. Goldberg, E. L. *et al.* Ketogenesis activates metabolically protective  $\gamma\delta$  T cells in visceral adipose tissue. *Nat. Metab.* **2**, 50–61 (2020).
172. Bennstein, S. B. Unraveling Natural Killer T-Cells Development. *Front. Immunol.* **8**, (2018).
173. Lynch, L. *et al.* Invariant NKT cells and CD1d<sup>+</sup> cells amass in human omentum and are depleted in patients with cancer and obesity. *Eur. J. Immunol.* **39**, 1893–1901 (2009).
174. Lynch, L. *et al.* Adipose Tissue Invariant NKT Cells Protect against Diet-Induced Obesity and Metabolic Disorder through Regulatory Cytokine Production. *Immunity* **37**, 574–587 (2012).
175. Huh, J. Y. *et al.* A Novel Function of Adipocytes in Lipid Antigen Presentation to iNKT Cells. *Mol. Cell. Biol.* **33**, 328–339 (2013).
176. Huh, J. Y. *et al.* Deletion of CD1d in Adipocytes Aggravates Adipose Tissue Inflammation and Insulin Resistance in Obesity. *Diabetes* **66**, 835–847 (2017).
177. Huh, J. Y., Park, Y. J. & Kim, J. B. Adipocyte CD1d determines adipose inflammation and insulin resistance in obesity. *Adipocyte* 1–8 (2018)  
doi:10.1080/21623945.2018.1440928.
178. B Cell Development, Activation and Effector Functions. *Primer Immune Response* 111–142 (2014) doi:10.1016/B978-0-12-385245-8.00005-4.
179. Wang, Y., Liu, J., Burrows, P. D. & Wang, J.-Y. B Cell Development and Maturation. in *B Cells in Immunity and Tolerance* (ed. Wang, J.-Y.) 1–22 (Springer, 2020).  
doi:10.1007/978-981-15-3532-1\_1.
180. Nishimura, S. *et al.* Adipose Natural Regulatory B Cells Negatively Control Adipose Tissue Inflammation. *Cell Metab.* **18**, 759–766 (2013).
181. García-Hernández, M. H. *et al.* Frequency of regulatory B cells in adipose tissue and peripheral blood from individuals with overweight, obesity and normal-weight. *Obes. Res. Clin. Pract.* **12**, 513–519 (2018).

182. Shen, L. *et al.* B-1a Lymphocytes Attenuate Insulin Resistance. *Diabetes* **64**, 593–603 (2015).
183. Weisberg, S. P. *et al.* Obesity is associated with macrophage accumulation in adipose tissue. *J. Clin. Invest.* **112**, 1796–1808 (2003).
184. Xu, H. *et al.* Chronic inflammation in fat plays a crucial role in the development of obesity-related insulin resistance. (2003) doi:10.1172/JCI19451.
185. Weisberg, S. P. *et al.* CCR2 modulates inflammatory and metabolic effects of high-fat feeding. *J. Clin. Invest.* **116**, 115–124 (2006).
186. Nagareddy, P. R. *et al.* Adipose Tissue Macrophages Promote Myelopoiesis and Monocytosis in Obesity. *Cell Metab.* **19**, 821–835 (2014).
187. Feng, B. *et al.* Clodronate Liposomes Improve Metabolic Profile and Reduce Visceral Adipose Macrophage Content in Diet-Induced Obese Mice. *PLOS ONE* **6**, e24358 (2011).
188. Lumeng, C. N., Bodzin, J. L. & Saltiel, A. R. Obesity induces a phenotypic switch in adipose tissue macrophage polarization. (2007) doi:10.1172/JCI29881.
189. Lumeng, C. N., DelProposto, J. B., Westcott, D. J. & Saltiel, A. R. Phenotypic Switching of Adipose Tissue Macrophages With Obesity Is Generated by Spatiotemporal Differences in Macrophage Subtypes. *Diabetes* **57**, 3239–3246 (2008).
190. Wentworth, J. M. *et al.* Pro-Inflammatory CD11c+CD206+ Adipose Tissue Macrophages Are Associated With Insulin Resistance in Human Obesity. *Diabetes* **59**, 1648–1656 (2010).
191. Xu, X. *et al.* Obesity Activates a Program of Lysosomal-Dependent Lipid Metabolism in Adipose Tissue Macrophages Independently of Classic Activation. *Cell Metab.* **18**, 816–830 (2013).

192. Kratz, M. *et al.* Metabolic Dysfunction Drives a Mechanistically Distinct Proinflammatory Phenotype in Adipose Tissue Macrophages. *Cell Metab.* **20**, 614–625 (2014).
193. Pirzgalska, R. M. *et al.* Sympathetic neuron–associated macrophages contribute to obesity by importing and metabolizing norepinephrine. *Nat. Med.* **23**, 1309–1318 (2017).
194. Hill, D. A. *et al.* Distinct macrophage populations direct inflammatory versus physiological changes in adipose tissue. *Proc. Natl. Acad. Sci.* **115**, E5096–E5105 (2018).
195. Jaitin, D. A. *et al.* Lipid-Associated Macrophages Control Metabolic Homeostasis in a Trem2-Dependent Manner. *Cell* **178**, 686–698.e14 (2019).
196. Hill et al. - 2018 - Distinct macrophage populations direct inflammation.pdf.
197. Stefanovic-Racic, M. *et al.* Dendritic Cells Promote Macrophage Infiltration and Comprise a Substantial Proportion of Obesity-Associated Increases in CD11c<sup>+</sup> Cells in Adipose Tissue and Liver. *Diabetes* **61**, 2330–2339 (2012).
198. Bertola, A. *et al.* Identification of Adipose Tissue Dendritic Cells Correlated With Obesity-Associated Insulin-Resistance and Inducing Th17 Responses in Mice and Patients. *Diabetes* **61**, 2238–2247 (2012).
199. Cho, K. W. *et al.* Adipose Tissue Dendritic Cells Are Independent Contributors to Obesity-Induced Inflammation and Insulin Resistance. *J. Immunol.* **197**, 3650–3661 (2016).
200. Ghosh, A. R. *et al.* Adipose Recruitment and Activation of Plasmacytoid Dendritic Cells Fuel Metaflammation. *Diabetes* **65**, 3440–3452 (2016).
201. Hannibal, T. D. *et al.* Deficiency in plasmacytoid dendritic cells and type I interferon signalling prevents diet-induced obesity and insulin resistance in mice. *Diabetologia* **60**, 2033–2041 (2017).

202. Mayadas, T. N., Cullere, X. & Lowell, C. A. The Multifaceted Functions of Neutrophils. *Annu. Rev. Pathol. Mech. Dis.* **9**, 181–218 (2014).
203. Pillay, J. *et al.* In vivo labeling with <sup>2</sup>H<sub>2</sub>O reveals a human neutrophil lifespan of 5.4 days. *Blood* **116**, 625–627 (2010).
204. Hidalgo, A., Chilvers, E. R., Summers, C. & Koenderman, L. The Neutrophil Life Cycle. *Trends Immunol.* **40**, 584–597 (2019).
205. Martin, C. *et al.* Chemokines Acting via CXCR2 and CXCR4 Control the Release of Neutrophils from the Bone Marrow and Their Return following Senescence. *Immunity* **19**, 583–593 (2003).
206. Evrard, M. *et al.* Developmental Analysis of Bone Marrow Neutrophils Reveals Populations Specialized in Expansion, Trafficking, and Effector Functions. *Immunity* **48**, 364-379.e8 (2018).
207. Eash, K. J., Greenbaum, A. M., Gopalan, P. K. & Link, D. C. CXCR2 and CXCR4 antagonistically regulate neutrophil trafficking from murine bone marrow. *J. Clin. Invest.* **120**, 2423–2431 (2010).
208. Teng, T.-S., Ji, A., Ji, X.-Y. & Li, Y.-Z. Neutrophils and Immunity: From Bactericidal Action to Being Conquered. *J. Immunol. Res.* **2017**, 1–14 (2017).
209. Yin, C. & Heit, B. Armed for destruction: formation, function and trafficking of neutrophil granules. *Cell Tissue Res.* **371**, 455–471 (2018).
210. Papayannopoulos, V. Neutrophil extracellular traps in immunity and disease. *Nat. Rev. Immunol.* **18**, 134–147 (2018).
211. Elgazar-Carmon, V., Rudich, A., Hadad, N. & Levy, R. Neutrophils transiently infiltrate intra-abdominal fat early in the course of high-fat feeding. *J. Lipid Res.* **49**, 1894–1903 (2008).

212. Hadad, N. *et al.* Induction of Cytosolic Phospholipase A2 $\alpha$  Is Required for Adipose Neutrophil Infiltration and Hepatic Insulin Resistance Early in the Course of High-Fat Feeding. *Diabetes* **62**, 3053–3063 (2013).
213. Talukdar, S. *et al.* Neutrophils mediate insulin resistance in mice fed a high-fat diet through secreted elastase. *Nat. Med.* **18**, 1407–1412 (2012).
214. Wang, Q. *et al.* Myeloperoxidase Deletion Prevents High-Fat Diet–Induced Obesity and Insulin Resistance. *Diabetes* **63**, 4172–4185 (2014).
215. Kawanishi, N., Niihara, H., Mizokami, T., Yada, K. & Suzuki, K. Exercise training attenuates neutrophil infiltration and elastase expression in adipose tissue of high-fat-diet-induced obese mice. *Physiol. Rep.* **3**, e12534 (2015).
216. Braster, Q. *et al.* Inhibition of NET Release Fails to Reduce Adipose Tissue Inflammation in Mice. *PLOS ONE* **11**, e0163922 (2016).
217. Revelo, X. S. *et al.* Nucleic Acid-Targeting Pathways Promote Inflammation in Obesity-Related Insulin Resistance. *Cell Rep.* **16**, 717–730 (2016).
218. Nijhuis, J. *et al.* Neutrophil Activation in Morbid Obesity, Chronic Activation of Acute Inflammation. *Obesity* **17**, 2014–2018 (2009).
219. Brotfain, E. *et al.* Neutrophil functions in morbidly obese subjects. *Clin. Exp. Immunol.* **181**, 156–163 (2015).
220. Hagman, D. K. *et al.* The short-term and long-term effects of bariatric/metabolic surgery on subcutaneous adipose tissue inflammation in humans. *Metabolism* **70**, 12–22 (2017).
221. D’Abbondanza, M. *et al.* Increased plasmatic NETs by-products in patients in severe obesity. *Sci. Rep.* **9**, 14678 (2019).
222. Liu, J. *et al.* Genetic deficiency and pharmacological stabilization of mast cells reduce diet-induced obesity and diabetes in mice. *Nat. Med.* **15**, 940–945 (2009).

223. Tanaka, A., Nomura, Y., Matsuda, A., Ohmori, K. & Matsuda, H. Mast cells function as an alternative modulator of adipogenesis through 15-deoxy-delta-12, 14-prostaglandin J<sub>2</sub>. *Am. J. Physiol.-Cell Physiol.* **301**, C1360–C1367 (2011).
224. Ishijima, Y., Ohmori, S. & Ohneda, K. Mast cell deficiency results in the accumulation of preadipocytes in adipose tissue in both obese and non-obese mice. *FEBS Open Bio* **4**, 18–24 (2014).
225. Hirai, S. *et al.* Involvement of mast cells in adipose tissue fibrosis. *Am. J. Physiol.-Endocrinol. Metab.* **306**, E247–E255 (2014).
226. Kumar, D. *et al.* Temporal immunometabolic profiling of adipose tissue in HFD-induced obesity: manifestations of mast cells in fibrosis and senescence. *Int. J. Obes.* **43**, 1281–1294 (2019).
227. Gutierrez, D. A., Muralidhar, S., Feyerabend, T. B., Herzig, S. & Rodewald, H.-R. Hematopoietic Kit Deficiency, rather than Lack of Mast Cells, Protects Mice from Obesity and Insulin Resistance. *Cell Metab.* **21**, 678–691 (2015).
228. Zhou, Y. *et al.* Leptin Deficiency Shifts Mast Cells toward Anti-Inflammatory Actions and Protects Mice from Obesity and Diabetes by Polarizing M2 Macrophages. *Cell Metab.* **22**, 1045–1058 (2015).
229. Vosshenrich, C. A. & Di Santo, J. P. Developmental programming of natural killer and innate lymphoid cells. *Curr. Opin. Immunol.* **25**, 130–138 (2013).
230. Boulenouar, S. *et al.* Adipose Type One Innate Lymphoid Cells Regulate Macrophage Homeostasis through Targeted Cytotoxicity. *Immunity* **46**, 273–286 (2017).
231. O’Sullivan, T. E. *et al.* Adipose-Resident Group 1 Innate Lymphoid Cells Promote Obesity-Associated Insulin Resistance. *Immunity* **45**, 428–441 (2016).
232. O’Rourke, R. W. *et al.* Systemic NK cell ablation attenuates intra-abdominal adipose tissue macrophage infiltration in murine obesity. *Obesity* **22**, 2109–2114 (2014).

233. Wensveen, F. M. *et al.* NK cells link obesity-induced adipose stress to inflammation and insulin resistance. *Nat. Immunol.* **16**, 376–385 (2015).
234. Theurich, S. *et al.* IL-6/Stat3-Dependent Induction of a Distinct, Obesity-Associated NK Cell Subpopulation Deteriorates Energy and Glucose Homeostasis. *Cell Metab.* **26**, 171-184.e6 (2017).
235. Mantell, B. S. *et al.* Mice Lacking NKT Cells but with a Complete Complement of CD8<sup>+</sup> T-Cells Are Not Protected against the Metabolic Abnormalities of Diet-Induced Obesity. *PLoS ONE* **6**, e19831 (2011).
236. Kotas, M. E. *et al.* Impact of CD1d Deficiency on Metabolism. *PLoS ONE* **6**, e25478 (2011).
237. Schipper, H. S. *et al.* Natural killer T cells in adipose tissue prevent insulin resistance. (2012) doi:10.1172/JCI62739.
238. Ji, Y. *et al.* Activation of Natural Killer T Cells Promotes M2 Macrophage Polarization in Adipose Tissue and Improves Systemic Glucose Tolerance via Interleukin-4 (IL-4)/STAT6 Protein Signaling Axis in Obesity. *J. Biol. Chem.* **287**, 13561–13571 (2012).
239. Wu, H. *et al.* T-Cell Accumulation and Regulated on Activation, Normal T Cell Expressed and Secreted Upregulation in Adipose Tissue in Obesity. *Circulation* **115**, 1029–1038 (2007).
240. Rocha, V. Z. *et al.* Interferon- $\gamma$ , a Th1 Cytokine, Regulates Fat Inflammation: A Role for Adaptive Immunity in Obesity. *Circ. Res.* **103**, 467–476 (2008).
241. McGillicuddy, F. C. *et al.* Interferon  $\gamma$  Attenuates Insulin Signaling, Lipid Storage, and Differentiation in Human Adipocytes via Activation of the JAK/STAT Pathway. *J. Biol. Chem.* **284**, 31936–31944 (2009).
242. Boldrini, V. de O., Farias, A. dos S. & Degasperri, G. R. Deciphering targets of Th17 cells fate: From metabolism to nuclear receptors. *Scand. J. Immunol.* **90**, e12793 (2019).

243. Winer, S. *et al.* Obesity predisposes to Th17 bias. *Eur. J. Immunol.* **39**, 2629–2635 (2009).
244. Shin, J. H., Shin, D. W. & Noh, M. Interleukin-17A inhibits adipocyte differentiation in human mesenchymal stem cells and regulates pro-inflammatory responses in adipocytes. *Biochem. Pharmacol.* **77**, 1835–1844 (2009).
245. Zúñiga, L. A. *et al.* IL-17 Regulates Adipogenesis, Glucose Homeostasis, and Obesity. *J. Immunol.* **185**, 6947–6959 (2010).
246. Nishimura, S. *et al.* CD8<sup>+</sup> effector T cells contribute to macrophage recruitment and adipose tissue inflammation in obesity. *Nat. Med.* **15**, 914–920 (2009).
247. Jiang, E. *et al.* Essential Role of CD11a in CD8<sup>+</sup> T-Cell Accumulation and Activation in Adipose Tissue. *Arterioscler. Thromb. Vasc. Biol.* **34**, 34–43 (2014).
248. Winer, D. A. *et al.* B cells promote insulin resistance through modulation of T cells and production of pathogenic IgG antibodies. *Nat. Med.* **17**, 610–617 (2011).
249. DeFuria, J. *et al.* B cells promote inflammation in obesity and type 2 diabetes through regulation of T-cell function and an inflammatory cytokine profile. *Proc. Natl. Acad. Sci.* **110**, 5133–5138 (2013).
250. Kim, D.-H. & Do, M.-S. BAFF knockout improves systemic inflammation via regulating adipose tissue distribution in high-fat diet-induced obesity. *Exp. Mol. Med.* **47**, e129–e129 (2015).
251. Ying, W. *et al.* Adipose tissue B2 cells promote insulin resistance through leukotriene LTB4/LTB4R1 signaling. (2017) doi:10.1172/JCI90350.
252. Tanigaki, K. *et al.* Hyposialylated IgG activates endothelial IgG receptor FcγRIIB to promote obesity-induced insulin resistance. *J. Clin. Invest.* **128**, 309–322 (2018).
253. Frasca, D. *et al.* Identification and Characterization of Adipose Tissue-Derived Human Antibodies With “Anti-self” Specificity. *Front. Immunol.* **11**, (2020).

254. Chalasani, N. *et al.* The diagnosis and management of nonalcoholic fatty liver disease: Practice guidance from the American Association for the Study of Liver Diseases. *Hepatology* **67**, 328–357 (2018).
255. Wong, V. W.-S., Adams, L. A., de Lédinghen, V., Wong, G. L.-H. & Sookoian, S. Noninvasive biomarkers in NAFLD and NASH — current progress and future promise. *Nat. Rev. Gastroenterol. Hepatol.* **15**, 461–478 (2018).
256. Anstee, Q. M., Reeves, H. L., Kotsiliti, E., Govaere, O. & Heikenwalder, M. From NASH to HCC: current concepts and future challenges. *Nat. Rev. Gastroenterol. Hepatol.* **16**, 411–428 (2019).
257. Sanyal, A. J. Past, present and future perspectives in nonalcoholic fatty liver disease. *Nat. Rev. Gastroenterol. Hepatol.* **16**, 377–386 (2019).
258. Szanto, K. B., Li, J., Cordero, P. & Oben, J. A. Ethnic differences and heterogeneity in genetic and metabolic makeup contributing to nonalcoholic fatty liver disease. *Diabetes Metab. Syndr. Obes. Targets Ther.* **12**, 357–367 (2019).
259. Younossi, Z. *et al.* Global burden of NAFLD and NASH: trends, predictions, risk factors and prevention. *Nat. Rev. Gastroenterol. Hepatol.* **15**, 11–20 (2018).
260. Glatz, J. F. C., Luiken, J. J. F. P. & Bonen, A. Membrane Fatty Acid Transporters as Regulators of Lipid Metabolism: Implications for Metabolic Disease. *Physiol. Rev.* **90**, 367–417 (2010).
261. Alves-Bezerra, M. & Cohen, D. E. Triglyceride Metabolism in the Liver. *Compr. Physiol.* **8**, 1–22 (2017).
262. Vanni, E., Marengo, A., Mezzabotta, L. & Bugianesi, E. Systemic Complications of Nonalcoholic Fatty Liver Disease: When the Liver Is Not an Innocent Bystander. *Semin. Liver Dis.* **35**, 236–249 (2015).

263. Lambert, J. E., Ramos–Roman, M. A., Browning, J. D. & Parks, E. J. Increased De Novo Lipogenesis Is a Distinct Characteristic of Individuals With Nonalcoholic Fatty Liver Disease. *Gastroenterology* **146**, 726–735 (2014).
264. Wang, Y., Viscarra, J., Kim, S.-J. & Sul, H. S. Transcriptional regulation of hepatic lipogenesis. *Nat. Rev. Mol. Cell Biol.* **16**, 678–689 (2015).
265. Donnelly, K. L. *et al.* Sources of fatty acids stored in liver and secreted via lipoproteins in patients with nonalcoholic fatty liver disease. *J. Clin. Invest.* **115**, 1343–1351 (2005).
266. Roumans, K. H. M. *et al.* Hepatic saturated fatty acid fraction is associated with de novo lipogenesis and hepatic insulin resistance. *Nat. Commun.* **11**, 1891 (2020).
267. Saggerson, D. Malonyl-CoA, a Key Signaling Molecule in Mammalian Cells. *Annu. Rev. Nutr.* **28**, 253–272 (2008).
268. Park, E. C. *et al.* Inhibition of CYP4A Reduces Hepatic Endoplasmic Reticulum Stress and Features of Diabetes in Mice. *Gastroenterology* **147**, 860–869 (2014).
269. ND, A. M. Non-Alcoholic Fatty Liver Disease, an Overview. *Integr. Med. Clin. J.* **18**, 42–49 (2019).
270. Mota, M., Banini, B. A., Cazanave, S. C. & Sanyal, A. J. Molecular mechanisms of lipotoxicity and glucotoxicity in nonalcoholic fatty liver disease. *Metabolism* **65**, 1049–1061 (2016).
271. Polyzos, S. A., Kountouras, J. & Mantzoros, C. S. Obesity and nonalcoholic fatty liver disease: From pathophysiology to therapeutics. *Metabolism* **92**, 82–97 (2019).
272. Kim, D. & Kim, W. R. Nonobese Fatty Liver Disease. *Clin. Gastroenterol. Hepatol.* **15**, 474–485 (2017).
273. Albhaisi, S., Chowdhury, A. & Sanyal, A. J. Non-alcoholic fatty liver disease in lean individuals. *JHEP Rep.* **1**, 329–341 (2019).
274. Romeo, S. *et al.* Genetic variation in PNPLA3 confers susceptibility to nonalcoholic fatty liver disease. *Nat. Genet.* **40**, 1461–1465 (2008).

275. Sookoian, S. & Pirola, C. J. Meta-analysis of the influence of I148M variant of patatin-like phospholipase domain containing 3 gene (PNPLA3) on the susceptibility and histological severity of nonalcoholic fatty liver disease. *Hepatology* **53**, 1883–1894 (2011).
276. Liu, Y.-L. *et al.* Carriage of the PNPLA3 rs738409 C >G polymorphism confers an increased risk of non-alcoholic fatty liver disease associated hepatocellular carcinoma. *J. Hepatol.* **61**, 75–81 (2014).
277. Singal, A. G. *et al.* The Effect of PNPLA3 on Fibrosis Progression and Development of Hepatocellular Carcinoma: A Meta-analysis. *Am. J. Gastroenterol.* **109**, 325–334 (2014).
278. Speliotes, E. K., Butler, J. L., Palmer, C. D., Voight, B. F. & Hirschhorn, J. N. PNPLA3 variants specifically confer increased risk for histologic nonalcoholic fatty liver disease but not metabolic disease. *Hepatology* **52**, 904–912 (2010).
279. Wei, J. *et al.* Prevalence and Severity of Nonalcoholic Fatty Liver Disease in Non-Obese Patients: A Population Study Using Proton-Magnetic Resonance Spectroscopy. *Am. J. Gastroenterol.* **110**, 1306–1314 (2015).
280. Adams, L. A. *et al.* Cholesteryl ester transfer protein gene polymorphisms increase the risk of fatty liver in females independent of adiposity. *J. Gastroenterol. Hepatol.* **27**, 1520–1527 (2012).
281. Musso, G., Cassader, M., Bo, S., Michieli, F. D. & Gambino, R. Sterol Regulatory Element-Binding Factor 2 (SREBF-2) Predicts 7-Year NAFLD Incidence and Severity of Liver Disease and Lipoprotein and Glucose Dysmetabolism. *Diabetes* **62**, 1109–1120 (2013).
282. Dongiovanni, P. *et al.* Transmembrane 6 superfamily member 2 gene variant disentangles nonalcoholic steatohepatitis from cardiovascular disease. *Hepatology* **61**, 506–514 (2015).

283. Musso, G. *et al.* Dietary habits and their relations to insulin resistance and postprandial lipemia in nonalcoholic steatohepatitis. *Hepatology* **37**, 909–916 (2003).
284. Yasutake, K. *et al.* Nutritional investigation of non-obese patients with non-alcoholic fatty liver disease: The significance of dietary cholesterol. *Scand. J. Gastroenterol.* **44**, 471–477 (2009).
285. Matsuzawa, N. *et al.* Lipid-induced oxidative stress causes steatohepatitis in mice fed an atherogenic diet. *Hepatology* **46**, 1392–1403 (2007).
286. Wouters, K. *et al.* Dietary cholesterol, rather than liver steatosis, leads to hepatic inflammation in hyperlipidemic mouse models of nonalcoholic steatohepatitis. *Hepatology* **48**, 474–486 (2008).
287. McCarthy, E. M. & Rinella, M. E. The Role of Diet and Nutrient Composition in Nonalcoholic Fatty Liver Disease. *J. Acad. Nutr. Diet.* **112**, 401–409 (2012).
288. Chung, M. *et al.* Fructose, high-fructose corn syrup, sucrose, and nonalcoholic fatty liver disease or indexes of liver health: a systematic review and meta-analysis. *Am. J. Clin. Nutr.* **100**, 833–849 (2014).
289. Ipsen, D. H., Tveden-Nyborg, P. & Lykkesfeldt, J. Normal weight dyslipidemia: Is it all about the liver? *Obesity* **24**, 556–567 (2016).
290. Katsuki, A. *et al.* Increased Visceral Fat and Serum Levels of Triglyceride Are Associated With Insulin Resistance in Japanese Metabolically Obese, Normal Weight Subjects With Normal Glucose Tolerance. *Diabetes Care* **26**, 2341–2344 (2003).
291. Park, B. J. *et al.* Visceral adipose tissue area is an independent risk factor for hepatic steatosis. *J. Gastroenterol. Hepatol.* **23**, 900–907 (2008).
292. Sinn, D. H. *et al.* Lean non-alcoholic fatty liver disease and development of diabetes: a cohort study. *Eur. J. Endocrinol.* **181**, 185–192 (2019).

293. Mak, L.-Y. *et al.* Global Epidemiology, Prevention, and Management of Hepatocellular Carcinoma. *Am. Soc. Clin. Oncol. Educ. Book* 262–279 (2018)  
doi:10.1200/EDBK\_200939.
294. Coronel-Castillo, C. E., Qi, X., Contreras-Carmona, J., Ramírez-Pérez, O. L. & Méndez-Sánchez, N. Nonalcoholic fatty liver disease and nonalcoholic steatohepatitis in HIV infection: a metabolic approach of an infectious disease. *Expert Rev. Gastroenterol. Hepatol.* **13**, 531–540 (2019).
295. Bessone, F., Dirchwolf, M., Rodil, M. A., Razori, M. V. & Roma, M. G. Review article: drug-induced liver injury in the context of nonalcoholic fatty liver disease – a physiopathological and clinical integrated view. *Aliment. Pharmacol. Ther.* **48**, 892–913 (2018).
296. Canfora, E. E., Meex, R. C. R., Venema, K. & Blaak, E. E. Gut microbial metabolites in obesity, NAFLD and T2DM. *Nat. Rev. Endocrinol.* **15**, 261–273 (2019).
297. Wigg, A. J. The role of small intestinal bacterial overgrowth, intestinal permeability, endotoxaemia, and tumour necrosis factor alpha in the pathogenesis of non-alcoholic steatohepatitis. *Gut* **48**, 206–211 (2001).
298. Miele, L. *et al.* Increased intestinal permeability and tight junction alterations in nonalcoholic fatty liver disease. *Hepatology* **49**, 1877–1887 (2009).
299. Le Roy, T. *et al.* Intestinal microbiota determines development of non-alcoholic fatty liver disease in mice. *Gut* **62**, 1787–1794 (2013).
300. Mouries, J. *et al.* Microbiota-driven gut vascular barrier disruption is a prerequisite for non-alcoholic steatohepatitis development. *J. Hepatol.* **71**, 1216–1228 (2019).
301. Ye, J.-Z. *et al.* Dynamic alterations in the gut microbiota and metabolome during the development of methionine-choline-deficient diet-induced nonalcoholic steatohepatitis. *World J. Gastroenterol.* **24**, 2468–2481 (2018).

302. Schneider, K. M. *et al.* Intestinal Microbiota Protects against MCD Diet-Induced Steatohepatitis. *Int. J. Mol. Sci.* **20**, 308 (2019).
303. Duarte, S. M. B. *et al.* Gut microbiome composition in lean patients with NASH is associated with liver damage independent of caloric intake: A prospective pilot study. *Nutr. Metab. Cardiovasc. Dis.* **28**, 369–384 (2018).
304. Yuan, J. *et al.* Fatty Liver Disease Caused by High-Alcohol-Producing *Klebsiella pneumoniae*. *Cell Metab.* **30**, 675-688.e7 (2019).
305. Arab, J. P., Arrese, M. & Trauner, M. Recent Insights into the Pathogenesis of Nonalcoholic Fatty Liver Disease. *Annu. Rev. Pathol. Mech. Dis.* **13**, 321–350 (2018).
306. Jenne, C. N. & Kubes, P. Immune surveillance by the liver. *Nat. Immunol.* **14**, 996–1006 (2013).
307. Iqbal, A. Liver immunology and Cross-talk. *Trop. Gastroenterol.* **37**, (2016).
308. Freitas-Lopes, M. A., Mafra, K., David, B. A., Carvalho-Gontijo, R. & Menezes, G. B. Differential Location and Distribution of Hepatic Immune Cells. *Cells* **6**, 48 (2017).
309. Oda, M., Yokomori, H. & Han, J.-Y. Regulatory mechanisms of hepatic microcirculation. *Clin. Hemorheol. Microcirc.* **29**, 167–182 (2003).
310. Svistounov, D. *et al.* The Relationship between Fenestrations, Sieve Plates and Rafts in Liver Sinusoidal Endothelial Cells. *PLoS ONE* **7**, (2012).
311. Häussinger, D. & Kordes, C. Space of Disse: a stem cell niche in the liver. *Biol. Chem.* **401**, 81–95 (2019).
312. Warren, A. *et al.* T lymphocytes interact with hepatocytes through fenestrations in murine liver sinusoidal endothelial cells. *Hepatology* **44**, 1182–1190 (2006).
313. Cai, J., Zhang, X.-J. & Li, H. The Role of Innate Immune Cells in Nonalcoholic Steatohepatitis. *Hepatol. Baltim. Md* **70**, 1026–1037 (2019).
314. Krenkel, O. & Tacke, F. Liver macrophages in tissue homeostasis and disease. *Nat. Rev. Immunol.* **17**, 306–321 (2017).

315. Varol, C., Mildner, A. & Jung, S. Macrophages: development and tissue specialization. *Annu. Rev. Immunol.* **33**, 643–675 (2015).
316. Kieusseian, A., Brunet de la Grange, P., Burlen-Defranoux, O., Godin, I. & Cumano, A. Immature hematopoietic stem cells undergo maturation in the fetal liver. *Dev. Camb. Engl.* **139**, 3521–3530 (2012).
317. Cheng, H., Zheng, Z. & Cheng, T. New paradigms on hematopoietic stem cell differentiation. *Protein Cell* **11**, 34–44 (2020).
318. Yona, S. *et al.* Fate Mapping Reveals Origins and Dynamics of Monocytes and Tissue Macrophages under Homeostasis. *Immunity* **38**, 79–91 (2013).
319. Scott, C. L. *et al.* Bone marrow-derived monocytes give rise to self-renewing and fully differentiated Kupffer cells. *Nat. Commun.* **7**, 10321 (2016).
320. Sakai, M. *et al.* Liver-Derived Signals Sequentially Reprogram Myeloid Enhancers to Initiate and Maintain Kupffer Cell Identity. *Immunity* **51**, 655–670.e8 (2019).
321. Ju, C. & Tacke, F. Hepatic macrophages in homeostasis and liver diseases: from pathogenesis to novel therapeutic strategies. *Cell. Mol. Immunol.* **13**, 316–327 (2016).
322. David, B. A. *et al.* Combination of Mass Cytometry and Imaging Analysis Reveals Origin, Location, and Functional Repopulation of Liver Myeloid Cells in Mice. *Gastroenterology* **151**, 1176–1191 (2016).
323. Heymann, F. & Tacke, F. Immunology in the liver — from homeostasis to disease. *Nat. Rev. Gastroenterol. Hepatol.* **13**, 88–110 (2016).
324. Breous, E., Somanathan, S., Vandenberghe, L. H. & Wilson, J. M. Hepatic regulatory T cells and Kupffer cells are crucial mediators of systemic T cell tolerance to antigens targeting murine liver. *Hepatol. Baltim. Md* **50**, 612–621 (2009).
325. Thomson, A. W. & Knolle, P. A. Antigen-presenting cell function in the tolerogenic liver environment. *Nat. Rev. Immunol.* **10**, 753–766 (2010).

326. Kristiansen, M. *et al.* Identification of the haemoglobin scavenger receptor. *Nature* **409**, 198–201 (2001).
327. Willekens, F. L. A. *et al.* Liver Kupffer cells rapidly remove red blood cell–derived vesicles from the circulation by scavenger receptors. *Blood* **105**, 2141–2145 (2005).
328. Wrighting, D. M. & Andrews, N. C. Interleukin-6 induces hepcidin expression through STAT3. *Blood* **108**, 3204–3209 (2006).
329. Theurl, M. *et al.* Kupffer cells modulate iron homeostasis in mice via regulation of hepcidin expression. *J. Mol. Med.* **86**, 825 (2008).
330. Wang, Y. *et al.* Plasma cholesteryl ester transfer protein is predominantly derived from Kupffer cells. *Hepatology. Baltim. Md* **62**, 1710–1722 (2015).
331. Theurl, I. *et al.* On-demand erythrocyte disposal and iron recycling requires transient macrophages in the liver. *Nat. Med.* **22**, 945–951 (2016).
332. Dou, L., Ono, Y., Chen, Y., Thomson, A. & Chen, X. Hepatic Dendritic Cells, the Tolerogenic Liver Environment, and Liver Disease. *Semin. Liver Dis.* **38**, 170–180 (2018).
333. Chen, Y. *et al.* Distinct response of liver myeloid dendritic cells to endotoxin is mediated by IL-27. *J. Hepatol.* **51**, 510–519 (2009).
334. Peng, H., Wisse, E. & Tian, Z. Liver natural killer cells: subsets and roles in liver immunity. *Cell. Mol. Immunol.* **13**, 328–336 (2016).
335. Liver-resident NK cells confer adaptive immunity in skin-contact inflammation - PubMed.
336. Daussy, C. *et al.* T-bet and Eomes instruct the development of two distinct natural killer cell lineages in the liver and in the bone marrow. *J. Exp. Med.* **211**, 563–577 (2014).
337. Zhang, L. H., Shin, J. H., Haggadone, M. D. & Sunwoo, J. B. The aryl hydrocarbon receptor is required for the maintenance of liver-resident natural killer cells. *J. Exp. Med.* **213**, 2249–2257 (2016).

338. Mackay, L. K. *et al.* Hobit and Blimp1 instruct a universal transcriptional program of tissue residency in lymphocytes. *Science* **352**, 459–463 (2016).
339. Sojka, D. K. *et al.* Tissue-resident natural killer (NK) cells are cell lineages distinct from thymic and conventional splenic NK cells. *eLife* **3**, e01659 (2014).
340. Marquardt, N. *et al.* Cutting edge: identification and characterization of human intrahepatic CD49a<sup>+</sup> NK cells. *J. Immunol. Baltim. Md 1950* **194**, 2467–2471 (2015).
341. Radaeva, S. *et al.* Natural killer cells ameliorate liver fibrosis by killing activated stellate cells in NKG2D-dependent and tumor necrosis factor-related apoptosis-inducing ligand-dependent manners. *Gastroenterology* **130**, 435–452 (2006).
342. Gur, C. *et al.* NKp46-mediated killing of human and mouse hepatic stellate cells attenuates liver fibrosis. *Gut* **61**, 885–893 (2012).
343. Wang, Y. & Zhang, C. The Roles of Liver-Resident Lymphocytes in Liver Diseases. *Front. Immunol.* **10**, 1582 (2019).
344. Li, F. *et al.* The microbiota maintain homeostasis of liver-resident  $\gamma\delta$ T-17 cells in a lipid antigen/CD1d-dependent manner. *Nat. Commun.* **8**, 13839 (2017).
345. Crosby, C. M. & Kronenberg, M. Tissue-specific functions of invariant natural killer T cells. *Nat. Rev. Immunol.* **18**, 559–574 (2018).
346. Monticelli, L. A. *et al.* Transcriptional regulator Id2 controls survival of hepatic NKT cells. *Proc. Natl. Acad. Sci. U. S. A.* **106**, 19461–19466 (2009).
347. Germanov, E. *et al.* Critical role for the chemokine receptor CXCR6 in homeostasis and activation of CD1d-restricted NKT cells. *J. Immunol. Baltim. Md 1950* **181**, 81–91 (2008).
348. Geissmann, F. *et al.* Intravascular immune surveillance by CXCR6<sup>+</sup> NKT cells patrolling liver sinusoids. *PLoS Biol.* **3**, e113 (2005).
349. Treiner, E. *et al.* Selection of evolutionarily conserved mucosal-associated invariant T cells by MR1. *Nature* **422**, 164–169 (2003).

350. Kurioka, A., Walker, L. J., Klenerman, P. & Willberg, C. B. MAIT cells: new guardians of the liver. *Clin. Transl. Immunol.* **5**, e98 (2016).
351. Huang, W. *et al.* The Role of CD1d and MR1 Restricted T Cells in the Liver. *Front. Immunol.* **9**, (2018).
352. Downey, A. M., Kapłonek, P. & Seeberger, P. H. MAIT cells as attractive vaccine targets. *FEBS Lett.* **593**, 1627–1640 (2019).
353. Legoux, F. *et al.* Microbial metabolites control the thymic development of mucosal-associated invariant T cells. *Science* (2019) doi:10.1126/science.aaw2719.
354. van Wilgenburg, B. *et al.* MAIT cells are activated during human viral infections. *Nat. Commun.* **7**, 11653 (2016).
355. Slichter, C. K. *et al.* Distinct activation thresholds of human conventional and innate-like memory T cells. *JCI Insight* **1**, (2016).
356. Yong, Y. K. *et al.* Hyper-Expression of PD-1 Is Associated with the Levels of Exhausted and Dysfunctional Phenotypes of Circulating CD161<sup>++</sup>TCR iV $\alpha$ 7.2<sup>+</sup> Mucosal-Associated Invariant T Cells in Chronic Hepatitis B Virus Infection. *Front. Immunol.* **9**, 472 (2018).
357. Mehal, W. Z., Azzaroli, F. & Crispe, I. N. Immunology of the healthy liver: Old questions and new insights. *Gastroenterology* **120**, 250–260 (2001).
358. Zhang, H., Jiang, Z. & Zhang, L. Dual effect of T helper cell 17 (Th17) and regulatory T cell (Treg) in liver pathological process: From occurrence to end stage of disease. *Int. Immunopharmacol.* **69**, 50–59 (2019).
359. Li, M. *et al.* A wave of Foxp3 + regulatory T cell accumulation in the neonatal liver plays unique roles in maintaining self-tolerance. *Cell. Mol. Immunol.* **17**, 507–518 (2020).
360. Wawman, R. E., Bartlett, H. & Oo, Y. H. Regulatory T Cell Metabolism in the Hepatic Microenvironment. *Front. Immunol.* **8**, (2018).

361. Chen, Y.-Y. *et al.* Human intrahepatic regulatory T cells are functional, require IL-2 from effector cells for survival, and are susceptible to Fas ligand-mediated apoptosis. *Hepatology* **64**, 138–150 (2016).
362. Steinert, E. M. *et al.* Quantifying Memory CD8 T Cells Reveals Regionalization of Immunosurveillance. *Cell* **161**, 737–749 (2015).
363. Fernandez-Ruiz, D. *et al.* Liver-Resident Memory CD8<sup>+</sup> T Cells Form a Front-Line Defense against Malaria Liver-Stage Infection. *Immunity* **45**, 889–902 (2016).
364. Olsen, T. M., Stone, B. C., Chuenchob, V. & Murphy, S. C. Prime-and-Trap Malaria Vaccination To Generate Protective CD8<sup>+</sup> Liver-Resident Memory T Cells. *J. Immunol.* **201**, 1984–1993 (2018).
365. Holz, L. E. *et al.* CD8<sup>+</sup> T Cell Activation Leads to Constitutive Formation of Liver Tissue-Resident Memory T Cells that Seed a Large and Flexible Niche in the Liver. *Cell Rep.* **25**, 68-79.e4 (2018).
366. Feau, S., Arens, R., Togher, S. & Schoenberger, S. P. Autocrine IL-2 is required for secondary population expansion of CD8(+) memory T cells. *Nat. Immunol.* **12**, 908–913 (2011).
367. Pallett, L. J. *et al.* IL-2<sup>high</sup> tissue-resident T cells in the human liver: Sentinels for hepatotropic infection. *J. Exp. Med.* **214**, 1567–1580 (2017).
368. Sutti, S. & Albano, E. Adaptive immunity: an emerging player in the progression of NAFLD. *Nat. Rev. Gastroenterol. Hepatol.* **17**, 81–92 (2020).
369. Allman, D. & Pillai, S. Peripheral B cell subsets. *Curr. Opin. Immunol.* **20**, 149–157 (2008).
370. Tsiantoulas, D., Sage, A. P., Mallat, Z. & Binder, C. J. Targeting B cells in atherosclerosis: closing the gap from bench to bedside. *Arterioscler. Thromb. Vasc. Biol.* **35**, 296–302 (2015).

371. Cai, X., Zhang, L. & Wei, W. Regulatory B cells in inflammatory diseases and tumor. *Int. Immunopharmacol.* **67**, 281–286 (2019).
372. Huang, W. *et al.* Depletion of liver Kupffer cells prevents the development of diet-induced hepatic steatosis and insulin resistance. *Diabetes* **59**, 347–357 (2010).
373. Lanthier, N. *et al.* Kupffer cell depletion prevents but has no therapeutic effect on metabolic and inflammatory changes induced by a high-fat diet. *FASEB J. Off. Publ. Fed. Am. Soc. Exp. Biol.* **25**, 4301–4311 (2011).
374. Nati, M. *et al.* The role of immune cells in metabolism-related liver inflammation and development of non-alcoholic steatohepatitis (NASH). *Rev. Endocr. Metab. Disord.* **17**, 29–39 (2016).
375. Schuster, S., Cabrera, D., Arrese, M. & Feldstein, A. E. Triggering and resolution of inflammation in NASH. *Nat. Rev. Gastroenterol. Hepatol.* **15**, 349–364 (2018).
376. Kazankov, K. *et al.* The role of macrophages in nonalcoholic fatty liver disease and nonalcoholic steatohepatitis. *Nat. Rev. Gastroenterol. Hepatol.* **16**, 145–159 (2019).
377. Bieggs, V. *et al.* Role of scavenger receptor A and CD36 in diet-induced nonalcoholic steatohepatitis in hyperlipidemic mice. *Gastroenterology* **138**, 2477–2486, 2486.e1–3 (2010).
378. Bieggs, V. *et al.* Trapping of oxidized LDL in lysosomes of Kupffer cells is a trigger for hepatic inflammation. *Liver Int. Off. J. Int. Assoc. Study Liver* **33**, 1056–1061 (2013).
379. Stienstra, R. *et al.* Kupffer cells promote hepatic steatosis via interleukin-1beta-dependent suppression of peroxisome proliferator-activated receptor alpha activity. *Hepatol. Baltim. Md* **51**, 511–522 (2010).
380. Wan, J. *et al.* M2 Kupffer cells promote M1 Kupffer cell apoptosis: a protective mechanism against alcoholic and nonalcoholic fatty liver disease. *Hepatol. Baltim. Md* **59**, 130–142 (2014).

381. Deshmane, S. L., Kremlev, S., Amini, S. & Sawaya, B. E. Monocyte chemoattractant protein-1 (MCP-1): an overview. *J. Interferon Cytokine Res. Off. J. Int. Soc. Interferon Cytokine Res.* **29**, 313–326 (2009).
382. Baeck, C. *et al.* Pharmacological inhibition of the chemokine CCL2 (MCP-1) diminishes liver macrophage infiltration and steatohepatitis in chronic hepatic injury. *Gut* **61**, 416–426 (2012).
383. Zhang, X. *et al.* CXC chemokine receptor 3 promotes steatohepatitis in mice through mediating inflammatory cytokines, macrophages and autophagy. *J. Hepatol.* **64**, 160–170 (2016).
384. Seki, E. *et al.* CCR1 and CCR5 promote hepatic fibrosis in mice. *J. Clin. Invest.* **119**, 1858–1870 (2009).
385. Heymann, F. *et al.* Hepatic macrophage migration and differentiation critical for liver fibrosis is mediated by the chemokine receptor C-C motif chemokine receptor 8 in mice. *Hepatol. Baltim. Md* **55**, 898–909 (2012).
386. Idrissova, L. *et al.* TRAIL receptor deletion in mice suppresses the inflammation of nutrient excess. *J. Hepatol.* **62**, 1156–1163 (2015).
387. Miura, K., Yang, L., van Rooijen, N., Ohnishi, H. & Seki, E. Hepatic recruitment of macrophages promotes nonalcoholic steatohepatitis through CCR2. *Am. J. Physiol. Gastrointest. Liver Physiol.* **302**, G1310-1321 (2012).
388. Beattie, L. *et al.* Bone marrow-derived and resident liver macrophages display unique transcriptomic signatures but similar biological functions. *J. Hepatol.* **65**, 758–768 (2016).
389. Seidman, J. S. *et al.* Niche-Specific Reprogramming of Epigenetic Landscapes Drives Myeloid Cell Diversity in Nonalcoholic Steatohepatitis. *Immunity* **52**, 1057-1074.e7 (2020).

390. Tran, S. *et al.* Impaired Kupffer Cell Self-Renewal Alters the Liver Response to Lipid Overload during Non-alcoholic Steatohepatitis. *Immunity* **53**, 627-640.e5 (2020).
391. Remmerie, A. *et al.* Osteopontin Expression Identifies a Subset of Recruited Macrophages Distinct from Kupffer Cells in the Fatty Liver. *Immunity* **53**, 641-657.e14 (2020).
392. Segers, F. M. *et al.* Complement alternative pathway activation in human nonalcoholic steatohepatitis. *PloS One* **9**, e110053 (2014).
393. Seki, E. *et al.* TLR4 enhances TGF-beta signaling and hepatic fibrosis. *Nat. Med.* **13**, 1324–1332 (2007).
394. Feng, M. *et al.* Kupffer-derived matrix metalloproteinase-9 contributes to liver fibrosis resolution. *Int. J. Biol. Sci.* **14**, 1033–1040 (2018).
395. Pellicoro, A. *et al.* Elastin accumulation is regulated at the level of degradation by macrophage metalloelastase (MMP-12) during experimental liver fibrosis. *Hepatology. Baltim. Md* **55**, 1965–1975 (2012).
396. Fallowfield, J. A. *et al.* Scar-associated macrophages are a major source of hepatic matrix metalloproteinase-13 and facilitate the resolution of murine hepatic fibrosis. *J. Immunol. Baltim. Md 1950* **178**, 5288–5295 (2007).
397. Karlmark, K. R. *et al.* Hepatic recruitment of the inflammatory Gr1+ monocyte subset upon liver injury promotes hepatic fibrosis. *Hepatology. Baltim. Md* **50**, 261–274 (2009).
398. Wang, X. *et al.* STING expression in monocyte-derived macrophages is associated with the progression of liver inflammation and fibrosis in patients with nonalcoholic fatty liver disease. *Lab. Invest.* **100**, 542–552 (2020).
399. Ramachandran, P. *et al.* Differential Ly-6C expression identifies the recruited macrophage phenotype, which orchestrates the regression of murine liver fibrosis. *Proc. Natl. Acad. Sci. U. S. A.* **109**, E3186-3195 (2012).

400. Duffield, J. S. *et al.* Selective depletion of macrophages reveals distinct, opposing roles during liver injury and repair. *J. Clin. Invest.* **115**, 56–65 (2005).
401. Henning, J. R. *et al.* Dendritic cells limit fibroinflammatory injury in nonalcoholic steatohepatitis in mice. *Hepatology* **58**, 589–602 (2013).
402. Sutti, S. *et al.* CX3CR1-expressing inflammatory dendritic cells contribute to the progression of steatohepatitis. *Clin. Sci. Lond. Engl. 1979* **129**, 797–808 (2015).
403. Ibrahim, J. *et al.* Dendritic cell populations with different concentrations of lipid regulate tolerance and immunity in mouse and human liver. *Gastroenterology* **143**, 1061–1072 (2012).
404. Heier, E.-C. *et al.* Murine CD103<sup>+</sup> dendritic cells protect against steatosis progression towards steatohepatitis. *J. Hepatology* **66**, 1241–1250 (2017).
405. Aarts, S. *et al.* Depletion of CD40 on CD11c<sup>+</sup> cells worsens the metabolic syndrome and ameliorates hepatic inflammation during NASH. *Sci. Rep.* **9**, 14702 (2019).
406. Connolly, M. K. *et al.* In liver fibrosis, dendritic cells govern hepatic inflammation in mice via TNF- $\alpha$ . *J. Clin. Invest.* **119**, 3213–3225 (2009).
407. Jiao, J. *et al.* Dendritic cell regulation of carbon tetrachloride-induced murine liver fibrosis regression. *Hepatology* **55**, 244–255 (2012).
408. Mogilenko, D. A. *et al.* Metabolic and Innate Immune Cues Merge into a Specific Inflammatory Response via the UPR. *Cell* **177**, 1201-1216.e19 (2019).
409. Haas, J. T. *et al.* Transcriptional Network Analysis Implicates Altered Hepatic Immune Function in NASH development and resolution. *Nat. Metab.* **1**, 604–614 (2019).
410. Margraf, A., Ley, K. & Zarbock, A. Neutrophil Recruitment: From Model Systems to Tissue-Specific Patterns. *Trends Immunol.* **40**, 613–634 (2019).
411. Rensen, S. S. *et al.* Increased hepatic myeloperoxidase activity in obese subjects with nonalcoholic steatohepatitis. *Am. J. Pathol.* **175**, 1473–1482 (2009).

412. Rensen, S. S. *et al.* Neutrophil-derived myeloperoxidase aggravates non-alcoholic steatohepatitis in low-density lipoprotein receptor-deficient mice. *PLoS One* **7**, e52411 (2012).
413. Pulli, B. *et al.* Myeloperoxidase–Hepatocyte–Stellate Cell Cross Talk Promotes Hepatocyte Injury and Fibrosis in Experimental Nonalcoholic Steatohepatitis. *Antioxid. Redox Signal.* **23**, 1255–1269 (2015).
414. Ou, R. *et al.* Neutrophil depletion improves diet-induced non-alcoholic fatty liver disease in mice. *Endocrine* **57**, 72–82 (2017).
415. Huang, H. *et al.* Damage-associated molecular pattern-activated neutrophil extracellular trap exacerbates sterile inflammatory liver injury. *Hepatology* **62**, 600–614 (2015).
416. Li, H. *et al.* Hepatocytes and neutrophils cooperatively suppress bacterial infection by differentially regulating lipocalin-2 and neutrophil extracellular traps. *Hepatology* **68**, 1604–1620 (2018).
417. Tosello-Trampont, A.-C. *et al.* NKp46+ natural killer cells attenuate metabolism-induced hepatic fibrosis by regulating macrophage activation in mice. *Hepatology* **63**, 799–812 (2016).
418. Gomez-Santos, L. *et al.* Inhibition of natural killer cells protects the liver against acute injury in the absence of glycine N-methyltransferase. *Hepatology* **56**, 747–759 (2012).
419. Marçais, A. *et al.* Regulation of mouse NK cell development and function by cytokines. *Front. Immunol.* **4**, 450 (2013).
420. Marçais, A. *et al.* The metabolic checkpoint kinase mTOR is essential for IL-15 signaling during the development and activation of NK cells. *Nat. Immunol.* **15**, 749–757 (2014).

421. Chung, J. W. *et al.* Osteopontin promotes the development of natural killer cells from hematopoietic stem cells. *Stem Cells Dayt. Ohio* **26**, 2114–2123 (2008).
422. Leavenworth, J. W., Verbinnen, B., Wang, Q., Shen, E. & Cantor, H. Intracellular osteopontin regulates homeostasis and function of natural killer cells. *Proc. Natl. Acad. Sci. U. S. A.* **112**, 494–499 (2015).
423. Viel, S. *et al.* Alteration of Natural Killer cell phenotype and function in obese individuals. *Clin. Immunol. Orlando Fla* **177**, 12–17 (2017).
424. Michelet, X. *et al.* Metabolic reprogramming of natural killer cells in obesity limits antitumor responses. *Nat. Immunol.* **19**, 1330–1340 (2018).
425. Assmann, N. *et al.* Srebp-controlled glucose metabolism is essential for NK cell functional responses. *Nat. Immunol.* **18**, 1197–1206 (2017).
426. Syn, W.-K. *et al.* NKT-associated hedgehog and osteopontin drive fibrogenesis in non-alcoholic fatty liver disease. *Gut* **61**, 1323–1329 (2012).
427. Maricic, I. *et al.* Differential Activation of Hepatic Invariant NKT Cell Subsets Plays a Key Role in Progression of Nonalcoholic Steatohepatitis. *J. Immunol. Baltim. Md 1950* **201**, 3017–3035 (2018).
428. Wolf, M. J. *et al.* Metabolic activation of intrahepatic CD8<sup>+</sup> T cells and NKT cells causes nonalcoholic steatohepatitis and liver cancer via cross-talk with hepatocytes. *Cancer Cell* **26**, 549–564 (2014).
429. Herrero-Cervera, A., Vinué, Á., Burks, D. J. & González-Navarro, H. Genetic inactivation of the LIGHT (TNFSF14) cytokine in mice restores glucose homeostasis and diminishes hepatic steatosis. *Diabetologia* **62**, 2143–2157 (2019).
430. Tay, S. S. *et al.* Intrahepatic activation of naive CD4<sup>+</sup> T cells by liver-resident phagocytic cells. *J. Immunol. Baltim. Md 1950* **193**, 2087–2095 (2014).
431. Sutti, S. *et al.* Adaptive immune responses triggered by oxidative stress contribute to hepatic inflammation in NASH. *Hepatology* **59**, 886–897 (2014).

432. The Role of Innate Cells Is Coupled to a Th1-Polarized Immune Response in Pediatric Nonalcoholic Steatohepatitis | SpringerLink.
433. Luo, X.-Y. *et al.* IFN- $\gamma$  deficiency attenuates hepatic inflammation and fibrosis in a steatohepatitis model induced by a methionine- and choline-deficient high-fat diet. *Am. J. Physiol. Gastrointest. Liver Physiol.* **305**, G891-899 (2013).
434. Tang, Y. *et al.* Interleukin-17 exacerbates hepatic steatosis and inflammation in non-alcoholic fatty liver disease. *Clin. Exp. Immunol.* **166**, 281–290 (2011).
435. Harley, I. T. W. *et al.* IL-17 signaling accelerates the progression of nonalcoholic fatty liver disease in mice. *Hepatology. Baltim. Md* **59**, 1830–1839 (2014).
436. Rau, M. *et al.* Progression from Nonalcoholic Fatty Liver to Nonalcoholic Steatohepatitis Is Marked by a Higher Frequency of Th17 Cells in the Liver and an Increased Th17/Resting Regulatory T Cell Ratio in Peripheral Blood and in the Liver. *J. Immunol. Baltim. Md 1950* **196**, 97–105 (2016).
437. Meng, F. *et al.* Interleukin-17 signaling in inflammatory, Kupffer cells, and hepatic stellate cells exacerbates liver fibrosis in mice. *Gastroenterology* **143**, 765-776.e3 (2012).
438. Tan, Z. *et al.* IL-17A plays a critical role in the pathogenesis of liver fibrosis through hepatic stellate cell activation. *J. Immunol. Baltim. Md 1950* **191**, 1835–1844 (2013).
439. Diedrich, T. *et al.* Characterization of the immune cell landscape of patients with NAFLD. *PloS One* **15**, e0230307 (2020).
440. Ghazarian, M. *et al.* Type I Interferon Responses Drive Intrahepatic T cells to Promote Metabolic Syndrome. *Sci. Immunol.* **2**, (2017).
441. Bhattacharjee, J. *et al.* Hepatic Natural Killer T-cell and CD8+ T-cell Signatures in Mice with Nonalcoholic Steatohepatitis. *Hepatology. Commun.* **1**, 299–310 (2017).
442. Breuer, D. A. *et al.* CD8+ T cells regulate liver injury in obesity-related nonalcoholic fatty liver disease. *Am. J. Physiol. Gastrointest. Liver Physiol.* **318**, G211–G224 (2020).

443. Wang, T. *et al.* The immunoregulatory effects of CD8 T-cell-derived perforin on diet-induced nonalcoholic steatohepatitis. *FASEB J. Off. Publ. Fed. Am. Soc. Exp. Biol.* **33**, 8490–8503 (2019).
444. Miyake, T. *et al.* B cell-activating factor is associated with the histological severity of nonalcoholic fatty liver disease. *Hepatol. Int.* **7**, 539–547 (2013).
445. Kawasaki, K. *et al.* Blockade of B-cell-activating factor signaling enhances hepatic steatosis induced by a high-fat diet and improves insulin sensitivity. *Lab. Investig. J. Tech. Methods Pathol.* **93**, 311–321 (2013).
446. Sutti, S. *et al.* BAFF neutralization ameliorates the evolution of experimental NASH. *J. Hepatol.* **68**, S340 (2018).
447. Nakamura, Y. *et al.* Depletion of B cell-activating factor attenuates hepatic fat accumulation in a murine model of nonalcoholic fatty liver disease. *Sci. Rep.* **9**, 977 (2019).
448. Mangelsdorf, D. J. *et al.* The nuclear receptor superfamily: the second decade. *Cell* **83**, 835–839 (1995).
449. Gustafsson, J.-A. Historical overview of nuclear receptors. *J. Steroid Biochem. Mol. Biol.* **157**, 3–6 (2016).
450. Gronemeyer, H., Gustafsson, J.-A. & Laudet, V. Principles for modulation of the nuclear receptor superfamily. *Nat. Rev. Drug Discov.* **3**, 950–964 (2004).
451. Kininis, M. & Kraus, W. L. A global view of transcriptional regulation by nuclear receptors: gene expression, factor localization, and DNA sequence analysis. *Nucl. Recept. Signal.* **6**, e005 (2008).
452. Blumberg, B. & Evans, R. M. Orphan nuclear receptors--new ligands and new possibilities. *Genes Dev.* **12**, 3149–3155 (1998).
453. Weikum, E. R., Liu, X. & Ortlund, E. A. The nuclear receptor superfamily: A structural perspective. *Protein Sci. Publ. Protein Soc.* **27**, 1876–1892 (2018).

454. Kumar, R. & Thompson, E. B. Transactivation functions of the N-terminal domains of nuclear hormone receptors: protein folding and coactivator interactions. *Mol. Endocrinol. Baltim. Md* **17**, 1–10 (2003).
455. Anbalagan, M., Huderson, B., Murphy, L. & Rowan, B. G. Post-translational modifications of nuclear receptors and human disease. *Nucl. Recept. Signal.* **10**, e001 (2012).
456. Rastinejad, F., Huang, P., Chandra, V. & Khorasanizadeh, S. Understanding nuclear receptor form and function using structural biology. *J. Mol. Endocrinol.* **51**, T1–T21 (2013).
457. Danielsen, M. Bioinformatics of nuclear receptors. *Methods Mol. Biol. Clifton NJ* **176**, 3–22 (2001).
458. Gronemeyer, H. & Moras, D. Nuclear receptors. How to finger DNA. *Nature* **375**, 190–191 (1995).
459. Schwabe, J. W., Chapman, L., Finch, J. T. & Rhodes, D. The crystal structure of the estrogen receptor DNA-binding domain bound to DNA: how receptors discriminate between their response elements. *Cell* **75**, 567–578 (1993).
460. Pawlak, M., Lefebvre, P. & Staels, B. General molecular biology and architecture of nuclear receptors. *Curr. Top. Med. Chem.* **12**, 486–504 (2012).
461. Wurtz, J. M. *et al.* A canonical structure for the ligand-binding domain of nuclear receptors. *Nat. Struct. Biol.* **3**, 206 (1996).
462. Moras, D. & Gronemeyer, H. The nuclear receptor ligand-binding domain: structure and function. *Curr. Opin. Cell Biol.* **10**, 384–391 (1998).
463. Weikum, E. R., Knuesel, M. T., Ortlund, E. A. & Yamamoto, K. R. Glucocorticoid receptor control of transcription: precision and plasticity via allostery. *Nat. Rev. Mol. Cell Biol.* **18**, 159–174 (2017).

464. Weikum, E. R., Tuntland, M. L., Murphy, M. N. & Ortlund, E. A. A Structural Investigation into Oct4 Regulation by Orphan Nuclear Receptors, Germ Cell Nuclear Factor (GCNF), and Liver Receptor Homolog-1 (LRH-1). *J. Mol. Biol.* **428**, 4981–4992 (2016).
465. Khorasanizadeh, S. & Rastinejad, F. Nuclear-receptor interactions on DNA-response elements. *Trends Biochem. Sci.* **26**, 384–390 (2001).
466. Fuller, P. J. The steroid receptor superfamily: mechanisms of diversity. *FASEB J. Off. Publ. Fed. Am. Soc. Exp. Biol.* **5**, 3092–3099 (1991).
467. Pratt, W. B., Galigniana, M. D., Morishima, Y. & Murphy, P. J. M. Role of molecular chaperones in steroid receptor action. *Essays Biochem.* **40**, 41–58 (2004).
468. O'Malley, B. W. & Tsai, M. J. Molecular pathways of steroid receptor action. *Biol. Reprod.* **46**, 163–167 (1992).
469. Tata, J. R. Signalling through nuclear receptors. *Nat. Rev. Mol. Cell Biol.* **3**, 702–710 (2002).
470. Lonard, D. M. & O'malley, B. W. Nuclear receptor coregulators: judges, juries, and executioners of cellular regulation. *Mol. Cell* **27**, 691–700 (2007).
471. Glass, C. K. & Rosenfeld, M. G. The coregulator exchange in transcriptional functions of nuclear receptors. *Genes Dev.* **14**, 121–141 (2000).
472. Tetel, M. J., Auger, A. P. & Charlier, T. D. Who's in charge? Nuclear receptor coactivator and corepressor function in brain and behavior. *Front. Neuroendocrinol.* **30**, 328–342 (2009).
473. Surjit, M. *et al.* Widespread negative response elements mediate direct repression by agonist-liganded glucocorticoid receptor. *Cell* **145**, 224–241 (2011).
474. Jetten, A. M., Kurebayashi, S. & Ueda, E. The ROR nuclear orphan receptor subfamily: critical regulators of multiple biological processes. *Prog. Nucleic Acid Res. Mol. Biol.* **69**, 205–247 (2001).

475. Jetten, A. M. Retinoid-related orphan receptors (RORs): critical roles in development, immunity, circadian rhythm, and cellular metabolism. *Nucl. Recept. Signal.* **7**, e003 (2009).
476. Giguère, V. *et al.* Isoform-specific amino-terminal domains dictate DNA-binding properties of ROR alpha, a novel family of orphan hormone nuclear receptors. *Genes Dev.* **8**, 538–553 (1994).
477. Chauvet, C., Bois-Joyeux, B. & Danan, J.-L. Retinoic acid receptor-related orphan receptor (ROR) alpha4 is the predominant isoform of the nuclear receptor RORalpha in the liver and is up-regulated by hypoxia in HepG2 human hepatoma cells. *Biochem. J.* **364**, 449–456 (2002).
478. André, E., Gawlas, K. & Becker-André, M. A novel isoform of the orphan nuclear receptor RORbeta is specifically expressed in pineal gland and retina. *Gene* **216**, 277–283 (1998).
479. He, Y. W., Deftos, M. L., Ojala, E. W. & Bevan, M. J. RORgamma t, a novel isoform of an orphan receptor, negatively regulates Fas ligand expression and IL-2 production in T cells. *Immunity* **9**, 797–806 (1998).
480. Moraitis, A. N. & Giguère, V. Transition from monomeric to homodimeric DNA binding by nuclear receptors: identification of RevErbAalpha determinants required for RORalpha homodimer complex formation. *Mol. Endocrinol. Baltim. Md* **13**, 431–439 (1999).
481. Schröder, M., Danielsson, C., Wiesenberg, I. & Carlberg, C. Identification of natural monomeric response elements of the nuclear receptor RZR/ROR. They also bind COUP-TF homodimers. *J. Biol. Chem.* **271**, 19732–19736 (1996).
482. Jetten, A. M. Retinoid-related orphan receptors (RORs): critical roles in development, immunity, circadian rhythm, and cellular metabolism. *Nucl. Recept. Signal.* **7**, (2009).

483. Giguère, V. Orphan nuclear receptors: from gene to function. *Endocr. Rev.* **20**, 689–725 (1999).
484. McBroom, L. D., Flock, G. & Giguère, V. The nonconserved hinge region and distinct amino-terminal domains of the ROR alpha orphan nuclear receptor isoforms are required for proper DNA bending and ROR alpha-DNA interactions. *Mol. Cell. Biol.* **15**, 796–808 (1995).
485. Burris, T. P. Nuclear hormone receptors for heme: REV-ERBalpha and REV-ERBbeta are ligand-regulated components of the mammalian clock. *Mol. Endocrinol. Baltim. Md* **22**, 1509–1520 (2008).
486. Emery, P. & Reppert, S. M. A rhythmic Ror. *Neuron* **43**, 443–446 (2004).
487. Moraitis, A. N., Giguère, V. & Thompson, C. C. Novel mechanism of nuclear receptor corepressor interaction dictated by activation function 2 helix determinants. *Mol. Cell. Biol.* **22**, 6831–6841 (2002).
488. Kurebayashi, S. *et al.* Selective LXXLL peptides antagonize transcriptional activation by the retinoid-related orphan receptor RORgamma. *Biochem. Biophys. Res. Commun.* **315**, 919–927 (2004).
489. Vitaterna, M. H., Takahashi, J. S. & Turek, F. W. Overview of circadian rhythms. *Alcohol Res. Health J. Natl. Inst. Alcohol Abuse Alcohol.* **25**, 85–93 (2001).
490. Mohawk, J. A., Green, C. B. & Takahashi, J. S. Central and peripheral circadian clocks in mammals. *Annu. Rev. Neurosci.* **35**, 445–462 (2012).
491. Ripperger, J. A. & Schibler, U. Circadian regulation of gene expression in animals. *Curr. Opin. Cell Biol.* **13**, 357–362 (2001).
492. Crumbley, C., Wang, Y., Kojetin, D. J. & Burris, T. P. Characterization of the core mammalian clock component, NPAS2, as a REV-ERBalpha/RORalpha target gene. *J. Biol. Chem.* **285**, 35386–35392 (2010).

493. Reppert, S. M. & Weaver, D. R. Coordination of circadian timing in mammals. *Nature* **418**, 935–941 (2002).
494. Solt, L. A. & Burris, T. P. Action of RORs and their ligands in (patho)physiology. *Trends Endocrinol. Metab.* **23**, 619–627 (2012).
495. CIRCA: Circadian gene expression profiles. <http://circadb.hogeschlab.org/mouse>.
496. Liu, C., Li, S., Liu, T., Borjigin, J. & Lin, J. D. Transcriptional coactivator PGC-1 $\alpha$  integrates the mammalian clock and energy metabolism. *Nature* **447**, 477–481 (2007).
497. Liu, A. C. *et al.* Redundant Function of REV-ERB $\alpha$  and  $\beta$  and Non-Essential Role for Bmal1 Cycling in Transcriptional Regulation of Intracellular Circadian Rhythms. *PLOS Genet.* **4**, e1000023 (2008).
498. Vu-Dac, N. *et al.* Transcriptional regulation of apolipoprotein A-I gene expression by the nuclear receptor ROR $\alpha$ . *J. Biol. Chem.* **272**, 22401–22404 (1997).
499. Raspé, E. *et al.* Transcriptional regulation of apolipoprotein C-III gene expression by the orphan nuclear receptor ROR $\alpha$ . *J. Biol. Chem.* **276**, 2865–2871 (2001).
500. Lind, U. *et al.* Identification of the human ApoAV gene as a novel ROR $\alpha$  target gene. *Biochem. Biophys. Res. Commun.* **330**, 233–241 (2005).
501. Wang, Y., Solt, L. A. & Burris, T. P. Regulation of FGF21 expression and secretion by retinoic acid receptor-related orphan receptor  $\alpha$ . *J. Biol. Chem.* **285**, 15668–15673 (2010).
502. Kallen, J. A. *et al.* X-ray structure of the hROR $\alpha$  LBD at 1.63 Å: structural and functional data that cholesterol or a cholesterol derivative is the natural ligand of ROR $\alpha$ . *Struct. Lond. Engl.* **10**, 1697–1707 (2002).
503. Bitsch, F. *et al.* Identification of natural ligands of retinoic acid receptor-related orphan receptor  $\alpha$  ligand-binding domain expressed in Sf9 cells--a mass spectrometry approach. *Anal. Biochem.* **323**, 139–149 (2003).

504. Boukhtouche, F., Mariani, J. & Tedgui, A. The 'CholesteROR' protective pathway in the vascular system. *Arterioscler. Thromb. Vasc. Biol.* **24**, 637–643 (2004).
505. Choi, W.-S. *et al.* The CH25H-CYP7B1-ROR $\alpha$  axis of cholesterol metabolism regulates osteoarthritis. *Nature* **566**, 254–258 (2019).
506. Chopra, A. R. *et al.* Absence of the SRC-2 coactivator results in a glycogenopathy resembling Von Gierke's disease. *Science* **322**, 1395–1399 (2008).
507. Kumar, N. *et al.* The benzenesulfoamide T0901317 [N-(2,2,2-trifluoroethyl)-N-[4-[2,2,2-trifluoro-1-hydroxy-1-(trifluoromethyl)ethyl]phenyl]-benzenesulfonamide] is a novel retinoic acid receptor-related orphan receptor-alpha/gamma inverse agonist. *Mol. Pharmacol.* **77**, 228–236 (2010).
508. Wang, Y. *et al.* Modulation of retinoic acid receptor-related orphan receptor alpha and gamma activity by 7-oxygenated sterol ligands. *J. Biol. Chem.* **285**, 5013–5025 (2010).
509. Sidman, R. L., Lane, P. W. & Dickie, M. M. Staggerer, a new mutation in the mouse affecting the cerebellum. *Science* **137**, 610–612 (1962).
510. Hamilton, B. A. *et al.* Disruption of the nuclear hormone receptor RORalpha in staggerer mice. *Nature* **379**, 736–739 (1996).
511. Steinmayr, M. *et al.* staggerer phenotype in retinoid-related orphan receptor alpha-deficient mice. *Proc. Natl. Acad. Sci. U. S. A.* **95**, 3960–3965 (1998).
512. A, M. *et al.* Severe atherosclerosis and hypoalphalipoproteinemia in the staggerer mouse, a mutant of the nuclear receptor RORalpha. *Circulation* **98**, (1998).
513. Lau, P. *et al.* The orphan nuclear receptor, RORalpha, regulates gene expression that controls lipid metabolism: staggerer (SG/SG) mice are resistant to diet-induced obesity. *J. Biol. Chem.* **283**, 18411–18421 (2008).
514. Kang, H. S. *et al.* Transcriptional profiling reveals a role for RORalpha in regulating gene expression in obesity-associated inflammation and hepatic steatosis. *Physiol. Genomics* **43**, 818–828 (2011).

515. Lau, P. *et al.* Rora deficiency and decreased adiposity are associated with induction of thermogenic gene expression in subcutaneous white adipose and brown adipose tissue. *Am. J. Physiol. Endocrinol. Metab.* **308**, E159-171 (2015).
516. Monnier, C., Auclair, M., Le Cam, G., Garcia, M.-P. & Antoine, B. The nuclear retinoid-related orphan receptor ROR $\alpha$  controls circadian thermogenic programming in white fat depots. *Physiol. Rep.* **6**, e13678 (2018).
517. Heinlein, U. A. & Wille, W. Evidence for a thymus-affecting, recessive mouse gene (sty) located between the staggerer (sg) and short-ear (se) loci on chromosome 9. *Cell Biol. Int. Rep.* **16**, 1247–1250 (1992).
518. Trenkner, E. & Hoffmann, M. K. Defective development of the thymus and immunological abnormalities in the neurological mouse mutation ‘staggerer’. *J. Neurosci. Off. J. Soc. Neurosci.* **6**, 1733–1737 (1986).
519. Han, Y.-H. *et al.* ROR $\alpha$  Decreases Oxidative Stress Through the Induction of SOD2 and GPx1 Expression and Thereby Protects Against Nonalcoholic Steatohepatitis in Mice. *Antioxid. Redox Signal.* **21**, 2083–2094 (2014).
520. Liu, Y. *et al.* Retinoic acid receptor-related orphan receptor  $\alpha$  stimulates adipose tissue inflammation by modulating endoplasmic reticulum stress. *J. Biol. Chem.* **292**, 13959–13969 (2017).
521. Zhang, Y. *et al.* The hepatic circadian clock fine-tunes the lipogenic response to feeding through ROR $\alpha/\gamma$ . *Genes Dev.* **31**, 1202–1211 (2017).
522. Kim, K. *et al.* ROR $\alpha$  controls hepatic lipid homeostasis via negative regulation of PPAR $\gamma$  transcriptional network. *Nat. Commun.* **8**, 162 (2017).
523. Kim, H.-J. *et al.* Liver-specific deletion of ROR $\alpha$  aggravates diet-induced nonalcoholic steatohepatitis by inducing mitochondrial dysfunction. *Sci. Rep.* **7**, 16041 (2017).
524. Molinaro, A. *et al.* Liver-specific ROR $\alpha$  deletion does not affect the metabolic susceptibility to western style diet feeding. *Mol. Metab.* **23**, 82–87 (2019).

525. Klar, J. *et al.* RAR-related orphan receptor A isoform 1 (RORa1) is disrupted by a balanced translocation t(4;15)(q22.3;q21.3) associated with severe obesity. *Eur. J. Hum. Genet. EJHG* **13**, 928–934 (2005).
526. Zhang, Y., Liu, Y., Liu, Y., Zhang, Y. & Su, Z. Genetic Variants of Retinoic Acid Receptor-Related Orphan Receptor Alpha Determine Susceptibility to Type 2 Diabetes Mellitus in Han Chinese. *Genes* **7**, (2016).
527. Chambers, J. C. *et al.* Genome-wide association study identifies loci influencing concentrations of liver enzymes in plasma. *Nat. Genet.* **43**, 1131–1138 (2011).
528. Kopmels, B. *et al.* Evidence for a hyperexcitability state of staggerer mutant mice macrophages. *J. Neurochem.* **58**, 192–199 (1992).
529. Dzhagalov, I., Giguère, V. & He, Y.-W. Lymphocyte Development and Function in the Absence of Retinoic Acid-Related Orphan Receptor  $\alpha$ . *J. Immunol.* **173**, 2952–2959 (2004).
530. Delerive, P. *et al.* The orphan nuclear receptor ROR $\alpha$  is a negative regulator of the inflammatory response. *EMBO Rep.* **2**, 42–48 (2001).
531. Besnard, S. *et al.* Expression and regulation of the nuclear receptor RORalpha in human vascular cells. *FEBS Lett.* **511**, 36–40 (2002).
532. Sun, Y. *et al.* Nuclear receptor ROR $\alpha$  regulates pathologic retinal angiogenesis by modulating SOCS3-dependent inflammation. *Proc. Natl. Acad. Sci. U. S. A.* **112**, 10401–10406 (2015).
533. Jaradat, M. *et al.* Modulatory role for retinoid-related orphan receptor alpha in allergen-induced lung inflammation. *Am. J. Respir. Crit. Care Med.* **174**, 1299–1309 (2006).
534. Stapleton, C. M. *et al.* Enhanced susceptibility of staggerer (RORalphasg/sg) mice to lipopolysaccharide-induced lung inflammation. *Am. J. Physiol. Lung Cell. Mol. Physiol.* **289**, L144–152 (2005).

535. Moffatt, M. F. *et al.* A large-scale, consortium-based genomewide association study of asthma. *N. Engl. J. Med.* **363**, 1211–1221 (2010).
536. Acevedo, N. *et al.* Interaction between retinoid acid receptor-related orphan receptor alpha (RORA) and neuropeptide S receptor 1 (NPSR1) in asthma. *PLoS One* **8**, e60111 (2013).
537. Friesenhagen, J. *et al.* Highly pathogenic influenza viruses inhibit inflammatory response in monocytes via activation of rar-related orphan receptor ROR $\alpha$ . *J. Innate Immun.* **5**, 505–518 (2013).
538. Saini, A. *et al.* An Accord of Nuclear Receptor Expression in M. tuberculosis Infected Macrophages and Dendritic Cells. *Sci. Rep.* **8**, (2018).
539. Wong, S. H. *et al.* Transcription factor ROR $\alpha$  is critical for nuocyte development. *Nat. Immunol.* **13**, 229–236 (2012).
540. Liu, Y. & Liu, Z. [Function and modulation of type II innate lymphoid cells and their role in chronic upper airway inflammatory diseases]. *Zhonghua Er Bi Yan Hou Tou Jing Wai Ke Za Zhi* **52**, 130–135 (2017).
541. Yang, X. O. *et al.* T helper 17 lineage differentiation is programmed by orphan nuclear receptors ROR alpha and ROR gamma. *Immunity* **28**, 29–39 (2008).
542. Baumjohann, D. *et al.* The microRNA cluster miR-17~92 promotes TFH cell differentiation and represses subset-inappropriate gene expression. *Nat. Immunol.* **14**, 840–848 (2013).
543. Wang, N. S. *et al.* Divergent transcriptional programming of class-specific B cell memory by T-bet and ROR $\alpha$ . *Nat. Immunol.* **13**, 604–611 (2012).
544. Malhotra, N. *et al.* ROR $\alpha$ -expressing T regulatory cells restrain allergic skin inflammation. *Sci. Immunol.* **13** (2018).
545. Kopmels, B. *et al.* Interleukin-1 Hyperproduction by In Vitro Activated Peripheral Macrophages from Cerebellar Mutant Mice. *J. Neurochem.* **55**, 1980–1985 (1990).

546. Kopmels, B., Mariani, J., Taupin, V., Delhay-Bouchaud, N. & Wollman, E. E. Differential IL-6 mRNA expression by stimulated peripheral macrophages of Staggerer and Lurcher cerebellar mutant mice. *Eur. Cytokine Netw.* **2**, 345–353 (1991).
547. Curtis, A. M. *et al.* Circadian control of innate immunity in macrophages by miR-155 targeting *Bmal1*. *Proc. Natl. Acad. Sci.* **112**, 7231–7236 (2015).
548. Han, Y.-H. *et al.* ROR $\alpha$  Induces KLF4-Mediated M2 Polarization in the Liver Macrophages that Protect against Nonalcoholic Steatohepatitis. *Cell Rep.* **20**, 124–135 (2017).
549. Kelly, P. M., Heryet, A. R. & McGee, J. O. Kupffer cell number is normal, but their lysozyme content is reduced in alcoholic liver disease. *J. Hepatol.* **8**, 173–180 (1989).
550. Manifold, I. H., Bishop, F. M., Cloke, P., Triger, D. R. & Underwood, J. C. Lysozyme in chronic liver disease: a biochemical and histological study. *J. Clin. Pathol.* **35**, 815–819 (1982).
551. van Vliet, A. CM., Bakker, W. H., Lindemans, J., Wilson, J. H. P. & van Zanten, R. A. A. Plasma lysozyme level and reticuloendothelial system function in human liver disease. *Clin. Chim. Acta* **113**, 193–199 (1981).
552. Farrell, G. *et al.* Mouse Models of Nonalcoholic Steatohepatitis: Toward Optimization of Their Relevance to Human Nonalcoholic Steatohepatitis. *Hepatology* **69**, 2241–2257 (2019).
553. Miller, A. M. *et al.* Inflammation-associated interleukin-6/signal transducer and activator of transcription 3 activation ameliorates alcoholic and nonalcoholic fatty liver diseases in interleukin-10-deficient mice. *Hepatology. Baltim. Md* **54**, 846–856 (2011).
554. Robertson, S. J. *et al.* Comparison of Co-housing and Littermate Methods for Microbiota Standardization in Mouse Models. *Cell Rep.* **27**, 1910-1919.e2 (2019).

555. Abram, C. L., Roberge, G. L., Hu, Y. & Lowell, C. A. Comparative analysis of the efficiency and specificity of myeloid-Cre deleting strains using ROSA-EYFP reporter mice. *J. Immunol. Methods* **408**, 89–100 (2014).
556. Morán-Salvador, E. *et al.* Cell-specific PPAR $\gamma$  deficiency establishes anti-inflammatory and anti-fibrogenic properties for this nuclear receptor in non-parenchymal liver cells. *J. Hepatol.* **59**, 1045–1053 (2013).
557. Garcia-Martinez, I. *et al.* Hepatocyte mitochondrial DNA drives nonalcoholic steatohepatitis by activation of TLR9. *J. Clin. Invest.* **126**, 859–864 (2016).
558. Weng, S.-Y. *et al.* IL-4 Receptor Alpha Signaling through Macrophages Differentially Regulates Liver Fibrosis Progression and Reversal. *EBioMedicine* **29**, 92–103 (2018).
559. He, L. *et al.* Enhancing the precision of genetic lineage tracing using dual recombinases. *Nat. Med.* **23**, 1488–1498 (2017).
560. de Hostos, E. L. The coronin family of actin-associated proteins. *Trends Cell Biol.* **9**, 345–350 (1999).
561. Drubin, D. G. & Nelson, W. J. Origins of cell polarity. *Cell* **84**, 335–344 (1996).
562. Mitchison, T. J. & Cramer, L. P. Actin-based cell motility and cell locomotion. *Cell* **84**, 371–379 (1996).
563. Search results | HUGO Gene Nomenclature Committee.  
<https://www.genenames.org/tools/search/#!/all?query=Coronin>.
564. Uetrecht, A. C. & Bear, J. E. Coronins: the return of the crown. *Trends Cell Biol.* **16**, 421–426 (2006).
565. Grogan, A. *et al.* Cytosolic phox proteins interact with and regulate the assembly of coronin in neutrophils. *J. Cell Sci.* **110 ( Pt 24)**, 3071–3081 (1997).
566. M, Y., C, D. C.-O., S, G. & Ws, T. Coronin function is required for chemotaxis and phagocytosis in human neutrophils. *J. Immunol. Baltim. Md 1950* **178**, (2007).

567. Moriceau, S. *et al.* Coronin-1 is associated with neutrophil survival and is cleaved during apoptosis: potential implication in neutrophils from cystic fibrosis patients. *J. Immunol. Baltim. Md 1950* **182**, 7254–7263 (2009).
568. Garin, J. *et al.* The Phagosome Proteome: Insight into Phagosome Functions. *J. Cell Biol.* **152**, 165–180 (2001).
569. Schüller, S., Neefjes, J., Ottenhoff, T., Thole, J. & Young, D. Coronin is involved in uptake of *Mycobacterium bovis* BCG in human macrophages but not in phagosome maintenance. *Cell. Microbiol.* **3**, 785–793 (2001).
570. Zheng, P.-Y. & Jones, N. L. *Helicobacter pylori* strains expressing the vacuolating cytotoxin interrupt phagosome maturation in macrophages by recruiting and retaining TACO (coronin 1) protein. *Cell. Microbiol.* **5**, 25–40 (2003).
571. Yan, M., Collins, R. F., Grinstein, S. & Trimble, W. S. Coronin-1 function is required for phagosome formation. *Mol. Biol. Cell* **16**, 3077–3087 (2005).
572. Itoh, S. *et al.* The Role of Protein Kinase C in the Transient Association of p57, a Coronin Family Actin-Binding Protein, with Phagosomes. *Biol. Pharm. Bull.* **25**, 837–844 (2002).
573. Jayachandran, R. *et al.* Survival of mycobacteria in macrophages is mediated by coronin 1-dependent activation of calcineurin. *Cell* **130**, 37–50 (2007).
574. Föger, N., Rangell, L., Danilenko, D. M. & Chan, A. C. Requirement for coronin 1 in T lymphocyte trafficking and cellular homeostasis. *Science* **313**, 839–842 (2006).
575. Shiow, L. R. *et al.* The actin regulator coronin 1A is mutant in a thymic egress-deficient mouse strain and in a patient with severe combined immunodeficiency. *Nat. Immunol.* **9**, 1307–1315 (2008).
576. Marshall, T. W., Aloor, H. L. & Bear, J. E. Coronin 2A regulates a subset of focal-adhesion-turnover events through the cofilin pathway. *J. Cell Sci.* **122**, 3061–3069 (2009).

577. T, N. *et al.* A neurally enriched coronin-like protein, ClipinC, is a novel candidate for an actin cytoskeleton-cortical membrane-linking protein. *J. Biol. Chem.* **274**, (1999).
578. T, M. Transcriptional regulation of a Purkinje cell-specific gene through a functional interaction between ROR alpha and RAR. *Genes Cells Devoted Mol. Cell. Mech.* **2**, (1997).
579. S, N., M, W. & Y, I. Prominent expression of nuclear hormone receptor ROR alpha in Purkinje cells from early development. *Neurosci. Res.* **28**, (1997).
580. H, I. Immunohistochemical characterization of the orphan nuclear receptor ROR alpha in the mouse nervous system. *J. Histochem. Cytochem. Off. J. Histochem. Soc.* **52**, (2004).
581. Lt, S. & A, M. Early postnatal Purkinje cells from staggerer mice undergo aberrant development in vitro with characteristic morphologic and gene expression abnormalities. *Brain Res. Dev. Brain Res.* **152**, (2004).
582. Rogg, M. *et al.* The WD40-domain containing protein CORO2B is specifically enriched in glomerular podocytes and regulates the ventral actin cytoskeleton. *Sci. Rep.* **7**, 15910 (2017).
583. Schwarz, A. *et al.* Coro2b, a podocyte protein downregulated in human diabetic nephropathy, is involved in the development of protamine sulphate-induced foot process effacement. *Sci. Rep.* **9**, (2019).
584. Wang, J. *et al.* MicroRNA and mRNA Interaction Network Regulates the Malignant Transformation of Human Bronchial Epithelial Cells Induced by Cigarette Smoke. *Front. Oncol.* **9**, (2019).
585. Gene Skyline. <http://rstats.immgen.org/Skyline/skyline.html>.
586. Cp, X., L, E., Mp, F., Ro, M. & Cs, C. Evolutionary and functional diversity of coronin proteins. *Subcell. Biochem.* **48**, (2008).
587. Kt, C., Sj, C. & Je, B. Unraveling the enigma: progress towards understanding the coronin family of actin regulators. *Trends Cell Biol.* **21**, (2011).

588. Balasubramanian, I. & Gao, N. From sensing to shaping microbiota: insights into the role of NOD2 in intestinal homeostasis and progression of Crohn's disease. *Am. J. Physiol. - Gastrointest. Liver Physiol.* **313**, G7–G13 (2017).
589. Wolf, A. J. *et al.* Phagosomal degradation increases TLR access to bacterial ligands and enhances macrophage sensitivity to bacteria. *J. Immunol. Baltim. Md 1950* **187**, 6002–6010 (2011).
590. Hancock, R. E. & Diamond, G. The role of cationic antimicrobial peptides in innate host defences. *Trends Microbiol.* **8**, 402–410 (2000).
591. Nash, J. A., Ballard, T. N. S., Weaver, T. E. & Akinbi, H. T. The peptidoglycan-degrading property of lysozyme is not required for bactericidal activity in vivo. *J. Immunol. Baltim. Md 1950* **177**, 519–526 (2006).
592. Zhang, X. *et al.* Human Lysozyme Synergistically Enhances Bactericidal Dynamics and Lowers the Resistant Mutant Prevention Concentration for Metronidazole to *Helicobacter pylori* by Increasing Cell Permeability. *Mol. Basel Switz.* **21**, (2016).
593. Lelouard, H. *et al.* Pathogenic bacteria and dead cells are internalized by a unique subset of Peyer's patch dendritic cells that express lysozyme. *Gastroenterology* **138**, 173-184.e1–3 (2010).
594. Rae, C. S., Geissler, A., Adamson, P. C. & Portnoy, D. A. Mutations of the *Listeria monocytogenes* peptidoglycan N-deacetylase and O-acetylase result in enhanced lysozyme sensitivity, bacteriolysis, and hyperinduction of innate immune pathways. *Infect. Immun.* **79**, 3596–3606 (2011).
595. Davis, K. M., Nakamura, S. & Weiser, J. N. Nod2 sensing of lysozyme-digested peptidoglycan promotes macrophage recruitment and clearance of *S. pneumoniae* colonization in mice. *J. Clin. Invest.* **121**, 3666–3676 (2011).
596. Markart, P. *et al.* Comparison of the microbicidal and muramidase activities of mouse lysozyme M and P. *Biochem. J.* **380**, 385–392 (2004).

597. Silverberg, M. S. *et al.* Ulcerative colitis-risk loci on chromosomes 1p36 and 12q15 found by genome-wide association study. *Nat. Genet.* **41**, 216–220 (2009).
598. Jostins, L. *et al.* Host-microbe interactions have shaped the genetic architecture of inflammatory bowel disease. *Nature* **491**, 119–124 (2012).
599. Pepys, M. B. *et al.* Human lysozyme gene mutations cause hereditary systemic amyloidosis. *Nature* **362**, 553–557 (1993).
600. Girnius, S. *et al.* A new lysozyme tyr54asn mutation causing amyloidosis in a family of Swedish ancestry with gastrointestinal symptoms. *Amyloid Int. J. Exp. Clin. Investig. Off. J. Int. Soc. Amyloidosis* **19**, 182–185 (2012).
601. Jean, E. *et al.* A new family with hereditary lysozyme amyloidosis with gastritis and inflammatory bowel disease as prevailing symptoms. *BMC Gastroenterol.* **14**, 159 (2014).
602. Ganz, T. Increased inflammation in lysozyme M-deficient mice in response to *Micrococcus luteus* and its peptidoglycan. *Blood* **101**, 2388–2392 (2003).
603. Markart, P., Korfhagen, T. R., Weaver, T. E. & Akinbi, H. T. Mouse Lysozyme M Is Important in Pulmonary Host Defense against *Klebsiella pneumoniae* Infection. *Am. J. Respir. Crit. Care Med.* **169**, 454–458 (2004).
604. Shimada, J. *et al.* Lysozyme M deficiency leads to an increased susceptibility to *Streptococcus pneumoniae*-induced otitis media. *BMC Infect. Dis.* **8**, 134 (2008).
605. Ogundele, M. O. A novel anti-inflammatory activity of lysozyme: modulation of serum complement activation. *Mediators Inflamm.* **7**, 363–365 (1998).
606. Kurasawa, T., Takada, K., Ohno, N. & Yadomae, T. Effects of murine lysozyme on lipopolysaccharide-induced biological activities. *FEMS Immunol. Med. Microbiol.* **13**, 293–301 (1996).

607. Ibrahim, H. R., Hamasaki, K. & Miyata, T. Novel peptide motifs from lysozyme suppress pro-inflammatory cytokines in macrophages by antagonizing toll-like receptor and LPS-scavenging action. *Eur. J. Pharm. Sci.* **107**, 240–248 (2017).
608. Liu, H. *et al.* Amelioration of oxidant stress by the defensin lysozyme. *Am. J. Physiol.-Endocrinol. Metab.* **290**, E824–E832 (2006).
609. Yu, S. *et al.* Paneth Cell-Derived Lysozyme Defines the Composition of Mucolytic Microbiota and the Inflammatory Tone of the Intestine. *Immunity* **53**, 398-416.e8 (2020).

## ANNEXES

LIMMA	Comparison	KO VS WT	KO VS WT	KO VS WT	KO VS WT	KO VS WT
Gene	Info	p-val	FDR,p-val	FC	log2(FC)	t-stat
Coro2b	coronin, actin binding protein	1,32E-06	0,03247	0,1984	-2,334	-8,324
Gm24561	predicted gene, 24561	0,009625	0,9149	0,2912	-1,78	-3,025
Phlda3	pleckstrin homology like domai	0,004162	0,8828	0,41	-1,286	-3,459
Gm25388	predicted gene, 25388	0,001078	0,7923	0,4129	-1,276	-4,166
Gm25819	predicted gene, 25819	0,002572	0,8828	0,42	-1,251	-3,709
Krtap19-9a	keratin associated protein 19-	0,007957	0,9149	0,4509	-1,149	-3,124
Arntl	aryl hydrocarbon receptor nucl	2,10E-06	0,03247	0,4522	-1,145	-7,983
Olf1217	olfactory receptor 1217	0,009464	0,9149	0,4684	-1,094	-3,034
Fam214a	family with sequence similarit	0,0002888	0,47	0,4699	-1,089	-4,881
5430437J10Rik	RIKEN cDNA 5430437J10 gene	0,0002152	0,4153	0,4718	-1,084	-5,046
Rfx7	regulatory factor X, 7	7,79E-05	0,2188	0,4723	-1,082	-5,631
Gm24009	predicted gene, 24009	0,009355	0,9149	0,4822	-1,052	-3,04
Cspg4	chondroitin sulfate proteoglyc	5,43E-05	0,2188	0,483	-1,05	-5,845
Gm22977	predicted gene, 22977	0,003356	0,8828	0,4828	-1,05	-3,57
Gm25447	predicted gene, 25447	0,0006434	0,6861	0,4895	-1,031	-4,442
4930583P06Rik	RIKEN cDNA 4930583P06 gene	0,007726	0,9149	0,4906	-1,027	-3,139
Gm25654	predicted gene, 25654	0,008567	0,9149	0,4973	-1,008	-3,086
Mir466g	microRNA 466g	0,007535	0,9149	0,4979	-1,006	-3,152
Gm24786	predicted gene, 24786	0,005475	0,9068	0,5069	-0,9802	-3,317
Gm25930	predicted gene, 25930	0,004391	0,8828	0,5073	-0,979	-3,431
Lmtk2	lemur tyrosine kinase 2	0,002561	0,8828	0,5108	-0,9691	-3,711
Tex9	testis expressed gene 9	0,0002751	0,47	0,5226	-0,9363	-4,908
Cd276	CD276 antigen	0,0008337	0,733	0,5247	-0,9305	-4,303

Olf378	olfactory receptor 378	0,004269	0,8828	0,5254	-0,9285	-3,446
Pilrb2	paired immunoglobulin-like type	0,00319	0,8828	0,5304	-0,9149	-3,597
Cry1	cryptochrome 1 (photolyase-like)	0,001448	0,8019	0,5345	-0,9038	-4,01
Olf596	olfactory receptor 596	0,0002002	0,4153	0,5375	-0,8956	-5,087
BC055324	cDNA sequence BC055324	0,002316	0,8828	0,5404	-0,8879	-3,763
Gm24855	predicted gene, 24855	0,001636	0,8432	0,5473	-0,8697	-3,945
Mir34a	microRNA 34a	0,009782	0,9149	0,5539	-0,8524	-3,017
Gm22459	predicted gene, 22459	0,005024	0,8828	0,5542	-0,8514	-3,361
Gm23443	predicted gene, 23443	0,001157	0,7923	0,5592	-0,8385	-4,129
Igkv6-14	immunoglobulin kappa variable	0,006672	0,9149	0,5648	-0,8241	-3,215
Olf1472	olfactory receptor 1472	0,003771	0,8828	0,5671	-0,8184	-3,51
Gm3414	NA	0,0001389	0,3303	0,5726	-0,8045	-5,295
Fam63b	NA	0,001252	0,7923	0,5733	-0,8026	-4,087
Hmga2-ps1	NA	0,002464	0,8828	0,5772	-0,7929	-3,731
Vmn1r57	vomer nasal 1 receptor 57	0,007601	0,9149	0,5831	-0,7781	-3,147
Cldn1	claudin 1	0,007146	0,9149	0,5877	-0,7669	-3,179
Adpgk	ADP-dependent glucokinase	1,55E-05	0,1592	0,5921	-0,7561	-6,625
Fam96a	NA	2,86E-05	0,2188	0,5953	-0,7482	-6,236
Ppp1r9a	protein phosphatase 1, regulat	0,008887	0,9149	0,5969	-0,7445	-3,067
Tas2r126	taste receptor, type 2, member	0,002502	0,8828	0,602	-0,7322	-3,723
Gm9789	predicted gene 9789	0,008113	0,9149	0,6033	-0,7291	-3,114
Vmn1r217	vomer nasal 1 receptor 217	5,84E-05	0,2188	0,6036	-0,7284	-5,802
Nnt	nicotinamide nucleotide transh	0,00494	0,8828	0,6045	-0,7261	-3,37
Tnfrsf12a	tumor necrosis factor receptor	0,005826	0,9149	0,6082	-0,7174	-3,285
Cpne5	copine V	0,003901	0,8828	0,6083	-0,7172	-3,492
C5ar2	complement component 5a receptor	0,0001261	0,3249	0,6097	-0,7138	-5,35

Olf172	olfactory receptor 172	0,0084 62	0,9149	0,6115	-0,7097	-3,092
B430319H 21Rik	RIKEN cDNA B430319H21 gene	0,0005 196	0,6179	0,6221	-0,6847	-4,558
Olf213	olfactory receptor 213	0,0080 1	0,9149	0,6238	-0,6809	-3,12
Klk8	kallikrein related- peptidase 8	0,0092 61	0,9149	0,6245	-0,6792	-3,045
Sfn	stratifin	0,0073 68	0,9149	0,625	-0,678	-3,164
Mrps2	mitochondrial ribosomal protei	0,0075 44	0,9149	0,6277	-0,672	-3,151
Myliip	myosin regulatory light chain	0,0002 22	0,4153	0,629	-0,6689	-5,029
Mir3475	microRNA 3475	0,0029 68	0,8828	0,6295	-0,6677	-3,634
Mrgpra6	MAS-related GPR, member A6	0,0024 67	0,8828	0,63	-0,6665	-3,73
B4galt5	UDP-Gal:betaGlcNAc beta 1,4-ga	0,0096 14	0,9149	0,6324	-0,6612	-3,026
Xlr5c	X-linked lymphocyte- regulated	0,0018 49	0,8663	0,6353	-0,6544	-3,881
Trp53i13	transformation related protein	0,0017 29	0,8625	0,6371	-0,6505	-3,916
Gm23404	predicted gene, 23404	0,0073 06	0,9149	0,6377	-0,649	-3,168
Nid2	nidogen 2	0,0087 57	0,9149	0,638	-0,6485	-3,074
2810417H1 3Rik	NA	0,0084 83	0,9149	0,6427	-0,6377	-3,091
Pdcd4	programmed cell death 4	0,0040 96	0,8828	0,6457	-0,6311	-3,467
Vmn1r42	vomeronasal 1 receptor 42	0,0085 87	0,9149	0,6459	-0,6307	-3,084
Adam30	a disintegrin and metallopepti	0,0066 9	0,9149	0,6493	-0,6231	-3,213
Vmn2r101	vomeronasal 2, receptor 101	0,0092 63	0,9149	0,6514	-0,6183	-3,045
Gm3287	predicted gene 3287	0,0096 55	0,9149	0,6519	-0,6172	-3,024
Gm13124	predicted gene 13124	0,0012 56	0,7923	0,6529	-0,615	-4,085
Zc3hav1l	zinc finger CCCH-type, antivir	0,0033 08	0,8828	0,6561	-0,608	-3,578
Rps27l	ribosomal protein S27- like	5,47E- 05	0,2188	0,657	-0,6059	-5,841
Gm26535	predicted gene, 26535	0,0038 91	0,8828	0,6591	-0,6015	-3,494
Trerf1	transcriptional regulating fac	0,0042 26	0,8828	0,662	-0,5951	-3,451
Defa-ps1	defensin, alpha, pseudogene 1	0,0085 12	0,9149	0,6623	-0,5945	-3,089
Matn2	matrilin 2	0,0036 72	0,8828	0,667	-0,5843	-3,524

Syne2	spectrin repeat containing, nu	0,0049 45	0,8828	0,6677	-0,5826	-3,37
Mir30a	microRNA 30a	0,0024	0,8828	0,6692	-0,5794	-3,745
Arl9	ADP-ribosylation factor-like 9	0,0082 89	0,9149	0,6707	-0,5764	-3,103
Pptc7	PTC7 protein phosphatase homol	0,0048 36	0,8828	0,6722	-0,5731	-3,381
Taf1b	TATA-box binding protein assoc	0,0003 578	0,5029	0,6732	-0,5708	-4,763
Tifab	TRAF-interacting protein with	0,0045 47	0,8828	0,6741	-0,5691	-3,413
Gm10037	predicted gene 10037	0,0065 82	0,9149	0,6747	-0,5677	-3,222
Gm26518	NA	0,0051 45	0,8988	0,676	-0,5649	-3,349
Ttll3	tubulin tyrosine ligase-like f	0,0033 13	0,8828	0,677	-0,5628	-3,577
Cyct	cytochrome c, testis	0,0035 85	0,8828	0,6778	-0,561	-3,536
Adgrl3	adhesion G protein-coupled rec	0,0079 84	0,9149	0,6793	-0,5579	-3,122
1700102P08Rik	RIKEN cDNA 1700102P08 gene	0,0080 4	0,9149	0,6797	-0,557	-3,118
Gm14409	predicted gene 14409	0,0011 89	0,7923	0,6809	-0,5545	-4,114
Vamp1	vesicle-associated membrane pr	0,0046 34	0,8828	0,6814	-0,5534	-3,403
Gm24471	predicted gene, 24471	0,0065 17	0,9149	0,682	-0,5521	-3,227
Tstd1	thiosulfate sulfurtransferase	0,0037 96	0,8828	0,6821	-0,552	-3,506
Il1rn	interleukin 1 receptor antagon	0,0090 19	0,9149	0,6822	-0,5517	-3,059
Lemd3	LEM domain containing 3	0,0085 44	0,9149	0,6836	-0,5488	-3,087
Mns1	meiosis-specific nuclear struc	0,0033 95	0,8828	0,6838	-0,5484	-3,564
Slc16a10	solute carrier family 16 (mono	0,0007 055	0,7037	0,684	-0,5479	-4,393
Smim3	small integral membrane protei	0,0091 83	0,9149	0,6841	-0,5478	-3,05
Ubash3b	ubiquitin associated and SH3 d	0,0039 85	0,8828	0,6861	-0,5436	-3,481
Mir223	microRNA 223	0,0068 95	0,9149	0,6862	-0,5432	-3,198
Peg13	paternally expressed 13	0,0033 6	0,8828	0,689	-0,5374	-3,57
Rara	retinoic acid receptor, alpha	0,0047 33	0,8828	0,6897	-0,5359	-3,392
Gm10521	predicted gene 10521	0,0049 33	0,8828	0,6898	-0,5358	-3,371
Ankrd49	ankyrin repeat domain 49	0,0040 67	0,8828	0,6904	-0,5346	-3,471

Gm16062	predicted gene 16062	0,0015 54	0,8353	0,691	-0,5332	-3,972
Lgals4	lectin, galactose binding, sol	0,0062	0,9149	0,6915	-0,5323	-3,253
Gm26067	predicted gene, 26067	0,0078 54	0,9149	0,6929	-0,5294	-3,131
Tmem86b	transmembrane protein 86B	0,0032 49	0,8828	0,6936	-0,5278	-3,587
Mxd4	Max dimerization protein 4	0,0011 82	0,7923	0,6939	-0,5271	-4,117
Gm24376	predicted gene, 24376	0,0033 8	0,8828	0,6945	-0,5259	-3,567
Tufm	Tu translation elongation fact	0,0049 72	0,8828	0,6957	-0,5236	-3,367
Prox1	prospero homeobox 1	0,0085 17	0,9149	0,6973	-0,5202	-3,089
E130112N 10Rik	NA	0,0010 64	0,7923	0,6977	-0,5194	-4,173
D930015E 06Rik	NA	0,0080 47	0,9149	0,6993	-0,5161	-3,118
Olf466	olfactory receptor 466	0,0033 43	0,8828	0,6998	-0,515	-3,572
Stk40	serine/threonine kinase 40	0,0070 56	0,9149	0,7006	-0,5133	-3,186
4930548J0 1Rik	RIKEN cDNA 4930548J01 gene	0,0019 95	0,8828	0,7011	-0,5123	-3,841
Slc17a1	solute carrier family 17 (sodi	0,0008 441	0,733	0,7021	-0,5103	-4,296
Cysl1r1	cysteinyl leukotriene receptor	0,0018 28	0,8663	0,7043	-0,5058	-3,887
Cfap36	cilia and flagella associated	0,0021 41	0,8828	0,7045	-0,5053	-3,804
Olf1300- ps1	olfactory receptor 1300, pseud	0,0070 39	0,9149	0,7045	-0,5052	-3,187
Gm20927	predicted gene, 20927	0,0018 1	0,8663	0,7055	-0,5033	-3,892
Nup54	nucleoporin 54	0,0064 77	0,9149	0,7059	-0,5025	-3,23
Sbk2	SH3-binding domain kinase fami	0,0059 47	0,9149	1,417	0,5029	3,274
Matn3	matrilin 3	0,0015 94	0,8353	1,422	0,5074	3,959
Cox7b2	cytochrome c oxidase subunit 7	0,0018 2	0,8663	1,432	0,5177	3,889
Gm10499	predicted gene 10499	0,0082 76	0,9149	1,433	0,5189	3,104
Gm24076	predicted gene, 24076	0,0043 9	0,8828	1,435	0,5215	3,431
Gm25625	predicted gene, 25625	0,0046 63	0,8828	1,435	0,5215	3,4
Gm12631	predicted gene 12631	0,0088 65	0,9149	1,446	0,5324	3,068
Gm4910	predicted pseudogene 4910	0,0033 63	0,8828	1,46	0,5458	3,569

Trip10	thyroid hormone receptor inter	0,00809	0,9149	1,462	0,5475	3,115
4932413F04Rik	RIKEN cDNA 4932413F04 gene	0,002466	0,8828	1,466	0,5519	3,731
Gm26600	predicted gene, 26600	0,000382	0,5135	1,469	0,5551	4,727
Tpcn2	two pore segment channel 2	0,009448	0,9149	1,471	0,5572	3,035
Hfe	homeostatic iron regulator	0,003623	0,8828	1,476	0,5616	3,531
OlfR837	olfactory receptor 837	0,0006329	0,6861	1,486	0,5714	4,451
1700047L14Rik	RIKEN cDNA 1700047L14 gene	0,003721	0,8828	1,488	0,5732	3,517
Zfp109	zinc finger protein 109	0,009147	0,9149	1,493	0,5781	3,052
Mir32	microRNA 32	0,002088	0,8828	1,499	0,5836	3,817
Tcrg-V4	T cell receptor gamma, variabl	0,003414	0,8828	1,5	0,5846	3,561
Bak1	BCL2-antagonist/killer 1	0,0004704	0,5954	1,513	0,5974	4,612
A530032D15Rik	RIKEN cDNA A530032D15Rik gene	0,006786	0,9149	1,519	0,6029	3,206
Fads2	fatty acid desaturase 2	0,006728	0,9149	1,525	0,6086	3,21
Adgrg1	adhesion G protein-coupled rec	0,004947	0,8828	1,537	0,62	3,369
Tspan4	tetraspanin 4	0,0002283	0,4153	1,549	0,631	5,013
Wars	tryptophanyl-tRNA synthetase	0,004545	0,8828	1,558	0,6397	3,413
2310009A05Rik	RIKEN cDNA 2310009A05 gene	0,00613	0,9149	1,559	0,641	3,259
LOC102637947	NA	0,002703	0,8828	1,562	0,6432	3,683
Mmp19	matrix metalloproteinase 19	0,006708	0,9149	1,567	0,6477	3,212
Zfp933	zinc finger protein 933	0,007343	0,9149	1,57	0,6509	3,165
Gm22062	predicted gene, 22062	0,006063	0,9149	1,572	0,6529	3,264
Gm22763	predicted gene, 22763	0,00998	0,9149	1,575	0,6557	3,007
Igkv3-4	immunoglobulin kappa variable	0,004069	0,8828	1,585	0,6644	3,47
Gm25846	predicted gene, 25846	0,00749	0,9149	1,586	0,6657	3,155
Gm23423	predicted gene, 23423	0,001069	0,7923	1,61	0,6867	4,171
Vmn1r56	vomer nasal 1 receptor 56	0,003882	0,8828	1,628	0,7028	3,495
Mir883b	microRNA 883b	0,003247	0,8828	1,633	0,7075	3,587

Cypt8	NA	0,0036 58	0,8828	1,638	0,712	3,526
Ceacam11	carcinoembryonic antigen-relat	0,0041 43	0,8828	1,642	0,7157	3,461
Krt17	keratin 17	0,0029 4	0,8828	1,643	0,7163	3,639
Gm24286	predicted gene, 24286	0,0032 52	0,8828	1,643	0,7167	3,587
Gm27701	predicted gene, 27701	0,0099 49	0,9149	1,653	0,7251	3,008
Gm23192	predicted gene, 23192	0,0045 03	0,8828	1,668	0,7384	3,418
Ighv1-20	immunoglobulin heavy variable	0,0045 3	0,8828	1,677	0,7455	3,415
Serpinb9e	serine (or cysteine) peptidase	0,0045 07	0,8828	1,684	0,7522	3,418
Gm10073	predicted pseudogene 10073	0,0003 513	0,5029	1,693	0,7594	4,773
Gm26489	predicted gene, 26489	0,0028 32	0,8828	1,712	0,7761	3,658
Gm23795	predicted gene, 23795	0,0057 7	0,9149	1,714	0,7777	3,29
Gm5388	predicted gene 5388	0,0090 26	0,9149	1,726	0,7878	3,059
Olf642	olfactory receptor 642	0,0047 72	0,8828	1,742	0,801	3,388
Phf11d	PHD finger protein 11D	0,0057 53	0,9149	1,744	0,8028	3,291
Cmpk2	cytidine monophosphate (UMP-CM	0,0015 72	0,8353	1,755	0,8112	3,967
Xdh	xanthine dehydrogenase	0,0037 89	0,8828	1,776	0,829	3,507
LOC10004 1057	NA	0,0047 89	0,8828	1,778	0,8301	3,386
Vmn2r85	vomeronasal 2, receptor 85	0,0012 08	0,7923	1,796	0,8448	4,106
Olf1109	olfactory receptor 1109	0,0098 8	0,9149	1,827	0,8692	3,012
Gm26078	predicted gene, 26078	0,0011 12	0,7923	1,842	0,8811	4,149
Vps13c	vacuolar protein sorting 13C	7,36E- 05	0,2188	1,85	0,8878	5,664
Cyp2c40	cytochrome P450, family 2, sub	0,0090 74	0,9149	1,863	0,8976	3,056
Ptafr	platelet-activating factor rec	0,0039 51	0,8828	1,864	0,8983	3,486
Gm26263	predicted gene, 26263	0,0008 535	0,733	1,867	0,901	4,291
B230209E 15Rik	RIKEN cDNA B230209E15 gene	0,0020 08	0,8828	1,886	0,9151	3,838
Neo1	neogenin	0,0004 814	0,5954	1,898	0,9242	4,6
Olf1274- ps	olfactory receptor 1274, pseud	0,0021 97	0,8828	1,909	0,9327	3,791

Myrf	myelin regulatory factor	0,0066 27	0,9149	1,946	0,9603	3,218
Esp16	exocrine gland secreted peptid	0,0025 05	0,8828	1,974	0,9814	3,722
Wfdc17	WAP four-disulfide core domain	0,0003 149	0,4869	2,027	1,02	4,833
Fcgr2b	Fc receptor, IgG, low affinity	0,0017 3	0,8625	2,061	1,043	3,916
Vmn2r68	vomeronal 2, receptor 68	0,0039 35	0,8828	2,067	1,047	3,488
Defb8	defensin beta 8	0,0009 135	0,7634	2,144	1,1	4,254
Gm26411	predicted gene, 26411	0,0039 22	0,8828	2,289	1,195	3,489
Lrg1	leucine-rich alpha-2- glycoprot	0,0027 19	0,8828	2,317	1,212	3,68
Gm23806	predicted gene, 23806	0,0055 61	0,9068	2,317	1,212	3,309
Mir1187	microRNA 1187	0,0066 18	0,9149	2,449	1,292	3,219
Ifit1b1	interferon induced protein wit	6,50E- 05	0,2188	2,521	1,334	5,739
Cxcl16	chemokine (C-X-C motif) ligand	0,0079 84	0,9149	2,533	1,341	3,122
Glce	glucuronyl C5-epimerase	5,00E- 05	0,2188	2,623	1,391	5,896
Crip1	cysteine-rich protein 1 (intes	0,0095 71	0,9149	2,951	1,561	3,028
Gm10509	predicted gene 10509	0,0079 52	0,9149	3,179	1,669	3,124
Mustn1	musculoskeletal, embryonic nuc	0,0021 24	0,8828	3,553	1,829	3,809

**Supplementary Table 1:** List of the modulated genes from microarrays performed on alveolar macrophages from lung of 14 weeks old naïve WT and MKO mice. Genes are sorted by log<sub>2</sub>( FC) value from downregulated to upregulated ones. n=6 mice per genotype.

**Saturated fatty acids promote GDF15 expression in macrophages through the PERK/eIF2/CHOP signaling pathway**

Laurent L'homme<sup>1,2</sup>, Benan Pelin Sermikli<sup>1</sup>, Bart Staels<sup>1</sup>, Jacques Piette<sup>2</sup>, Sylvie Legrand-Poels<sup>2,3,\*</sup>, David Dombrowicz<sup>1,3,\*</sup>

<sup>1</sup>Univ. Lille, INSERM, CHU Lille, Institut Pasteur de Lille, U1011-EGID, Lille, France.

<sup>2</sup>University of Liege, GIGA-Signal Transduction, Laboratory of Virology and Immunology, Liège, Belgium.

<sup>3</sup>DD and SLP contributed equally to this work.

\* Correspondence: [david.dombrowicz@pasteur-lille.fr](mailto:david.dombrowicz@pasteur-lille.fr) (DD) and [S.Legrand@ulg.ac.be](mailto:S.Legrand@ulg.ac.be) (SLP)

**Abstract:**

Growth differentiation factor-15 (GDF-15) and its receptor GFRAL are involved in the development of obesity and insulin resistance. GDF-15 level increases with obesity and is positively associated with disease progression. The molecular mechanism underlying GDF-15 production is unknown but macrophages have been recently proposed as a key source. In the present work, we sought for potential physiological activators of *GDF15* expression in macrophages and identified saturated fatty acids (SFAs) as strong inducers of *GDF15* expression and secretion. SFAs increase *GDF15* expression following the induction of an ER stress and the activation of the unfolded protein response through the PERK/eIF2/CHOP signaling pathway. The transcription factor CHOP directly binds *GDF15* promoter region and regulates *GDF15* expression. Unlike SFAs, unsaturated fatty acids do not promote *GDF15* expression and rather prevent both SFA-induced *GDF15* expression and ER stress. These results suggest that free fatty acids may be involved in the control of GDF-15 and provide new molecular insights about how diet and lipid metabolism may regulate the development of obesity and T2D.

**Keywords:**

GDF15; macrophage; obesity; saturated fatty acids; stearate; ER stress; CHOP.

## **Introduction**

Growth differentiation factor-15 (GDF-15) is a cytokine from the transforming growth factor-beta (TGF- $\beta$ ) superfamily. GDF-15 is positively associated with the development of several diseases including obesity (Dostálová et al., 2009; Vila et al., 2011), type 2 diabetes (T2D) (Bao et al., 2019; Kempf et al., 2012), non-alcoholic steatohepatitis (NASH) (Koo et al., 2018), cardiovascular diseases (Brown et al., 2002) and various cancers (Brown et al., 2003; Koopmann et al., 2004). In the past decades, GDF-15 has been extensively studied in cancer where it is mainly regulated by the transcription factor p53 and plays roles in apoptosis, proliferation, invasion, angiogenesis, metastasis, drug resistance and anorexia/cachexia (Johnen et al., 2007; Osada et al., 2007; Tsai et al., 2018). More recently, a growing interest about its role in metabolic diseases has emerged, particularly in obesity and T2D. Indeed, similar to its role on cancer-induced anorexia (Johnen et al., 2007), GDF-15 also regulates food intake in obesity models. Transgenic mice overexpressing *Gdf15* or mice injected with recombinant GDF-15 are protected against obesity and insulin resistance (IR) (Chrysovergis et al., 2014; Chung et al., 2017; Emmerson et al., 2017; Jung et al., 2018; Macia et al., 2012; Mullican et al., 2017). On the contrary, *Gdf15*-deficient mice are prone to obesity and IR (Tran et al., 2018).

Glial-derived neurotrophic factor receptor alpha-like (GFRAL) was recently identified as the GDF-15 receptor (Emmerson et al., 2017; Hsu et al., 2017; Mullican et al., 2017; Yang et al., 2017). The discovery of GFRAL and its highly restricted expression within the brainstem area postrema and the nucleus tractus solitaries (Emmerson et al., 2017; Hsu et al., 2017; Mullican et al., 2017; Yang et al., 2017) confirm earlier findings showing that GDF-15 activates neurons in these regions controlling food intake (Johnen et al., 2007; Tsai et al., 2014). Similar to *Gdf15* deficient mice, mice lacking

*Gf1a1* are prone to develop more severe obesity and IR (Hsu et al., 2017; Mullican et al., 2017). Besides the impact of GDF-15 on food intake contributing to the protection against obesity and T2D, anorectic-independent effects of GDF-15 on insulin sensitivity, lipolysis and fatty acid oxidation have been described (Chrysovergis et al., 2014; Chung et al., 2017; Hsu et al., 2017), suggesting that GDF-15 effects extend beyond the regulation of food intake.

GDF-15 is expressed by various cell types including adipocytes (Ding et al., 2009), hepatocytes (Li et al., 2018), myocytes (Chung et al., 2017) and epithelial cells (Park et al., 2017). GDF-15 was originally named macrophage inhibitory cytokine 1 (MIC-1) due to its ability to regulate macrophage activation (Bootcov et al., 1997). GDF-15 is also produced by macrophages themselves (Bootcov et al., 1997; Jung et al., 2018), suggesting that GDF-15 has an autocrine regulatory function. Macrophages are key components of the innate immunity not only playing important roles during infections and cancer but also in tissue development and metabolic homeostasis (Wynn et al., 2013). Macrophages colonize all the tissues early during embryological development and represent the most abundant immune cell type in most tissues (Perdiguerro and Geissmann, 2016). Tissue macrophage infiltration is also observed in most pathological conditions such as obesity, T2D and cancer (Wynn et al., 2013), indicating that macrophages may represent an important source of GDF-15 in these disorders. To support this hypothesis, overexpression of *Gdf15* in monocytes/macrophages lineage reduces body weight and IR (Macia et al., 2012). By contrast, reconstitution of macrophage-depleted mice with *Gdf15*-deficient macrophages increases body weight and IR compared to mice reconstituted with *Gdf15*-proficient macrophages (Jung et al., 2018), showing that GDF-15 production by macrophages is essential in obesity and T2D. Despite these findings demonstrating a role of macrophage-produced GDF-

15 in obesity and T2D, little is known about the regulation of GDF15 in macrophages in metabolic diseases.

One major regulator of GDF-15 in myocytes, hepatocytes and cancer cells is the endoplasmic reticulum (ER) stress (Chung et al., 2017; Li et al., 2018; Patel et al., 2019; Yang et al., 2010). Importantly, ER stress is also involved in the development of obesity and T2D and occurs in liver, pancreas and adipose tissue (Boden et al., 2008; Laybutt et al., 2007; Ozcan et al., 2004). Accumulation of misfolded proteins in ER lumen, referred as ER stress, occurs when the protein-folding machinery is overwhelmed (Walter and Ron, 2011). It may result from an increase of protein synthesis, a defect in post-translational modification, an impairment of protein degradation, an alteration in ER calcium concentration or a lipid bilayer stress. ER stress triggers a cellular response, called the unfolded protein response (UPR), to restore ER homeostasis or to induce cell death if the stress is chronic or substantial. Initiation of the UPR arises from the detection of misfolded proteins accumulation through three sensor proteins, inositol-requiring enzyme 1 $\alpha$  (IRE1 $\alpha$ ), PKR-like ER kinase (PERK) and activating transcription factor 6 (ATF6), that ultimately activate signaling cascades (Walter and Ron, 2011). Among the signaling pathways activated by the UPR, the integrated stress response (ISR) is highly important in ER stress resolution. ISR is initiated following the phosphorylation of the eukaryotic initiation factor 2 alpha (eIF2 $\alpha$ ) by PERK. Phosphorylation of eIF2 $\alpha$  regulates eIF2 complex activity and leads to a global decrease of mRNAs translation. Paradoxically, ISR increases the translation and expression of some mRNAs such as those encoding the transcription factors ATF4, ATF3 and CHOP. Together, these transcription factors regulate the expression of various genes critical to resolve ER stress. Interestingly, ISR and the transcription factor CHOP contribute to obesity and IR (Han et al., 2013;

Suzuki et al., 2017). Indeed, CHOP-deficient mice are more susceptible to obesity (Han et al., 2013), but the molecular mechanism underlying the protective role of CHOP remains unclear.

In the present work, we sought for potential physiological activators of *GDF15* expression in macrophages and identified saturated fatty acids (SFAs) as strong inducers of *GDF15* expression and secretion. We show that SFAs induce *GDF15* expression following induction of an ER stress. SFAs-induced ER stress initiates the activation of the eIF2 complex in a PERK-dependent manner and the expression of the transcription factor CHOP that directly binds *GDF15* promoter region and regulates *GDF15* expression. Interestingly, we show that unsaturated fatty acids (UFAs) prevent SFA-induced *GDF15* expression and ER stress, bringing new findings about how diet and lipid metabolism may regulate the development of obesity and T2D.

## **Materials and Methods**

### **Preparation of FFA solutions**

FFA solutions were prepared as previously described (L'homme et al., 2013). In summary, C16:0 (Sigma, #P0500), C16:1 (Sigma, #P9417), C18:0 (Sigma, #S4751), C18:1 (Sigma, #O1008) and C18:2 (Sigma, #L1376) were first dissolved in NaOH and then complexed with fatty acid free, low endotoxin BSA (Sigma, #A8806) at a FFA:BSA molar ratio of 3.4:1.

### **Cell culture and treatments**

Peripheral blood mononuclear cells (PBMCs) were purified by single step density gradient centrifugation with Ficoll-Paque PLUS (GE Healthcare) from buffy coat obtained from healthy donors after informed consent (Croix Rouge de Belgique and Etablissement Francais du Sang). Monocytes were isolated from PBMCs using CD14 MicroBeads (Miltenyi Biotec) according to the manufacturer's instructions. Monocyte-derived macrophages (MDMs) were generated by culturing freshly isolated monocytes in RPMI 1640 (Lonza) with 20% heat-inactivated FBS (Gibco), 100 IU/mL penicillin (Lonza), 100 IU/mL streptomycin (Lonza) and 100 ng/mL of human M-CSF premium grade (Miltenyi Biotec) for 7 days at 37°C under 5% CO<sub>2</sub> atmosphere before stimulation.

The THP-1 monocytic cell line (ATCC) were maintained between 0.5 and 2.0 × 10<sup>6</sup> cells/ml in RPMI 1640 (Lonza) supplemented with 10% heat-inactivated FBS (Gibco) and 25 µg/mL gentamycin (Gibco) at 37°C under 5% CO<sub>2</sub> atmosphere. THP-1 cells were differentiated into macrophage-like cells with 100 ng/ml of PMA (Sigma, #P8139) for 24 h, washed with PBS, and kept resting for one night in fresh supplemented medium before stimulation.

MDMs and PMA-differentiated THP-1 cells were treated with 100 to 200  $\mu$ M FFAs or 5  $\mu$ g/mL tunicamycin (Sigma #T7765) for 2 to 16 hours. Inhibitors, including pifithrin- $\alpha$  (Enzo Life Sciences #BML-GR325 ; 20  $\mu$ M), 4-phenylbutyric acid (PBA) (Sigma #P21005 ; 1 mM), GSK2606414 (Sigma #516535 ; 2  $\mu$ M), GSK2656157 (Santa Cruz #sc-490341 ; 2  $\mu$ M), trans-ISRIB (Tocris #5284 ; 1  $\mu$ M) and salubrinal (Tocris #2347 ; 50  $\mu$ M), were added 15 minutes before FFAs stimulation and maintained through the experiment. Cell viability for ER stress inhibitors and FFAs was assessed and non-toxic concentrations were selected (Fig. S1A-B).

### **siRNA transfection**

$2.5 \times 10^5$  THP-1 cells were transfected by using the HiPerFect Transfection reagent (Qiagen #301705) according to manufacturer's instructions (protocol for suspension cell lines). Predesigned siRNA targeting human IRE1 $\alpha$ , PERK, ATF6, CHOP and ATF3 were purchased from Integrated DNA Technologies (TriFECTa DsiRNA Kit). For IRE1 $\alpha$  and PERK, THP-1 cells were transfected before PMA differentiation and the treatment with FFAs performed 80 hours post-transfection. For ATF6, PMA-differentiated THP-1 cells were transfected for 32 hours before FFAs stimulation. CHOP and ATF3 siRNAs were transfected in PMA-differentiated THP-1 cells for 8 hours before FFAs treatment.

### **Cell viability assay**

Cell proliferation reagent WST-1 (Roche Applied Science #05015944001) was used to assess cell proliferation, viability and toxicity according to the manufacturer's instructions.  $1.5 \times 10^5$  THP-1 cells were differentiated with PMA in 96-well plate followed by treatment for 16 hours before addition of WST-1 reagent.

## **Luminex assay**

GDF-15 was measured in culture supernatants from MDMs by Luminex assay (R&D Systems) according to manufacturer's instructions. Beads were read on a Bio-Plex 200 system (Bio-Rad) or on a Bio-Plex MAGPIX system (Bio-Rad).

## **RT-qPCR**

Total RNAs were extracted with high pure RNA isolation kit (Roche Applied Science) or TRIzol reagent (Ambion) according to the manufacturer's recommendations. DNase treatment was performed on column for RNA isolation kit or after resuspension of RNA pellet for TRIzol extraction by using DNase I (Thermo Scientific, #EN0521). Purified RNAs were reverse-transcribed to complementary DNA (cDNA) by using the high capacity cDNA reverse transcription kit (Applied Biosystems, #4368813). qPCR was performed by using Brilliant II SYBR Green QPCR Master Mix (Agilent, #600828) and ran on a Mx3000P qPCR system (Agilent) or on a LightCycler 480 (Roche Applied Science). Gene expressions were calculated using the  $2^{-\Delta\Delta CT}$  method. OAZ1, a highly stable gene in human (de Jonge et al., 2007), was chosen as housekeeping gene. Primer sequences are provided in supplementary table 1.

## **Western blot**

Cells were lysed in total phospho lysis buffer (62.5 mM Tris-HCl at pH 6.8, 10% glycerol, 2% SDS, 3%  $\beta$ -mercaptoethanol, 0.03% bromophenol blue, 1 mM DTT, 1 mM sodium orthovanadate, 25 mM  $\beta$ -glycerophosphate, 15 mM sodium fluoride, 1 mM PMSF, and complete protease inhibitor cocktail) and subjected to SDS-PAGE. The following primary antibodies were used: anti-phospho-eIF2 $\alpha$  (Cell Signaling #9721), anti-eIF2 $\alpha$  (Cell Signaling #9722), anti-CHOP (Santa Cruz #sc-575), anti-HSP90

(Santa Cruz #sc-7947) and anti- $\beta$ -tubulin (Sigma #T5201). The secondary antibodies used for the revelation were Alexa Fluor 680 anti-mouse IgG (Jackson ImmunoResearch, #715-625-150), Alexa Fluor 790 anti-rabbit IgG (Jackson ImmunoResearch, #711-655-152), HRP-linked anti-rabbit IgG (Cell Signaling #7074) and HRP-linked anti-mouse IgG (Dako #7074). Fluorescent immunoblots were scanned with an OdysseyCLx Imaging System (LI-COR) and quantified with Image studio software (LI-COR). For chemoluminescent western blot, revelation was performed with ECL (Pierce) by using the digital imaging system ImageQuant LAS 4000 (GE Healthcare) and quantification achieved with the ImageQuant TL software (version 7.0, GE Healthcare). After phospho-eIF2 $\alpha$  revelation, a stripping step of 1 hour at 50°C with Tris-HCl pH 6.8, 2% SDS, 0.8%  $\beta$ -mercaptoethanol was performed before the detection of eIF2 $\alpha$ .

### **ChIP-qPCR**

After 16 hours of treatment with BSA or C18:0, PMA-differentiated THP-1 cells were washed twice with PBS and crosslinked with 1% methanol-free formaldehyde (Pierce #28908) for 10 minutes at room temperature. Crosslink was quenched by addition of glycine. Cells were scrapped in buffer 1 (50 mM HEPES-KOH pH 7.5, 0.25% Triton X100, 10% glycerol, 0.5 mM EGTA, 1 mM EDTA, 140 mM NaCl, 0.5% Igepal, 1 mM PMSF, cOmplete protease inhibitor cocktail) and incubated for 10 min at 4°C under agitation. Samples were centrifuged at 600g, washed with buffer 2 (10 mM Tris-HCl pH 8.0, 0.5 mM EGTA, 1 mM EDTA, 200 mM NaCl, 1 mM PMSF, cOmplete protease inhibitor cocktail) and centrifuged at 600g. Nuclei pellets were resuspended in buffer 3 (50 mM Tris-HCl pH 8.0, 10 mM EDTA, 1% SDS, 1 mM PMSF, cOmplete protease inhibitor cocktail), sonicated by using a Bioruptor Plus (Diagenode) and incubated with

2 µg antibody overnight at 4°C under agitation. Immunocomplexes were captured with protein A/G magnetic beads previously blocked with BSA and tRNA from yeast (Sigma #R5636). Beads were successively washed with buffer 4 (50 mM Tris-HCl pH 8.0, 1% Triton X100, 1 mM EDTA, 150 mM NaCl, 0.1% SDS), buffer 5 (50 mM Tris-HCl pH 8.0, 1% Triton X100, 1 mM EDTA, 500 mM NaCl, 0.1% SDS), buffer 6 (50 mM Tris-HCl pH 8.0, 1 mM EDTA, 500 mM LiCl, 0.5% sodium deoxycholate, 1% igepal) and TE (50 mM Tris-HCl pH 8.0, 1 mM EDTA). Beads were resuspended in elution buffer (1% SDS, 100mM NaHCO<sub>3</sub>) and incubated overnight at 65°C with agitation to reverse crosslink. DNA was purified with NucleoSpin gel and PCR Clean-up (Macherey-Nagel #740609) according to the manufacturer's instructions. qPCR was performed by using Brilliant II SYBR Green QPCR Master Mix (Agilent, #600828) and ran on a Mx3000P qPCR system (Agilent). The antibodies used were anti-CHOP (Santa Cruz #sc-575) and normal rabbit IgG (Cell Signaling #2729). Primer sequences are provided in supplementary table 1.

### **Statistical analyses**

All statistical analyses were carried out using GraphPad Prism 7 for Windows (GraphPad Software, Inc.) and presented as the means ± standard error of the mean (SEM). When one independent variable was involved, two-tailed Student's *t*-test was performed to compare two groups and one-way ANOVA with Dunnett's multiple comparisons test to compare more than two groups. Two-way ANOVA with Sidak's multiple comparisons test was performed when the experiment involved two independent variables. Tests used are described in the figure legends. Statistical significance was set at  $p < 0.05$ .

## **Results**

### **SFAs promote *GDF15* expression and secretion in macrophages**

To better understand how *GDF15* expression is regulated in macrophages, we analyzed a publicly available transcriptomic dataset of human primary macrophages treated with several physiological stimuli including cytokines, TLR ligands, glucocorticoid, prostaglandin, lipoprotein and free fatty acids (FFAs) (Fig. 1A) (Xue et al., 2014). FFAs, and particularly palmitate (C16:0) and stearate (C18:0), the two most common saturated fatty acids (SFAs), induced the highest *GDF15* expression. Since both FFAs and *GDF-15* concentrations increase in metabolic diseases (Bergman and Ader, 2000; Dostálová et al., 2009; Vila et al., 2011), FFAs may represent potential activators of *GDF15* expression. To confirm this finding, we treated human primary monocyte-derived macrophages (MDMs) with physiological concentrations of FFAs (100  $\mu$ M) (Hodson et al., 2008), including C16:0, C18:0 and their chain length-matched unsaturated fatty acids (UFAs) C16:1, C18:1 and C18:2. We confirmed that SFAs induced *GDF15* expression (Fig. 1B) and secretion (Fig. 1C) compared to the vehicle alone (BSA) in MDMs. C18:0 induced a stronger response than C16:0. Interestingly, UFAs were unable to induce *GDF15* expression and secretion.

### **ER stress, but not p53, is involved in SFAs-induced *GDF15* expression**

*GDF-15* was extensively studied for its role in cancer and shown to be mainly regulated by the transcription factor p53 (Osada et al., 2007) and the ER stress pathway (Yang et al., 2010). SFAs did not induce the common p53 target genes such as *CDKN1A*, encoding for p21, and *MDM2* (Fig. 2A-B) but strongly increased the expression of ER stress-related markers such as *HSP5A*, encoding for BIP, and the spliced form of *XBP1* mRNA in MDMs (Fig. 2C-D) (Walter and Ron, 2011).

Inhibition of p53 with pifithrin- $\alpha$  did not reverse C18:0-induced *GDF15* expression in MDMs (Fig. 2E) while ER stress inhibition by the chemical chaperone 4-phenylbutyric acid (PBA) decreased *GDF15* expression (Fig. 2F) and secretion (Fig. 2G). On the other hand, induction of an ER stress with tunicamycin, a glycosylation inhibitor leading to the accumulation of misfolded proteins in ER, increased ER stress marker (Fig. 2H) and *GDF15* expression (Fig. 2I), confirming that ER stress is able to induce *GDF15* expression in macrophages.

### **PERK/eIF2 $\alpha$ /CHOP pathway regulates SFAs-induced *GDF15* expression**

To better understand how ER stress leads to *GDF15* expression, we inhibited each of the three UPR branches by silencing IRE1 $\alpha$ , ATF6 or PERK through siRNA transfection in PMA-differentiated THP-1 cells. The human monocytic cell line THP-1, differentiable in macrophage-like cells by using PMA, was used for its better transfection efficiency compared to primary macrophages. SFAs induced *GDF15* expression and ER stress in PMA-differentiated THP-1 cells as observed in primary MDMs (Fig. S2A-B). While the expression of each ER stress sensor was significantly downregulated after transfection of the corresponding siRNA (Fig. S3A-C), only the PERK silencing decreased C18:0-induced *GDF15* expression (Fig. 3A & Fig. S3D-E). Pharmacological inhibition of PERK with GSK2606414 or GSK2656157 reduced C18:0-induced *GDF15* expression in PMA-differentiated THP-1 cells (Fig. 3B). PERK inhibition also decreased *GDF15* expression and secretion following stimulation with C18:0 in primary MDMs (Fig. 3C-D). Similarly to C18:0-mediated *GDF15* expression, tunicamycin-induced *GDF15* expression was prevented by PERK inhibitors (Fig. 3E), demonstrating that PERK pathway is involved in ER stress-induced *GDF15* expression in macrophages.

As a consequence of ER stress, PERK phosphorylates eIF2 $\alpha$  that activates the ISR and increases the expression of *ATF4*, *ATF3* and *DDIT3*, encoding for CHOP (Walter and Ron, 2011). In agreement with our results showing that SFAs initiated an ER stress, SFAs induced eIF2 $\alpha$  phosphorylation (Fig. S4A) and expression of *ATF4*, *ATF3* and *DDIT3* (Fig. S4B-D). Treatment with trans-ISRIB, an eIF2 complex inhibitor, decreased both C18:0- and tunicamycin-induced *GDF15* expression (Fig. 3F). In basal conditions and under ER stress, eIF2 $\alpha$  is dephosphorylated by PP1/CREP and PP1/GADD34 complexes driving a negative regulation of eIF2 activity. Interestingly and as anticipated, preventing dephosphorylation of eIF2 $\alpha$  by inhibiting these phosphatase complexes with salubrinal exacerbated C18:0- and tunicamycin-induced *GDF15* expression (Fig. 3G). Altogether, these results show that eIF2 signaling pathway, namely the ISR, regulates *GDF15* expression in macrophages.

*ATF3* and CHOP are two key transcription factors involved in ISR which are both induced by SFAs (Fig. S4C-D). Transfection of siRNA against *ATF3* or *DDIT3* mRNA shortly before C18:0 treatment allowed us to mainly prevent the increase of mRNA level induced by C18:0 (Fig. 4A-B). CHOP silencing decreased *GDF15* expression (Fig. 4C) while *ATF3* knock down did not (Fig. 4D). Analysis of *GDF15* promoter region revealed seven potential CHOP response elements (Fig. 4E). To determine whether CHOP is recruited in *GDF15* promoter in response to C18:0 treatment, we performed a ChIP assay for these response elements that we grouped in 4 sites (Fig. 4E). BSA alone showed no enrichment at any sites suggesting no or few basal binding of CHOP in *GDF15* promoter (Fig. 4F). This observation is correlated with an undetectable CHOP protein level under basal conditions (Fig. 4G). C18:0 increased CHOP protein level (Fig. 4G) and CHOP binding in *GDF15* promoter (Fig. 4F). These results suggest that CHOP regulates *GDF15* expression in macrophages by a direct binding to its

promoter. It is worth noting that all the previous treatments restraining *GDF15* expression such as PBA, PERK siRNAs, PERK inhibitors and trans-ISRIB also successfully decreased *DDIT3* expression (Fig. 5A-E), while treatments exacerbating *GDF15* expression such as p53 inhibitor pifithrin- $\alpha$  and salubrinal increased *DDIT3* expression (Fig. 5F-G). Collectively, these data demonstrate that C18:0 promote *GDF15* expression in macrophages following the induction of an ER stress through the PERK/eIF2/CHOP signaling pathway.

### **UFAs inhibit SFAs-induced ER stress and *GDF15* expression**

Unlike SFAs, UFAs did not induce *GDF15* expression and secretion (Fig. 1B-C). It has been previously reported that UFAs were able to prevent SFAs-induced cytokine production such as IL-1 $\beta$  or IL-6 (Gianfrancesco et al., 2019; L'homme et al., 2013; Macrae et al., 2013). To investigate whether UFAs prevent C18:0-induced *GDF15* expression, we treated PMA-differentiated THP-1 cells with C18:0 alone or in combination with an equimolar concentration of UFAs. C16:1, C18:1 and C18:2 were all able to prevent C18:0-induced *GDF15* expression (Fig. 6A). Since CHOP is involved in SFAs-induced *GDF15* expression, we next analyzed ER stress response upon co-treatment with C18:0 and UFAs. UFAs restrained C18:0-induced ER stress markers including the splicing of *XBP1* mRNA (Fig. 6B), eIF2 $\alpha$  phosphorylation (Fig. 6C) and the expression of *HSPA5* and *DDIT3* (Fig. 6D-E). In contrast, tunicamycin-induced *GDF15* expression (Fig. 6F) and ER stress (Fig. 6G-J) were not inhibited by UFAs co-treatment, suggesting that UFAs have no general effect on ER stress but specifically restrain SFAs effect on ER stress. The protection mediated by UFAs against C18:0-induced ER stress and CHOP upregulation likely account for the inhibition of *GDF15* expression. Taken together, our results show the complex action of FFAs on *GDF15*

regulation in macrophages with SFAs promoting GDF-15 production and UFAs counteracting SFAs effect.

## **Discussion**

The role of GDF-15 and its receptor GFRAL in the development and progression of obesity and T2D is well described (Chrysovergis et al., 2014; Chung et al., 2017; Emmerson et al., 2017; Hsu et al., 2017; Macia et al., 2012; Mullican et al., 2017; Tran et al., 2018; Yang et al., 2017), but the molecular mechanism accounting for the high expression of GDF-15 in these conditions is poorly understood. Obesity increases GDF15 expression in liver and adipose tissue (Patel et al., 2019). Parenchymal cells from these tissues; i.e. hepatocytes, preadipocytes and mature adipocytes; have been proposed as a source for this increased expression (Ding et al., 2009; Li et al., 2018; Patel et al., 2019). Macrophages are the main immune cell population in both adipose tissue and liver and expand with obesity (Wynn et al., 2013). Recently, it was showed that macrophages produce critical levels of GDF-15 in obese mice (Jung et al., 2018), suggesting that macrophages should also contribute to the obesity-associated increase of GDF-15. To better understand how *GDF15* expression may be regulated in macrophages, we investigated the effect of several physiological stimuli and identified SFAs as being able to promote GDF15 expression and secretion. C18:0 (stearate) induced a stronger *GDF15* expression than C16:0 (palmitate) at the same concentration. C18:0 is the second most important SFA, representing 12.5% of plasmatic FFAs while C16:0 reaches 28% (Hodson et al., 2008). Several studies reported a positive association for both C16:0 and C18:0 with obesity and T2D (Klein-Platat et al., 2005; Ma et al., 2015).

We showed that C18:0-induced *GDF15* expression is ER stress-dependent and involves the UPR via the PERK/eIF2/CHOP signaling pathway and a direct binding of the transcription factor CHOP in *GDF15* promoter. In basal conditions, macrophages express no or low level of CHOP, likely explaining the absence of CHOP binding in *GDF15* promoter and the lack of effect of ER stress, UPR and ISR inhibitors in unstimulated cells. The basal *GDF15* expression and secretion in macrophages is therefore ER stress-independent. Upon SFAs treatment, the PERK/eIF2/CHOP signaling pathway is activated leading to CHOP expression and binding to *GDF15* promoter, as well as *GDF15* expression and secretion by macrophages. Interestingly, the transcription factor CHOP has been involved in obesity development and CHOP-deficient mice are more susceptible to obesity (Han et al., 2013), similarly to *Gdf15*-deficient mice (Tran et al., 2018). The molecular mechanism accounting for the higher weight gain of CHOP-deficient mice is not elucidated but, given the role of CHOP in the regulation of *GDF15* and the role of GDF-15 on food intake, a decrease of GDF-15 level in these mice may play a role.

The role of ER stress and ISR on *GDF15* regulation was previously described in cancer cell (Yang et al., 2010), myocyte (Chung et al., 2017), gut epithelial cells (Park et al., 2017) and hepatocytes (Li et al., 2018). These works revealed that various ISR stimuli including the non-steroidal anti-inflammatory compound sulindac sulfide (Yang et al., 2010), mitochondrial UPR (Chung et al., 2017), enteropathogenic *Escherichia coli* (Park et al., 2017), tunicamycin (Li et al., 2018; Patel et al., 2019) and thapsigargin (Li et al., 2018; Patel et al., 2019) induce GDF-15. Despite the fact that different ER stress stimuli are described to promote *GDF15* expression, SFAs represent interesting physiological stimuli linking obesity and GDF-15. Indeed, obesity increases FFA levels and a disequilibrium in SFA/UFA balance is commonly associated with progression of

obesity and the development of complications such as T2D (Klein-Platat et al., 2005; Ma et al., 2015).

Previous studies have demonstrated that UFAs are able to prevent cytokines production by SFAs, as described for IL-6 (Macrae et al., 2013) and IL-1 $\beta$  (Gianfrancesco et al., 2019; L'homme et al., 2013). We observed that an equimolar concentration of UFAs also prevents C18:0-induced *GDF15* expression in macrophages. UFAs also suppress ER stress and CHOP expression, probably accounting for the inhibition of *GDF15* expression. Inhibition of ER stress by UFAs is specific to SFAs as UFAs were unable to protect against tunicamycin-induced ER stress and increase in *GDF15* expression. These results reveal the complexity of FFA-mediated regulation of inflammatory process and provide evidences than the ratio SFAs/UFAs may be more important than the absolute value of SFAs.

It remains currently unclear whether FFAs, and particularly SFAs, play a direct role in macrophages activation during obesity. *In vitro*, SFAs activate macrophages to produce pro-inflammatory cytokines such as TNF- $\alpha$  and IL-1 $\beta$  (Haversen et al., 2009; L'homme et al., 2013). In obese adipose tissue, macrophages develop a pro-inflammatory phenotype in line with the presence of metabolic stimuli such as SFAs (Kratz et al., 2014). We showed that SFAs induces expression and secretion of *GDF-15* by macrophages *in vitro* and further investigations are required to support this finding *in vivo*.

*GDF-15* is protective against obesity and T2D (Chrysovergis et al., 2014; Chung et al., 2017; Emmerson et al., 2017; Hsu et al., 2017; Macia et al., 2012; Mullican et al., 2017; Tran et al., 2018; Yang et al., 2017). However, *GDF-15* shows a positive correlation with obesity progression and the development of complications such as T2D (Bao et

al., 2019; Dostálová et al., 2009; Kempf et al., 2012; Vila et al., 2011). This puzzling discrepancy may result from SFAs properties. Since SFAs induce a pro-inflammatory phenotype in macrophages (Haversen et al., 2009), GDF-15 may be produced besides other cytokines and be considered as an independent marker of macrophage activation by SFAs. The positive association between GDF-15 level and obesity progression may therefore result from the pro-inflammatory status of SFAs-activated macrophages, given that pro-inflammatory macrophages are involved in the development of obesity complications (Wynn et al., 2013).

In conclusion, we show that SFAs promote GDF-15 expression and secretion in macrophages. SFAs-induced GDF15 expression involves ER stress and the PERK/eIF2/CHOP signaling pathway. UFAs prevent SFAs-induced *GDF15* expression and ER stress. These new findings provide new molecular insights about how diet and lipid metabolism may regulate the development of obesity and T2D.

### **Acknowledgments and funding**

This research has been funded by the Interuniversity Attraction Poles (IAP) program initiated by the Belgian Science Policy Office (BELSPO) (IAP grant P7/32) (to JP), the University of Liege and the European Union in the context of the FP7-PEOPLE-COFUND-BelPD project (to LL), the Leon Fredericq Foundation (to LL) and by grants from “European Genomic Institute for Diabetes” (E.G.I.D., ANR-10-LABX-46) (to DD & BS).

## **References**

- Bao, X., Borné, Y., Muhammad, I.F., Nilsson, J., Lind, L., Melander, O., Niu, K., Orho-Melander, M., and Engström, G. (2019). Growth differentiation factor 15 is positively associated with incidence of diabetes mellitus: the Malmö Diet and Cancer-Cardiovascular Cohort. *Diabetologia* 62, 78–86.
- Bergman, R.N., and Ader, M. (2000). Free fatty acids and pathogenesis of type 2 diabetes mellitus. *Trends Endocrinol. Metab.* 11, 351–356.
- Boden, G., Duan, X., Homko, C., Molina, E.J., Song, W., Perez, O., Cheung, P., and Merali, S. (2008). Increase in endoplasmic reticulum stress-related proteins and genes in adipose tissue of obese, insulin-resistant individuals. *Diabetes* 57, 2438–2444.
- Bootcov, M.R., Bauskin, A.R., Valenzuela, S.M., Moore, A.G., Bansal, M., He, X.Y., Zhang, H.P., Donnellan, M., Mahler, S., Pryor, K., et al. (1997). MIC-1, a novel macrophage inhibitory cytokine, is a divergent member of the TGF-beta superfamily. *Proc. Natl. Acad. Sci. U.S.A.* 94, 11514–11519.
- Brown, D.A., Breit, S.N., Buring, J., Fairlie, W.D., Bauskin, A.R., Liu, T., and Ridker, P.M. (2002). Concentration in plasma of macrophage inhibitory cytokine-1 and risk of cardiovascular events in women: a nested case-control study. *Lancet* 359, 2159–2163.
- Brown, D.A., Ward, R.L., Buckhaults, P., Liu, T., Romans, K.E., Hawkins, N.J., Bauskin, A.R., Kinzler, K.W., Vogelstein, B., and Breit, S.N. (2003). MIC-1 serum level and genotype: associations with progress and prognosis of colorectal carcinoma. *Clin. Cancer Res.* 9, 2642–2650.
- Chrysovergis, K., Wang, X., Kosak, J., Lee, S.-H., Kim, J.S., Foley, J.F., Travlos, G., Singh, S., Baek, S.J., and Eling, T.E. (2014). NAG-1/GDF-15 prevents obesity by increasing thermogenesis, lipolysis and oxidative metabolism. *Int J Obes (Lond)* 38, 1555–1564.
- Chung, H.K., Ryu, D., Kim, K.S., Chang, J.Y., Kim, Y.K., Yi, H.-S., Kang, S.G., Choi, M.J., Lee, S.E., Jung, S.-B., et al. (2017). Growth differentiation factor 15 is a myomitokine governing systemic energy homeostasis. *J. Cell Biol.* 216, 149–165.
- Ding, Q., Mracek, T., Gonzalez-Muniesa, P., Kos, K., Wilding, J., Trayhurn, P., and Bing, C. (2009). Identification of macrophage inhibitory cytokine-1 in adipose tissue and its secretion as an adipokine by human adipocytes. *Endocrinology* 150, 1688–1696.
- Dostálová, I., Roubíček, T., Bártlová, M., Mráz, M., Lacinová, Z., Haluzíková, D., Kaválková, P., Matoulek, M., Kasalický, M., and Haluzík, M. (2009). Increased serum concentrations of macrophage inhibitory cytokine-1 in patients with obesity and type 2 diabetes mellitus: the influence of very low calorie diet. *Eur. J. Endocrinol.* 161, 397–404.
- Emmerson, P.J., Wang, F., Du, Y., Liu, Q., Pickard, R.T., Gonciarz, M.D., Coskun, T., Hamang, M.J., Sindelar, D.K., Ballman, K.K., et al. (2017). The metabolic effects of GDF15 are mediated by the orphan receptor GFRAL. *Nat. Med.* 23, 1215–1219.

- Gianfrancesco, M.A., Dehairs, J., L'homme, L., Herinckx, G., Esser, N., Jansen, O., Habraken, Y., Lassence, C., Swinnen, J.V., Rider, M.H., et al. (2019). Saturated fatty acids induce NLRP3 activation in human macrophages through K<sup>+</sup> efflux resulting from phospholipid saturation and Na, K-ATPase disruption. *Biochim Biophys Acta Mol Cell Biol Lipids* 1864, 1017–1030.
- Han, J., Murthy, R., Wood, B., Song, B., Wang, S., Sun, B., Malhi, H., and Kaufman, R.J. (2013). ER stress signalling through eIF2 $\alpha$  and CHOP, but not IRE1 $\alpha$ , attenuates adipogenesis in mice. *Diabetologia* 56, 911–924.
- Haversen, L., Danielsson, K.N., Fogelstrand, L., and Wiklund, O. (2009). Induction of proinflammatory cytokines by long-chain saturated fatty acids in human macrophages. *Atherosclerosis* 202, 382–393.
- Hodson, L., Skeaff, C.M., and Fielding, B.A. (2008). Fatty acid composition of adipose tissue and blood in humans and its use as a biomarker of dietary intake. *Prog. Lipid Res.* 47, 348–380.
- Hsu, J.-Y., Crawley, S., Chen, M., Ayupova, D.A., Lindhout, D.A., Higbee, J., Kutach, A., Joo, W., Gao, Z., Fu, D., et al. (2017). Non-homeostatic body weight regulation through a brainstem-restricted receptor for GDF15. *Nature* 550, 255–259.
- Johnen, H., Lin, S., Kuffner, T., Brown, D.A., Tsai, V.W.-W., Bauskin, A.R., Wu, L., Pankhurst, G., Jiang, L., Junankar, S., et al. (2007). Tumor-induced anorexia and weight loss are mediated by the TGF-beta superfamily cytokine MIC-1. *Nat. Med.* 13, 1333–1340.
- de Jonge, H.J.M., Fehrmann, R.S.N., de Bont, E.S.J.M., Hofstra, R.M.W., Gerbens, F., Kamps, W.A., de Vries, E.G.E., van der Zee, A.G.J., te Meerman, G.J., and ter Elst, A. (2007). Evidence Based Selection of Housekeeping Genes. *PLoS ONE* 2, e898.
- Jung, S.-B., Choi, M.J., Ryu, D., Yi, H.-S., Lee, S.E., Chang, J.Y., Chung, H.K., Kim, Y.K., Kang, S.G., Lee, J.H., et al. (2018). Reduced oxidative capacity in macrophages results in systemic insulin resistance. *Nat Commun* 9, 1551.
- Kempf, T., Guba-Quint, A., Torgerson, J., Magnone, M.C., Haefliger, C., Bobadilla, M., and Wollert, K.C. (2012). Growth differentiation factor 15 predicts future insulin resistance and impaired glucose control in obese nondiabetic individuals: results from the XENDOS trial. *Eur. J. Endocrinol.* 167, 671–678.
- Klein-Platat, C., Draï, J., Oujaa, M., Schlienger, J.-L., and Simon, C. (2005). Plasma fatty acid composition is associated with the metabolic syndrome and low-grade inflammation in overweight adolescents. *Am. J. Clin. Nutr.* 82, 1178–1184.
- Koo, B.K., Um, S.H., Seo, D.S., Joo, S.K., Bae, J.M., Park, J.H., Chang, M.S., Kim, J.H., Lee, J., Jeong, W.-I., et al. (2018). Growth differentiation factor 15 predicts advanced fibrosis in biopsy-proven non-alcoholic fatty liver disease. *Liver Int.* 38, 695–705.
- Koopmann, J., Buckhaults, P., Brown, D.A., Zahurak, M.L., Sato, N., Fukushima, N., Sokoll, L.J., Chan, D.W., Yeo, C.J., Hruban, R.H., et al. (2004). Serum macrophage

inhibitory cytokine 1 as a marker of pancreatic and other periampullary cancers. *Clin. Cancer Res.* 10, 2386–2392.

Kratz, M., Coats, B.R., Hisert, K.B., Hagman, D., Mutskov, V., Peris, E., Schoenfelt, K.Q., Kuzma, J.N., Larson, I., Billing, P.S., et al. (2014). Metabolic dysfunction drives a mechanistically distinct proinflammatory phenotype in adipose tissue macrophages. *Cell Metab.* 20, 614–625.

Laybutt, D.R., Preston, A.M., Akerfeldt, M.C., Kench, J.G., Busch, A.K., Biankin, A.V., and Biden, T.J. (2007). Endoplasmic reticulum stress contributes to beta cell apoptosis in type 2 diabetes. *Diabetologia* 50, 752–763.

L'homme, L., Esser, N., Riva, L., Scheen, A., Paquot, N., Piette, J., and Legrand-Poels, S. (2013). Unsaturated fatty acids prevent activation of NLRP3 inflammasome in human monocytes/macrophages. *J. Lipid Res.* 54, 2998–3008.

Li, D., Zhang, H., and Zhong, Y. (2018). Hepatic GDF15 is regulated by CHOP of the unfolded protein response and alleviates NAFLD progression in obese mice. *Biochem. Biophys. Res. Commun.* 498, 388–394.

Ma, W., Wu, J.H.Y., Wang, Q., Lemaitre, R.N., Mukamal, K.J., Djoussé, L., King, I.B., Song, X., Biggs, M.L., Delaney, J.A., et al. (2015). Prospective association of fatty acids in the de novo lipogenesis pathway with risk of type 2 diabetes: the Cardiovascular Health Study. *Am. J. Clin. Nutr.* 101, 153–163.

Macia, L., Tsai, V.W.-W., Nguyen, A.D., Johnen, H., Kuffner, T., Shi, Y.-C., Lin, S., Herzog, H., Brown, D.A., Breit, S.N., et al. (2012). Macrophage inhibitory cytokine 1 (MIC-1/GDF15) decreases food intake, body weight and improves glucose tolerance in mice on normal & obesogenic diets. *PLoS ONE* 7, e34868.

Macrae, K., Stretton, C., Lipina, C., Blachnio-Zabielska, A., Baranowski, M., Gorski, J., Marley, A., and Hundal, H.S. (2013). Defining the role of DAG, mitochondrial function, and lipid deposition in palmitate-induced proinflammatory signaling and its counter-modulation by palmitoleate. *J. Lipid Res.* 54, 2366–2378.

Mullican, S.E., Lin-Schmidt, X., Chin, C.-N., Chavez, J.A., Furman, J.L., Armstrong, A.A., Beck, S.C., South, V.J., Dinh, T.Q., Cash-Mason, T.D., et al. (2017). GFRAL is the receptor for GDF15 and the ligand promotes weight loss in mice and nonhuman primates. *Nat. Med.* 23, 1150–1157.

Osada, M., Park, H.L., Park, M.J., Liu, J.-W., Wu, G., Trink, B., and Sidransky, D. (2007). A p53-type response element in the GDF15 promoter confers high specificity for p53 activation. *Biochem. Biophys. Res. Commun.* 354, 913–918.

Ozcan, U., Cao, Q., Yilmaz, E., Lee, A.-H., Iwakoshi, N.N., Ozdelen, E., Tuncman, G., Görgün, C., Glimcher, L.H., and Hotamisligil, G.S. (2004). Endoplasmic reticulum stress links obesity, insulin action, and type 2 diabetes. *Science* 306, 457–461.

Park, S.-H., Yu, M., Kim, J., and Moon, Y. (2017). C/EBP homologous protein promotes NSAID-activated gene 1-linked pro-inflammatory signals and enterocyte invasion by enteropathogenic *Escherichia coli*. *Microbes Infect.* 19, 110–121.

Patel, S., Alvarez-Guaita, A., Melvin, A., Rimmington, D., Dattilo, A., Miedzybrodzka, E.L., Cimino, I., Maurin, A.-C., Roberts, G.P., Meek, C.L., et al. (2019). GDF15 Provides an Endocrine Signal of Nutritional Stress in Mice and Humans. *Cell Metab.* 29, 707-718.e8.

Perdiguerro, E.G., and Geissmann, F. (2016). The development and maintenance of resident macrophages. *Nat. Immunol.* 17, 2–8.

Suzuki, T., Gao, J., Ishigaki, Y., Kondo, K., Sawada, S., Izumi, T., Uno, K., Kaneko, K., Tsukita, S., Takahashi, K., et al. (2017). ER Stress Protein CHOP Mediates Insulin Resistance by Modulating Adipose Tissue Macrophage Polarity. *Cell Rep* 18, 2045–2057.

Tran, T., Yang, J., Gardner, J., and Xiong, Y. (2018). GDF15 deficiency promotes high fat diet-induced obesity in mice. *PLoS ONE* 13, e0201584.

Tsai, V.W.-W., Manandhar, R., Jørgensen, S.B., Lee-Ng, K.K.M., Zhang, H.P., Marquis, C.P., Jiang, L., Husaini, Y., Lin, S., Sainsbury, A., et al. (2014). The anorectic actions of the TGF $\beta$  cytokine MIC-1/GDF15 require an intact brainstem area postrema and nucleus of the solitary tract. *PLoS ONE* 9, e100370.

Tsai, V.W.W., Husaini, Y., Sainsbury, A., Brown, D.A., and Breit, S.N. (2018). The MIC-1/GDF15-GFRAL Pathway in Energy Homeostasis: Implications for Obesity, Cachexia, and Other Associated Diseases. *Cell Metab.* 28, 353–368.

Vila, G., Riedl, M., Anderwald, C., Resl, M., Handisurya, A., Clodi, M., Prager, G., Ludvik, B., Krebs, M., and Luger, A. (2011). The relationship between insulin resistance and the cardiovascular biomarker growth differentiation factor-15 in obese patients. *Clin. Chem.* 57, 309–316.

Walter, P., and Ron, D. (2011). The unfolded protein response: from stress pathway to homeostatic regulation. *Science* 334, 1081–1086.

Wynn, T.A., Chawla, A., and Pollard, J.W. (2013). Macrophage biology in development, homeostasis and disease. *Nature* 496, 445–455.

Xue, J., Schmidt, S.V., Sander, J., Draffehn, A., Krebs, W., Quester, I., De Nardo, D., Gohel, T.D., Emde, M., Schmidleithner, L., et al. (2014). Transcriptome-based network analysis reveals a spectrum model of human macrophage activation. *Immunity* 40, 274–288.

Yang, H., Park, S.H., Choi, H.J., and Moon, Y. (2010). The integrated stress response-associated signals modulates intestinal tumor cell growth by NSAID-activated gene 1 (NAG-1/MIC-1/PTGF-beta). *Carcinogenesis* 31, 703–711.

Yang, L., Chang, C.-C., Sun, Z., Madsen, D., Zhu, H., Padkjær, S.B., Wu, X., Huang, T., Hultman, K., Paulsen, S.J., et al. (2017). GFRAL is the receptor for GDF15 and is required for the anti-obesity effects of the ligand. *Nat. Med.* 23, 1158–1166.

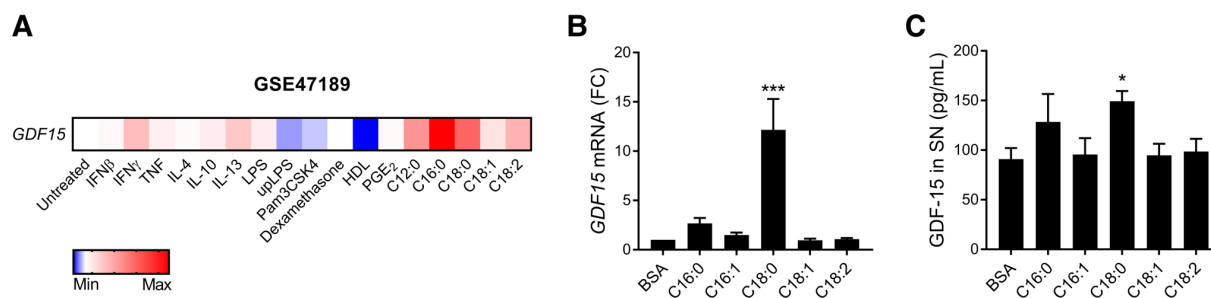


**Figure 1. SFAs promote *GDF15* expression and secretion in macrophages.**

**(A)** Heatmap representing *GDF15* expression in human primary macrophages treated with different stimuli. Further details are available in Xue et al., 2014 and under the accession number GSE47189. **(B-C)** MDMs were treated with 100  $\mu$ M FFA or BSA for 16 hrs. *GDF15* expression was assessed by RT-qPCR **(B)** and *GDF-15* secretion in SN was measured by luminex assay **(C)** ( $n = 5$ ).  $*p < 0.05$ ;  $***p < 0.001$  by one-way ANOVA with Dunnett's multiple comparisons test. Results are presented as mean  $\pm$  SEM. SN, supernatant. FC, Fold change.

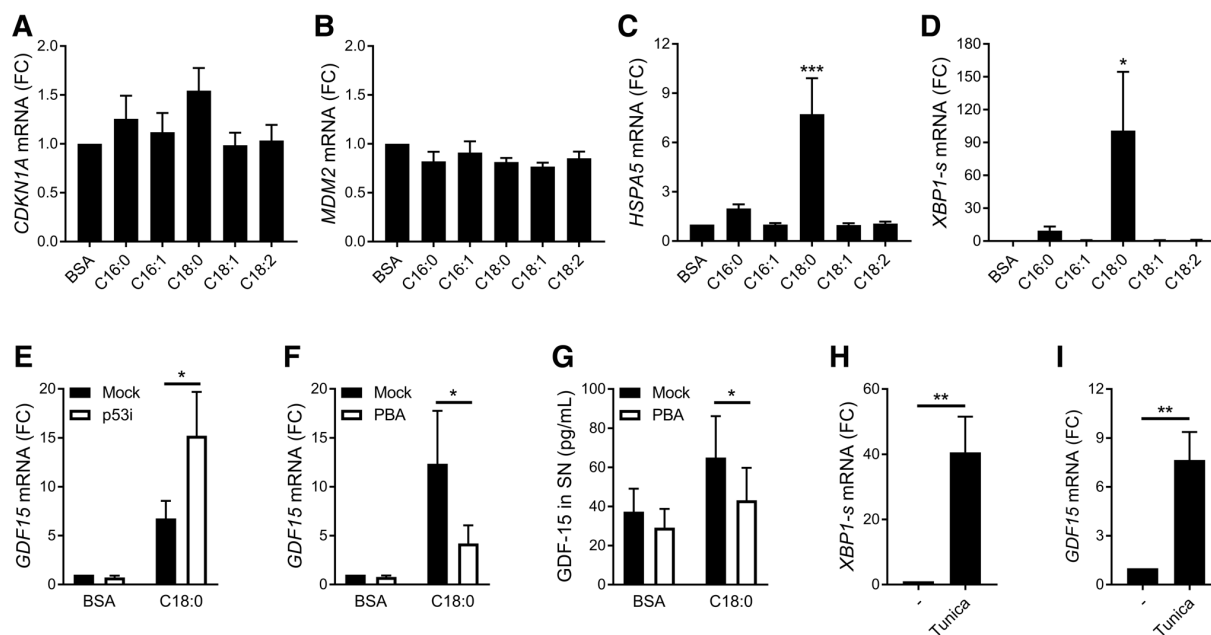


**Figure 2. Role of ER stress in SFAs-induced *GDF15* expression.**

(A-D) mRNA expression measured by RT-qPCR after treatment with 100  $\mu$ M FFAs for 16 hrs in MDMs ( $n = 5$ ). \* $p < 0.05$ ; \*\*\* $p < 0.001$  by one-way ANOVA with Dunnett's multiple comparisons test. (E-G) *GDF15* expression measured by RT-qPCR (E-F) and *GDF-15* secretion in SN measured by luminex assay (G) after stimulation of MDMs with 100  $\mu$ M C18:0 for 16 hrs in presence of 20  $\mu$ M pifithrin- $\alpha$  (p53i) ( $n = 3$ ) or 1 mM PBA ( $n = 5$ ). \* $p < 0.05$  by two-way ANOVA with Sidak's multiple comparisons test. (H-I) mRNA expression measured by RT-qPCR after treatment with 5  $\mu$ g/mL tunicamycin for 16 hrs in MDMs ( $n = 5$ ). \*\* $p < 0.01$  by Student's *t*-test. Results are presented as mean  $\pm$  SEM. SN, supernatant. FC, Fold change.

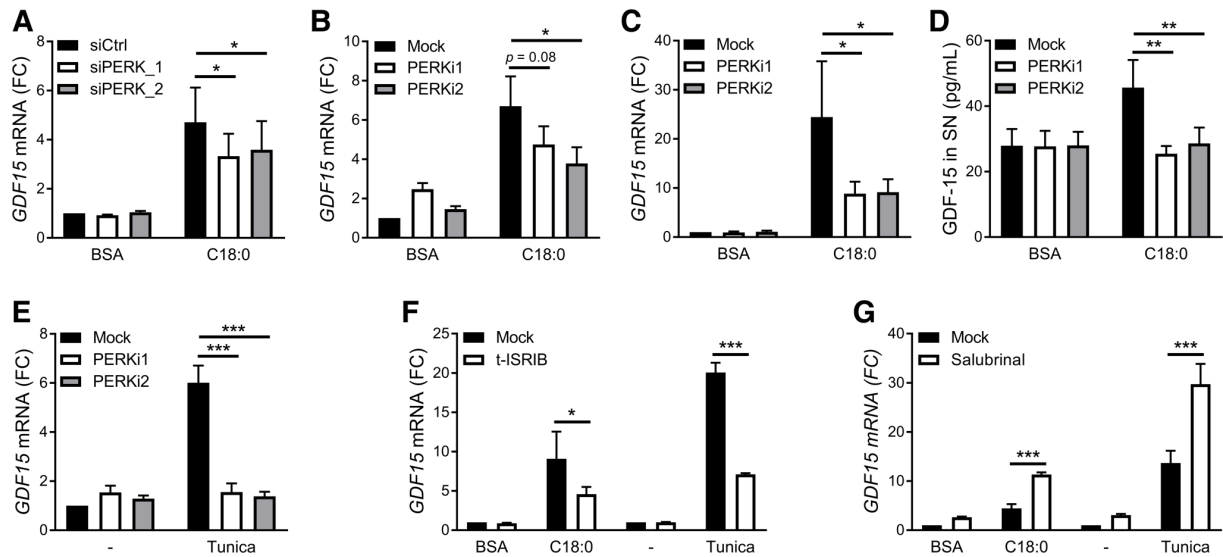


**Figure 3. Role of ISR in SFAs-induced *GDF15* expression.**

**(A-B)** *GDF15* expression measured by RT-qPCR in PMA-differentiated THP-1 cells treated with 200  $\mu$ M C18:0 for 16 hrs after PERK silencing by siRNA **(A)** ( $n = 5$ ) or in presence of 2  $\mu$ M GSK2606414 (PERKi1) or GSK2656157 (PERKi2) **(B)** ( $n = 5$ ). **(C-E)** *GDF15* expression measured by RT-qPCR **(C, E)** or *GDF-15* secretion in supernatant (SN) measured by luminex assay **(D)** in MDMs treated with 100  $\mu$ M C18:0 or 5  $\mu$ g/mL tunicamycin for 16 hrs in presence of 2  $\mu$ M GSK2606414 (PERKi1) or GSK2656157 (PERKi2) ( $n = 4$ ). **(F-G)** *GDF15* expression measured by RT-qPCR after treatment with 200  $\mu$ M C18:0 or 5  $\mu$ g/mL tunicamycin for 16 hrs in PMA-differentiated THP-1 cells in presence of 1  $\mu$ M trans-ISRIB or 50  $\mu$ M salubrinal ( $n = 5$ ). \* $p < 0.05$ , \*\* $p < 0.01$ , \*\*\* $p < 0.001$  by two-way ANOVA with Sidak's multiple comparisons test. Results are presented as mean  $\pm$  SEM. FC, Fold change.

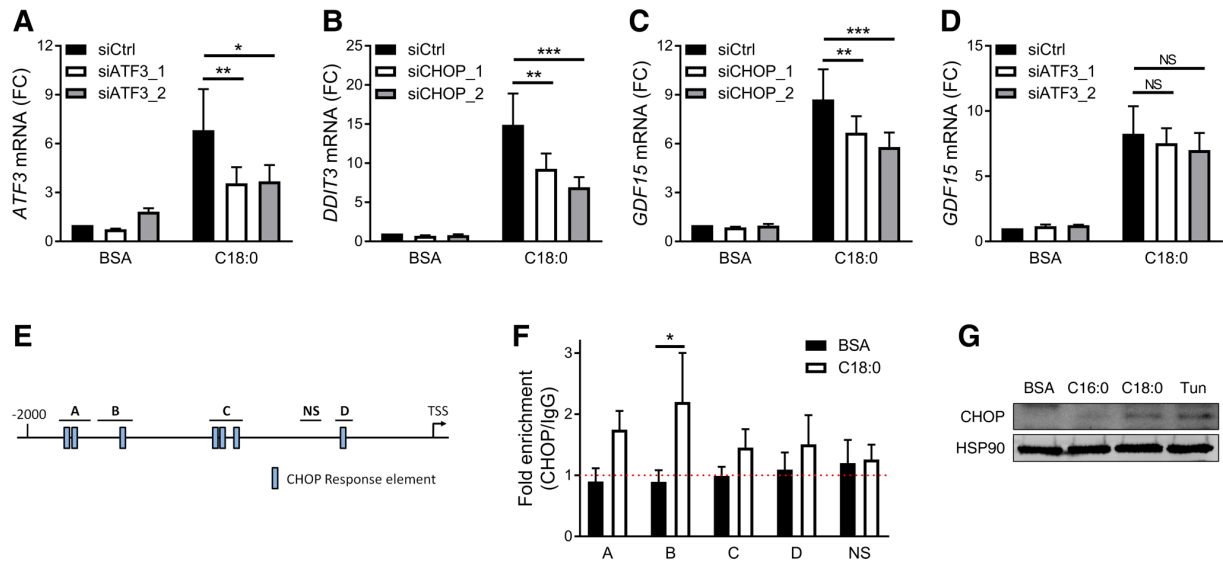


**Figure 4. Role of CHOP in SFAs-induced *GDF15* expression.**

**(A-D)** *GDF15* expression measured by RT-qPCR after treatment with 200  $\mu$ M C18:0 for 16 hrs in PMA-differentiated THP-1 after ATF3 or CHOP silencing by siRNA ( $n = 4$ ). **(E)** Schematic representation of *GDF15* promoter with the putative CHOP response elements and the regions analyzed in ChIP-qPCR. **(F)** CHOP binding in *GDF15* promoter measured by ChIP-qPCR in PMA-differentiated THP-1 cells treated with 200  $\mu$ M C18:0 for 16 hrs ( $n = 4$ ). **(G)** Analysis of CHOP expression by western blot after stimulation of PMA-differentiated THP-1 cells with 200  $\mu$ M SFAs or 5  $\mu$ g/mL tunicamycin for 24 hrs ( $n = 3$ ). \* $p < 0.05$ , \*\* $p < 0.01$ , \*\*\* $p < 0.001$  by two-way ANOVA with Sidak's multiple comparisons test. Results are presented as mean  $\pm$  SEM. FC, Fold change. TSS, transcription start site.

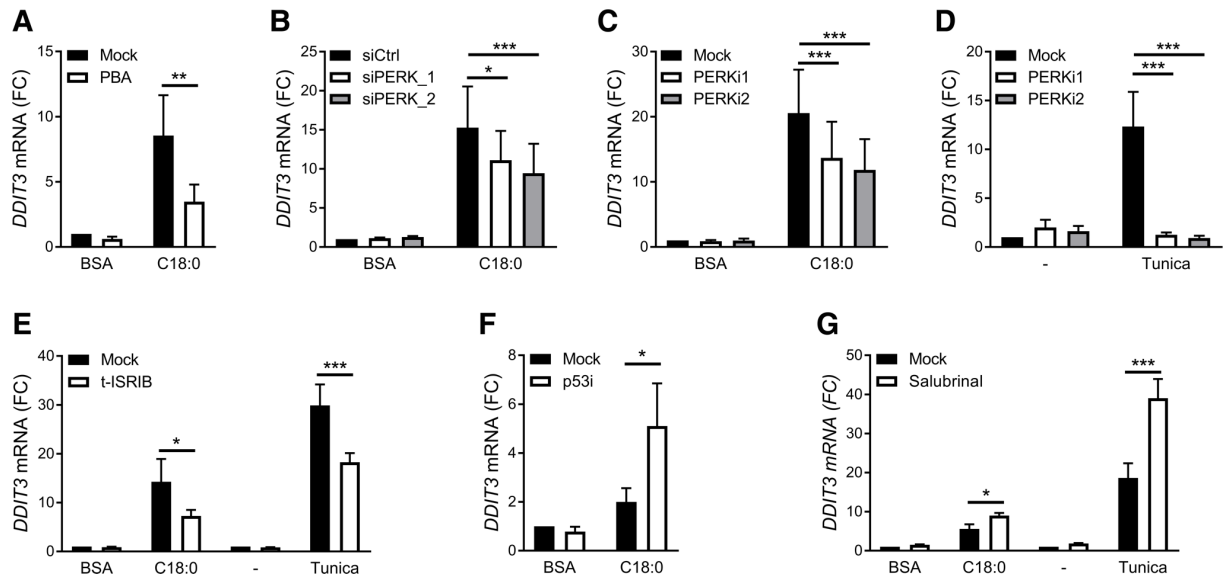


**Figure 5. CHOP regulation by pharmacological and siRNA strategies.**

(A-G) *DDIT3* expression measured by RT-qPCR after treatment with 100  $\mu$ M C18:0 in MDMs (A, C, D, F), 200  $\mu$ M C18:0 in PMA-differentiated THP-1 (B, E, G) or 5  $\mu$ g/mL tunicamycin for 16 hrs in presence of 1 mM PBA, 2  $\mu$ M GSK2606414 (PERKi1), 2  $\mu$ M GSK2656157 (PERKi2), 1  $\mu$ M trans-ISRIB, 20 $\mu$ M pifithrin- $\alpha$  (p53i), 50  $\mu$ M salubrinal or after PERK silencing by siRNA ( $n = 3-5$ ). \* $p < 0.05$ , \*\* $p < 0.01$ , \*\*\* $p < 0.001$  by two-way ANOVA with Sidak's multiple comparisons test. Results are presented as mean  $\pm$  SEM. FC, Fold change.

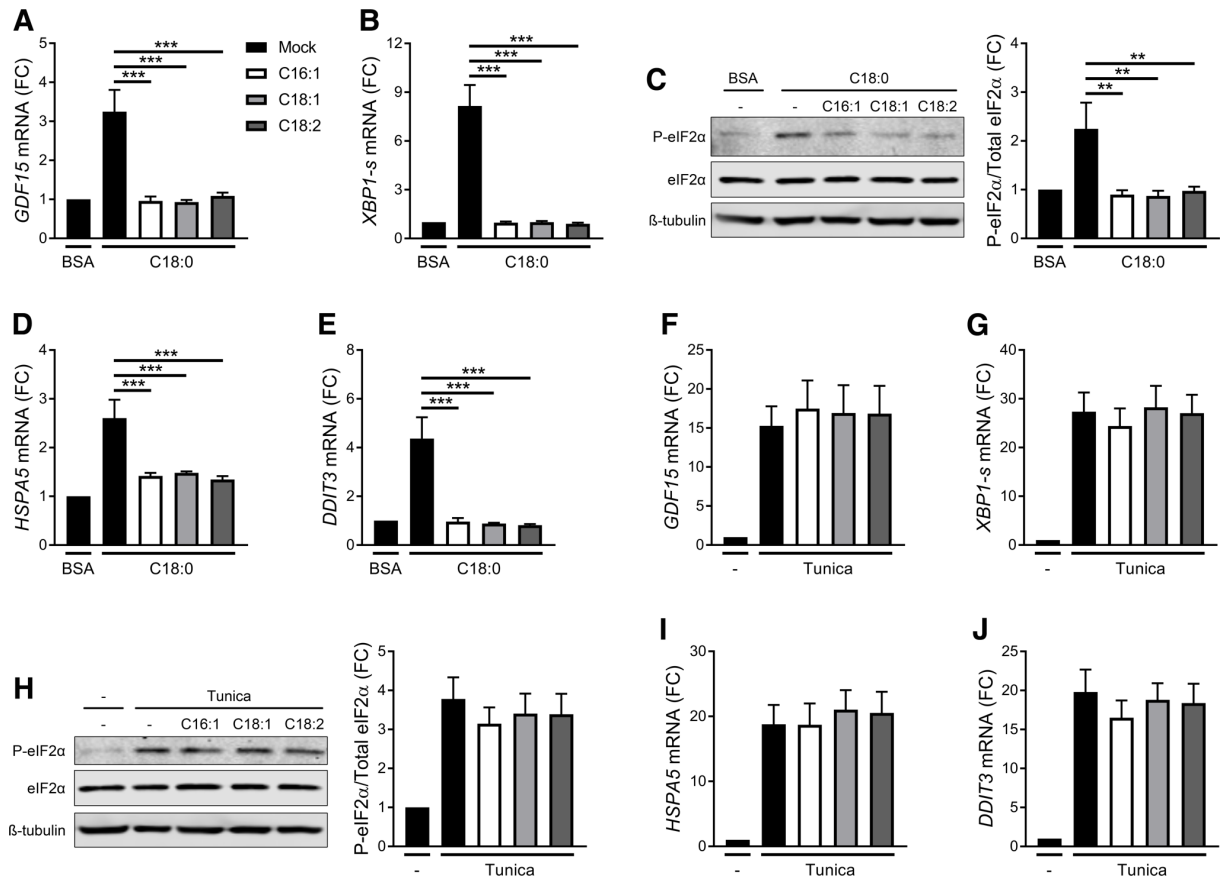


**Figure 6. UFAs prevent SFA-induced *GDF15* expression.**

**(A-J)** mRNA expression measured by RT-qPCR **(A-B, D-G, I-J)** and analysis of eIF2 $\alpha$  phosphorylation by western blot **(C, H)** after treatment with 200  $\mu$ M C18:0 or 5  $\mu$ g/mL tunicamycin in presence of 200  $\mu$ M UFAs for 16 hrs in PMA-differentiated THP-1 cells ( $n = 5$ ). \*\* $p < 0.01$ , \*\*\* $p < 0.001$  by one-way ANOVA with Dunnett's multiple comparisons test. Results are presented as mean  $\pm$  SEM. FC, Fold change.

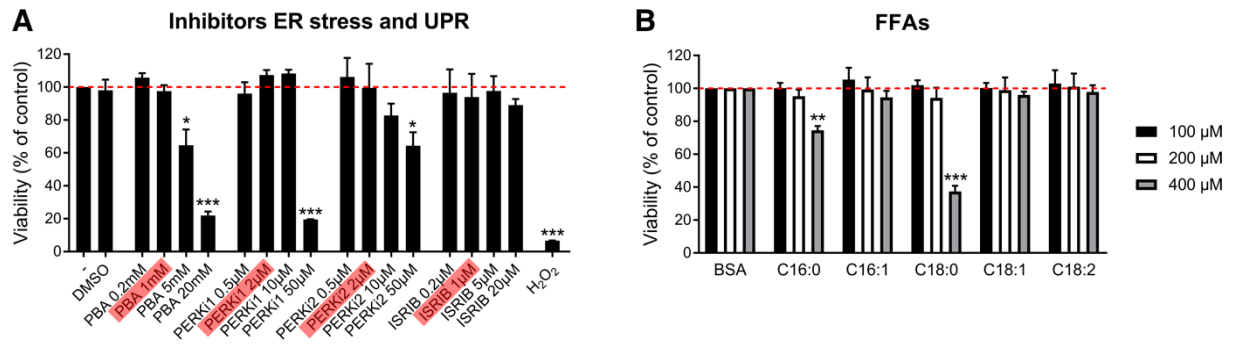


**Figure S1. Cell toxicity of inhibitors and FFAs**

**(A-B)** Cell viability was assessed with WST1 reagent in PMA-differentiated THP-1 cells treated for 16 hrs with inhibitors or FFAs at the indicated concentration ( $n = 3$ ). \* $p < 0.05$ , \*\* $p < 0.01$ , \*\*\* $p < 0.001$  by one-way ANOVA with Dunnett's multiple comparisons test for **(A)** and by two-way ANOVA with Sidak's multiple comparisons test for **(B)**. Results are presented as mean  $\pm$  SEM.

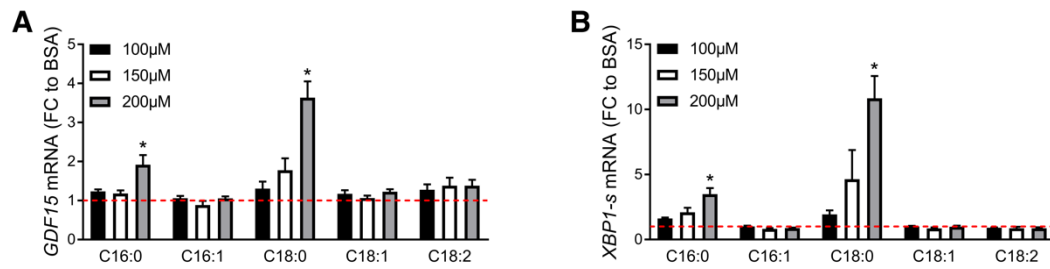


**Figure S2. SFAs induce *GDF15* expression and ER stress in PMA-differentiated THP1 cells**

**(A-B)** mRNA expression measured by RT-qPCR after treatment with the indicated concentration of FFAs for 16 hrs in PMA-differentiated THP-1 cells ( $n = 5$ ).  $*p < 0.05$  by two-way ANOVA with Sidak's multiple comparisons test. Results are presented as mean  $\pm$  SEM. FC, Fold change.

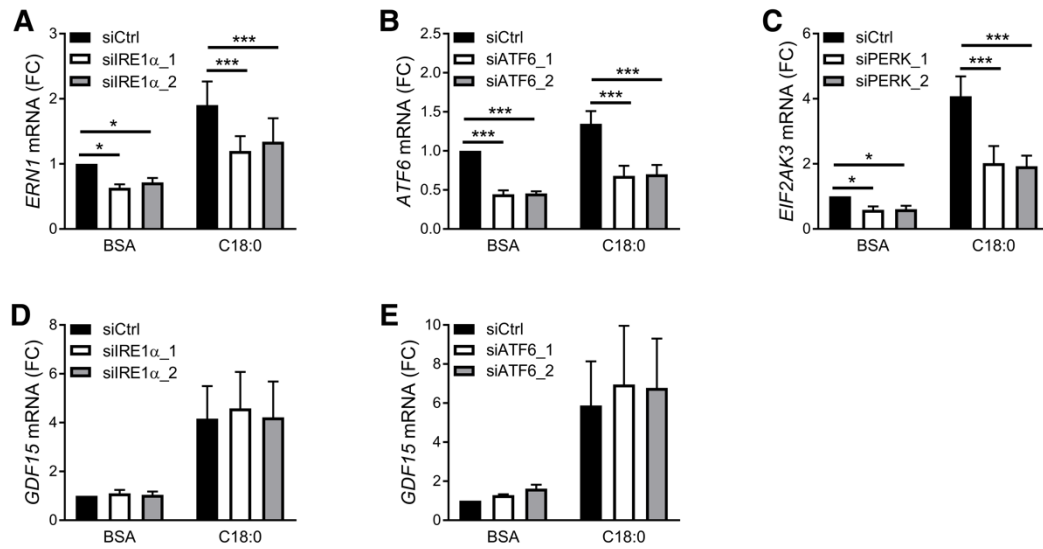


**Figure S3.** IRE1 $\alpha$ , ATF6 and PERK silencing in PMA-differentiated THP1 cells

(A-E) mRNA expression measured by RT-qPCR after treatment with 200  $\mu$ M C18:0 for 16 hrs in PMA-differentiated THP-1 cells after IRE1 $\alpha$ , ATF6 or PERK silencing by siRNA ( $n = 5$ ).  $p < 0.05$ , \*\*\* $p < 0.001$  by two-way ANOVA with Sidak's multiple comparisons test. Results are presented as mean  $\pm$  SEM. FC, Fold change.

**Table S1.** List of primers used in RT-qPCR and ChIP-qPCR.

<b>RT-qPCR</b>	<b>Forward</b>	<b>Reverse</b>
GDF15	GCAAGAACTCAGGACGGTGA	TGGAGTCTTCGGAGTGCAAC
OAZ1	GGATCCTCAATAGCCACTGC	TACAGCAGTGGAGGGAGACC
CDKN1A	GCGAGGCACAAGGGTACAAGACAG	TAATGGCGGGCTGCATCCAG
MDM2	GCCCTTCGTGAGAATTGGCT	AAAGCCCTCTTCAGCTTGTGT
HSPA5	TAGCGTATGGTGCTGCTGTC	TTTGTCAAGGGTCTTTCACC
XBP1 spliced isoform	CTGAGTCCGCAGCAGGTG	ACTGGGTCCAAGTTGTCCAG
ERN1	AGCAGTTAGAGAGAGGGCGGG	CTGGAGGGGGACAGTGATGT
ATF6	CAATTGGAAGCAGCAAATGA	ACCGAGGAGACGAGACTGAA
EIF2AK3	GTGGGACCAAGACCGTGAAA	CGACAACCCAGAGCTGAACA
ATF4	TCAAACCTCATGGGTTCTCC	GTGTCATCCAACGTGGTCAG
DDIT3	GAACCAGGAAACGGAAACAGA	TCTCCTTCATGCGCTGCTT
ATF3	ATTGTCCGGGCTCAGAATGG	ACCACGACTGCTTAGCTCTG

<b>ChIP-qPCR GDF15</b>	<b>Forward</b>	<b>Reverse</b>
Promoter site A	GCTGGAGCTTGCAGGTTGG	AAAATTTCAAGAAATTAACCGGTCGTG
Promoter site B	ACCACGACCGGTTAATTTCTGAA	AAAAATTAATAACTCTAGCCCCTGGC
Promoter site C	TGCTCTTGTTGATCAGGCGGA	CTGGGCTTGGTGGTGGGATTA
Promoter site D	AGAATGAGTAGGAGTTCTCCAGAGG	CATAGGAGGCACTTGATAAACTGGG
Promoter site NS	ATTATGAATCCTGTGAGGATGGCTT	ATTATCTTCCAGTCTAAGCAGGGT